Numerical Simulation of a Metro Train Fire

by

Boon Hui Chiam

Supervised by

Michael Spearpoint
and
Dr. Charley Fleischmann

Fire Engineering Research Report 05/1
June 2005

A thesis submitted in partial fulfilment of the requirements for the degree of Master of Engineering in Fire Engineering

Department of Civil Engineering
University of Canterbury
Private Bag 4800
Christchurch, New Zealand

For a full list of reports please visit http://www.civil.canterbury.ac.nz/fire/fe_resrch_reps.html

Abstract

This research thesis presents the simulation of fire growth and flame spread within a metro train in an underground trainway using Fire Dynamics Simulator (FDS) Computational Fluid Dynamics (CFD) model. The motivation of the study is to predict the heat release rate (HRR) and specifically the peak value for emergency tunnel ventilation system design. Even though currently there are several methods that can be used to estimate the HRR for a metro train, it appears that the current methods cannot realistically predict the HRR because factors such as the burning behaviour of materials; and/or the train and tunnel geometries that affect the HRR are not considered. This project attempts to incorporate these factors in the FDS model.

The study evaluated the design of metro trains proposed for the new Circle Line under construction in Singapore. In this research, two modelling approaches were proposed. The first modelling approach prescribed the Cone Calorimeter heat release rate per unit area (HRRPUA) while the other prescribed the heat of vaporisation. The difference between the two is the prescribed constant which governed the rate of pyrolysis. Cone Calorimeter tests were conducted for the surface exposed materials to evaluate the train car materials' reaction to fire and to derive the material properties for input into the FDS model.

In this research, three common fire scenarios have been identified for simulation. They were fire on top of the seat (arson), fire in the corner (arson and electrical fault) and undercarriage fire (electrical fault). The common fire scenarios were expanded to account for ventilation factors. A total of 13 credible fire scenarios were investigated.

As it has been found that prescribing the material properties values derived from the Cone Calorimeter test data were not able to accurately predict the ignition and fire growth for the materials simulated. A combination of derived and calibrated properties values has been prescribed in the final simulations.

In the final simulations, the two modelling approaches predicted the same fire severity for different fire scenarios. The simulations indicated that it is important to prevent direct airflow through the train compartment as it may support fire spread if there is a large ignition source. The simulations also indicated that for a scenario that will progress to flashover under the influence of high ventilation airflow velocity, the fire spread to adjacent cars will be very rapid if there is no door installed between the metro train cars.

Two peak HRR values have been proposed for the design of emergency tunnel ventilation system for the metro train under consideration based on the simulations. A peak HRR value of 5 MW has been proposed for a metro train fire at the station trackway and a peak HRR value of 10 MW has been proposed for a metro train fire in the tunnel.

Acknowledgments

Throughout the course of this research project, I have received assistance and support from a large number of people who I would like to acknowledge:

- My supervisor, Mike Spearpoint and co-supervisor, Dr. Charley Fleishmann for their guidance throughout the course of the project.

- My employer, the Land Transport Authority (LTA), Singapore for providing me a scholarship to pursue the Master of Engineering in Fire Engineering degree course.

- My colleagues in the LTA, particularly Sandra Tay who proofread sections of this report; and Joseph Tan for his prompt response of information I have requested.

- The other MEFE students, particularly Ming Wei who has assisted me in conducting the Cone Calorimeter tests.

- Fire technicians, Grant Dunlop and Bob Smith, CAD manager, Joost Stenfert Kroese and librarian, Christine McKee.

- Dr. Kevin McGrattan from NIST for providing the FDS model for the Cone Calorimeter to carry out the FDS predictions of small-scale test results.

- Vince Dowling from CSIRO for providing papers on their research work on train fire.

- My friend, Dr. Jonathan Tai for sharing his research experiences and proofreading this report.

- My family for their unwavering support.

Table of Contents

List of Figures

List of Tables

Nomenclature

Symbol	Description	Unit
A	Pre-exponential factor	m/s
A_A	Annular area (i.e. tunnel cross-sectional area minus train cross-sectional area)	m^2
A_{sur}	Surface area	m^2
C	Empirical constant (Equation 3.11)	-
C_{calib}	Calibration constant (Equation 8.1)	$kg^{0.5}m^{0.5}K^{0.5}$
$C_{nat\ con}$	Coefficient for natural convection	-
c	Specific heat	kJ/kgK
c_p	Specific heat of ambient air at constant pressure	kJ/kgK
D	Equivalent circular diameter	m
D_s	Instantaneous measure of the smoke optical density at a particular instant in time	-
D^*	Characteristic fire diameter	m
E	Amount of energy released by complete combustion per unit mass of oxygen consumed	kJ/kg
E_A	Activation energy	kJ/kmol
E_{CO}	Heat release per mass unit of oxygen consumed for the combustion of CO	kJ/kg of O_2
Fr	Froude number	-
f	External force vector (excluding gravity)	-
g	Acceleration due to gravity	m/s^2
$grade$	Gradient	°
H	Height	m
h	Enthalpy	J
h_{con}	Convection heat transfer coefficient	kW/m^2K
h_{tot}	Total heat transfer coefficient	kW/m^2K

I	Radiation intensity	W/m^2
I_s	Flame spread index	-
K_{grade}	Grade correction factor	-
k	Thermal conductivity	W/mK
k_{max}	Maximum extinction coefficient	m^{-1}
L	Characteristic length	m
M	Molecular weight	kg/kmol
$\dot{m}$	Mass loss rate	kg/s
$\dot{m}_{ex}$	Mass flow rate in the Cone Calorimeter exhaust duct	kg/s
p	Pressure	Pa
Pr	Prandtl number	-
$\dot{Q}$	Heat release rate	kW or MW
$\dot{Q}^*$	Characteristic heat release rate	kW or MW
q_{rad}	Radiative heat flux vector	-
$\dot{q}$	Heat release rate for small-scale test	kW
$\dot{q}_{cr}$	Critical heat flux	kW/m^2
$\dot{q}_e$	Exposure heat flux	kW/m^2
R^2	Correlation coefficient	-
Re	Reynolds number	-
RH	Relative humidity	%
r	Stoichiometric air/fuel ratio	kg/kg
SEA	Specific extinction area	m^2/kg
s	Stoichiometric oxidizer/fuel ratio	kg/kg
T	Ignition temperature	°C or K
T_{ex}	Gas temperature at the orifice plate	K
t	Time	s
U	Overall heat transfer coefficient	$W/m^2K.$
u	Vector describing the velocity in the u, v and w directions	-
V	Velocity	m/s

W	Width	m
X	Mole fraction	-
x	Vector describing the position in the x, y and z directions	-
Y	Mass fraction	-
Y_F^I	Fuel mass fraction in the fuel stream	-
Z	Mixture fraction	-

Greek symbol	**Description**	**Unit**
ψ	HRR enhancement	-
ρ	Density	kg/m^3
δ	Thickness	m
χ	Combustion efficiency factor	-
χ_{rad}	Radiative loss fraction	-
τ	Viscous stress tensor	Pa
$\Re$	Universal gas constant	kJ/kmolK
v	Stoichiometric coefficients	-
κ	Local absorption coefficient	-
ϕ	Oxygen depletion fraction	-
α	Volumetric expansion factor	-
σ	Stefan-Boltzmann's constant (5.67×10^{-11})	kW/m^2K^4
ε	Surface emissivity at ignition	-
δx	Nominal grid size	mm
$\Delta H_{c,eff}$	Effective heat of combustion	kJ/kg or MJ/kg
ΔH_v	Heat of vaporisation	kJ/kg or MJ/kg
ΔP	Pressure drop across the orifice plate	Pa

List of superscripts	Description	Unit
$\dot{}$	Per unit time	s^{-1}
$'$	Per unit length	m^{-1}
$''$	Per unit area	m^{-2}
$'''$	Per unit volume	m^{-3}
*	Characteristic	
∞	Ambient	
A	Concentration in the analyser	
a	Incoming air	
e	Exhaust gas	
n	Power value between the ranges of 0.547 to 1	

List of subscripts	Description
1,2,3,4	Number used to differentiate the HRR contribution of metro train cars at different fire development stage
∞	Ambient
a	Property of air
b	Blackbody
CO	Property of carbon monoxide
CO_2	Property of carbon dioxide
con	Convective
cr	Critical value
e	External
eff	Effective
F	Fuel
FO	Flashover
f	Flame or fire
g	Gas
i	Chemical species
ig	Ignition

int	Initial
is	Ignition source
max	Maximum value
min	Minimum value
*O*2	Property of oxygen
P	Products
peak	Peak value
rad	Radiative
sur	Surface
t	Tunnel
tot	Total
VL	Loss of visibility

List of Abbreviations	**Description**
ASET	Available safe egress time
ASTM	American Society for Testing and Materials
ac	Alternating current
ave	Average
BART	Bay Area Rapid Transit, US
BR	British Rail, UK
CCL	Circle Line, Singapore
CEN	European Committee for Standardisation
CENELEC	European Committee for Electrical Standardisation
CFD	Computational fluid dynamics
CFE	Critical flux at extinguishment
CO	Carbon monoxide
CO_2	Carbon dioxide
CRF	Critical radiant flux
CSIRO	Commonwealth Scientific and Industrial Research Organization
dc	Direct current
EN	European standard
ERRI	European Railway Research Institute

EWL	East West Line, Singapore
FAA	Federal Aviation Administration
FDS	Fire Dynamics Simulator
FED	Fractional effective dose
FIRESTARR	Fire Standardisation Research of Railway vehicles
FRP	Fibreglass reinforced polymer
FO	Flashover
FSTL	Fire Science and Technology Laboratory
FTA	Federal Transit Administration
HGVs	Heavy good vehicles
HRR	Heat release rate
HRRPUA	Heat release rate per unit area
H_2O	Water
IEC	International Electrotechnical Commission
IS	Ignition source
ISO	International Organization for Standardization
LTA	Land Transport Authority, Singapore
LUL	London Underground Limited, UK
Max	Maximum
MTRC	Mass Transit Rail Corporation, Hong Kong
NA	Not available
NBS	National Bureau of Standards, now NIST
NEL	North East Line, Singapore
NFPA	National Fire Protection Association
NI	Not ignition
NIST	National Institute of Standards and Technology
NR	Not required
NSL	North South Line, Singapore
n/a	Not applicable
n/r	Not required
OSU	Ohio State University, US
O_2	Oxygen
QFRS	Queensland Fire and Rescue Service, Australia

RSET	Required safe egress time
R&D	Research and Development
SEPTA	Southeastern Pennsylvania Transportation Agency, US
SFPE	Society of Fire Protection Engineers
STDEV	Standard deviation of average value
UIC	International Union of Railways
UITP	International Union of Public Transport
UK	United Kingdom
US	United States
USCG	US Coast Guard
UMTA	Urban Mass Transit Administration, now FTA
VOF4	Rate of smoke generation in the first 4 minutes
WMATA	Washington Metropolitan Area Transit Authority, US

1 Introduction

A mass rapid transit or metro system is a public transportation system, using electric-powered rolling stock running in its own right-of-way on guideway facilities at-grade, underground, or elevated, free from interference with other ground traffic, to transport large volumes of passengers at high speeds and with short headway, in the city and its adjacent areas. In many cases, at least a portion of the rails are placed in tunnels dug beneath the surface of a city in which case the system may be called the subway or the underground (Anon 2004a).

Metro systems are being recognised as an effective and efficient way to solve transport problems in congested cities and new lines are being planned and built throughout the world. In designing a metro system, fire safety is one of the high priorities in view of the volume of passengers being transported. It is even more vital if the system is built underground as fire incident in an underground trainway is considerably different from fire in a building in term of fire development, evacuation and rescue operations (Wolinska 2002).

For a metro train fire, it is important that the emergency tunnel ventilation system is able to control the direction of smoke movement in order to provide a clear and safe path for evacuation of passengers and to facilitate fire-fighting operations. In a tunnel, the predominant method for achieving this objective is for the emergency tunnel ventilation system to develop sufficient longitudinal airflow movement past the fire site so that all the smoke and hot gases will be forced in an opposite direction of evacuation (Hettinger and Barnett 1991). This is usually achieved by operating the emergency tunnel ventilation system in a push-pull ventilation mode whereby ventilation fans at one end of the tunnel will be in supply mode and the other end in extraction mode (Luk 2004). The design criterion is to maintain an annular airflow rate past the fire site higher than the critical velocity to prevent the upper layer of heated air from flowing in the direction opposite to the forced ventilation (a phenomenon called “back-layering”) which will hinder the safe evacuation of passengers.

For a metro train fire at the station trackway i.e. the section of track next to the station platform, one of the ventilation strategies is to operate the tunnel ventilation fans at both ends of the station in extraction mode to extract the smoke and hot gases generated from the fire (Luk 2004) so that to maintain a tenable environment along the means of escape within the station (Chua 2003).

The capacity of the emergency tunnel ventilation system must be adequately designed to cope with the most onerous/ worst case train fire scenarios in the tunnel and at the station trackway. In the design, the fire heat release rate (HRR) generated from the burning train is one of the key parameters that dictates the air velocity i.e. the critical velocity required to prevent back-layering (Hettinger and Barnett 1991). It is also one of the parameters that determines the performance of the emergency tunnel ventilation system (Chua 2003). The HRR value is dependent upon the quantity and nature of the combustible materials in the metro train car, the physical configuration of the metro train (i.e. length, width, size of windows, and doors, etc), and the type of metro train car construction (Hettinger and Barnett 1991) and is the single most important factor contributing to the fire severity (Babrauskas and Peacock 1992).

Although many metro systems/lines have already been built worldwide, there is little known of the actual HRR of a metro train. Several methods of determining the HRR exist. The most common method involves taking the complete fire load and dividing it by an assumed time. The assumed time is taken from the historical observations of actual metro train fires.

Another method involves summation of HRR per unit area (HRRPUA) of surface materials. The HRRPUA for all the surface materials are obtained from small-scale tests e.g. Cone Calorimeter tests (ASTM E 1354 2004; ISO 5660-1:2002; ISO 5660-2:2002; ISO 5660-3:2003; NFPA 271 2004 edition).

There are also attempts to use a post-flashover zone model to predict the HRR of a metro train. The design assumes the fire is ventilation controlled and therefore has a constant burning rate.

The above methods do not consider the burning behaviour of materials; and/or do not consider the physical configuration of the metro train, the type of metro train car construction and the tunnel geometry.

Some designers determine the HRRs of major items such as car seat and lining materials. The HRRs of these major items are either obtained by conducting a series of tests or from references; or derived from the fire load of these major items. The HRR of the metro train is then estimated by analysis. Among the methods used to determine the HRRs of major items, conducting fire tests are considered to be the most appropriate but conducting full-scale fire tests are expensive. Furthermore the HRRs obtained from the open-air burning experiments may not represent the HRRs in the metro train compartment and the tunnel environment because of radiant heat feedback from the fire and the influence of airflow from the emergency tunnel ventilation system.

1.1 Impetus for the research

It appears that the current methods cannot realistically predict the HRR of a metro train in an underground trainway. A new method/approach that incorporates factors that affect the HRR of a metro train needs to be developed.

This research project attempts to use computational fluid dynamics (CFD) model to simulate fire growth and flame spread within a metro train in an underground trainway. The motivation of the study is to predict the HRR and specifically the peak HRR for emergency tunnel ventilation system design. Cone Calorimeter tests will be conducted for the exposed surface materials in the metro train. Materials' thermo-physical properties will be derived using existing procedures for input into a CFD model.

A CFD model is chosen instead of zone model because of the complexity in the metro train geometry. CFD modelling can be time consuming but it is currently the most state-of-the-art tool used by the fire engineering community. CFD modelling is not new in the transportation industries as it is a common tool used to check on the effectiveness of emergency tunnel ventilation design (using a pre-defined HRR) (Könnecke and Schneider 2004; Sinai 2004).

The CFD model used in this research is Fire Dynamics Simulator (FDS) Version 4 developed by National Institute of Standards and Technology (NIST). FDS is used because it is currently the most advanced and widely used CFD model for fire simulation (VTT 2003) and is available in the public domain. The author recognises that fire growth modelling is still in its infancy. However, extensive studies have been carried out to validate FDS predictions of fire growth and flame spread e.g. Liang (2002); Hietaniemi et al. (2004). FDS has also been successfully used to reconstruct several fire incidents e.g. Madrzykowski, et al. (2002); Vettori et al. (2002); McGrattan and Hamins (2003). The results from those studies are promising. This raises the level of confidence in using FDS to carry out this research. Detailed review of validation work of FDS can be found in McGrattan (2004).

Besides predicting the HRR, this research project also allows us to gain valuable insight and understanding of how fire may grow, spread and develop in a underground trainway which may be useful in planning evacuation and fire fighting procedures and designing fire safety systems for metro systems by eliminating guess work on the fire development.

1.2 Objective of this research

The objectives of this research project are:

a) Identify and incorporate factors that affect fire development of a metro train in an underground trainway into the FDS model.
b) Identify credible fire scenarios for a metro train for simulation.
c) Evaluate the metro train car materials' reaction to fire and derive the materials' thermo-physical properties from Cone Calorimeter test data.
d) Carry out FDS simulation to examine the fire growth and flame spread within a metro train in and underground trainway and to predict the HRR.

1.3 Limitation of this research

In this research, the physical configuration of the metro train, the type of metro train car construction and tunnel geometries are based on the new Circle Line (CCL) under construction in Singapore. This is because the author is familiar with the project as he has been involved in the design stage. The other reasons are because the drawings for the CCL metro train and tunnel are made available and the exposed surface material samples for the CCL metro train are provided by the Land Transport Authority (LTA), Singapore for the study.

No full-scale fire test has been conducted to verify the modelling results. This is due to the cost involved in burning a metro train; and lack of facilities and equipment that are required to conduct the full-scale test. However, HRR estimations based on existing methods are used to compare the modelling results.

Because the material properties derived from Cone Calorimeter test data are used as input into the CFD model, the main assumptions made for the simulations are:

a) The thermal properties such as the thermal conductivity and the specific heat are constant.
b) The heat release rate properties such as the heat of combustion and the heat of vaporisation (gasification) are constant. Time average values are derived from the Cone Calorimeter test data and are used.
c) The burning behaviour of materials in the real fire scenario is the same as the small-scale tests.

1.4 Organisation of this report

This report consists of 12 Chapters. Chapter 2 presents the literature reviewed. Chapter 3 outlines the main assumptions and equations behind FDS to give a brief overview and broad understanding of the concepts behind the fire model. The underlying theory of FDS in predicting fire growth and flame spread will also be described.

Chapter 4 outlines the approach taken in this research. Chapter 5 gives a brief description of the CCL metro train and tunnel. Chapter 6 discusses the possible fire scenarios for the CCL metro train. The credible fire scenarios are identified for FDS simulation. Chapter 7 describes the trial simulations carried out. The trial simulations serve two purposes:

a) Carry out grid sensitivity study to decide on the grid size to be used for the final simulations.
b) Identify any unforeseen issue or problem that may be encountered during the simulations.

Chapter 8 describes the Cone Calorimeter tests. It also describes the procedures to derive the Cone Calorimeter heat release rates and the thermo-physical properties of the materials. The observations during the tests and the results will also be presented. In Chapter 9, FDS predictions of Cone Calorimeter test results will be covered.

Chapter 10 presents the HRR calculations based on the current methods. The estimations serve as baseline for comparison with the final simulation results. Then Chapter 11 describes the final simulations; presents and discusses the final simulation results. And finally, Chapter 12 concludes this report.

2 Literature review

The literature review focuses on metro trains rather than all pubic transport vehicles. However in some Sections, studies from other public transport vehicles are covered because they provide useful information and/ or are considered relevant to this research project.

There are four parts in this Chapter. Part one reports the HRRs based on full-scale tests conducted. It also reports the HRRs during actual train fire incidents as quoted in various literature. Part two reviews and comments on the current methods of estimating the HRR for a metro train; and gives a summary of the peak HRR values adopted by various metro lines for the emergency tunnel ventilation system design. Part three reviews the research programs related to fire safety studies of rail cars and part four reviews the other studies relevant to this research project.

2.1 HRRs of metro trains – From full-scale tests and historical observations

2.1.1 Full-scale tests - EUREKA project (EUREKA 1995; Ingason et al. 1994)

SP-Fire Technology conducted a series of full-scale tests of vehicles (a passenger train car, a bus, a metro train car, a simulated truck load) and two wood crib tests in a tunnel (Ingason et al. 1994). The study was a joint project between nine western European countries with a project name EUREKA EU 499 “Fires in Tunnels” (EUREKA 1995). The tunnel used for the fire tests was a 2.3 km long abandoned copper-mine in north Norway. The main layout of the tunnel is shown in Figure 2.1.

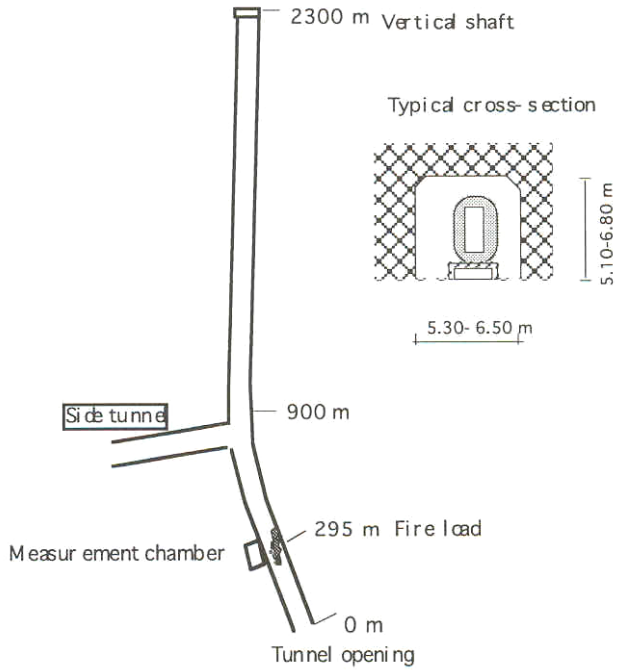

Figure 2.1: Layout and typical cross-section of the tunnel (reproduced from Ingason et al. (1994))

The HRRs for the fire tests were calculated using oxygen consumption technique. Among the six fire tests, only one test (one of the wood crib tests) was carried out with forced ventilation. The difference in peak HRR for the wood cribs tests, with and without forced ventilation, was found to be substantial. The full-scale tests for the passenger train car (Intercity train), the metro train car and the wood cribs tests are discussed below.

Passenger train car (Intercity train)

The passenger train car was 20.6 m long by 2.7 m wide and 3 m high. The number of seats was 80 and the total fire load of the seats was nearly 9000 MJ (note that the type of seat was not stated in the report). The fire load for the train car was calculated to be 77000 MJ. The ignition source was 7.3 litres of isopropanol, corresponding to 200 MJ, which is the fire load of one seat (Richter and Vauquelin 1994). The HRR reached 13.5 MW after 25 minutes with a second peak of 12 MW after 100 minutes. The heat release rate curve is shown in Figure 2.2.

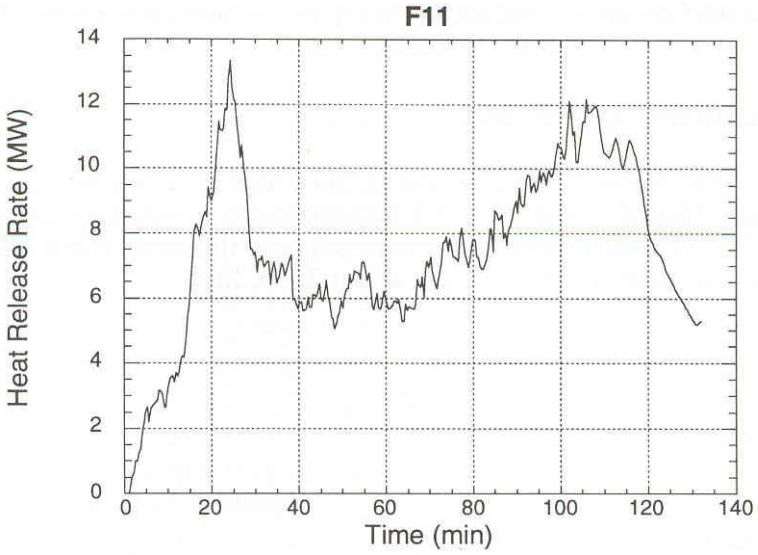

Figure 2.2: HRR curve for a passenger train car (reproduced from Ingason et al. (1994))

From the HRR curve, it can be seen that the passenger train car has not burnt out even after 130 minutes. This might be due to the high fire load content of the passenger train car. A total heat released of 58500 MJ was estimated by integrating the HRR curve from 0 to 130 minutes. This total heat released value was approximately 80% of the total fire load estimated for the passenger train car. However, this total heat released value was likely to be underestimated since the passenger train car was still releasing high amount of energy at 130 minutes.

Metro train car

The metro train car was 18 m long by 2.8 m wide and 3 m high made of aluminium. The number of seats was 40 and they were made of polyurethane foam covered with textiles (note that the type of textiles was not stated in the report). The total fire load of the seats was calculated to be 6000 MJ whereas the total fire load of the metro train car was calculated to be 41300 MJ. Two ignition source sizes were quoted by two independent references. Richter and Vauquelin (1994) quoted 0.77 litres of isopropanol while FIT Workpackage2 (2003) quoted 6.3 kg (≈ 8 litres) isopropanol. It is not clear which quoted ignition source size is correct. In the experiment, the HRR reached 35 MW in about five minutes. The HRR curve for the metro train car is shown in Figure 2.3. A total heat released of 36900 MJ was estimated by integrating the HRR curve from 0 to 117 minutes. This total heat released value was approximately 90% of the total fire load estimated for the metro train car.

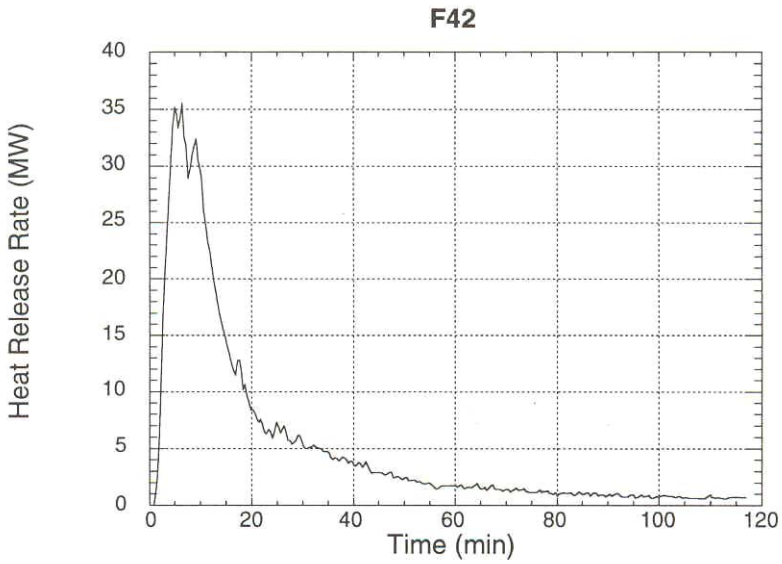

Figure 2.3: HRR curve for a metro train car (reproduced from Ingason et al. (1994))

It was noted that although it was the same experiment, Steinert (1994) reported a peak HRR of only 24 MW for the same test. The difference was due to the method used to evaluate the HRR. Ingason et al. (1994) used the oxygen consumption technique while Steinert (1994) used the enthalpy flows of CO_2 / CO mass flows for the determination of the HRR. Even so, both have assumed that the heat release per unit mass of O_2 consumed is 13100 kJ/kg of O_2 in their calculation.

From Figure 2.2 and Figure 2.3, it can be seen that the peak HRR of the metro car was much higher (almost 3 times) even though its fire load was lower than the passenger train car. This indicated that fire load tells nothing about burning behaviour of materials. The results suggested that for the full-scale tests, the seats used in the metro train car were much easier to burn compared to the seats of passenger train car.

Wood cribs tests

The wood cribs tests consisted of 950 kg wood crib stacks measuring 3.2 m long by 0.8 m wide and 2.4 m high. Two tests were conducted, one with forced ventilation and the other without. For the test with forced ventilation, the average air velocity over the tunnel cross section was 2.9 m/s. The HRR curves for the two tests are shown in Figure 2.4 and Figure 2.5.

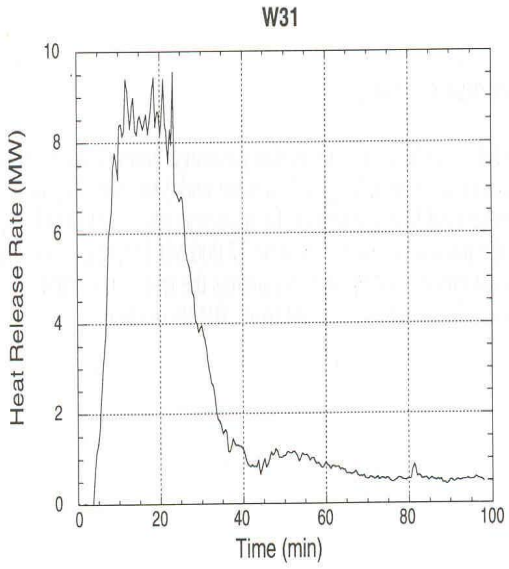

Figure 2.4: HRR curve for wood cribs (without forced ventilation) (reproduced from Ingason et al. (1994))

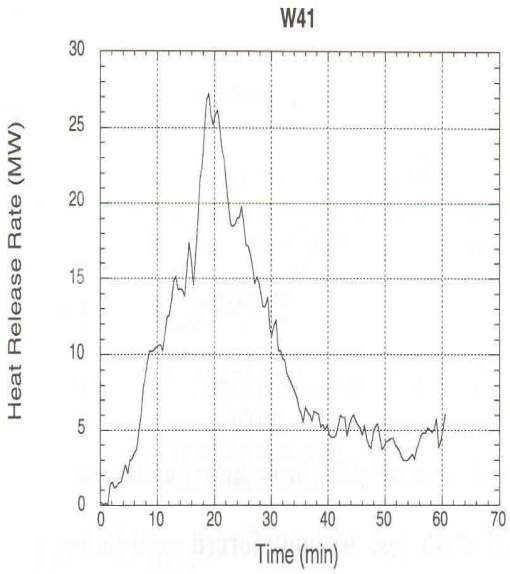

Figure 2.5: HRR curve for wood cribs (with forced ventilation) (reproduced from Ingason et al. (1994))

From the HRR curves for the two wood cribs tests, it can be seen that the peak HRR increased by almost 3 times under the influence of the forced ventilation. How the forced ventilation might affect the HRRs of the passenger train car, metro train car or other vehicles tested however was not discussed in Ingason et al. (1994).

Important findings from EUREKA-project (Haack 1994; Richter 1994)

The following important findings from EUREKA-project as reported in Haack (1994) and Richter (1994) are relevant to this project:

a) Vehicles with roof constructed of steel were able to withstand the heat whereas vehicles with roof constructed of aluminium were completely destroyed at a rather early stage of the fire tests.
b) Maximum temperatures of about 700 to 1000°C were measured for fire tests of rail cars. The metro car with aluminium body resulted in higher temperature compared to the metro car or passenger cars with steel bodies.
c) Modern outfitting in newer rail cars makes them much more resistant to ignition than older vehicles.

2.1.2 Japanese full-scale tests (Hasemi et al. 2004)

It was reported in Hasemi et al. (2004) that based on the full-scale tests of trains compliant with the Japanese regulations, the HRR values of the trains were between 10 to 20 MW. However, the details of the full-scale tests were not covered in the paper.

2.1.3 HRRs – Estimated /calculated based on actual fires

Usually, tunnel fire incidents are thoroughly investigated. The details such as the fire development, extinguishing and rescue work, etc will not be discussed here. However, the causes of the fires and the HRRs estimated /calculated based on information available on the fires as reported in various literature are presented.

Daegu metro train fire, Korea, 18 Feb 2003

The cause of fire was due to arson. The arsonist started fire when he was on a train of Subway Line 1 in Daegu, South Korea, by spreading flammable liquid (reportedly two PET bottles full of petrol) into one of the carriages of a six-car train when it reached Jungangno Station (Anon 2004c). An estimated HRR value of at least 20 MW was reported in Chow (2004) and Park (2004).

Kaprun tunnel fire, Austria, 11 Nov 2000

This was not a metro train fire but a cable-rail fire within a 43° inclined, 3.4km long tunnel. The cause of the fire was due to faulty heater (radiator) in the driver's cab. Peak HRR of between 15 to 50 MW was reported in FIT Workpackage2 (2003). The estimation was based on model scale experiments performed in a tunnel with the same slope.

Baku metro train fire, Azerbaijan, 28 Oct 1995

A fully loaded five-car metro train stopped about 200 m after the Uldus station due to sparkover/ electric arc in the electrical equipment in the rear bogie of the fourth car. A hole was created through the floor of the fourth car (blowtorch effect due to a hole in an air compressor) and the cable fire under the car started to spread upwards through the hole and ignited the seats. The fire spread rapidly to the fifth car. The peak HRR value for the fourth and the fifth cars was estimated to be about 100 MW at around 30 to 45 minutes after the train came to a stop as reported in FIT Workpackage2 (2003). The HRR was estimated based on the time frame of fire development and the size of the tunnel cross-section.

Montreal metro train fires, Canada, 12 Dec 1971 and 23 Jan 1974

On the 12 Dec 1971, a train collided with the end of the tunnel at the Henri Bourassa metro station, followed by a short circuit and a fire which spread to train-sets stationed nearby. An average HRR value of 20.5 MW was reported in Associated Engineers (1980).

On 23 Jan 1974, faulty rubber tyres on a train caused a short circuit south of the Rosemard station, starting a fire and leading to the destruction of nine vehicles and 300 m of cabling. An average HRR value of 26.4 MW was reported in Associated Engineers (1980).

Comments on HRRs estimated /calculated based on actual metro train fires

The quoted HRR values for the Kaprun tunnel cable-rail car fire (15 MW to 50 MW) and the Batu tunnel metro fire (100 MW) were extremely high. If the HRR values for these two fires were estimated based on the size of the tunnel or the slope of tunnel (for the case of the Kaprun tunnel cable-rail fire), it was likely to be over estimated.

The average HRR values were quoted for the two Montreal metro train fires. The peak HRR values were expected to be much higher.

2.2 Current methods of estimating the HRR of a metro train

This Section reviews and comments on the current methods of estimating the HRR of a metro train. A total five methods are presented namely the traditional method, the summation method, the post-flashover model method, the Arup Fire method and the Frankfurt metro fire model.

2.2.1 Traditional method

The traditional method (Dowling and Delichatsios 2000; Dowling and White 2004) of estimating HRR involves taking the complete fire load in MJ and dividing it by an assumed time. This method was first used to estimate the HRR of a metro train in 1975 (Later discussion referred to as Design scenario – 1975). The assumed time is based on observations of two Montreal metro system fires. Since then, the method has gone through a few revisions in order to reflect the observations from other train fires (Later discussion referred to as Design scenario - 1983) and also to account for metro car design and construction advancements especially in terms of materials selection (Later discussion referred to as Design scenario – 1989) (Hettinger and Barnett 1991; Kennedy et al. 1998). The different revisions are discussed below.

Design scenario - 1975

The 1975 fire scenario was developed to reflect the observations of two Montreal metro system fires (January 1974 and December 1971). In both fires, flashover occurred about twenty minutes after the onset of the fire and the average time of combustion of each vehicle was about one hour. A relatively constant heat release rate is estimated for this scenario based on the assumption that the average heat release rate over the duration of the fire is equal to the rate of a single burning car i.e.:

$$\frac{Total\ \ fire\ load\ \ per\ car\ (MJ)}{Time\ (s)} = \frac{Time\ \ fire\ load\ \ per\ car}{3600}\ (MW) \qquad \text{Equation 2.1}$$

This method of estimating the HRR was used for the design of emergency tunnel ventilation system of the original sections of the Atlanta (MARTA) system as well as the Baltimore, Buffalo, Hong Kong and Pittsburgh metro systems (Hettinger and Barnett 1991).

Design scenario - 1983

The first revision to the design fire scenario was made as a result of the observations of the Bay Area Rapid Transit (BART) metro system fire in San Francisco, California, in January 1979 and the Toronto metro system fire in Canada in October 1976. Multiple cars were involved in these fire incidents, with the fire transmitted to the adjacent car approximately twenty minutes after flashover. In each incident, all combustibles above and below the car floor[1] and less than one-half of the floor material were burnt in the first car. The fires were generally limited to the above-floor combustibles in the second and succeeding cars.

In calculating the HRR for this scenario, an initial fire size $\dot{Q}_{\text{int}}$ of 0.7 MW is assumed for the metro cars and lasted for 20 minutes. The HRR for the first involved car $\dot{Q}_1$ is calculated using Equation 2.2 while the HRR for the second and succeeding cars $\dot{Q}_2$ is calculated using Equation 2.3. The peak HRR is then obtained by summing up the heat release rates based on the fire development as shown in Table 2.1.

$$\dot{Q}_1 = \text{Fire heat release rate for first involved car} = \frac{\text{Above floor fire load } (MJ) + \text{Below floor fire load } (MJ) + \frac{1}{2}\,\text{Floor heat load } (MJ) - \dot{Q}_{\text{int}}\ (MW)\ x\ 1200\ (s)}{3600\ (s)} \qquad \text{Equation 2.2}$$

$$\dot{Q}_2 = \text{Fire heat release rate for second and succeeding cars} = \frac{\text{Above floor fire load } (MJ)\ - \dot{Q}_{\text{int}}\ (MW)\ x\ 1200\ (s)}{3600\ (s)} \qquad \text{Equation 2.3}$$

1 The train is divided into above floor, floor and below floor when calculating the HRR using the traditional method. Above floor refers to the car interior equipment and materials, which also includes the floor covering. Floor refers to the structural floor of the train whilst below floor refers to the undercarriage equipment and materials.

Time period (min)	Car no.	HRR of car (MW)	Peak HRR (MW)	Remark
0 – 20	1	$\dot{Q}_{int}$	$\dot{Q}_{int}$	1st car at initial burning phase.
20 – 40	1 2	$\dot{Q}_1$ $\dot{Q}_{int}$	$\dot{Q}_1 + \dot{Q}_{int}$	1st car flashover. 2nd car at initial burning phase.
40 – 60	1 2 3	$\dot{Q}_1$ $\dot{Q}_2$ $\dot{Q}_{int}$	$\dot{Q}_1 + \dot{Q}_2 + \dot{Q}_{int}$	1st continues to burn. 2nd car flashover. 3rd car at initial burning phase.
60 – 80	1 2 3 4	$\dot{Q}_1$ $\dot{Q}_2$ $\dot{Q}_2$ $\dot{Q}_{int}$	$\dot{Q}_1 + \dot{Q}_2 + \dot{Q}_2 + \dot{Q}_{int}$	1st and 2nd cars continue to burn. 3th car flashover. 4th car at initial burning phase.
80 -100	2 3 4 5	$\dot{Q}_2$ $\dot{Q}_2$ $\dot{Q}_2$ $\dot{Q}_{int}$	$\dot{Q}_2 + \dot{Q}_2 + \dot{Q}_2 + \dot{Q}_{int}$	1st car completely burnt out. 2nd and 3rd cars continue to burn. 4th car flashover. 5th car at initial burning phase.

Table 2.1: Fire development based on design scenario - 1983

This scenario was used for the designs of the MOS-1 section of the LA Metro Red Line system as well as the Los Angeles (Blue Line), Philadelphia (SEPTA), and the newer sections of the Atlanta metro system (Hettinger and Barnett 1991).

Design scenario - 1989

The second revision to the design fire scenario was made to incorporate the impact of the recommendations contained in NFPA 130 "Standard for Fixed Guideway Transit Systems" (NFPA 130 2003 edition), originally issued in 1983 by the Fixed Guideway Transit Systems Technical Committee of the National Fire Protection Association (NFPA). NFPA 130 contained guidelines developed by the Urban Mass Transit Administration (UTMA), now Federal Transit Administration (FTA), for test standards which limit flammability and smoke emission characteristics for materials used in construction of transit vehicles. Note that the 2000 and 2003 edition of NFPA 130 addressed fixed guideway transit and passenger rail systems, and changes have been made throughout the document to incorporate passenger rail requirements.

Subsequently, the vehicles for many older metro systems (including BART and Toronto) have been retrofitted and fire-hardened to meet the NFPA 130 requirements. Vehicle seats which previously could be ignited by a newspaper are now fire-resistant to the point that a kerosene-soaked rag will not ignite the seat material. New vehicles are specified to meet (or exceed) the NFPA 130 requirements (Hettinger and Barnett 1991; Kennedy et al. 1998).

The flashover and fire-transmission rates for the design of metro systems whose vehicles met these more stringent design standards were re-evaluated. However, because there were no major fires involving metro vehicles in US since the development of the NFPA 130, the recognised improvements due to the NFPA 130 cannot be directly quantified. Therefore, the revised value for these parameters were assumed to increase from 20 minutes to 30 minutes (Hettinger and Barnett 1991; Kennedy et al. 1998). The design equations are revised as shown in Equations 2.4 and 2.5.

$$\dot{Q}_1 = \text{Fire heat release rate for first involved car} = \frac{\text{Above floor fire load } (MJ) + \text{Below floor fire load } (MJ) + \frac{1}{2}\,\text{Floor heat load } (MJ) - Q_{\text{int}}\ (MW)\,x\,1800\ (s)}{3600\ (s)} \qquad \text{Equation 2.4}$$

$$\dot{Q}_2 = \text{Fire heat release rate for second and succeeding cars} = \frac{\text{Above floor fire load } (MJ)\ - Q_{\text{int}}\ (MW)\,x\,1800\ (s)}{3600\ (s)} \qquad \text{Equation 2.5}$$

For this scenario, up to two cars are considered to be fully involved at any given time due to the thirty minutes fire development (flashover) and fire transmission times. This scenario was used in the design of the Seattle, Shanghai, Taipei (Hettinger and Barnett 1991) and Singapore East West Line (EWL), North South Line (NSL) and North East Line (NEL) metro systems (Lim 2005).

Although the traditional method was usually used to estimate the HRR for the design of emergency tunnel ventilation system, however it has been noted that in some designs, a safety factor of e.g. 2, was included to account for uncertainties (Amtrak 2004).

Circle Line, Singapore

Circle Line (CCL), Singapore is currently under construction. The HRR of the CCL metro train was estimated based on the same methodology as the design fire scenarios –1983 and 1989 for the design of emergency tunnel ventilation system. Although the same methodology is used, there are a few modifications to the assumptions. In the CCL design, the design consultant has conservatively assumed that the fire transmitted to the adjacent car in 10 minutes after flashover (compared to 20 minutes in design scenario - 1983 and 30 minutes in design scenario 1989). The initial fire size Q_{int} of 0.7 MW was also used with a burning period of 30 minutes (same as design fire scenario – 1989).

In their design, they have included a combustion efficiency factor χ of 0.7 (Meinhardt 2002) noting the fact that not all combustibles will be consumed during the fire (Drysdale 1998; Karlsson and Quintiere 2000). The metro car's floor has 45 minutes fire resistance rating (Renie and Prevot 2003). This was also accounted for in the design calculation.

As in design scenario – 1989, up to two cars are considered to be fully involved at any given time. The design equations used for the calculation of HRR are shown below:

$$\dot{Q}_1 = Fire\ heat\ release\ rate\ \ of\ \ below\ \ floor\ combustibles\ \ \ for\ \ first\ involved\ \ car$$
$$= \frac{(Below\ \ floor\ \ fire\ load\ \ (MJ))\chi - Q_{\text{int}}\ (MW)\,x\,1800\ (s)}{3600\ (s)} \qquad \text{Equation 2.6}$$

$$\dot{Q}_2 = Fire\ heat\ release\ rate\ \ for\ \ first\ involved\ \ car$$
$$(Above\ \ floor\ \ fire\ load\ \ (MJ) + Below\ \ floor\ \ fire\ load\ \ (MJ)$$
$$= \frac{+\frac{1}{2}\ Floor\ \ fire\ load\ \ (MJ))\chi - Q_{\text{int}}\ (MW)\,x\,1800\ (s)}{3600\ (s)} \qquad \text{Equation 2.7}$$

$$\dot{Q}_3 = Fire\ heat\ release\ rate\ of\ \ floor\ \&\ above\ \ floor\ combustibles\ \ for\ \ first\ involved\ \ car$$
$$= \frac{(Above\ \ floor\ \ fire\ load\ \ (MJ) + \frac{1}{2}\ Floor\ \ fire\ load\ \ (MJ))\chi - Q_{\text{int}}\ (MW)\,x\,1800\ (s)}{3600\ (s)} \qquad \text{Equation 2.8}$$

Note: Under floor combustibles have completely burnt out.

$$\dot{Q}_4 = Fire\ heat\ release\ rate\ \ for\ \text{sec}ond\ \ and\ \ succeeding\ \ cars$$
$$= \frac{(Above\ \ floor\ \ fire\ load\ \ (MJ))\chi\ - Q_{\text{int}}\ (MW)\,x\,1800\ (s)}{3600\ (s)} \qquad \text{Equation 2.9}$$

Equations 2.6 and 2.8 are newly added to account for the fire resistance rating of the floor. Equations 2.7 and 2.9 are modification of Equations 2.4 and 2.5 respectively to include the combustion efficiency factor χ. A 10 MW fire was estimated for the design of emergency tunnel ventilation system in CCL (Meinhardt 2002).

2.2.2 Summation method

NFPA 130 (2003 edition) Annex D contains a non-mandatory method for determining "hazard load" in MJ/m^3 of train car volume. Based on previous work by Smith (1976), a heat release rate test is utilised to determine a 180-second average heat release and smoke emission. The Ohio State University (OSU) apparatus (ASTM-E-906 2004) is specified for use in an example calculation.

The surface materials are exposed to exposure heat flux levels as shown in Table 2.2 to simulate an initiating fire. The exposure heat flux levels are selected according to the surface materials' orientation and location.

Surface	**Exposure heat flux level (kW/m^2)**
Seat	10
Floor	10
Window	15
Light fixture cover	15
Lower wall	15
Ceiling	35

Table 2.2: Exposure heat flux on surface materials

The 180-second average heat release and smoke emission values are multiplied by the exposed surface area for each material and totalled. Finally, the total values are divided by the volume of the vehicle to obtain "fire and smoke load" for the vehicle per unit volume. A suggested performance criterion of 3 MJ/m^3 is included, as the maximum allowable loading to assure self-propagating fire would not occur with an initiating fire consisting of the equivalent of 0.45 kg of newsprint or 0.23 kg of lighter fluid. This method is used to evaluate the overall material flammability in the metro car. It did not provide a complete description of a fire (Peacock and Braun 1999) nor was it used to estimate the fire size.

In 1997, Duggan (1997) published a method that summed rates of heat release per unit area of exposed surface materials. In this method, the surface materials or components are tested in Cone Calorimeter and the entire HRR curve for each material is used. Higher exposure heat flux levels are proposed so as to reflect the exposure conditions of a real fire. The exposure heat flux levels used are shown in Table 2.3.

Surface	Exposure heat flux (kW/m^2)
Horizontal supine ('Floor-like' orientation) – Floor covering and seat trim base	20 or 25
Vertical ('Wall-like' orientation) – Wall panels, seat trim back and seat shell back	35
Horizontal prone ('Ceiling-like' orientation) – Ceiling panels	50

Table 2.3: Exposure heat fluxes for Cone Calorimeter testing in Duggan (1997) method

The heat release rate per unit area (HRRPUA) curves of these exposed surface materials (determined from Cone Calorimeter tests) are multiplied by their exposed areas in the metro car. The 'HRR curves' of all the exposed surface materials are then summed up. A notional 1.5 MW continuous ignition source is added and taken to represent a severe luggage stack fire. In the example calculation given in Duggan (1997), the result was smoothed using a rolling average of 20 s to merge the peaks which were close together as Duggan is in opinion that the peaks are unlikely to be close together in a real fire. When the data was reviewed against the emergency tunnel ventilation system design capacity, Duggan suggested a notional value be included to account for other miscellaneous surfaces and items within the car. In the example calculation, he used a notional value of 3 MW for these unknown.

Dowling and Delichatsios (2000; 2001) reported that in Hong Kong, the Mass Transit Rail Corporation (MTRC) has included a requirement that the total sum of HRR of all the surface materials in a metro train car shall not exceed 5 MW at any time. In order to obtain this data, all the surface materials must be tested in the Cone Calorimeter. MTRC accepts the calculations based on the method published by Duggan (1997).

Dowling and White (2004) commented on the above method, highlighting that the assumption is at odds with what is known about fire growth in an enclosure. The method may result in a grossly over estimation of HRR because it assumes all surface materials to be involved in the combustion simultaneously. Furthermore the calculation is usually done for one car only, and disregards any contribution from the sub-floor components. They stated that even though the result is expressed in MW, it does not provide any estimation of a likely fire size.

In 2000, Dowling and Delichatsios (2000) published a methodology that attempted to allow for fire spread within a train car. The method is similar to Duggan method except that it assumed that because of the square cylinder shape of a train car, fire could not commence on all surfaces at the same instance. It arbitrarily chooses a rolling ignition that involves 10 % of a train car each minute.

2.2.3 Post-flashover model method

In 1991, Hettinger and Barnett (1991) published a method that used the post-flashover computer model, COMPF2 (Babrauskas 1979) to predict the HRR of a metro train car interior (above floor). The assumption for the model is that fire is ventilation controlled during the post-flashover regime and therefore the burning rate is simply a function of the oxygen available for combustion.

The technique used to predict the ventilation controlled burning rate was to have the COMPF2 model automatically adjusts the burning rate during the simulation so as to produce the maximum temperature in the fire compartment.

Two basic scenarios were modelled. The first scenario assumed that the vehicle's doors remained closed and all of the windows opened. The latter assumption was made because it was expected that the maximum fire temperatures would result in failure of either the window safety glass or the elastomer which hold the window glass. The second scenario was modelled with opened side doors as well as opened windows.

As the original version of COMPF2 could only account for one opening, the source code of COMPF2 was modified so that multiple opening at various elevations could be modelled.

In their study, they reported that the excess oxygen introduced by the emergency tunnel ventilation system would not significantly increase the estimated HRR.

Heat loss from the compartment by conduction was modelled but due to the limitations of the COMPF2 model, fixed thermal properties were used and only one value was used for the door, partition and ceiling even though they were constructed of different materials with different thickness. Because COMPF2 is not able to model more than one burning item, material properties of a generic polycarbonate were used. Polycarbonate was selected because Hettinger and Barnett were in opinion that after vehicle flashover, the fire-resistant plastics would exhibit material properties similar to those of polycarbonate plastics. Combustion efficiency factor χ was included and 'net' heat of combustion was based on weighted average for the combustible materials in the train.

Hettinger and Barnett carried out sensitivity analyses, varying the combustion efficiency factor χ from 0.55 to 0.8, and varying the 'net' heat of combustion from 13.65 to 19.77 MJ/kg. In all cases, the mass of fuel was varied so that the total heat content of the rail car was constant. The calculated HRRs varied from 4 to 15.1 MW depending on the scenario simulated; the combustion efficiency factor and 'net' heat of combustion used. A HRR of 12.9 MW (based on the second scenario, combustion efficiency factor χ of 0.8 and 'net' heat of combustion of 13650 kJ/kg) was recommended in the paper.

As the HRR obtained using COMPF2 only accounted for the combustibles in the train car interior (above floor), the traditional method was used to calculate the HRRs of the floor and below floor combustibles. The HRRs were then added up to give a peak HRR value of 18 MW for the train car. It has been noted that in calculating the HRR for the floor, Hettinger and Barnett assumed 25 % of the floor assembly to be consumed during a fire (compared to 50 % in traditional method). This value was based on observation during factory fire tests of the floor assembly.

Only one car was assumed to be involved in the fire for the above study. Hettinger and Barnett concluded that fire was unlikely to spread to other cars because gas temperature of 540°C (from their study) was not high enough to cause failure of safety glass windows in the train cars downstream of the fire. Furthermore, the car ends had a stainless shell therefore fire would not be able to transmit directly from car to car.

The above method was used for ventilation system upgrade study for the Washington DC (WMATA) system and several other ventilation studies.

The use of COMPF2 to predict the HRR of a metro train was also reported in Kennedy et al. (1998). The approach was the same as Hettinger and Barnett study including the fire load for the train cars. However, the train cars in Kennedy et al. study were assumed to have polycarbonate windows instead of safety glass windows. It was assumed in Kennedy et al. study that the polycarbonate windows would melt and fall out in cars downstream of the fire, resulting in a multi-car fire with succeeding cars being involved every 30 minutes. The peak HRR for the duration of the fire was estimated to be 23.1 MW, with two cars being fully involved at any one time.

2.2.4 Arup Fire method

Arup Fire developed a fire dynamics model to predict the HRRs of an older type train car and a modern train car (used in St Paul's City Thameslink, London) based on a scenario where the train car was approaching flashover when it entered the underground station (Arup 2004). The model used results from Furniture Calorimeter tests specified for upholstered car seats and lining materials. The older type train car had upholstered seats and combustible linings and a HRR value of 16 MW was computed (Arup 2004). The modern train car had retardant upholstered seats and a HRR value of 7 MW was estimated (Barber et al. 1994).

The techniques developed for the model were later used to assess the rail cars in Thailand. No Furniture Calorimeter test was conducted. The HRR data of major items was mostly obtained from SFPE Handbook (SFPE 2002). Peak HRR values of 16.3 MW and 14 MW were reported for a sleeper car and a wooden seat car respectively (Barber et al. 1994).

2.2.5 Frankfurt metro fire model

According to research work done by Wilk (2002), a HRR value of 5.6 MW 30 minutes after the start of the fire was computed for the underground metro train car (U-Bahn) used in city of Frankfurt. The HRR was derived by performing a series of fire tests and detailed combustion analysis for the train car (Könnecke and Schneider 2004). The ignition source was assumed to be a baby carriage (buggy) loaded with shopping goods inside the motor coach (train car) caused by arson (Mauser 2005) and the fire spreads successively to the benches (seat), doors, enclosure (wall) lining materials and the driver’s cab. A delay time before ignition was estimated for each component depending on their location in train car and the HRRs totalled to obtain the peak HRR.

2.2.6 Comments on the current methods

Traditional method

a) In the traditional method, the fire load of the combustible materials in the train is the key parameter used to estimate the HRR but fire load tells nothing above the burning behaviour of the materials. The EUREKA-project full-scale tests for the passenger train car and metro train cars illustrated this point. Therefore this method is unable to distinguish whether the materials have good fire performance.
b) The burning duration, the fire development (flashover) time and the fire transmission time are approximated based on historical observations of metro train fires. But not all the trains and tunnels are identical. The quantity and burning behaviour of materials; the geometries of the train and tunnel; and the ventilation will have major influence on the fire development and burning duration.
c) Nevertheless, this method does have an advantage, as it seems to be able to 'account' for all the combustibles in the train car.

Summation method

a) NFPA Standard 130 "hazard load analysis" and Duggan method of estimating the HRR assumes that every part of every material ignites and burns simultaneously. In reality, different propensities for ignition, flame spread, and heat release make both the hazard load analysis and the HRR estimation highly conservative.
b) Although Duggan method of estimating the HRR may be an improvement of the traditional method because it accounts for the burning behaviour of the materials inside the train car, improvements are needed to ensure the estimation is realistic.
c) The calculation is done for one car only, and ignores any contribution from the sub-floor components. Furthermore, the geometries of the train car and tunnel; and ventilation are not considered. All these will be dealt with in this research project.

Post-flashover model method

a) In the paper, the authors reported that the excess oxygen introduced by the emergency tunnel ventilation system would not significantly increase the estimated HRR. This might be because the effect of the emergency tunnel ventilation was evaluated along the length of the train car exterior (with the side windows and side doors opened). If there is scenario where the emergency tunnel ventilation airflow is able to flow directly into the train car compartment, this might not be the case.

b) COMPF2 is only able to account for burning within a compartment. Burning outside the compartment is not accounted for. The HRR may be under-predicted because of this reason.

c) For a ventilation-controlled fire, the HRR can be calculated using Equation 2.10 (Drysdale 1998). $\frac{\Delta H_{c,eff}}{r}$ in Equation 2.10 gives the energy released per unit mass of air (kJ/kg of air). In the study, the stoichiometric air/fuel ratio r was calculated based on a generic material (polycarbonate) but the 'net' heat of combustible based on weighted average for the combustible materials in the train was used. This has resulted in relatively low energy released per unit mass of air (1039 to 1505 kW/kg of air compared to 3050 kW/kg of air given in most literature such as Drysdale (1998); Karlsson and Quintiere (2000) and Tewarson (2002)) during the combustion process. After flashover, if the fire-resistant plastics exhibit material properties similar to those of generic polycarbonate plastic as suggested by the authors, the HRR may be under-predicted because a generic polycarbonate plastic has an effective heat of combustion of about 30000 kJ/kg (SFPE 2002).

$$\dot{Q} = \dot{m}_a \frac{\Delta H_{c,eff}}{r} \qquad \text{Ventilation Controlled Fire} \qquad \text{Equation 2.10}$$

d) The burning behaviour of the actual materials in the train car used was not considered even though material properties of polycarbonate were used.

Arup Fire method and Frankfurt metro fire model

a) The ARUP Fire method and the Frankfurt metro fire model of estimating the HRR for a metro train are almost identical. The HRRs of major items such as seat and lining materials are first obtained. Ignition of second and succeeding items are then estimated by analysis. Among the methods used to determine the HRRs of major items, conducting fire tests are considered to be the most appropriate but conducting full-scale fire tests are expensive. Furthermore the HRRs obtained from the open-air burning experiments may not represent the HRRs in the metro train compartment and the tunnel environment because of radiant heat feedback from the fire and the influence of airflow from the emergency tunnel ventilation system.
b) It also seems that the calculation is done for one car only, and ignores any contribution from the sub-floor components.

2.2.7 Peak HRR values adopted by various metro lines

Different peak HRR values were being used for the design of emergency tunnel ventilation system. The peak HRR values ranged from 5 MW to 31.1 MW, depending on the method used to derive the HRR. The peak HRR values adopted by some metro lines are shown in Table 2.4.

Country	Metro Line	Peak HRR (MW)	Reference
Singapore	North South Line (NSL)	24 MW	(Chua 2003)
Singapore	East West Line (EWL)	24 MW	(Chua 2003)
Singapore	North East Line (NEL)	15 MW	(Chua 2003)
Singapore	Circle Line (CCL)	10 MW	(Chua 2003)
Australia	New South Link	10 MW	(Chua 2003)
Hong Kong	Lantau Airport Line (LAL)	5 MW	(Chua 2003)
Hong Kong	Airport Express Line (AEL)	10 MW	(Chua 2003)
Thailand,	Chaloem Ratchamongkhon MRT line, Bangkok	7 MW	(Drake and Meeks 2000; Yau et al. 2002)
Greece	Athens metro	10 MW	(Castro et al. 1997)
UK	St Paul's City Thameslink, London	16 MW	(Arup 2004)
USA	Mount Lebanon Tunnel light rail transit, Pittsburgh, PA	13.2 MW	(Kennedy and Patel 1988)
USA	Amtrak New York City Tunnels	31.1 MW	(Amtrak 2004)
USA	Ventilation system upgrade study for Washington DC (WMATA) system	18 MW	(Hettinger and Barnett 1991)
USA	Ventilation system upgrade study for Washington DC (WMATA) system	23.1 MW	(Kennedy et al. 1998)

Table 2.4: Peak HRR values adopted by some metro lines

2.3 Fire safety studies of rail cars

This Section reviews the work done on fire safety studies of rail cars. All the studies reviewed focused on assessing the potential fire hazard of interior materials used in rail cars except one which was conducted to assess the HRR of a rail car.

Although some of the fire safety studies were not specifically for metro train cars, they provided useful information such as size of ignition sources, fire scenarios, etc. Most importantly some of the studies supported the approach and methodology taken in this research project.

2.3.1 A Fire Hazard Evaluation of the Interior of WMATA Metrorail Cars (Braun 1975)

In 1975, under a contract with the Washington Metropolitan Area Transit Authority (WMATA), the National Bureau of Standards (NBS), now NIST, conducted a series of fire tests to assess potential fire and smoke hazards represented by various materials that were being incorporated in the new metro cars. The study was conducted in three parts:

a) Small-scale laboratory tests were performed on materials from the various components used on the interior of the new metro car.
b) For economic reason, a non-destructive test using smoke bomb was conducted to ascertain the likelihood of fire or smoke from an ignition below the floor system to penetrate to the car interior through the floor.
c) Seven fire tests were conducted on a mock-up car interior in order to determine the overall effects of an assembled system as compared to the fire performance characteristics of the individual components

The criteria used to evaluate the full-scale tests were: a) there shall be no significant spread of fire from the seat of ignition; and b) the smoke level shall be such as to allow egress in a reasonable time from a burning car.

The tests were conducted using one of the following ignition sources:

a) A paper trash bag containing one full sheet of newspaper – 0.03 kg
b) 0.45 kg of loosely stacked newspaper
c) 0.91 kg of loosely stacked newspaper equivalent of a 'Sunday newspaper'

The fire was at one of the following locations:

a) On the floor – in the aisle
b) On the floor - beneath the seat
c) On a seat

Main conclusions and recommendations from the study were:

a) The floor was unlikely to allow rapid penetration of fire and smoke from a fire beneath the car.
b) The carpet and the ceiling did not contribute significantly to the initial fire hazards
c) While the small-scale test results indicated that the car interior materials might not be readily ignited by very small ignition sources, the full-scale results showed that the materials failed to perform in their end-use configuration as would have been predicted.
d) The nylon-covered polyurethane seat cushions and PVC acrylic wall linings were potential sources of hazard since fire spread did occur beyond the area of origin. These components were recommended to be replaced or upgraded.

2.3.2 Fire Hazard Evaluation of BART Vehicles (Braun 1978)

In 1978, at the request of the UMTA, the NBS conducted a limited fire hazard analysis of the metro cars used on the Bay Area Rapid Transit (BART) metro system in San Francisco, California. The purpose of the study was to ascertain if any aspect of the design details or the material specifications relating to the metro car could result in an environment that had a high probability for developing into hazardous fire situation.

A survey of fire and smoke incidents on metro cars of the BART metro system from March 1975 to Nov 1976 revealed that majority of the incidents were found to start below the floor due to subsystem failures such as brake failure. The importance of fire penetration resistance of the floor assembly was highlighted. By comparing the floor assembly with earlier tests (see Section 2.3.1), the report recommended that the floor assembly to be hardened.

Except for electrical fires, the report considered three probable locations for an interior ignition source. They were:

a) On the floor – in the aisle
b) On the floor – beneath the seat
c) On a seat

The likelihood of occurrence of the ignition source located in the aisle to result in flame spread was concluded to be low as it would require an 'inordinately large amount' of fuel (unfortunately, "inordinately large amount' was not defined). This scenario was not considered further. For the two other ignition locations, flame spread was postulated. The report recommended the nylon/vinyl-covered polyurethane seats to be replaced as they represented a significant hazard based on earlier tests (see Section 2.3.1). The report also recommended using an intumescent coating on the wall and ceiling liner to improve fire protection and installation of fire detection system to indicate the presence of a fire on board a train.

It has been noted that the study relied on limited test results from fire tests conducted by BART for the fire hazard analysis. No fire test was conducted in the study itself. From the report, it also has been noted that the test methods specified by the Operator were no longer in use in the current guideline/standard (FRA requirement/ NFPA 130).

2.3.3 Fire Test of Amtrak Passenger Rail Vehicle Interiors (Peacock and Braun 1984)

In 1984, under the funding by the Federal Railroad Administration (FRA), the NBS conducted a series of fire test to assess the burning behaviour of the interior of passenger rail vehicles. Three types of fire tests were performed:

a) Small-scale laboratory tests to study the flammability and smoke generation characteristics of individual materials.
b) Full-scale calorimeter tests on seats to determine the rate of heat release from burning seat assemblies.
c) Full-scale tests on mock-up of the interior of cars to investigate the potential for fire hazard in a fully furnished vehicle.

The materials used in the tests were typical materials from the Amtrak fleet of 1984.The small-scale tests, included in the study, were used to evaluate ignition, flame spread, smoke emission and rate of heat release of individual materials. The results were compared to the results from the full-scale tests. In the full-scale calorimeter tests of seats, full size upholstered specimens of seat cushions and seat backs were tested to measure the rate of heat release. The seats were mounted on incombustible seat frames, which were similar to the seat frames used in the Amtrak fleet. Four seats were tested in the furniture calorimeter. The upholstery of the different seats was made of polyurethane, fire resistant polychloroprene, fire resistant polyurethane and low smoke polychloroprene. Ignition of the seats was accomplished with an ignition source consisting of 50 sheets of newspaper weighing approximately 1.06 kg. The maximum heat release rate of the burning seats ranged from 30 kW for the fire resistant polyurethane seat to 139 kW for the polyurethane seat (see Figure 2.6).

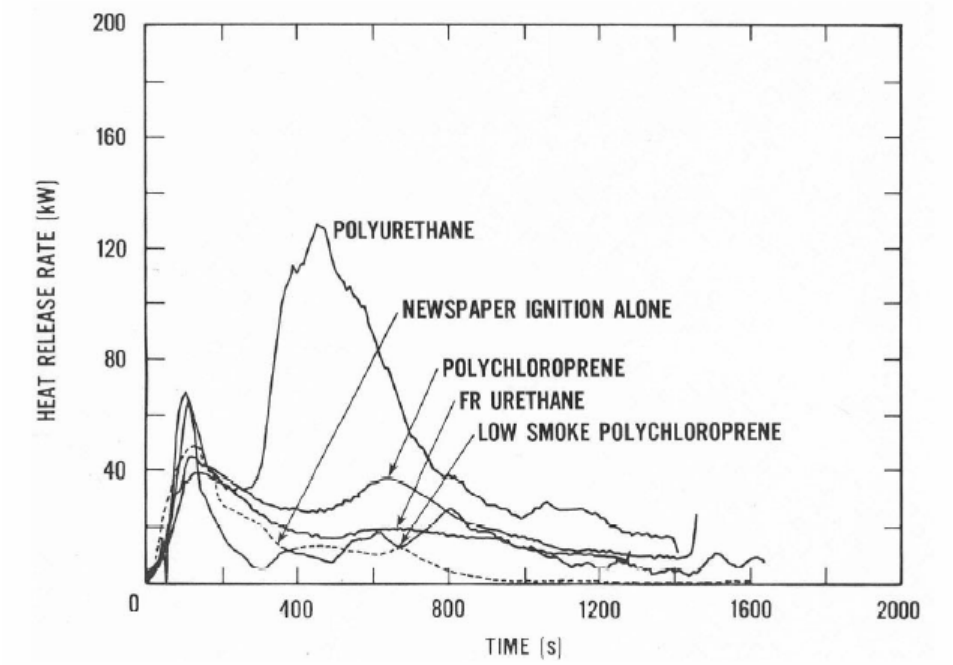

Figure 2.6: HRR curves for the experiments with seats in the Furniture Calorimeter (reproduced from Peacock and Braun (1984))

A total of eight full-scale mock-up tests were performed in the study. The enclosure (see Figure 2.7) used in the tests was made of steel studding with a covering of perforated steel sheets on the walls and the ceiling. The size of the enclosure was 2.4 m wide by 3.6 m long by 2.4 m high which was identical to an ISO 9705 room.

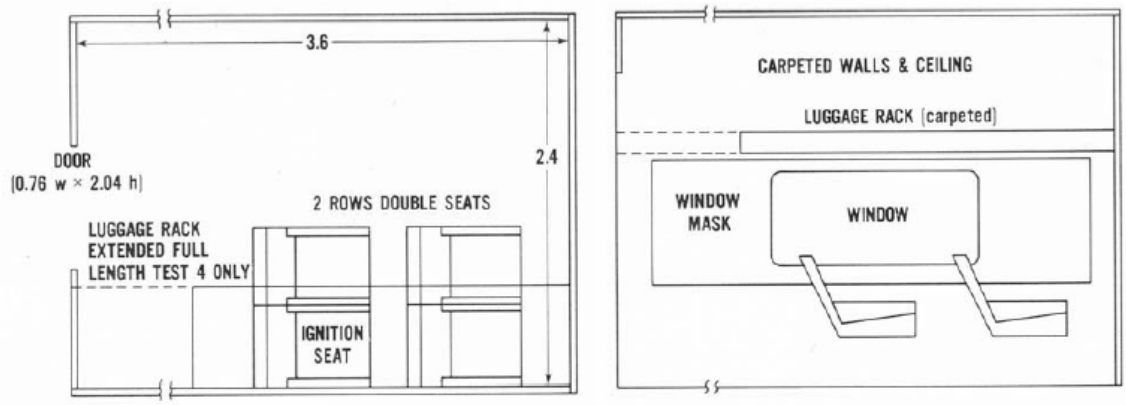

Figure 2.7: The full-scale mock-up (reproduced from Peacock and Braun (1984))

The wall and ceiling carpeting were glued directly onto the perforated steel sheets. A luggage rack, lined with carpeting materials, extended to the rear of the second seat assembly in three of the tests (tests 1 to 3) and the entire length of the compartment in five tests (tests 4 to 8). In four of the tests (tests 1 to 4), the seats were mounted in the enclosure and in the remaining four tests (tests 5 to 8), only the incombustible seat

assemblies (steel seat frame and calcium silicate board supported the newspaper for ignition) were installed. The window glazing and the window masks were installed close to the seat assemblies. The only opening to the enclosure was the 0.76 m wide and 2.04 m high doorway. In the eight mock-up tests different combinations of materials were used to simulate present as well as possible future interior material configurations.

The ignition source used was 50 sheets of newspaper (100 sheets of newspaper for tests 6 and 8) placed on the rear seat closest to the window. During the tests, measurements of temperature, heat flux, gas velocity, gas concentration, smoke density and rate of heat release were made. The maximum heat release rate varied from 40 to 4400 kW in the experiments as shown in Figure 2.8.

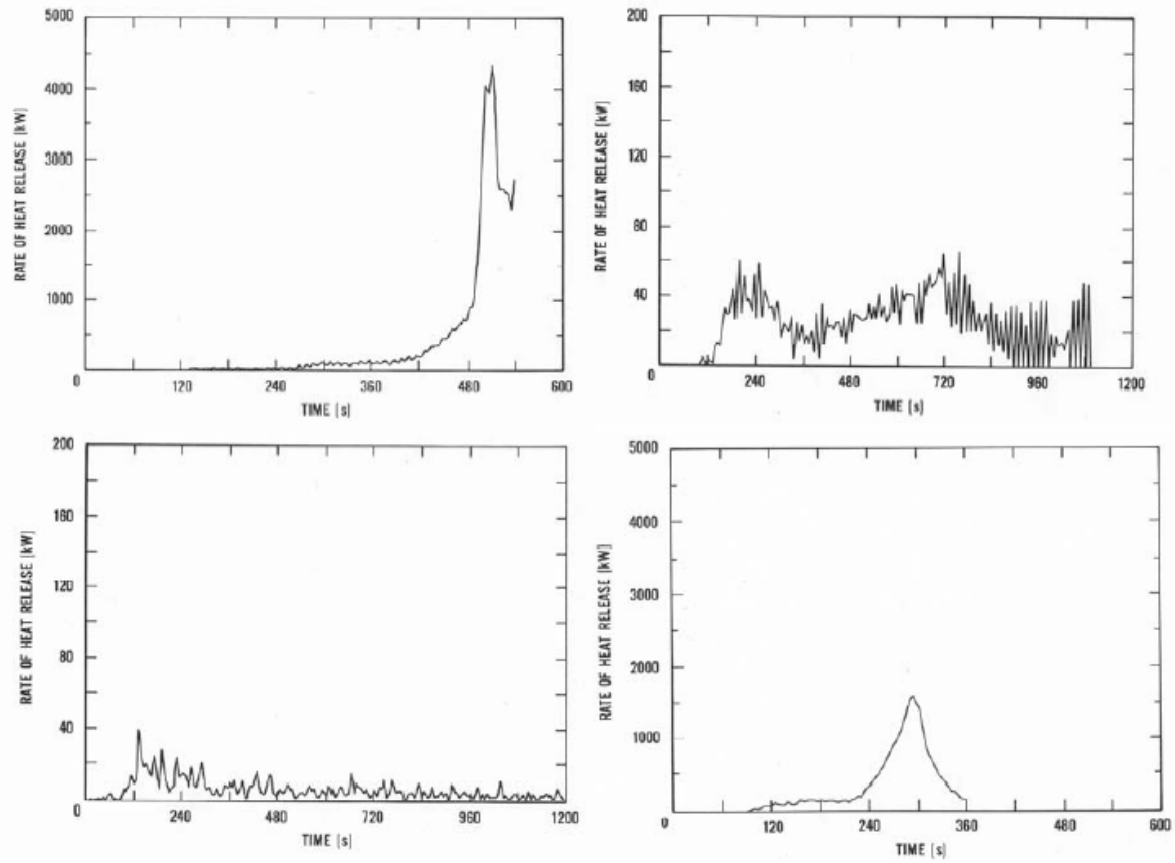

Figure 2.8: HRR curves for the full-scale tests (test 1 upper left, test 2 upper right, test 3 lower left and test 4 lower right) (reproduced from Peacock and Braun (1984))

The four fully furnished full-scale mock-up tests (tests 1 to 4), i.e. the tests where combustible seating arrangements were used, could be divided into two categories. The two categories were those tests in which full room involvement was obtained (tests 1 and 4) and those tests in which few, if any, hazardous conditions were observed (tests 2 and 3). In test 1 and 4, the initial fire in the seats caused the carpeting beneath the luggage rack to ignite, which lead to a serious fire. The lower HRR from the seats as well as the shortened luggage rack in tests 2 and 3 prevented the carpeting from being ignited, which in turn, prevented a severe fire. Thus, it was concluded that an ignition source that provided enough heat for a sufficient period of time to ignite the carpeting material beneath the luggage rack was likely to cause a severe fire.

Another conclusion drawn from the study was that the small-scale tests on individual materials could be used to predict trends in a full-scale fire performance for a given full-scale geometry. However, when the geometry of the full-scale test room was changed, the chosen small-scale tests failed to reflect the effects of these changes. In the light of this conclusion a vehicle interior evaluation protocol was suggested. According to the protocol a small number full-scale tests should be performed to determine a set of acceptable materials for the given geometry of the evaluated vehicle. This could be followed by a series of small-scale tests to evaluate alternative materials. Materials, which are equal or better than the materials tested in the full-scale tests, can then be substituted without further full-scale testing.

One of the specific recommendations made in the study based on the results of the performed tests was that particular attention should be paid to ensure that the materials used as wall coverings adjacent to seating would resist ignition and subsequent spread of fire.

2.3.4 Fire Safety of Passenger Trains (Peacock et al. 2004; Peacock and Braun 1999; Peacock et al. 1998; Peacock et al. 2002; Peacock et al. 1995)

In a paper presented by a group of researchers from NIST (Peacock et al. 1995), they concluded that an alternative approach that used HRR-based test methods, incorporated with fire modelling and fire hazard analysis, to assess potential hazards under real fire conditions could provide a more credible and cost-effective means to predict the fire performance of passenger train materials. They quoted that studies by Barnett (1992); Cappuccio (1992); ERRI (1992a); ERRI (1992b); Parker (1994); Smith (1983) on transit system analysis; Schirmer Engineering Corporation (1990) on Amtrak stations, tunnels, and train cars; and Burdett et al. (1989) on King's Cross subway station, all supported this new direction for passenger train fire safety.

As the current FRA-cited test methods and performance criteria only provide a relative ranking of materials under the specified exposure conditions, quantitative data which can be used for the fire modelling and hazard analysis are not available (note that the test methods and performance criteria contained in the FRA fire safety guidelines and the NFPA 130 are almost similar as they were adapted from guidelines developed by the UMTA (also see Section 2.2.1). NFPA 130 and FRA test methods and performance criteria are summarised in Appendix A of this report for comparison and reference.).

To assess the feasibility and to demonstrate the practicality and effectiveness of HRR-based test methods and fire hazard analysis techniques, a comprehensive three-phase passenger train fire safety research program was developed by Volpe Transportation Systems Center (Volpe Center) and conducted by NIST under the sponsorship of the FRA Office of Research and Development (R&D). The results from the research program are intended to provide:

a) The FRA with addition information so that appropriate fire safety performance requirements can be developed for inclusion in the proposed passenger equipment rule.

b) Rail car builders and passenger train system operators with increased flexibility to permit incorporation of innovative materials and designs in future passenger rail cars.

Phase I of the research focused on the evaluation of passenger train interior materials using the Cone Calorimeter test method which provided the quantitative data for the fire modelling. The Cone Calorimeter test data was compared with data from FRA-cited small-scale test methods to determine relative material fire performance. In Phase II, large-scale tests were conducted with selected interior material component assemblies using Furniture Calorimeter. The data from the Cone Calorimeter (smoke data) and Furniture Calorimeter (HRR data) tests was used as input into fire model as part of the fire hazard analysis. The impact of car geometry, detection and suppression systems, and egress time on the safety of passengers and crew for representative intercity passengers coach, dining, and sleeping railcar designs were also evaluated. Phase III involved real-scale testing of a full size rail car. The real-scale test results were compared with the small and large-scale tests results conducted in the first two phases of the research and were used to verify the use of the fire hazard analysis based on the computer model.

Phase I (Peacock and Braun 1999)

Extensive survey of the U.S passenger train and other transportation vehicles fire safety requirements, European passenger train fire safety requirements (French, German, British, and the International Union of Railways (UIC)) were covered in Chapter 2 of the Phase I report. The survey of the U.S passenger train and other transportation vehicles fire safety requirements revealed that there was considerable overlap in the existing U.S. transportation approach to fire safety. It has been noted that the Federal Aviation Administration (FAA) and U.S. Coast Guard (USCG) have both accepted the use of HRR as a means to evaluate material fire performance for aircraft and marine vessels.

The survey also concluded that the existing European approaches to passenger train fire safety were generally similar to U.S approach. All of them relied on small-scale test methods to evaluate individual material fire performance with key objectives of prevent fire, retard its growth and spread, and provide adequate evacuation time for passenger and crew. Although the current small-scale test methods are useful as a screening tool to select materials, they are unable to account for interactions between materials and for different end-use geometries which is a major concern. It was reported that this has led to several European country efforts and coordinated European Railway Research Institute (ERRI) and Commission for European Standardisation (CEN) activities to develop assessment tools for fire hazard evaluation based on a combination of Cone Calorimeter, Furniture Calorimeter, real-scale testing, and computer modelling of passenger train interior assembly fires.

The cited European research programs and brief reviews of the programs in Peacock and Braun (1999) are partially reproduced below (points a to e) as they contained information relevant to this project:

a) The British Rail (BR) small-scale (Cone-Calorimeter) test program which was targeted at developing a database of HRR data for all rails materials in current use (Young 1995). Real-scale assembly tests in a Furniture Calorimeter were also conducted as part of the ERRI research effort. BR has also conducted several real-scale test burns of existing coaches and sleeping cars on open trackways.
b) The London Underground Limited (LUL) worked on testing of materials using Cone Calorimeter. In the test, LUL selected an exposure of 50 kW/m^2 for 20 minutes as a suitable exposure for material evaluation consistent with testing exposures and fire experiences in the United Kingdom (Young 1995).
c) Study by SP-Fire Technology on seat flammability in buses and rail transit trains using small-scale and real-scale tests. In the small-scale tests, the Cone Calorimeter was selected to provide ignition and heat release rate data. In real-scale tests, the maximum heat release rate of a seat assembly, about 200 kW, was not sufficient to ignite the panels or the ceiling ‘fast enough’. Ignition of adjacent seats was noted in the real-scale mock-up tests (Göransson and Lundqvist 1990).

d) The EUREKA project (also see Section 2.1.1) whereby the following major conclusions were made (EUREKA 1995):
   - Large amounts of smoke and hot gases produced can quickly fill the entire tunnel reducing visibility to less than 1m.
   - In major incidents, flashover occurred after 7 to 10 minutes and total burning duration lasted from 30 minutes to several hours.

e) Research by ERRI where they considered the use of the Cone Calorimeter to be the only small-scale apparatus suitable for providing useful data for computer modelling (ERRI 1992a). In a test application, ERRI used the HAZARD I fire model (Peacock et al. 1991) to simulate a fire in the British 3 m test cube and concluded that the use of the model to simulate fires in a railway vehicle was feasible (ERRI 1992b). ERRI has conducted Cone Calorimeter and Furniture Calorimeter to provide input data for fire and hazard modelling of passenger coaches (ERRI 1994; ERRI 1995).

In NIST's Phase I study, a total of 30 materials classified into five board categories were selected for the Cone Calorimeter tests. They were:

a) Seat and mattress assemblies
b) Wall and window surfaces
c) Curtains, drapes and fabrics
d) Floor covering
e) Miscellaneous components.

Although the materials were from Amtrak rail car, they represented a range of those typically used in US passenger trains.

An exposure level of 50 kW/m^2 was chosen as a suitable exposure for material evaluation consistent with exposure level in the existing FRA-cited test methods and exposure levels in actual fires.

The Cone Calorimeter test data was compared with data from FRA-cited small-scale test methods to determine relative material fire performance. For majority of the materials, the Cone Calorimeter results provide a good correlation with the FRA-cited test results. However, some materials which had low flame spread index I_s (calculated from ASTM E 162 or ASTM D 3675 test data) had higher HRR values in the Cone Calorimeter tests. The results suggested that although these materials had low flame spread index I_s, they might contribute to fire development by releasing high amount of heat when ignited.

Phase II (Peacock et al. 2002)

The Phase II study includes conducting large-scale tests of selected interior material component assemblies using Furniture Calorimeter. The data from the Cone Calorimeter and Furniture Calorimeter tests was used as input into the CFAST zone model of the fire model HAZARD I developed by NIST. The egress time was calculated using egress model from HAZARD I, airEXODUS^{TM} (Galea et al. 2001) and network model developed by Hagiwara. The latter two egress models were used so that relative comparison could be made since egress model from HAZARD I is only appropriate for residential occupancies. The available safe egress time (ASET) was then compared with the required safe egress time (RSET) as part of the fire hazard analysis (note that the fire analysed were only examples demonstrating the use of fire hazard analysis techniques and did not represent an evaluation of any particular existing car configuration or actual hazard as highlighted in the report). Three types of rail passenger cars were evaluated: typical single level coach, bi-level dining and bi-level sleeping cars.

In considering the fire scenarios, both interior fire and exterior fire were evaluated. Besides electrical-related interior fires, the report also identified several locations of interior ignition source in a passenger train which include:

a) On the floor;
b) On the floor - beneath a seat, mattress, or table;
c) On a seat, mattress, or table;
d) In a trash container; or
e) On a luggage rack.

For exterior fire, it was reported that hot wheels caused by problems with brakes or bearings were the source of most exterior fire using conventional rail. Exterior fire sources for metro systems were also mentioned in the report, which included third rail power, propulsion, and braking systems. It was highlighted that consideration must be given to the probable results of sub-floor ignition because detection could come late in the fire development and suppression could be difficult.

However, modelling of the exterior fire impact upon rail car passengers and train crew is beyond the capabilities of computer models or other computational methods. Therefore, the focus of the fire scenario development for the Phase II study was only on interior fire scenarios.

The following fire scenarios were identified:

a) An ignition under a coach seat by a small source (crumpled newspaper)
b) Fire in a trash bag on a coach seat or in a sleeping compartment
c) Overheated equipment (motor, pump, battery failure) in a sleeping car; and
d) A 'Sterno' can igniting a tablecloth in a dining or lounge car.

The scenarios identified were consistent with past passenger fires and those described in the ASTM rail assessment guide (ASTM E 2061 2000).

Ignition sources used for the large-scale tests are shown in Table 2.5. They were selected to represent a range of initial fire conditions that might occur in a passenger train (in line with the ignition sources in the fire scenarios identified).

S/no	Ignition Source	Remark
1	TB 133 burner (Ohlemiller and Villa 1992)	- At 17 kW for 80 s - Used for flammability of commercial seating furniture. - Simulate ignition of several sheets of crumpled newspaper - Burner located 0.025 m above seat cushion and 0.05 m from back cushion.
2	Gas sand burner	- At 25 kW or 50 kW throughout the experiment - 0.17 square burner
3	Round gas burner	- At 280 kW at the start of the test and was increased to 400 kW approximately 300 s into the test - 0.27 m diameter burner
4	Trash bag filled with newspaper, 2.7 kg	- Simulate the burning characteristics of actual Amtrak train trash bags - Represent a severe ignition source that may be present on the train - Peak HRR for the trash bags averaged 203 ± 35 kW including the 25 kW sand bag burner used to ignite the bags. Average HRR over the entire duration of burning was 77 ± 24 kW

Table 2.5: Ignition sources used for the large-scale tests

A total of twenty-nine large-scale tests of selected interior material component assemblies using Furniture Calorimeter were conducted as shown in Table 2.6.

Test no	Assemblies tested in Furniture Calorimeter	Ignition source
1-7	Trash bag from Amtrak train (of different weight)	Gas sand burner at 25 kW
8-10	Trash bag filled with newspaper, 2.7 kg	Gas sand burner at 25 kW
11-14	Coach seat assembly	TB 133 burner, Round gas burner at 280 and 400 kW, Trash bag filled with newspaper, 2.7 kg
15-16	Lower bed with bedding and pillow	Trash bag filled with newspaper, 2.7 kg
17	Upper & Lower beds with bedding, pillow, and window drapes	Trash bag filled with newspaper, 2.7 kg
18,19	Wall carpet on wall	Gas sand burner at 50 kW
20,21	Wall carpet on wall and ceiling	Gas sand burner at 50 kW
22-24	Window drape	Gas sand burner at 25 kW
25-27	Privacy curtain	Gas sand burner at 25 kW
28	Window with gaskets, frame, and mask	Gas sand burner at 50 kW
29	Window with gaskets, frame, mask, and drapes	Trash bag filled with newspaper, 2.7 kg

Table 2.6: Large-scale tests of selected interior material component assemblies using Furniture Calorimeter

Main conclusions from the large-scale tests were:

a) Trash bags were considered to be a credible large ignition source that could lead to fire growth and spread. The HRR values of actual trash bags from an Amtrak overnight train ranged from 53 to 284 kW. For the trash bag filled with newspaper which was used as the ignition source for many of the assembly tests, had a peak HRR of 203 ± 35 kW.
b) Component materials that comply with the current FRA fire safety criteria were difficult to ignite. The Phase II report stated that it would require ignition source strength of 2 to 10 times those used for similar materials and products found outside of the rail transportation environment.
c) However, if severe ignition existed, some of the materials e.g. wall carpeting and window glazing, which were difficult to ignite, would produce high HRR values once ignited and would contribute to the fire growth.

Phase III (Peacock et al. 2004)

Seventeen real-scale assembly tests were conducted within an Amtrak passenger rail coach car. Among the seventeen tests, five were fire growth and spread tests conducted to evaluate the representative hazard of existing passenger rail car component material configuration. The five fire growth and spread tests are shown in Table 2.7.

Test no	Test type	Ignition source
13	Window drape	Gas sand burner (at 25 kW) on lower edge
14	Corner test	Trash bag filled with newspaper, 2.7 kg, in corner next to wall carpet and FRP panel
15	Seating area	Gas sand burner at 25 kW below seat
16		TB 133 burner (at 17 kW for 80 s) on seat
17		Trash bag filled with newspaper, 2.7 kg, on seat

Table 2.7: Five fire growth and spread tests

Most of the tests were terminated when there was significant flame spread. This was to prevent extensive damage to the car so that additional tests can be conducted.

For the five flame spread and growth tests, significant flame spread was observed for tests using trash bag as ignition source. This was consistent with the conclusions from the Phase II report.

One of the objectives of the Phase III study was to compare the real-scale test results with the small and large-scale tests results conducted in the first two phases of the research. It has been found that the small-scale Cone Calorimeter test results, full–scale components material assembly tests and real-scale tests all showed similar ranking of materials from low HRR to high HRR. It is also worthwhile to mention that the report recognized that in practice, a major advantage of HRR data from a device like the Cone Calorimeter has the ability to use these data in appropriate model to predict full-scale performance which coincides with the approach taken in this research project.

2.3.5 FIRESTARR (Briggs et al. 2001a; Briggs et al. 2001b; Tallec et al. 2001)

FIRESTARR is a European joint project established to assist the work of European standardisation committees CEN/CENELEC in drafting a Part 2 (Requirements for the fire behaviour of materials and components) for a 7-part European Standard prEN45545 “Fire protection on railway vehicles”. The aim of the new standard is to protect passengers and staff from danger caused by fire onboard a train.

FIRESTARR project was initiated as the CEN group realised that there were no common test procedures and that the fire safety of different products was not properly investigated.

FIRESTARR stands for FIRE STAndardisation Research of Railway vehicles and is a joint project that consists of 11 different partners around Europe. The main technical objectives of the project were:

a) To identify the fire risks onboard European trains and to define the most likely and relevant fire scenarios
b) To select the most appropriate test methods to evaluate the reaction-to-fire behaviour, according to key fire critical effects like ignitability, time to uncontrolled fire (flashover), time to loss of visibility and time to lethal conditions
c) To obtain test results for a representative range of railway products. The products are divided into the three groups: surface products (e.g. wall, ceiling panels, seat frame and floor coverings), furniture and electrical components.
d) To recommend a classification system for these ranges of products and to validate the proposals with real-scale experiments on different parts of European trains.

Note that the review of FIRESTARR project will be on the surface products only as they are considered more relevant to the metro train evaluated in this research project.

Statistical analysis of fires from the FIRESTARR study revealed that except in particular cases e.g. electrical defect, arson was the main fire risk on board European trains and that in most cases, the fires started on the vandalized seat. Three fire scenarios were identified in the interior of railway vehicles for the study:

a) Arson on a seat due to a cigarette lighter or burning newspaper
b) High temperature in electrical components due to electrical defects
c) Fire in toilet due to a cigarette or burning newspaper.

Exterior fire scenario e.g. sparks from brakes or by combustion of fuel after a major collision, was not considered because model trains are protected against sparks and because major collisions were extremely rare in railways as quoted in the report.

The FIRESTARR group assumed the fire was ventilation controlled when the windows were sealed but when the windows were broken, the fire became fuel controlled. Fuel controlled fire was used as the basis for the test.

Small-scale, large-scale and real-scale tests were conducted. The set of test methods selected must be able to measure the five parameters identified as FIRST (flame spread (F), ignitability (I), heat release (R), smoke opacity (S) and toxicity (T)) for evaluation of reaction to fire for the three product groups. These five parameters were found to be similar to what Rakaczky (1980) considered as the most important flammability areas. The test methods must also be representative of at least one of the fire development stages (Initial stage, early developing stage, developing stage (pre-flashover) and developed stage (post-flashover)).

A number of test methods were selected for the small-scale tests. Test methods were either EN or ISO/IEC standard. Where international method was found not to be applicable, national standards e.g. French NFX, Germany DIN, were used. Among the small-scale tests selected for surface products, the Cone Calorimeter was utilised to measure the ignitability parameter (ISO 5660 Part 1), heat release parameter (ISO 5660 Part 1) and smoke opacity parameter (ISO 5660 Part 2). The key parameters for analysis from the Cone Calorimeter tests are:

a) Time to ignition t_{ig}
b) Peak heat release rate $\dot{q}''_{peak}$
c) Average $\dot{q}''$ values for the first 180 and 300 s after ignition i.e. $\dot{q}''_{180}$ and $\dot{q}''_{300}$
d) Total heat released q''
e) Total smoke produced using specific extinction area SEA
f) Maximum extinction coefficient $k_{\max}$

In the Cone Calorimeter tests, an exposure heat flux level of 35 kW/m^2 was used to simulate an early developing fire and 50 kW/m^2 was used to simulate a developing fire.

For real-scale tests of surface products, a room (see Figure 2.9) with dimensions of a real railway compartment (about 9 m^3) was placed under the hood of room corner test ISO 9705 (ISO 9705:1993). In order to define the burner (burning seat) and simulate thermal attack (on wall and ceiling) during real fire, a series of preliminary tests with seats were conducted. From the preliminary tests, FIRESTARR group came out with the following conclusions:

a) An open door condition allowed the seat to produce higher intensity fire. This was the fire considered to reproduce the thermal attack on walls and ceilings during real fire.
b) The thermal attack on ceiling was never bigger than the attack on the wall.

Two burner sizes were stated in different sections of the report.

a) Burner which was able to reach 180 kW in 5 minutes producing thermal attack of 40, or maximum 50 kW/m^2 on the walls
b) Burner which reached 75 kW for 2 minutes followed by 150 kW for 8 minutes producing thermal attack of 40 kW/m^2.

The latter was likely to be the one used in the real-scale tests.

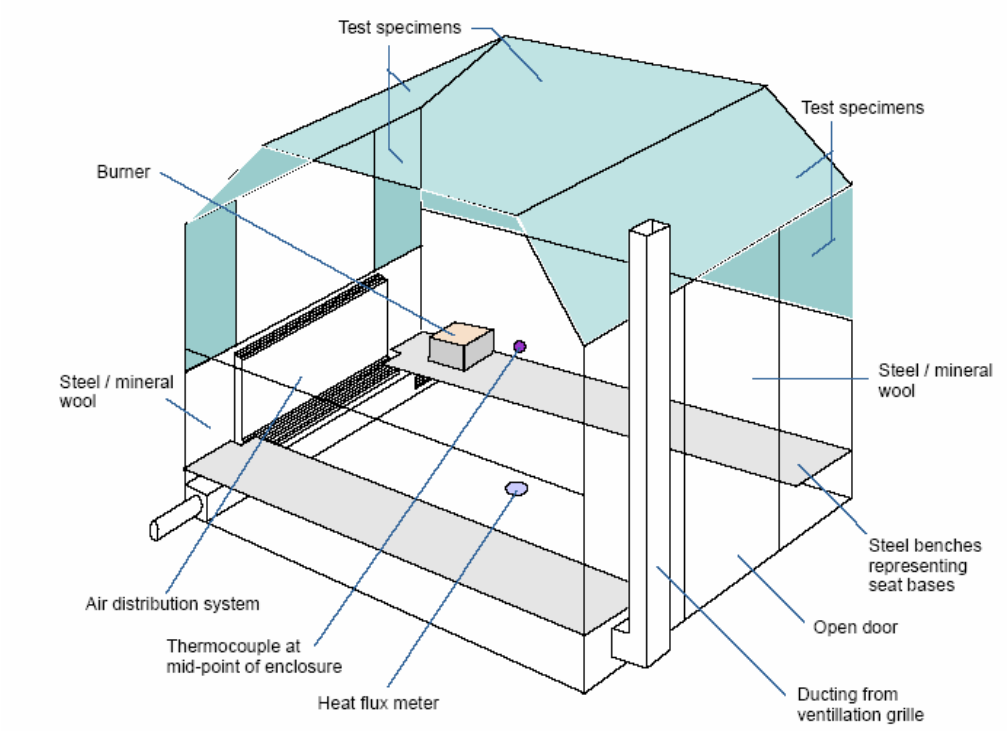

Figure 2.9: Schematic view of 9 m^3 compartment (reproduced from (Briggs et al. 2001a))

Some correlations were found between the small-scale and real-scale tests for surface products (mainly wall and ceiling) as discussed below:

a) For materials which provide flashover, there is a correlation between the real-scale and small-scale (ISO 5660 at 50 kW/m^2 exposure heat flux level).
b) For fire growth parameters, the following correlations were found:

- Heat release rate (real-scale) and $\dot{q}''_{180}$ and $\dot{q}''_{180}$ (ISO 5660 at 35 and 50 kW/m^2 exposure heat flux levels)
- Total heat released (real-scale) and total heat released (ISO 5660 at 35 kW/m^2 exposure heat flux level) only for materials with flashover.

c) For smoke parameters, correlation was found between smoke production rate (real-scale) and rate of smoke generation in the first 4 minutes (VOF4) (ISO 5659-2 at 25 kW/m^2 with pilot flame and 50 kW/m^2 without pilot flame)

d) For toxicity parameters, fractional effective dose (FED) (real-scale) was found to correlate with combination of parameters in small-scale that was, index toxicity multiple by total mass loss (with the index toxicity from UITP E6 test at 400 or 600°C and the total mass loss from ISO 5660 test at 35 or 50 kW/m^2 exposure heat flux levels).

Following these findings, the FIRESTARR group recommended test methods, test conditions and classification criteria for wall and ceiling products as shown in Table 2.8.

Class A is for high performance product suitable for use in train with underground or tunnel operations. Class B is medium performance product for use in train with non-underground or non-tunnel operations and Class C is for low performance product which is only suitable for use in low risk, limited use applications only.

For flooring products, no real-scale compartment/corridor tests were carried out in the FIRESTARR project. The recommended test methods were based on the analysis of results obtained in small-scale and also information coming from the EN work for building product. The test methods, test conditions and classification criteria for flooring products are shown in Table 2.9.

Fire Critical Effect	Parameter	Test method	Test condition	Classification Criteria		
				Class A	Class B	Class C
Ease of Initiation	F	ISO 5658-2	Exposure heat flux gradient from 50 to 1.5 kW/m^2	CFE $\geq$ 37 kW/m^2	CFE $\geq$ 30 kW/m^2	CFE $\geq$ 10 kW/m^2
	I	ISO 5660-1	Exposure heat flux level of 50 kW/m^2	No ignition	Ignition	Ignition
Fire Growth	R	ISO 5660-1	Exposure heat flux level of 50 kW/m^2	No FO or $t_{FO} \geq 390$ s	$t_{FO} \geq 240$ s	n/r
Smoke opacity	S	ISO 5659-2	Exposure heat flux level of 50 kW/m^2 (Without pilot flame)	$t_{VL} \geq 390$ s	$t_{VL} \geq 390$ s	n/r
Smoke Lethality	T	ISO 5660-1	Mass loss measurement at 35 kW/m^2 exposure heat flux level	FED<1.0	FED<10.0	n/r
		UITP E6	400°C			

Table 2.8: Test methods, test conditions and classification criteria for wall and ceiling products (adopted from Briggs et al. (2001a))

Note:

1) CFE is critical flux at extinguishment (ISO 5658-2)
2) FO is flashover in 10 m^3 compartment as calculation from ISO 5660-1 data at 50 kW/m^2 exposure heat flux level using the correlation equation derived
3) t_{FO} is time to flashover in compartment as calculation from ISO 5660-1 data at 50 kW/m^2 exposure heat flux level using the correlation equation derived
4) t_{VL} is time to loss of visibility in 40 m^3 corridor as calculation from ISO 5659-2 data using the correlation equation derived
5) FED is fractional effective dose calculated from UITP E6 data and ISO 5660-1 data at 35 kW/m^2 exposure heat flux level using the correlation equation derived
6) n/r is not required

Fire Critical Effect	Parameter	Test method	Test condition	Classification Criteria		
				Class A	Class B	Class C
Ease of Initiation	F	Pr EN ISO 9239-1	Exposure heat flux gradient from 11 to 1 kW/m^2	CRF $\geq$ 8.0 kW/m^2	CRF $\geq$ 4.5 kW/m^2	CF $\geq$ 3.0 kW/m^2
	I	ISO 5660-1	Exposure heat flux of 25 kW/m^2	No Ignition	Ignition	Ignition
Fire Growth	R	ISO 5660-1	Exposure heat flux of 25 kW/m^2	$q^{"} \leq 75$ MJ/m^2	$q^{"} \leq 120$ MJ/m^2	n/r
Smoke opacity	S	ISO 5659-2	Exposure heat flux of 25 kW/m^2 (+pf)	VOF4 $\leq$ 100	VOF4 $\leq$ 1000	n/r
			Exposure heat flux of 25 kW/m^2 (-pf)	VOF4 $\leq$ 100	VOF4 $\leq$ 200	n/r
Smoke Lethality	T	ISO 5660-1	Mass loss measurement[a]	FED<1.0	FED<10.0	n/r
		UITP E6	400 or 600°C			

a Exposure heat flux level for Cone Calorimeter test 5660-1 was not stated in Briggs et al. (2001a)

Table 2.9: Test methods, test conditions and classification criteria for flooring products (adopted from Briggs et al. (2001a))

Note:

1) CRF is critical radiant flux. It is the radiant flux at which the flame extinguishes or the radiant flux after a test period of 30 minutes, which ever is the lower (i.e. the flux corresponding with the further extent of flame spread).
2) VOF4 is smoke rate index in the first 4 minutes
3) ISO 5660-1, ISO 5659-2 and UITP E6 tests with the proposed test conditions are optional for measurements on parameters smoke production rate and are only required if specified by Regulators.
4) n/r is not required

2.3.6 Conducting a Full-Scale Experiment on a Rail Passenger Car (White and Dowling 2004)

Commonwealth Scientific and Industrial Research Organization (CSIRO)'s Fire Science and Technology Laboratory (FSTL) conducted a series of rail passenger car fire experiments on a collaborative basis with a rail operator and Queensland Fire and Rescue Service (QFRS). The objectives of the experiments were to:

a) Investigate the fire size resulting from application of different ignition sources in a typical rail passenger vehicle;
b) Establish an understanding of how fire develops and spreads in a typical rail passenger vehicle; and
c) Enhance understanding of the link between material flammability properties and total fire size.

Note that FSTL is currently analysing the experimental data therefore no results have been presented.

A total of ten experiments were conducted. Nine of them were ignition experiments and one (fully developed fire) involved burning of approximately half the vehicle fitted with typical interior materials. The combination of interior car materials selected for the experiments was intended as representative of a typical Australian suburban rail passenger vehicle.

As no suitable existing tunnel or large enclosure was available for the experiments, they were carried out in the open air. Therefore combustion products could not be collected for measuring heat release rate by oxygen consumption calorimetry. The analysis and estimation of heat release rate was by 'other means' using the temperature, flow, radiation heat flux, etc data collected during the experiments. 'Other means' quoted in the paper include:

a) Matching existing fire plume and ceiling jet correlations with observations to estimate the HRR.
b) Based on conservation of energy and mass to estimate the HRR.

c) Use of fire model such as FDS to estimate the HRR by iteratively inputting a "best guess" HRR to the CFD model and comparing the resulting temperature distribution and smoke plumes with those actually observed.

The ignition sources and ignition source locations for the ignition experiments are shown in Table 2.10.

Test no	Ignition source
1	300 g crumpled newspaper piled on seat against wall
2	600 g crumpled newspaper piled on seat against wall
3	150 g timber crib on seat against wall
4	400 g timber crib on seat against wall
5	500 ml kerosene poured onto slashed seat adjacent wall
6	450 g crumpled newspaper piled on seat against wall
7	450 g crumpled newspaper piled on floor in corner behind steel seat shell
8	300 g crumpled newspaper piled on floor in corner behind GRP seat shell
9	600 g timber crib on seat against wall

Table 2.10: Ignition sources and ignition source locations for the ignition experiments

As for the last experiment, the ignition source used was 1 kg of crumpled newspapers piled on the floor in a corner behind the end seat shell.

Cone Calorimeter tests for major combustible materials present in the carriage were also conducted. The exposure heat flux levels for the materials were selected based on their end use orientations. Supine materials were tested at 25 kW/m^2 exposure heat flux level, vertical materials were tested at 35kW/m^2 and prone materials were tested at 50 kW/m^2. The Cone Calorimeter heat release rate curves, as highlighted in the paper, will be used to calculate the HRR using method similar to Duggan (1997) (see Section 2.2.2). However, the calculation may be modified to match experimentally observed spread rates.

2.3.7 Conclusions drawn from previous research

The following conclusions are drawn from previous research.
(The reference indicates from which study the conclusions are drawn.)

a) In metro vehicle interior tests, the design of seat assemblies and wall linings are important factors in fire growth (Braun 1975; Braun 1978). In passenger rail car, the design of wall coverings adjacent to seating is the key to the fire growth (Peacock and Braun 1984).
b) Ignition source sizes used for full-scale and real-scale tests have increased progressively for each newer study as interior materials used in newer rail car which complied with the current small-scale test methods' performance criteria are more difficult to ignite (Braun 1975; Briggs et al. 2001a; Peacock et al. 2004; Peacock and Braun 1984; Peacock et al. 2002; White and Dowling 2004).
c) In almost all the studies, the newspaper is identified as an ignition source. An electrical fault is also considered but the ignition size is hard to define (Braun 1975; Briggs et al. 2001a; Peacock et al. 2004; Peacock and Braun 1984; Peacock et al. 2002; White and Dowling 2004).
d) In addition to electrical defects, the locations of ignition source to be considered are the corner area and the seat area (Braun 1975; Braun 1978; Briggs et al. 2001a; Peacock et al. 2004; Peacock and Braun 1984; Peacock and Braun 1999; Peacock et al. 2002).
e) An ignition source size between 150 to 200 kW is required to reproduce a thermal attack of 40 to 50 kW/m^2 on walls and ceilings and develop significant fire growth and flame spread (Briggs et al. 2001a; Peacock et al. 2004).
f) In US, an exterior fire is still considered as a potential fire scenario. However in EU, exterior fire is less of a concern as modern trains are protected against sparks and because major collisions are extremely rare in railways (Braun 1978; Briggs et al. 2001a; Peacock et al. 2002).

g) Nearly all the current efforts in transportation vehicle fire safety are focused on the use of HRR data to measure material fire performance (Barnett 1992; Briggs et al. 2001a; Burdett et al. 1989; Cappuccio 1992; ERRI 1992a; ERRI 1992b; Parker 1994; Peacock 1993; Peacock and Braun 1999; Schirmer Engineering Corporation 1990; Young 1995).

h) Cone Calorimeter test data can provide useful data for computer modelling (ERRI 1992a; Peacock 1993; Peacock and Braun 1999) .

i) An exposure level of 50 kW/m^2 is chosen as a suitable exposure for material evaluation using Cone Calorimeter consistent with exposure level in the existing test methods and exposure levels in actual fires (Peacock and Braun 1999; Young 1995). It has been found that at this exposure, there are correlations between HRR data from the Cone Calorimeter and real-scale tests (Briggs et al. 2001a; Peacock et al. 2004).

2.4 Studies relevant to this research project

Numerous studies have been carried out on fire safety in tunnels. While most studies focus on ensuring the systems are adequately designed (whereby in most cases, the HRR is predefined) e.g. Brennan and Lim (2003); Könnecke and Schneider (2004); Luo and Yau (2002) and Sinai (2004), some specific studies focus on examining factors such as tunnel and tunnel size; forced ventilation; tunnel slope, have on the HRR of a burning vehicle in a tunnel which are relevant to this research project.

2.4.1 Tunnel and tunnel size

Casale and Marlair (1994) conducted fire experiments for heptane and noted that the burning rate of a pool fire in a tunnel was higher than expected in the open air. They suggested that it might be due to significant re-radiation from the heated walls.

Carvel et al. (2001a) from Heriot-Watt University investigated in detail the differences between the HRR of fires in tunnels with the HRR of similar fires in the open air. No fire test was conducted in their study. The data was from study of fire tests in tunnels recorded in various literature. The HRRs for car, wooden crib and pool fires were compared. From the study, they concluded that in many instances the confining geometry of the tunnel enhanced the HRR of a fire significantly and the degree of enhancement appeared to increase with the fire dimensions up to a point where fire became ventilation controlled. However for pool fires, they found that the amount of enhancement was very much dependent on the nature of the fuel.

In another paper (Carvel et al. 2001c), they published an empirical formula which relates the fire width W_f, tunnel width W_t and HRR enhancement ψ. The formula is in the form of:

$$\psi = 24\left(\frac{W_f}{W_t}\right)^3 + 1 \qquad \text{Equation 2.11}$$

They suggested that the formula is valid for most fires involving cars, wooden cribs and kerosene & heptane pools in tunnels with a rectangular aspect. For fires in tunnels with a concave ceiling, the formula under-predicts the value of ψ by up to 10%.

2.4.2 Forced ventilation

The researchers from Heriot-Watt University also investigated the influence of longitudinal ventilation on the HRR for fires in tunnels (Carvel et al. 1999a; Carvel et al. 1999b; Carvel et al. 2001b; Carvel et al. 2001d). Five different fires were investigated: fires involving heavy good vehicles (HGVs); passenger cars; and three different sizes of pool fires. The study was probabilistic in nature, producing a probability distribution of HRR for each of the cases at four different longitudinal ventilation velocities (2, 4, 6 and 10 m/s). The results from the study indicated that the HRR of a HGV would be greatly enhanced by longitudinal ventilation; there was a high probability that a HGV fire would have a HRR about five times and 10 times greater with a forced ventilation velocity of 4m/s and 10m/s respectively than with natural ventilation. The results were somewhat in line with findings by Bettis et al. (1994) who carried out reduced-scale experiments for HGVs. Bettis et al. (1994) reported that with decrease in ventilation rate, the HRR also reduced, particularly the large fires where a strong correlation between the HRR and the ventilation velocity was observed.

For pool fires, however, the study predicted that forced ventilation would have an 'enflaming' effect on small and medium pool fires at low ventilation rates, but that higher ventilation would tend to reduce the HRR of a fire. On the other hand, for large pool fires, forced ventilation appeared to have an 'enflaming' effect at all ventilation rates. For car fires, there was no significant variation of the HRR with forced ventilation.

2.4.3 Tunnel slope

Rail tunnel is normally sloped between stations for practical reasons. Depending on the tunnel alignment and the soil conditions, the gradient of a rail tunnel varies from 0° to 3° (Lim 2005) and has direct influence on the critical velocity. Wu (2003) studies the effects of tunnel slope on the critical velocity both experimentally and by CFD simulations. When the tunnel is less than 15º, he found that the critical velocity increased linearly with slope.

When calculating the critical velocity, the effects of tunnel slope is accounted for by grade correction factor K_{grade} and is given by Equation 2.12 (Associated Engineers 1980).

$$K_{grade} = 1 + 0.0374(grade)^{0.8} \qquad \text{Equation 2.12}$$

A sloped tunnel increases the critical velocity and hence the ventilation rate of the emergency tunnel ventilation system. In Section 2.4.2, the effect of forced ventilation on the HRR has been discussed. Therefore, it can be concluded that a sloped tunnel will has 'indirect' effect on the HRR of a burning vehicle. However its 'direct' effect on the HRR is not clear, as there is little or no specific study in this area. The only study that may be relevant is study on trench effect. However from studies on trench effect e.g. Drysdale et al. (1992), a gradient of 3° might be too gentle to have significant effect on the HRR. Therefore, it was decided not to investigate this further to limit the scope of this project.

2.4.4 Conclusions drawn from specific studies

Although the results from the above studies might not be directly applicable to this research project, they do highlight the significance of tunnel environment on the HRR of a fire in a tunnel. For the effect of tunnel and tunnel size on the HRR, it can be accounted for in the simulation conducted in this research. The effect of forced ventilation can also be investigated. However, the direct effect of a sloped tunnel on the HRR will not be investigated to limit the scope of this research.

It is important to highlight that there are others ongoing /completed research programs on tunnel fire safety e.g. Memorial tunnel fire tests (FHWA 2004), Runehamar fire tests (SP 2004), PIARC research program (PIARC 1999). However, these programs have different objectives (some only main for road tunnel) which are beyond the scope of this research project and therefore are not covered in the literature review.

3 Fire Dynamics Simulator (FDS)

This Chapter outlines the main assumptions and equations behind the FDS to give a brief overview and broad understanding of the concepts behind the model. The underlying theory of FDS in predicting fire growth and flame spread will be described. The details covered in this Chapter are mainly referenced from Carlsson (2003); Cox (1995); Floyd et al. (2001) and McGrattan (2004).

3.1 Hydrodynamics model

FDS solves numerically a form of the Navier-stokes equations for low-speed, thermally driven flow with an emphasis on smoke and heat transport from fires. The core algorithm is an explicit predictor-corrector scheme, second order accuracy in space and time. Turbulence is treated by means of the Smagorinsky form of Large Eddy Simulation (LES), in which large-scale eddies are computed directly and the sub-grid dissipative processes are modelled. It is possible to perform a Direct Numerical Simulation (DNS), in which dissipative terms are computed directly, if the underlying numerical grid is fine enough (McGrattan 2004). In this project, LES approach has been employed due to practical reasons (grid resolution and computing power) and therefore only theory behind LES approach is presented.

Four conservation equations (mass, species, momentum and energy) for a thermally-expandable multi-component mixture of ideal gases are being solved in FDS. They will be individually discussed in later Sections.

3.1.1 Conservation of mass

The general conservation of mass equation states that the rate of mass storage within a given control volume, due to density changes, is balanced by the net rate of inflow of mass by convection. In the case of a steady flow situation, the conservation of mass equation states that what flows in must comes out (Cox 1995). The equation is written as:

$$\frac{\partial \rho}{\partial t} + \nabla . \rho u = 0 \qquad \text{Equation 3.1}$$

Where the first term describes the density changes with time and the second term defines the mass convection. u is the vector describing the velocity in the u, v and w directions.

3.1.2 Conservation of species

In the presence of a vector u, the conservation of mass fraction Y of a chemical species i is given by:

$$\frac{\partial}{\partial t}(\rho Y_i) + \nabla . \rho Y_i u = \nabla . \rho D_i \nabla Y_i + \dot{m}_i''' \qquad \text{Equation 3.2}$$

Where the first term on the left side represents the accumulation of species due to change in density with time, the second term is the inflow and outflow of species from the control volume due to convection. The right side gives the terms for the inflow or outflow of species from the control volume due to diffusion and the production rate of particular species within the control volume caused by chemical reaction.

3.1.3 Conservation of momentum

The equation for the conservation of momentum is derived by applying Newton's second law of motion, which states that the rate of momentum of a fluid element is equal to the sum of the forces acting on it (Cox 1995). The equation is written as:

$$\rho\left(\frac{\partial u}{\partial t}+(u.\nabla)u\right)=-\nabla p+\nabla.\tau+\rho g+f \qquad \text{Equation 3.3}$$

Here the left hand side represents the increase in momentum and inertia forces, while the right hand side comprises forces acting on it. These forces include pressure p, gravity g, an external force vector f (which represents the drag associated with sprinkler droplets that penetrate the control volume) and a measure of the viscous stress tensor τ acting on the fluid within the control volume. Among these forces, gravity is the most important because it represents the influence of buoyancy on the flow.

3.1.4 Conservation of energy

The equation for conservation of energy is the first law of thermodynamics which states that increase in energy of the control volume is equal to the heat added minus the work done by expansion. In FDS, the conservation of energy is in the form of:

$$\left(\frac{\partial}{\partial t}(\rho h)+\nabla.\rho hu\right)=\left(\frac{\partial p}{\partial t}+u.\nabla p\right)+q'''-\nabla.q_{rad} \qquad \text{Equation 3.4}$$
$$+\nabla.k\nabla T+\sum_i \nabla.h_i\rho D_i\nabla Y_i$$

Here the left side describes the net rate of energy accumulation, whereas the right side comprises of the various energy gain or loss terms that contribute to this energy accumulation. These include the pressure work term, energy driving the system, represented by HRR per unit volume $\dot{q}'''$, the radiative heat flux vector q_{rad} and the convective term $\nabla.k\nabla T$. The last term represents the energy change associated with species inter-diffusion.

3.1.5 Equation of State

The conservation equations are supplemented by an equation of state relating the thermodynamic quantities (McGrattan 2004). In FDS, the equation of state is in the form of:

$$p = \rho T \Re \sum_i (Y_i / M_i) \qquad \text{Equation 3.5}$$

3.2 Combustion model

There are two types of combustion models used in FDS. The choice depends on the type of simulation approach chosen. For LES approach, a mixture fraction-based combustion model is used.

The mixture fraction combustion model approximates the combustion process in both space and time so that the fire can be simulated more efficiently (Floyd et al. 2001). It assumes that large-scale transport phenomena due to convection and radiation can be simulated directly, but physical processes occurring at small length and time scales must be represented in an approximate manner (McGrattan 2004). This assumption is essential because the actual rate of chemical processes that control the combustion energy release are too complex and computationally expensive to be included, even in reduced form, in practical CFD simulations (Carlsson 2003).

In mixture fraction-based combustion model, combustion is calculated from the mixing rates of fuel and oxidant. The chemical reactions between fuel and oxygen are taken to follow a single one-step stoichiometric reaction.

$$v_F Fuel + v_{O2} O_2 \rightarrow \sum_i v_{P,i}\ Products \qquad \text{Equation 3.6}$$

Where the numbers v_i are the stoichiometric coefficients for the overall combustion process that reacts fuel 'F' with oxygen '$O2$' to produce a number of products 'P'.

The model assumes that the combustion is mixing-controlled and that all species of interest can be represented by a single variable known as mixture fraction $Z(x,t)$. The mixture fraction is a conserved quantity representing the fraction of material at a given location that originated in the fuel stream and is defined as:

$$Z = \frac{sY_F - (Y_{O2} - Y_{O2}^{\infty})}{sY_F^I + Y_{O2}^{\infty}}; s = \frac{v_{O2} M_{O2}}{v_F M_F} \qquad \text{Equation 3.7}$$

Where Y_F^I is the fuel mass fraction in the fuel stream, M_F is the fuel molecular weight, M_{O2} is the oxygen molecular weight.

By design, Z varies from one in the region containing only fuel, to zero where the oxygen mass fraction equals its ambient value Y_{O2}^{∞}.

The reaction is assumed to proceed infinitely fast, meaning that all mixtures of oxygen and fuel react instantaneously as they mix such that both fuel and oxygen cannot coexist. This will result in both fuel and oxygen vanishing at a certain instant where their mass fractions Y_i drop to zero. Equation 3.7 can therefore be simplified to obtain the flame mixture fraction Z_f:

$$Z_f = \frac{Y_{O2}^{\infty}}{sY_F^I + Y_{O2}^{\infty}} \qquad \text{Equation 3.8}$$

The flame mixture fraction Z_f defines the flame by prescribing a two-dimensional surface, known as flame sheet, in a three dimensional space (McGrattan 2004).

The assumption that fuel and oxidizer cannot co-exist also leads to the state relation between the oxygen mass fraction Y_o and the mixture fraction Z as shown in Equation 3.9.

$$Y_{O2}(Z) = \begin{cases} Y_{O2}^{\infty}(1 - Z/Z_f) & Z < Z_f \\ 0 & Z > Z_f \end{cases} \qquad \text{Equation 3.9}$$

The mass fraction of all the other species of interest can be also described by individual state relations based on the mixture fraction. These state relations can be determined by analysis of the stoichiometric reaction of the particular fuel under consideration. Figure 3.1 illustrates the state relations of various species for propane. From Figure 3.1, the point where the fuel and oxygen lines meet at a mass fraction of zero is where the flame sheet is defined, as mentioned earlier.

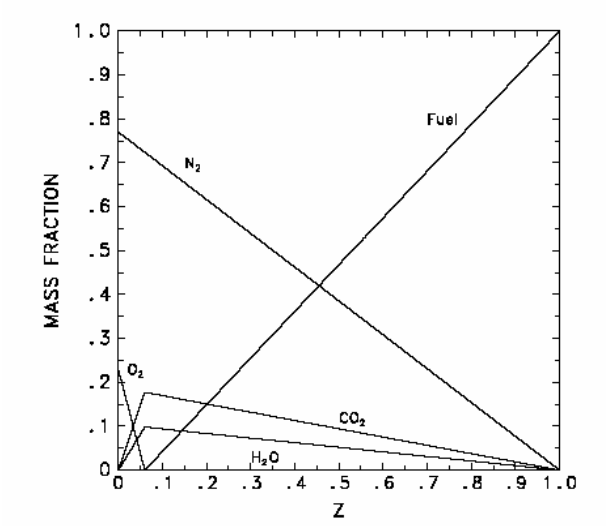

Figure 3.1: State relations for propane (reproduced from McGrattan (2004))

In FDS, the local HRR is estimated using a rather simple method based on oxygen consumption calorimetry. The oxygen consumption rate is calculated from the mass fraction and the corresponding local HRR can then be calculated from:

$$\dot{q}''' = \Delta H_{O2} \dot{m}'''_{O2} \qquad \text{Equation 3.10}$$

This is the concept used in FDS. McGrattan (2004) explains in details how an expression for the local HHR is derived from the conservation equations and state relations for numerical simulation.

3.2.1 Enhancements to the mixture fraction combustion model

The mixture fraction model described in the previous Section has several limitations, both numerical and physical. Its numerical limitations are related to the grid resolution. If the grid is coarse, the fire will not be adequately resolved. This will result in the flame surface, as defined by the mixture fraction $Z = Z_f$, to underestimate the observed flame height. Consequently, the HRR will be under-estimated. To overcome this problem, a different value of Z is used to define the combustion region for a better estimation of the flame height.

The expression that is used to calculate this different value mixture fraction $Z_{f,eff}$ is:

$$\frac{Z_{f,eff}}{Z_f} = \min\left(1, C\frac{D^*}{\delta x}\right) \qquad \text{Equation 3.11}$$

Where C is an empirical constant (that is independent of the scenario being simulated), D^* is the characteristic fire diameter, which is given as:

$$D^* = \left(\frac{\dot{Q}}{\rho_\infty c T_\infty \sqrt{g}}\right)^{\frac{2}{5}} \qquad \text{Equation 3.12}$$

and δx is the nominal grid size.

Another problem with coarse grid is that a disproportionate amount of the combustion energy is released near the edges of the fire source. To avoid too much of the energy from being released too close to the fire source when coarse grid is used, there is a maximum bound imposed on the local heat release rate per unit area of flame sheet. This upper bound is based on a simple analysis in which the fire is assumed to be conical in shape with the surface area A_{sur}, and a flame height H_f given by:

$$\frac{H_f}{D} = 3.7\dot{Q}^{*2/5} - 1.02 \qquad \text{Equation 3.13}$$

The surface area of a real flame is larger than that of a cone, so the upper board estimate will prevent too much energy from being released too close to the fire when a coarse grid is used, but will be high enough not to interfere with the calculation when the grid is well resolved. Any energy that is 'clipped' off due to the upper bound is redistributed over the entire flame volume automatically (McGrattan 2004).

The physical limitation of the mixture fraction combustion model is that it assumes the fuel and oxygen burn instantaneously when mixed. The assumption of fast chemistry does not normally place any restrictions on the calculations that are typical, i.e. well-ventilated fires. However, if a fire is in an under-ventilated compartment, or if a suppression agent like water mist or CO_2 is introduced, fuel and oxygen may mix but combustion may not occur. Also, a shear layer with high strain rate separating the fuel stream from an oxygen supply can prevent combustion to take place (McGrattan 2004). To overcome this physical limitation, a simple model has been implemented for flame extinction in FDS. This model relates the flame extinction to the oxygen concentration and the temperature as shown in Figure 3.2. When the gas environment falls in the 'No Burn' zone, the state relations (see Figure 3.1) are no longer valid for values of Z below stoichiometric, since now some fuel may be mixed with the other combustion products (McGrattan 2004).

This enable FDS to simulate under-ventilated or fire suppression scenarios described above where most CFD codes fail to predict burning behaviour accurately (Carlsson 2003).

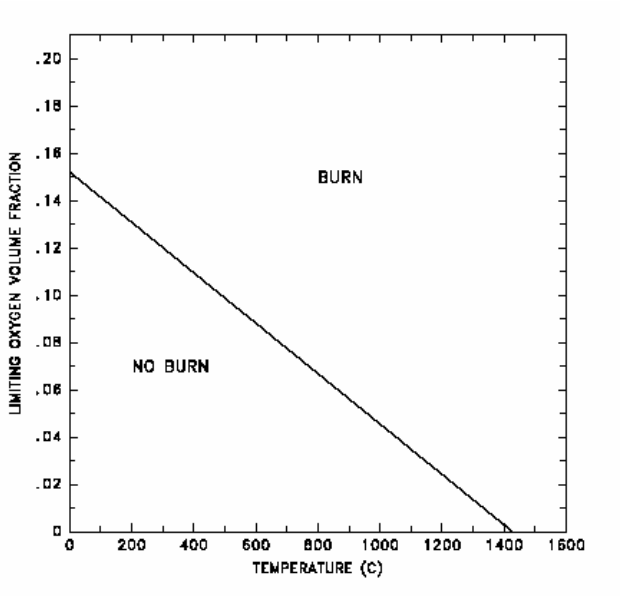

Figure 3.2: Oxygen-temperature phase space showing where combustion is allowed and not allowed to take place (reproduced from McGrattan (2004))

3.3 Thermal radiation model

In FDS, a Finite Volume approach has been adopted in solving the Radiative Transport Equation (RTE) for a non-scattering grey gas to compute the radiative heat flux. This is explained in more detail in McGrattan (2004).

A major point to be highlighted is that different approach (or equation) has been used to calculate the source term (radiation intensity) I_b for the grid cells through which the flame sheet cuts. This is because the temperatures are averaged across the grid cell and are therefore considerably lower than would be expected for a particular point in a diffusion flame. Because radiation is dependent on the forth power of temperature, this will affect the accuracy of radiation heat flux calculated from those particular grids. Elsewhere i.e. outside flame zone, there is greater confidence in the computed temperature, and the original equation for source term can assume its ideal value there (McGrattan 2004). The equations used to calculate the source term are shown in Equation 3.14.

$$\kappa I_b = \begin{cases} \kappa\sigma T^4/\pi & \textit{Outside flame zone} \\ \chi_{rad}\dot{q}'''/4\pi & \textit{Inside flame zone} \end{cases}$$ Equation 3.14

Where σ is the Stefan-Boltzmann constant, $\dot{q}'''$ is the HRR per unit volume and χ_{rad} is the local fraction of that HRR emitted as thermal radiation. κ is the local absorption coefficient and is dependent on the mixture fraction and temperature; and is determined by a sub-model implemented in FDS called RADCAL (McGrattan 2004).

3.4 Convection heat flux

The calculation of convective heat flux depends on whether one is performing DNS or LES. In LES calculation, the convective heat flux to the surface is obtained from a combination of natural and forced convection correlations (McGrattan 2004).

$$\dot{q}_c'' = h_{con}\Delta T\ ;\ h_{con} = \max\left[C_{nat\ con}|\Delta T|^{\frac{1}{3}}, \frac{k}{L}0.037\,\mathrm{Re}^{\frac{4}{5}}\,\mathrm{Pr}^{\frac{1}{3}} \right]$$ Equation 3.15

Where ΔT is the difference between the wall and the gas temperature, $C_{nat\ con}$ is the coefficient for natural convection, L is the characteristic length related to the size of the physical obstruction, k is the thermal conductivity of the gas, and the Reynolds number Re and Prandtl number Pr are based on the gas flowing past the obstruction.

3.5 Pyrolysis model

FDS includes a simple model for ignition and surface-flame spread, in which an ignition temperature is assigned to the combustible surface. The rate of pyrolysis being governed by a user prescribed constant which is either a rate of heat release per unit of the surface area HRRPUA or a heat of vaporisation (gasification) ΔH_v.

If HRRPUA is prescribed, the surface will burn like a burner when it has reached its ignition temperature. If heat of vaporisation is prescribed, the burning rate of the fuel will depend on the net heat feedback to the surface from the fire. For thermoplastic fuel, the calculation of net heat feedback will depend on whether the surface material is thermally-thick or thermally-thin.

If the surface material is assumed to be thermally thick, one-dimensional heat conduction equation for the material temperature $T(x,t)$ is applied in the direction x pointing into the solid (the point $x = 0$ represents the surface). The equation is given by:

$$\rho c \frac{\partial T}{\partial t} = \frac{\partial}{\partial x}\left(k \frac{\partial T}{\partial x}\right); -k \frac{\partial T}{\partial x}(0,t) = \dot{q}''_{con} + \dot{q}''_{rad} - \dot{m}'' \Delta H_v \qquad \text{Equation 3.16}$$

where ρ , c and k are the temperature dependent density, specific heat and conductivity of the materials respectively; $\dot{q}''_{con}$ is the convective and q''_{rad} is the (net) radiative heat flux at the surface, $\dot{m}''$ is the mass loss rate per unit area and ΔH_v is the heat of vaporisation. Fuel pyrolysis is assumed to take place at the surface thus the heat required to vaporize the fuel is extracted from the incoming energy flux. The pyrolysis rate is estimated using a single-step Arrhenius rate law of the first order, written as:

$$\dot{m}'' = A \rho e^{-E_A / \Re T} \qquad \text{Equation 3.17}$$

The value of the pre-exponential factor A and the activation energy E_A are chosen such that the burning takes place very close to a given ignition temperature. These parameters are probably the most difficult to choose when using a model of this kind. The values found in the literature are not consistent with each other and can differ by one order of magnitude or more (Carlsson 2003). If A and E_A are not known, which is usually the case, user can prescribe the critical mass flux rate and the ignition temperature. This will direct the code to choose A and E_A so that the fuel burns at the critical mass flux rate when its surface temperature reaches ignition temperature

(McGrattan and Forney 2004). The latter method is used in this project. Besides prescribing the critical mass flux rate and the ignition temperature, the maximum burning rate of the fuel will also be prescribed so that to prevent excess pyrolysis. The intent is to limit the burning rate of the fuel to its measured maximum.

If the surface material is assumed to be thermally-thin, that is, its temperature is assumed uniform across its width, $T(t)$ is affected by gains and losses due to convection, radiation and pyrolysis. The thermal lag of the material is a function of the product of its density, specific heat and thickness δ. The heat transfer equation is given by:

$$\frac{\partial T}{\partial t} = \frac{\dot{q}''_{con} + \dot{q}''_{rad} - \dot{m}'' \Delta H_v}{\rho c \delta} \qquad \text{Equation 3.18}$$

The convective and radiative fluxes are summed over the front and back surface of the thin fuel. The back surface is assumed to face an ambient temperature void by default in FDS unless otherwise specified (McGrattan 2004). The pyrolysis rate for a thermally-thin fuel is also estimated using Equation 3.17.

The heat transfer and pyrolysis for the charring fuels e.g. wood and liquid fuels e.g. methanol are different from the thermoplastic fuel. They are not covered here since these fuels are not simulated in this project. The details however can be found in McGrattan (2004); McGrattan and Forney (2004).

3.6 Stretching the grid

In FDS, the grid cells that fill the computational domain are uniform in size by default. However, one or two of the three coordinate directions can be specified to be non-uniform (McGrattan and Forney 2004). This can be done by using the TRNX, TRNY and/or TRNZ namelist groups. This function will be used in this project so that to capture the important features of the train that is much smaller than the defined grid size.

4 Approach

This Chapter outlines the approach taken in this project to accomplish the objectives. Nine major steps are taken in this project and are discussed below.

1) Train car construction; train car and tunnel geometries

The first step is to identify the amount and type of combustible materials, its location, and orientation in the train car (to be discussed in Chapter 5). The focus will be on the exposed surface materials in the train car interior since they are the fuels being modelled in FDS. They are the main combustibles and will be the first to ignite and involve in the fire. Miscellaneous items such as electrical cables, electrical components, air-conditioning (air-con) duct, air-con components, thermal insulation, etc are not included because there items are either housed in the underseat boxes, equipped cubicle assembly, driver console assembly, behind wall construction or inside the ceiling. These items will only be involved when the exposed surface materials melt, drip or collapse and it is beyond the capabilities of fire models or other computational methods to simulate these phenomena. Therefore, it is assumed that these items will only involved during the late stage of the fire and have little effect on the peak HRR.

The sub-floor components i.e. floor and below floor combustibles, are also not included. However means to incorporate the contribution of sub-floor components is proposed as discussed below.

Sub-floor components

Due to the complexity of undercarriage geometry, materials used, etc, it is beyond the scope of this project to model fire growth and flame spread in the undercarriage. When considering exterior fire scenario, it is assumed that the exterior fire has propagated above floor and burned in the car interior. The fire size of the exterior fire will be estimated using the traditional method. This will account for the contribution of the sub-floor components. The estimated fire size is used as an ignition source in the car interior for the simulation. This approach allowed both interior and exterior fire scenarios to be examined in the study.

The train and tunnel geometries are factors that will affect the fire development and will also be accounted for in the simulation.

2) Gather information on mechanical and thermal properties of bounding surfaces

The material in the bounding surfaces of the train can affect the hot gas temperature considerably and thereby the heat flux to the burning surface. Most of the material properties are not available from the train supplier and therefore need to be gathered from references or calculated. Information required included the thickness δ, thermal conductivity k, specific heat c and density ρ. Material properties for the concrete tunnel wall also need to be sought since they affect the tunnel temperature.

3) Set up FDS model

The third step is to set up FDS model. This will be carried out based on the actual train and tunnel geometries.

4) Modelling approach

Two modelling approaches are proposed in this project. The difference between the two is the prescribed constant which governed the rate of pyrolysis as discussed in Chapter 3 i.e. one modelling approach prescribed heat of vaporisation while the other prescribed HRRPUA. The modelling approach prescribing the heat of vaporisation is a more realistic method of simulating fire compared to the modelling approach by prescribing the HRRPUA as rate of pyrolysis is dependant on heat feedback from fire and not a user prescribed constant. However, the latter approach is included in the project as an attempt to improve on the HRR estimation method developed by Duggan (1997) by considering factors that affect the fire development

In Duggan (1997) method, the surface materials are tested in the Cone Calorimeter at an exposure heat flux levels selected according to their orientation in the train car. The proposed exposure heat flux levels are in the range of 20 (or 25) kW/m^2 ('floor-like' orientation material) to 50 kW/m^2 ('ceiling-like' orientation material).

These exposure conditions can be related to unwanted fires. Three types of flaming fires have been categorised by the British Standards Institution (BSI 1988) in its Code of Practice for the Assessment of Toxic Hazards in Fire in Buildings and Transport. They are:

a) Developing fires, flaming (pre-flashover)
b) Fully-developed fires, high ventilation (post-flashover fuel-controlled fires)
c) Fully-developed fires, low ventilation (post-flashover ventilation-controlled fires)

According to Peacock and Braun (1999), the heat flux levels found in fires are:

a) Developing fires – 20 to 50 kW/m^2
b) Fully-developed fires – 50 to 75 kW/m^2

The heat flux levels for developing fires are found to be consistent with values quoted in a number of literature e.g. Babrauskas (2002) and Briggs et al. (2001a). In Briggs et al. (2001a), exposure heat flux of 35 kW/m^2 and 50 kW/m^2 were used to simulate early developing fire and developing fire respectively. Cone Calorimeter test at exposure heat flux level of 25 kW/m^2 was included in their proposed test methods for floor products.

However, for post-flashover fires, substantially higher heat flux levels were reported in Babrauskas (2002) as shown in Table 4.1 below. The reported values were based on experimental results of heat fluxes measurement in post-flashover room fires.

	Heat flux (kW/m^2)		
	Ceiling	**Walls**	**Floor**
Maximum	106-176	116-229	119-143
Average	68-147	91-194	-

Table 4.1: Heat fluxes measured in post-flashover room fires (adopted from Babrauskas (2002))

This information suggests that the exposure conditions proposed by Duggan (1997) could only represent conditions within a train car which is progressing towards, or is at flashover. For the modelling approach based on HRRPUA, the rate of heat release from the fuel surface will follow the prescribed Cone Calorimeter HRRPUA curve (of the fuel) once its surface reached the ignition temperature. FDS is not able to adjust the HRRPUA curve according to the heat feedback from the fire. This is one of the limitations of FDS. Therefore using the HRRPUA curve at heat fluxes proposed by Duggan (1997) is likely to over predict the HRR during the early stage of the fire. Because of add-on effect, it may inaccurately predict flashover even though in an actual fire, flashover may not happen.

Therefore for material which is difficult to ignite, using the HRRPUA curve at heat fluxes proposed by Duggan (1997) will be conservative; however, for a material which is easily combustible, it may under predict the HRR. As rail car materials that comply with the stringent small-scale tests performance criteria are difficult to ignite (Peacock et al. 2002), it was decided that heat flux levels proposed by Duggan 1997) be used in the current study but modified according to the scheme as shown in Table 4.2 to simplify the modelling input.

Surface	$\dot{q}_e''$ **(kW/m^2)**
Floor	25
Wall, seat and driver console assembly	35
Ceiling	50

Table 4.2: Exposure heat flux levels for Cone Calorimeter testing in the modelling approach based on HRRPUA

Note that as the Cone Calorimeter test will be conducted under controlled conditions, the computed HRRPUA curve may not represent the HRR of the material when the material is burning in a real train fire scenario especially under the influence of emergency tunnel ventilation airflow. However, in order to proceed with the simulation, it is assumed that the burning behaviour of material in the real fire scenario will be the same as small-scale test. This is one of the main assumptions made for modelling approach based on HRRPUA.

5) Determine credible fire scenarios for CCL train

The fifth step is to determine the credible fire scenarios for simulation. The common fire scenarios will be identified through statistical data, expert opinion, conclusions drawn from the literature review and analysis of the CCL metro train car construction. The credible type, size and location of ignition source will be identified. Ventilation factors also will also be addressed.

6) Cone Calorimeter tests and material properties

Cone Calorimeter tests will be carried out to evaluate the train car materials' reaction to fire and to derive the material properties for input into the FDS model. The train car materials provided by LTA are shown in Table 4.3.

S/no	Component	Material
1	Seat	Fiberglass reinforced polymer (FRP) polyester
2	Floor covering	Styrene butadiene
3	Wall panel	Aluminum panel with a thin coat of powder paint on its exposed surface
4	Window	Laminated safety glass
5	Bellows (Inner)	WPE Vamac compound ref 22-003
6	Bellows (Outer)	WPE Vamac compound ref 22-004
7	Air-con duct	Glass wool with the outer surface covered with aluminum paper sheet

Table 4.3: Train car materials provided by LTA

The seat, floor covering, wall panel and window are exposed surface materials in the train. However only the seat, floor covering and wall panel samples will be tested in the Cone Calorimeter since the window is not combustible. These three samples will be tested under at least three exposure heat flux levels so that there is sufficient data to derive the material properties. Note that besides the seat, a number of components in the train car e.g. underseat boxes, driver console assembly, are also made of FRP polyester (see Chapter 5). Since only the seat sample is available for the Cone Calorimeter test, it is assumed that other components made of the same material will have the same material properties as the seat sample. The ceiling and door panels are also assumed to have the same material properties as the wall panel sample since they are made of the same material.

The bellows (Inner) and bellows (Outer) are part of the train car gangway (see Chapter 5, Figure 5.6). The gangway is the end sections of the train car used to couple and provide flexible connection between the train cars. The bellows (Inner) and bellows (Outer) are distinguished by their colour, which are grey and black respectively. The bellows and the air-con duct will be also tested in the Cone Calorimeter however the results will not be used for the modelling. They are tested to examine their ignitability and flammability which might be useful in future study.

The following information will be derived from the Cone Calorimeter test data for input into FDS model:

a) Cone Calorimeter HRRPUA curve at various exposure heat flux levels
b) Ignition temperature T_{ig}
c) Effective heat of combustion $\Delta H_{c,eff}$
d) Heat of vaporisation ΔH_v
e) Critical mass flux $\dot{m}''_{cr}$
f) Maximum burning rate $\dot{m}''_{\max}$
g) The thermal inertia $k\rho c$ i.e. the product of thermal conductivity k, density ρ and specific heat c at ignition temperature if the surface material is thermally thick. The product of density ρ, specific heat c and thickness δ at ignition temperature if the surface material is thermally thin

7) FDS predictions of Cone Calorimeter test results

FDS predictions of Cone Calorimeter test results i.e. the time to ignition and heat release rate, will be conducted. This step is particularly important as no full-scale test will be conducted to validate the train fire modelling results. Therefore it is essential to check whether the material properties derived (and used as input into the fire model) are able to provide reasonable prediction of the experimental test results before they are used for simulation of train fires. Depending on the results, the material properties may need to be adjusted /calibrated to improve the fire model prediction.

8) Trial Simulations

Trial simulations will be carried out a) for grid sensitivity study to decide on the grid size to be used for the final simulations b) to identify any unforeseen issue or problem that may be encountered during the simulations.

9) Final Simulations

Final simulations will be carried out to assess the fire spread within a metro train car and to the adjacent cars; to assess the likelihood of flashover and to predict the HRR.

5 Train car and tunnel geometries

This Chapter gives a brief description of the configuration and construction of the Circle Line (CCL) metro train. It also describes briefly the fire protection systems onboard the train; outlines the test methods and performance criteria for the metro train car materials; and gives a summary of fire loads in the metro train cars. The tunnel geometries are also briefly covered. The information for the CCL metro train is mainly obtained from Alstom (2004); Renie and Prevot (2003); RTI (2002) and Tan (2005b).

5.1 Circle Line train

CCL is the fourth metro line currently under construction in Singapore. The line will be 33.3 km long with about 29 stations. Like the previous metro line, North East Line (NEL), CCL will be driverless, fully automatic and entirely underground. The main features of CCL train will be the same as NEL which include:

a) Air-conditioning system
b) Passenger information system
c) Closed circuit television (CCTV) system
d) Public address (PA) system
e) Fully equipped desk (driver console assembly) for manual operation.
f) Fire and smoke detection system
g) Fire rated floor construction (at least 45 minutes)
h) Redundancy for every major components to ensure seamless train operation in automatic mode

The CCL train cars come in two configurations, a MC-car and a T-car as shown in Figure 5.1 and Figure 5.2 respectively. Both configurations are almost identical. The main difference in layout between the two cars is that the MC-car has an end mask (train head) that housed the driving console assembly and the detrainment door. The driving console is used for manual operation of the train while the detrainment door is used for detrainment of passengers in a tunnel during an emergency incident.

An operational train is made by coupling one T-car between two MC-cars. The gangway at the end section(s) of the train cars are used to couple and provide flexible connection between the cars. No door is fitted between cars and therefore passengers can move freely from one car to the other through the 1.4 m wide gangway access. When the train cars are mechanically coupled to each other, the cars are also automatically coupled electrically.

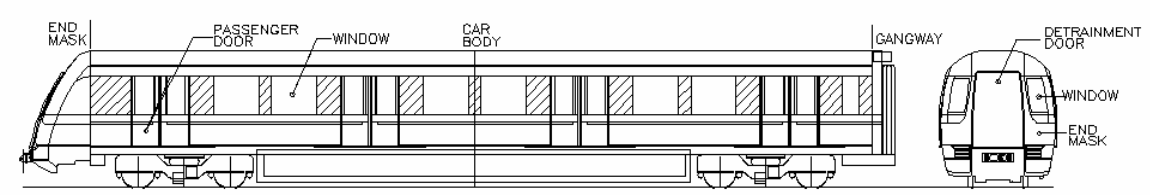

Figure 5.1: MC-car – Side and front elevations (adopted from Alstom (2001a) and Alstom (2001c))

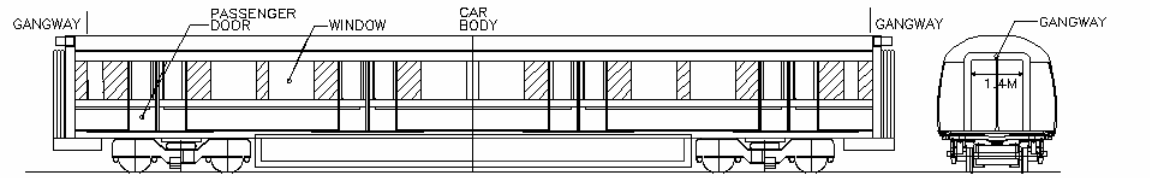

Figure 5.2: T-car – Side and front elevations (adopted from Alstom (2001a) and Alstom (2001d))

The length of the MC-car and T-car are 23.45 m and 22.8 m respectively. When the cars are coupled together, the length of the train is about 70 m. The width of the train is 3.2 m and the height of the floor above the upper edge of the rail is about 1.1 m.

There are six windows and four electrically driven bi parting type (sliding) passenger doors located on either side of each car. There are two smaller windows located at each set of passenger door. At the front of the MC-car is the end mask with an emergency detrainment door and two small side windows fitted to the front end of it. The driver console assembly is also located at the front of the MC-car.

The 'brain' of the train is the Train Integrated Management System (TIMS). This system is designed to controls the major sub-systems (see Figure 5.3) within the train in a co-ordinated manner so that to provide a safe and managed environment for train operation. Its major function is to monitor and provide overriding control of the major sub-systems and at the same time reports any variation to normal operation to the Operational Control Centre (OCC).

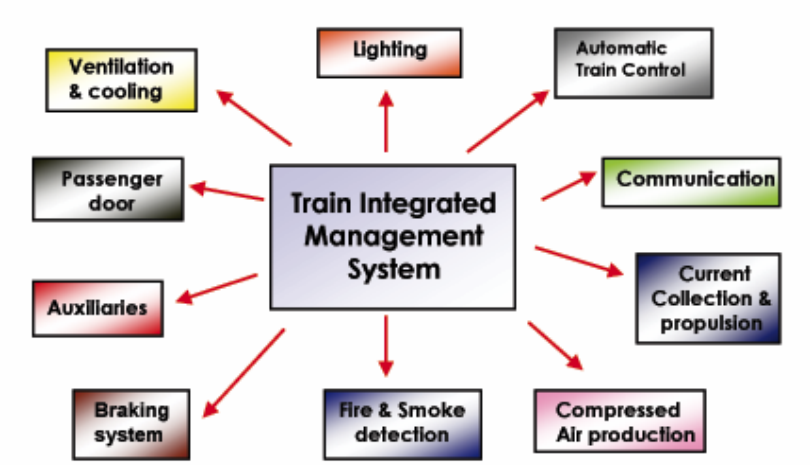

Figure 5.3: TIMS and major sub-systems (adopted from RTI (2002))

A pick-up shoe mounted at the under carriage of the MC-car collects 750 volts dc power supply from the 3rd rail laid along the side of the rail track. A propulsion system converts the supply from 750 volts dc to a variable voltage/ frequency three-phase ac supply and delivers it to the traction motors to drive the train. An auxiliary supply invertor and Delta to Star connected transformer located at the under carriage of the T-car convert the supply to provide 400 volts ac and 230 volts ac to all the auxiliary equipment. 400 volts 3 phase power supply is required for the operation of air-conditioning module, battery chargers and the main compressor drive motor. A set of batteries and battery charger are provided on each car to supply 110 volts dc power for the control systems.

5.1.1 Car interior design

The seating arrangement in the MC-car and T-car are shown in Figure 5.4 and Figure 5.5 respectively. The MC-car has 50 seats while the T-car has 46 seats and spaces for two wheel chairs. The design capacity of the train is 960 passengers including the standing spaces.

The passenger seat is made of moulded FRP polyester and is fixed to an aluminium frame. The FRP polyester is treated with flame retardant additive to improve the resistant against unwanted fire. The sides of each set of row of seats are against the sidewall and/or the glass screen.

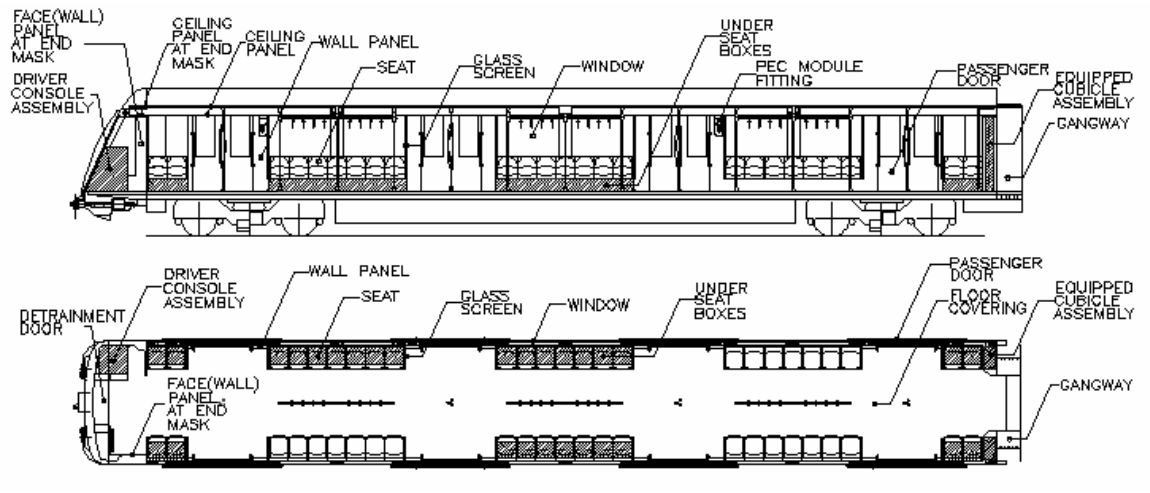

Figure 5.4: MC-car – Side and plan views (adopted from Alstom (2001a))

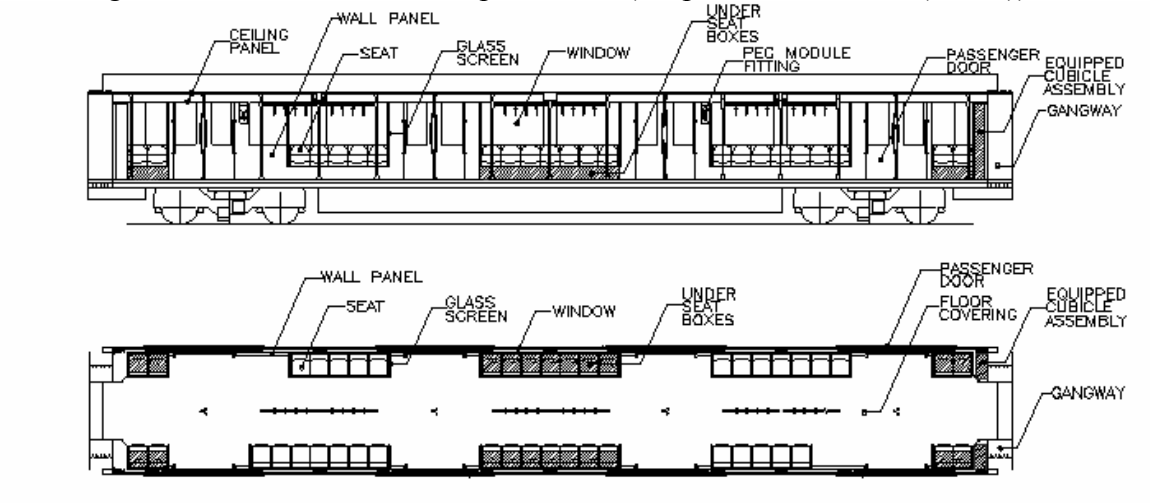

Figure 5.5: T-car - Side and plan views (adopted from Alstom (2001a))

The under seat boxes, located under designated seat locations, and the equipped cubicle assemblies, located at the right-hand end of the train cars, housed the electrical and electronic equipments. The Passenger Emergency Communication (PEC) module fitting, located at alternate door, housed the PEC. The PEC is used for direct communication with the OCC during emergency. These three components are also made of FRP polyester.

The walls and ceiling panels are made of aluminium with a thin coat of powder paint on its exposed surface. The noise and temperature insulation layer for the wall and ceiling consists of glass wool. Both sides of the passenger door are made of aluminium panels with glass wool sandwiched in between.

Each car has two air-con evaporator units housed within the roof duct. The air-con duct is made of glass wool with the outer surface covered with aluminium paper sheet. The air-con supply slot diffusers run along each side of the car with the air-con return grilles located near the two ends of each car. The air-con diffusers and grilles are made of aluminium. Lighting is provided by fluorescent tubes under diffusers. Lighting strips run the full length of each car on each side of the car next to the air-con diffusers.

The floor covering is made of styrene butadiene, a type of synthetic rubber. The floor covering is also treated with flame retardant additive.

The main components for the gangway are the bellows (Inner and Outer). The bellows (Inner) and bellows (Outer) are made of WPE Vamac compound, a type of elastomer material. The bellows (Inner) and bellows (Outer) are distinguished by their colour, which is grey and black respectively as shown in Figure 5.6. The inner surface of the gangway is protected with aluminium panel and therefore the bellows will not be exposed. The panel can be seen in Figure 5.7.

Figure 5.6: Gangway – Bellows (Inner and Outer)

Figure 5.7: Inner surface of gangway

The wall (face) and ceiling panels at the end mask; the detrainment door and the driver console assembly are also made of FRP polyester. All the windows in the train cars are made of laminated safety glass.

5.1.2 Car exterior design

The framework of the car body is made of aluminium with an outer covering of welded aluminium plates. The end mask at the front of the MC-car is made of FRP polyester. The floor construction that separates the under carriage equipment from the train car compartment consists of Okoume plywood floor hut assembly and steel under frame. The floor construction is fire rated to at least 45 minutes.

5.2 Fire protection systems onboard the train

Two types of fire detection system are provided onboard the train. One system used smoke detectors while the other used fire wire. For the smoke detector system, optical smoke detectors are used to monitor the air circulating in the car and to produce an alarm signal when smoke is detected. The source of any smoke may originate from the car interior or be drawn in from the tunnel. For the fire wire system, fire wires are arranged in loops and run through selected equipment cases and cabinets. Excessive heat will cause the insulation to melt and the conductors to short together. This condition is detected by a fire control panel which then generate a fire detection signal. Information and/or alarm will be sent to the OCC for emergency response upon detection of fire.

Besides the fire detection systems, there are also two dry chemical (Class ABC) type fire extinguishers provided in each car for early fire suppression.

5.3 Test methods and performance criteria

Based on information contained in Renie and Prevot (2003), the materials are tested in accordance with test methods and performance criteria specified in NFPA 130 (see Appendix A) or NFF (Normalisation Française – Chapitre F – Ferroviaire (French Standard – Chapter F – Railway rolling stock)) Standards. The applicable NFF Standards are summarised in Table 5.1 below.

S/no	Standard	Title
1	NFF 16-101	Rolling stock - Fire behaviour – Materials choosing (Category A1)
2	NFF 16-102	Rolling stock – Fire behaviour – Materials choosing, application for electric equipments
3	NFF 63-808	Railway Rolling Stock – Halogen free, electrical conductors and cables with thin insulation, and protective layers
4	NFF 63-826	Railway Rolling Stock – Halogen free electrical conductors and cables
5	NFF 63-827	Railway Rolling Stock – Halogen free electrical conductors, class 120°C

Table 5.1: Applicable NFF Standards

5.4 Train cars fire load schedule

Based on the information contained in Renie and Prevot (2003), the fire loads of the combustibles in the MC-car and the T-car are summarised in Table 5.2 and Table 5.3 below. The information will be used for HRR estimation based on traditional method in Chapter 10 of this report. From Table 5.2 and Table 5.3, it can be seen that the seat (including other components that are made of FRP polyester) and the floor covering represent the greatest percentage of above floor fire load found in the train. The paint is used on the interior and the exterior surfaces of the cars and is included as separate item in Table 5.2 and Table 5.3, therefore the fire load for the wall, the ceiling and the door panels are shown as nil. The fire load contribution from the paint is found to be insignificant compared with the fire loads from other exposed surface materials mentioned above.

As for the fire load below floor, the main contributors are the wire insulation and the battery frame. The contributions from other components are found to be comparatively lower.

Designation	Location	Main material	Heat of combustion (MJ / Kg)	Weight per car (Kg)	Fire loading per car (MJ)
MC-car fire load above floor					
Seat (including underseat boxes)	Car interior	FRP polyester	13.0	306	3970
Equiped Cubicle Assembly	Car interior	FRP polyester	16.9	36	612
PEC Module Fitting	Car interior	FRP polyester	12.6	21	263
End Mask (80%)	Car interior and exterior	FRP polyester	13.9	136	1890
Driving Console Assembly (including wall (face) and ceiling panel)	Car interior	FRP polyester	12.5	94	1182
Detrainment Door	Car interior	FRP polyester	19.5	85	1658
Floor covering	Car interior	Styrene butadiene	17.9	238	4270
Air-con duct	Inside ceiling	Glass wool with the outer surface covered with aluminium paper sheet	5.2	75	385
ACMV miscellaneous items	Inside ceiling and behind wall panel	Fibreglass, Silicon	29.4	23	666
Thermal Insulation	Between wall panel and car body	Glass wool	1.4	61	88
Door Seal	Door	EPDM 772 (Rubber)	27.2	62	1682
Window Seal	Window	SIKATACK PLUS BOOSTER, POLYAMID 6.6, Rubber, Neoprene	27.6	36	991
Gangway (80%)	Gangway	WPE Vamac compound	11.1	141	1562
Electrical components	Mainly concealed inside ceiling and behind wall	Different materials among electrical components	20.3	30	606
Miscellaneous items	Mainly concealed inside ceiling and behind wall	Different materials among miscellaneous items	28.0	23	632

Windows	Car interior	Laminated Safety glass	-	-	-
Wall, ceiling and door panels	Car interior	Aluminium	-	-	-
Paint	Car interior and exterior	Paint	7.9	36	284
		Subtotal	14.8	1402	20743
MC-car fire load for floor					
Floor	Floor	Okoume plywood	33.9	107	3632
		Subtotal	33.9	107	3632
MC-car fire load below floor					
Gangway (20%)	Gangway	WPE Vamac compound	10.6	31	329
End Mask (20%)	Car exterior	FRP Polyester	13.7	58	802
Wire Insulation	Undercarriage	Different materials	19.9	133	2640
Battery frame	Undercarriage	Plywood NAVYRAIL (XSPD)	35.1	69	2433
Pneumatic, Brake System and Bogie Equipment	Undercarriage	Paint, plastic, rubber	28.3	44	1257
Electrical components	Undercarriage	Different materials among electrical components	20.6	4	74
Miscellaneous items	Undercarriage	Different materials among miscellaneous items	9.9	36	357
		Subtotal	21.0	376	7892
			17.1	1885	32267

Note: Fire load for gangway and end mask have been splitted into two parts: 80% of the fire load is above floor and 20% is below floor.

Table 5.2: Fire loads of the combustibles in the MC-car

Designation	Location	Main material	Heat of combustion (MJ / Kg)	Weight per car (Kg)	Fire loading per car (MJ)
T-car fire load above floor					
Seat (including underseat boxes)	Car interior	FRP polyester	13.0	281	3644
Equiped Cubicle Assembly	Car interior	FRP polyester	16.3	68	1113
PEC Module Fitting	Car interior	FRP polyester	12.5	27	332
Floor covering	Car interior	Styrene butadiene	17.9	244	4376
Air-con duct	Inside ceiling	Glass wool with the outer surface covered with aluminium paper sheet	5.2	95	492
ACMV Misc Items	Inside ceiling and behind wall panel	Fibreglass, Silicon	29.6	20	598
Thermal Insulation	Between wall panel and car body	Glass wool	1.5	64	93
Door Seal	Door	EPDM 772 (Rubber)	27.2	62	1681
Window Seal	Window	SIKATACK PLUS BOOSTER, POLYAMID 6.6, Rubber, Neoprene	27.6	41	1134
Gangway (80%)	Gangway	WPE Vamac compound	11.0	287	3147
Electrical components	Mainly concealed inside ceiling and behind wall	Different materials among electrical components	21.6	22	485
Miscellaneous items	Mainly concealed inside ceiling and behind wall	Different materials among miscellaneous items	28.4	18	505
Windows	Car interior	Laminated Safety glass	-	-	-
Wall, ceiling and door panels	Car interior	Aluminium	-	-	-
Paint	Car interior and exterior	Paint	7.9	36	284
		Subtotal	14.1	1265	17884

T-car fire load for floor					
Floor	Floor	Okoume plywood .	33.6	113	3789
		Subtotal	33.6	113	3789
T-car fire load for below floor					
Gangway (20%)	Gangway	WPE Vamac compound	10.6	62	658
Pneumatic, Brake System	Undercarriage	Paint, plastic, rubber	26.1	30	779
Wire Insulation	Undercarriage	Different materials	19.4	226	4381
Battery frame	Undercarriage	Plywood NAVYRAIL (XSPD)	35.1	69	2433
Electrical components	Undercarriage	Different materials among electrical	17.9	3	62
Miscellaneous components	Undercarriage	Different materials among misc items	10.2	36	369
		Subtotal	20.4	426	8683
			16.8	1805	30355

Note: Fire load for gangway has been splitted into two parts: 80% of the fire load is above floor and 20% is below floor

Table 5.3: Fire loads of the combustibles in the T-car

5.5 Tunnel geometries

CCL will be entirely underground. The concrete tunnel is either constructed by cut and cover technique or by boring using tunnel-boring machine (TBM). The advantages of the latter method are that it can avoids almost any disturbance to existing streets and buildings; and the need to carry out diversion of utilities commonly buried not far below city streets.

A typical cut and cover tunnel section on a straight alignment is shown in Figure 5.8 and a typical bored tunnel section on a straight alignment is shown in Figure 5.9. As shown in the Figures, the side walls of the tunnel are the tunnel services such as tunnel drainage pipe, tunnel lighting, power supply cables, signalling and communication cables, etc. The lower left hand side of the Figures show the 3rd rail which carry the electrical power supply for the train as discussed earlier. The lower right hand side of the Figures show a 0.8 m wide tunnel walkway which is used by authorised staff when maintaining / inspecting services during or after revenue hour.

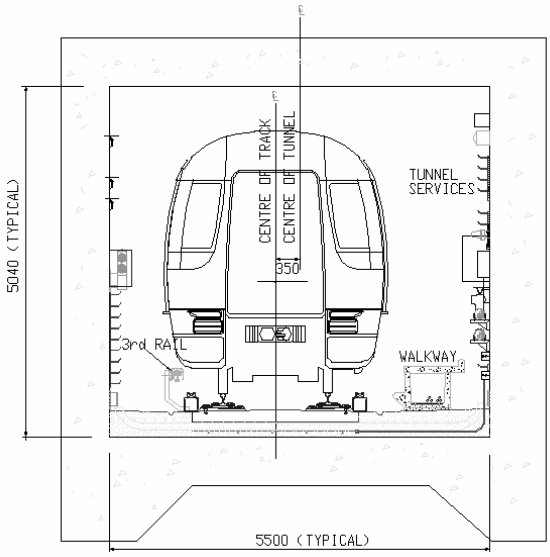

Figure 5.8: Typical cut and cover tunnel section on a straight alignment (adopted from Alstom (2001a) and Alstom (2001b))

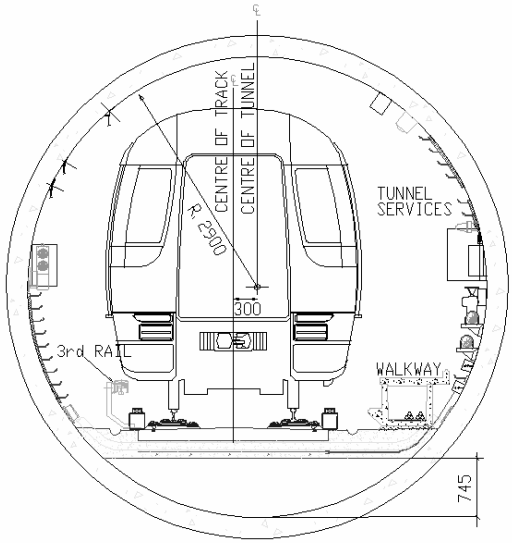

Figure 5.9: Typical bored tunnel section on a straight alignment (adopted from Alstom (2001a) and Alstom (2001b))

6 Design fire scenarios

This Chapter discusses the possible fire scenarios for the CCL metro train. The credible fire scenarios are identified and simulated using FDS to identify fire locations that will result in fire with the highest fire severity, assess the fire development and predict the HRR.

A three-step process is applied to identify the credible fire scenarios. The first step involves review of existing fire statistics data of metro train fires. This will allow the common fire scenarios to be identified. A few simple but important questions can be answered in this step e.g. the cause of the fire, the type, size and location of the ignition source. The second step defines the fire scenarios for the simulation and the third step predicts how the fires could probably develop.

6.1 Fire statistics

No metro train fire incident was reported in Singapore since the first metro line opened in Nov 1987 (Soo 2005; Tan 2005a). In order to determine the main causes of fires in metro trains, it is necessary to use data from other countries e.g. USA, UK, etc. Appendix B provides a compilation of major metro train fires around the world from 1970 to 2003. The survey has revealed three causes of fires:

a) An accident due to a derailment or a collision followed by an electrical short circuit
b) Electrical faults either in the interior or exterior of metro train car
c) Arson (Usually in the metro train car interior)

Fire due to a derailment or a collision followed by an electrical short circuit was rare (only one incident – Montreal, Canada, 12 Dec1971), in line with the finding by Briggs et al. (2001a) that it only occurred in very old vehicles. Fire due to electrical faults and arson were the main causes of metro train fires which inline with the statistical data complied by Tipping (2004). Statistical data complied by Tipping (2004) is shown in Table 6.1 for easy reference.

Cause of fire	Frequency	%
Arson fires (interior)	145	68
Electrical faults (interior)	8	4
Small Fires (interior)	2	1
Electrical faults (undercarriage)	57	27
Total	212	100

Table 6.1: Source of fire (adopted from Tipping (2004))

Analysing the data in Appendix B revealed that beside electrical faults, for interior car scenarios, the ignition sources ranged from discarded cigarettes to flammable liquid; and the locations of ignition sources were usually on the seat or on the floor. For exterior fire scenarios, short circuit and overheating of equipment in the undercarriage were the main causes of fires.

Statistical analysis of the fires occurring in interior of rail cars by Briggs et al. (2001a) indicated that fires caused by arson on a seat due to a cigarette lighter or burning newspaper were the most probable. They have also identified high temperature in electrical equipment due to electrical defects as one of the common fire scenarios. Munro et al. (2002) analysed the data for rail vehicles fires from New South Wales rail safety incident database and concluded that seat fires had the highest consequences compared to other fire scenarios such as those due to electrical defects, started on the floor or occurred at the exterior of the rail car.

Even though statistical data could provide useful information for developing fire scenario, Munro et al. (2002) and Peacock et al. (2002) have stressed that it would be inappropriate to select fire scenarios solely based on statistical data as it was only an indicator of the scenarios that have occurred. Relevant expert judgement would be required to identify a foreseeable (Munro et al. 2002) but potentially the most dangerous (Peacock et al. 2002) or with the highest consequences fire scenario. In this project, expert opinions were sought by having discussion with staff from the transit regulator when developing the fire scenarios.

6.2 Fire scenarios

From the statistical data, discussion with staff from the transit regulator, conclusions drawn from the literature reviews of fire safety studies of rail cars and detailed analysis of the train cars construction, the following common fire scenarios for train cars are identified.

Common interior fire scenario

Common fire scenario '1' -	Fire due to burning newspaper or flammable liquid placed on the seat in the centre of train cars (Arson)
Common fire scenario '2a' -	Fire due to burning newspaper or flammable liquid in the corner next to the face panel and driver console assembly (Arson)
Common fire scenario '2b' -	Overheating of electrical equipment at the driver console assembly (Electrical fault)

Note: Common fire scenarios '2a' and '2b' are being investigated as one single fire scenario, which later will be known as 'Common fire scenario '2' - Fire in the corner next to the face panel and driver console assembly (Arson or electrical fault)'.

Common exterior fire scenario

Common fire scenario '3' -	Undercarriage fire due to electrical short circuit or overheating of light voltage (LV) equipment or battery charger (Electrical fault)

These common fire scenarios are consistent with past metro train fires. The scenarios consider observations from real-scale tests that seat and wall linings are important factors in fire growth (Braun 1975; Braun 1978). The locations of ignition source are selected taking into account the locations of combustibles in the train car. The ignition source types simulate fires that have or could credibly occur.

In all the above common fire scenarios, train is disabled in the tunnel. A non-incident train is stopped behind the incident train and therefore required the emergency tunnel ventilation airflow to be set in a direction that prevents smoke from flowing towards the non-incident train regardless of the train fire location. This is probably the worst situation that could happen during a metro train fire incident.

The fire scenario is illustrated in Figure 6.1. Appendix C of this report provides additional information on the emergency tunnel ventilation system operating directions for various fire scenarios, which can be referenced to for additional information.

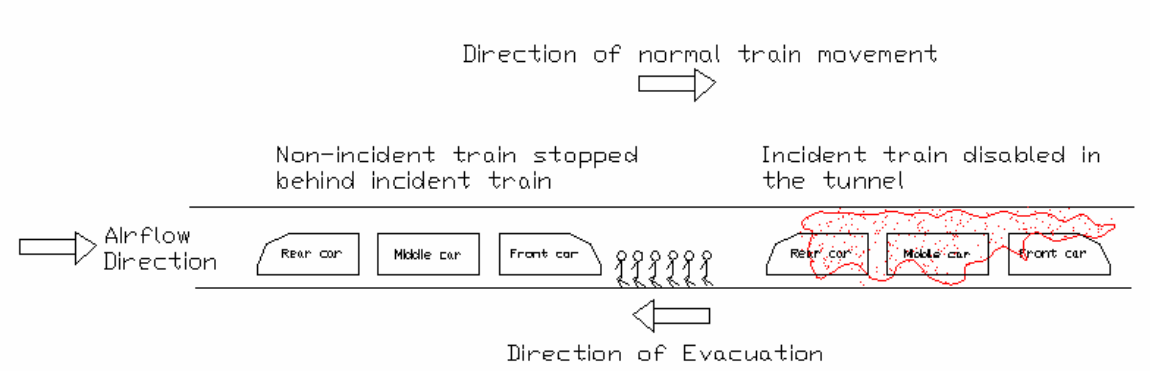

Figure 6.1: Train fire in a tunnel

It is notable that the above only addressed the type and location of the credible ignition source in a train car and the emergency tunnel ventilation mode during the fire incident. It did not take into consideration if the train doors were opened or closed; or the windows would fail. These are important factors that would influence the fire development. Furthermore the location where the fire initiated in the three-car train has also not been considered up to this point.

This lead to the following questions to be answered:

a) Is the detrainment door(s) opened? If yes, one end or two ends?
b) Is the passenger door(s) opened? If yes, how many doors opened?
c) Would the window(s) fail? If yes, how many windows failed?
d) Fire located in rear car, centre car or front car[1]?

1 Front car refers to the front MC-car in the direction of train movement. Centre car refers to the T-car and rear car refers to the MC-car at the rear of the train. These terms will be used throughout this and the later Chapters.

The answers for the first two questions will depend on situations. Even though evacuation is normally through the detrainment door (in a direction whereby smoke free path is created by the emergency tunnel ventilation system), it is still possible for the passengers to open the detrainment door at the other end of the train by simply activating a push button on it as shown in Figure 6.2. They could also escape through the passenger door by turning on the emergency handle switch (EHS) beside each door as shown in Figure 6.3. According to the emergency procedure by the train operator, the train doors should be closed (by the staff) after the evacuation if it is possible and safe to do so (Tan 2005a).

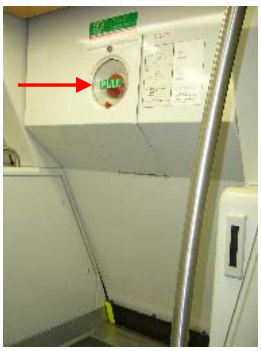

Figure 6.2: Detrainment door push button

Figure 6.3: Emergency handle switch (EHS)

The possibilities of failure for the window depend on the properties of the glass, the compartment gas temperature and the seal that holds the glass. Laminated safety glass is used for the window and door glass but there is no information on laminated safety glass performance under fire condition. The only information available is their performance during cold (normal) condition. It has been stated that when laminated safety glass fractured under impact, the broken fragments of the glass will remain bond to the plastic interlayer (Anon 2004b). This information is inadequate to assure that the safety glass will not fail because the plastic interlayer may melt during the fire. There is also a possibility of failure due to the seal that holds the glass (Mauser 2005).

Fire can be in the rear car, middle car or front car (see Figure 6.1). Rear car fire is likely to have a high consequence if the detrainment doors are opened, as fire is likely to propagate in the direction of airflow. Middle car fire might result in higher consequence as fire could spread in two directions when the detrainment doors are closed. Front car fire however is likely to have less consequence compared to the other two locations and therefore will not be considered further. Note that for middle car fire, only fire on the seat (fire scenario 1) and undercarriage fire (fire scenario 2) are applicable.

The possible sub-fire scenarios that could probably occur can be expanded as shown in Figure 6.4 and Figure 6.5. Figure 6.4 shows the possible sub-fire scenarios for rear car fire while Figure 6.5 shows the possible sub-fire scenarios for middle car fire. At this stage, it is only limited to answering yes or no to the first three questions.

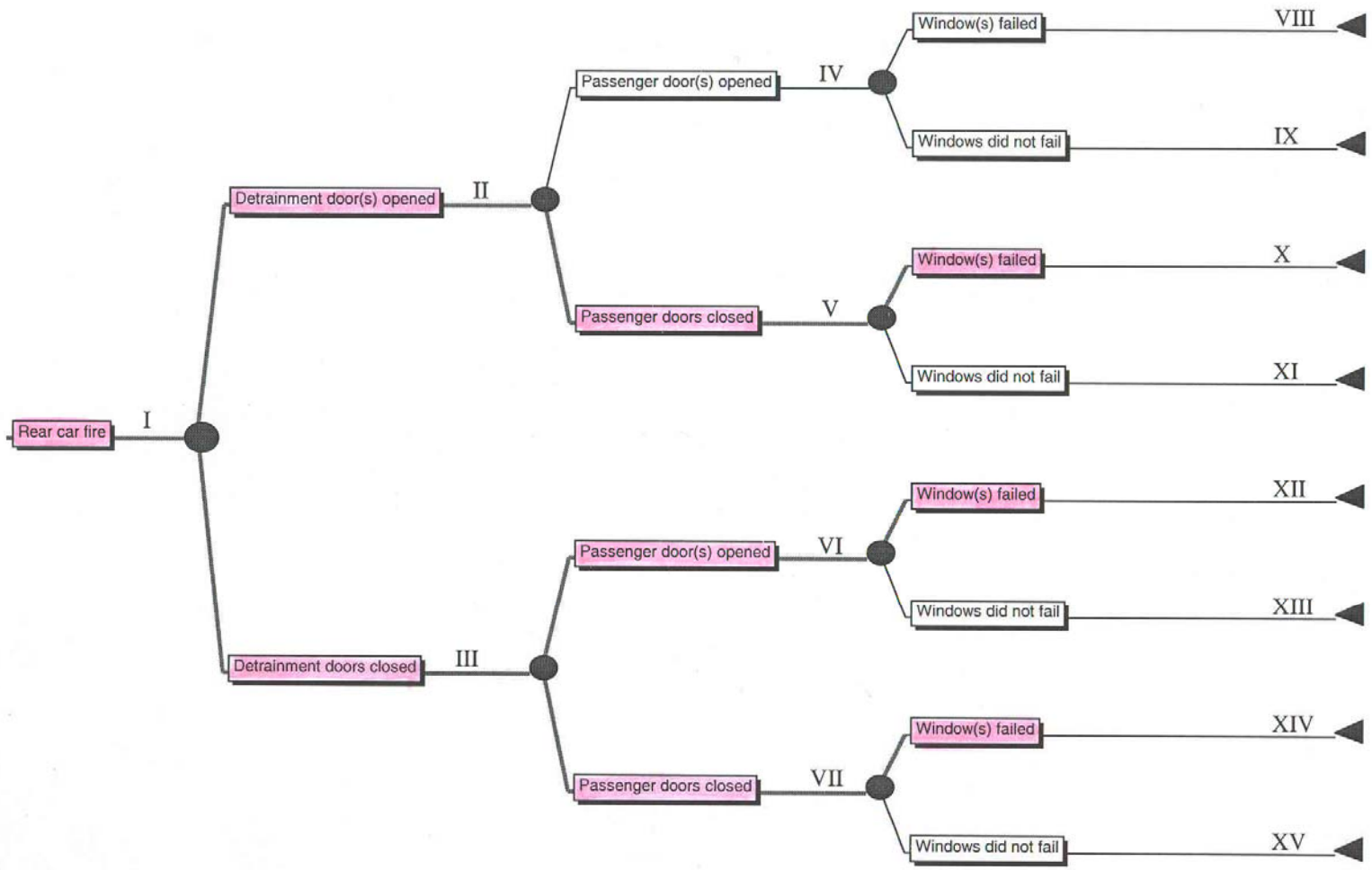

Note : For common fire scenarios '1', '2' and '3'.

Figure 6.4: Possible sub-fire scenarios for a rear car fire

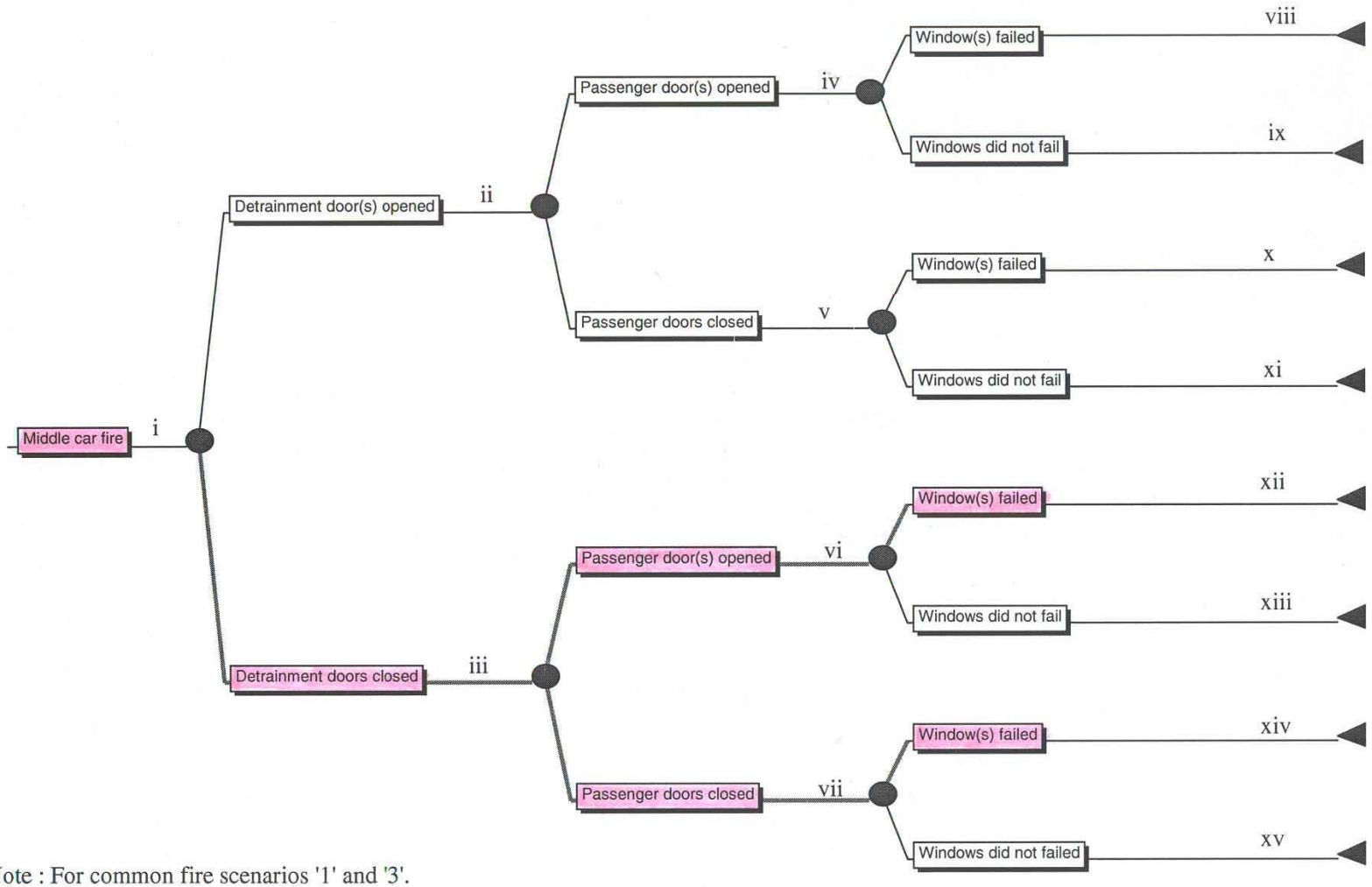

Note : For common fire scenarios '1' and '3'.

Figure 6.5: Possible sub-fire scenarios for a middle car fire

It can be seen from Figure 6.4 and Figure 6.5 that each common fire scenario (i.e. common fire scenarios '1', '2' and '3') can expand to eight sub-fire scenarios. It is not feasible and practical to simulate all possible scenarios and therefore it is necessary to focus on scenarios with the highest consequence and/or of particular interest.

The following five possible sub-scenarios are considered:

Real car fire

Common fire scenarios '1', '2' and '3'	Sub-scenario 'A' – (path I-II-V-X)	Both detrainment doors opened, all passenger doors closed, window failure
	Sub-scenario 'B' – (path I-III-VI-XII)	Both detrainment doors closed, 1st and 4th passenger doors facing the walkway opened, window failure
	Sub-scenario 'C' – (path I-III-VII-XIV)	All doors closed, window failure

Middle car fire

Common fire scenarios '1' and '3'	Sub-scenario 'D' – (path i-iii-vi-xii)	Both detrainment doors closed, 1st and 4th passenger doors facing the walkway opened, window failure
	Sub-scenario 'E' – (path i-iii-vii-xiv)	All doors closed, window failure

In all the sub-scenarios, it is assumed that window failure is possible. The failure might be due to the safety glass itself or the seal which holds the glass. This is the most onerous scenario that could happen as window failure will provide ventilation for the fire to grow to peak. Window failure will be simulated by assuming that window will fail when the 'detectors' located at the window (in the model) reach a specified temperature. This will be discussed in detail in Chapter 7.

In sub-scenario 'A', detrainment doors at both ends of the train are assumed to be opened. This sub-scenario is selected because it allows the forced (tunnel) ventilation airflow to 'fan' the fire thus causing it to propagate in the direction of airflow as mentioned earlier. Having passenger doors opened might reduce the compartment temperature as hot gases could escape from those doors. If too much hot gas escapes, it might not or would take a longer time to attain full car involvement. Therefore it is more conservative to assume the passenger doors are closed.

Sub-scenario 'B' assumes both the detrainment doors are closed while the 1st and 4th passenger doors of the train car are opened. 1st and 4th passenger doors are opened so that to resemble the opening condition of sub-scenario 'A' but to simulate scenario whereby there is little influence from the forced ventilation on the fire. It is evident from studies by Carvel et al. (1999a); Carvel et al. (1999b); Carvel et al. (2001b) and Carvel et al. (2001d) that forced ventilation might not necessary promote fire growth. This sub-scenario allows the effect of forced ventilation to be investigated. Most importantly, this scenario can also used to represent a train fire scenario at the station trackway i.e. the section of track next to the station platform. For a train fire at the station trackway, the passenger doors will be opened for evacuation. In CCL design, the tunnel ventilation fans at both ends of the station will be operated in exhaust mode (see Appendix C). There is little influence from the forced ventilation on the fire during a train fire scenario at the station trackway based on study by Hettinger and Barnett (1991) and therefore can be represented by sub-scenario 'B'.

Sub-scenario 'C' assumes that there is sufficient air within the compartment for fire to grow. Because hot gases and smoke are contained within the low ceiling compartment, the gas temperature might accelerate and cause window failure. This sub-scenario is included to examine whether this may occur; and if it does occur, what is the fire severity?

Sub-scenarios 'D' and 'E' are similar to sub-scenarios 'B' and 'C' except that fire location is at the middle car. These two fire scenarios might result in higher consequence because fire could spread in two directions. Note that detrainment doors opened and passenger doors closed sub-scenario is not studied for middle car. This is because the forced ventilation is likely to cause the fire to propagate in the direction of airflow and therefore resulting in only up to two cars involved in the fire compared to three in other sub-scenarios. For sub-scenario 'D', it can also be used to represent a train fire scenario at station trackway for the same reason as discussed earlier.

In summary, the fire scenarios to be studied in this project are tabulated in Table 6.2 for easy reference. The fire scenarios to be studied are named according to the common fire scenario and sub-scenario combinations as shown in the last column of Table 6.2. The various fire scenarios will be simulated using FDS to identify fire locations that will result in fire with the highest fire severity, assess the fire development and predict the HRR.

S/no	Description of fire location and type of fire	Description of ventilation condition	Fire scenario
1	Rear car, fire on the seat (Arson)	Both detrainment doors opened, all passenger doors closed	1A
2	Rear car, fire in the corner (Arson or electrical fault)	Both detrainment doors opened, all passenger doors closed	2A
3	Rear car, undercarriage fire (Electrical fault)	Both detrainment doors opened, all passenger doors closed	3A
4	Rear car, fire on the seat (Arson)	Both detrainment doors closed, 1st and 4th passenger doors facing the walkway opened	1B
5	Rear car, fire in the corner (Arson or electrical fault)	Both detrainment doors closed, 1st and 4th passenger doors facing the walkway opened	2B
6	Rear car, undercarriage fire (Electrical fault)	Both detrainment doors closed, 1st and 4th passenger doors facing the walkway opened	3B
7	Rear car, fire on the seat (Arson)	All doors closed	1C
8	Rear car, fire in the corner (Arson or electrical fault)	All doors closed	2C
9	Rear car, undercarriage fire (Electrical fault)	All doors closed	3C
10	Middle car, fire on the seat (Arson)	Both detrainment doors closed, 1st and 4th passenger doors facing the walkway opened	1D
11	Middle car, undercarriage fire (Electrical fault)	Both detrainment doors closed, 1st and 4th passenger doors facing the walkway opened	3D
12	Middle car, fire on the seat (Arson)	All doors closed	1E
13	Middle car, undercarriage fire (Electrical fault)	All doors closed	3E

Note: Forced ventilation and window failure will be simulated for all scenarios.

Table 6.2: Summary of fire scenarios to be simulated

It is important to highlight that the factors that influence the fire development include:

a) Amount and type of fuel, its location, orientation in the train.
b) Train and tunnel geometries.
c) The material properties of the train boundaries.
d) The size and location of the ignition source.
e) The size and location of openings.

Although this project attempts to address all these factors in the simulation, it is not possible to deal with the unknown. The greatest unknown is probably the items (fuels) being brought onto the train by the passengers. One of the possible items that might be brought onto the train is the luggage bag. Peacock et al. (2002) quoted a peak HRR of 200 kW for a burning luggage. Morgan and De Smedt (2002) quoted a peak HRR of 500 kW for two carry-on bags touching and burning simultaneously. The HRR curve for the latter is shown in Figure 6.6. From the Figure, it is found that the average HRR is approximately 200 kW with a burning period of about 1800 s.

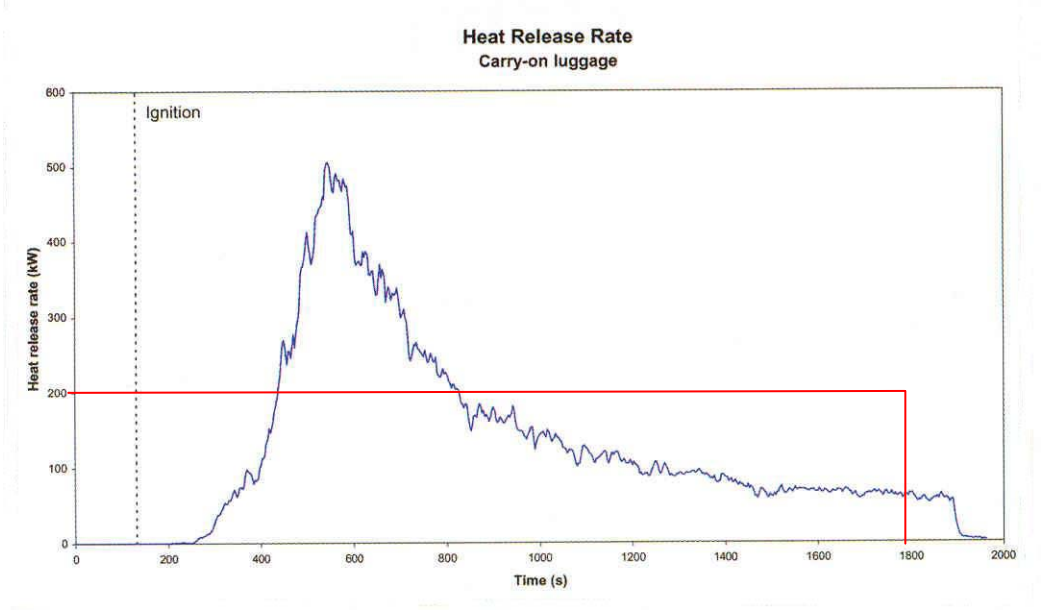

Figure 6.6: HRR curve of two carry-on bags (adopted from Morgan and De Smedt (2002))

As items brought onto the train will be scattered and not piled high in one localised location (note: there is no luggage rack in CCL train), it is unlikely that all the items would ignite at once and contribute significantly to the HRR of the metro train. However, the author does have to acknowledge that the item brought onto the train might contribute to the fire growth. Therefore in considering the ignition source for

simulation, the fire size of the ignition source is assumed to be constant throughout the assumed burning duration to account for the contribution of this unknown. The ignition source fire size and burning duration for the simulations are discussed in Chapter 7 of this report.

6.3 Fire development

Once the fire scenarios have been identified, the next step is to predict how they could be developed.

A typical fire development process for a metro train is shown in Figure 6.7. The worst fire scenarios will be to follow the path from a to k or aa to k shown in Figure 6.7. The fire starts with ignition source, which might be in the interior or exterior of the train car. If the fire is unattended or not suppressed, and there is sufficient amount ventilation and fuel, fire would grow in intensity. For interior car fire, the first item ignited by the ignition source would be the seat back or the face panel and the driver console assembly depending on the fire scenario in concern. For an exterior fire, the first item ignited is likely to be the wiring. For exterior fire scenario, the fire needs to propagate through the 45 minutes fire resistance rated floor before it could burn in the car interior. To allow for the worst, it is assumed that propagation through floor is possible.

For all the scenarios, fires grow in the interior car could be postulated. Fires grow can be either by increased burning rate, by flame spread over the first ignited item, or by ignition of nearby surface. Gas temperature in the interior car increases and reaches about 600°C. With sufficient amount of ventilation and fuel, the fire could progress to full car involvement in which all exposed combustible surfaces ignite simultaneously, with a very rapid increase in HRR. This very rapid and sudden transition from a growing fire to a fully developed fire is called flashover (Karlsson and Quintiere 2000).

When the burning car is fully involved in the fire, the heat is sufficient to spread the fire to adjacent cars since the there is no door installed between the train cars. The fire development process repeats in the succeeding cars. Not all cars might be fully involved at the same time. When the second and/or third cars are fully developed, the first burning car might be in its decay phase.

Observations of actual metro train fires have shown that the flame spread between cars occurs above the floor line. The fire resistance rated floor would usually prevent the fire from spreading to the below floor equipment or burning the floor itself (Hettinger and Barnett 1991). This is assumed to be the case in this project.

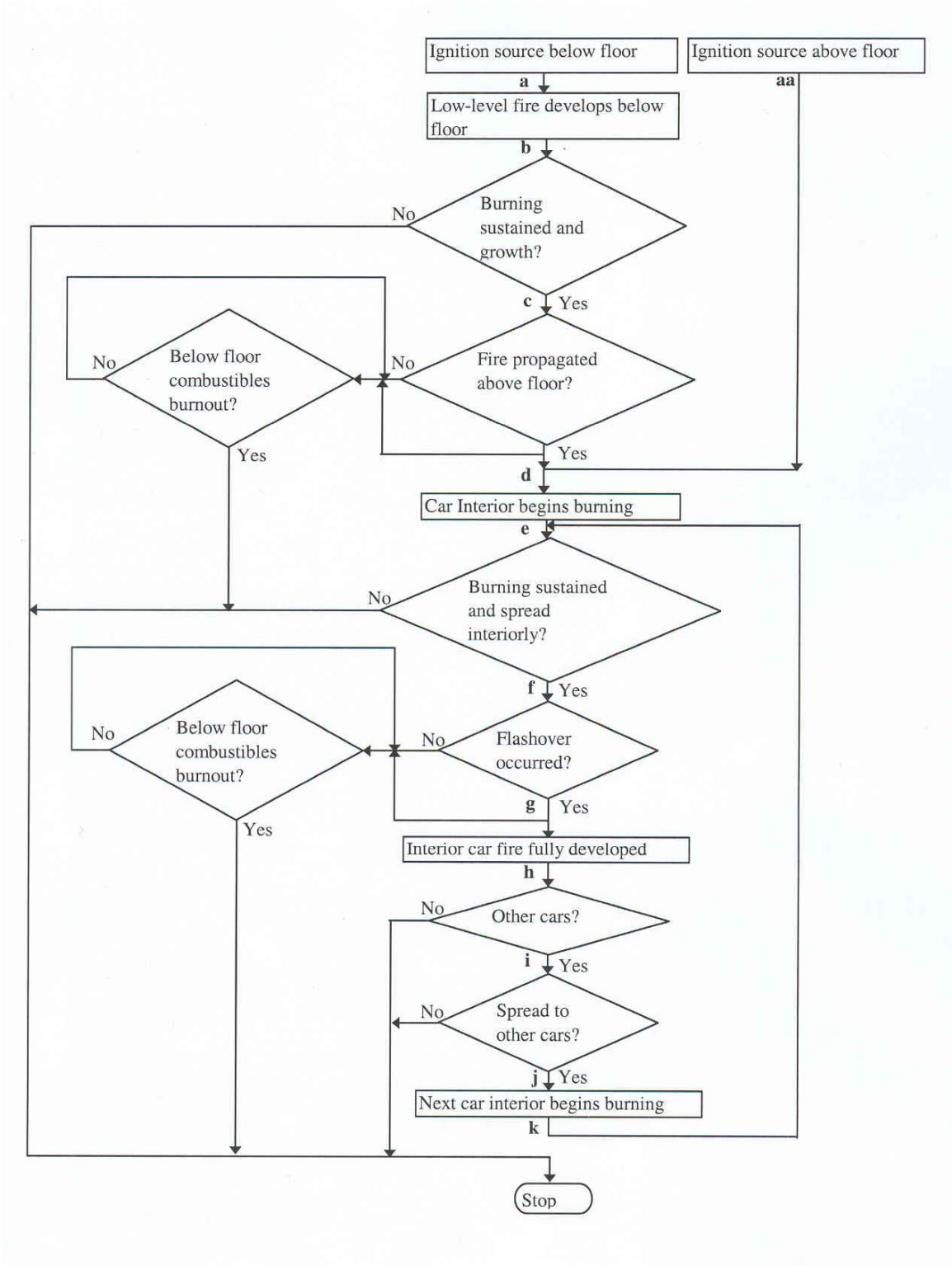

Note:

1) The fire is unattended throughout the burning duration.
2) The fire is contained to the above floor in the second and succeeding cars due to the presence of the fire resistance floor.

Figure 6.7: Typical metro train fire development flow diagram

7 Trial simulations

This Chapter describes the trial simulations carried out. It also presents and discusses the trial simulation results. The trial simulations serve two purposes:

a) Carry out grid sensitivity study to decide on the grid size to be used for the final simulations.
b) Identify any unforeseen issue or problem that may be encountered during the simulations.

The trial simulations were carried out before the Cone Calorimeter tests were conducted. Therefore the material properties were obtained from various references and not from the actual materials. Each simulation would require a couple of days (One to 12 days depending on grid size, fire scenario and computer speed) to complete. The computers used for the simulations were either Intel(R) Pentium(R) 4, 2.8 GHz, 1 GB RAM or Intel(R) Pentium 4(R), 3.2 GHz, 2 GB RAM computers. In order to ensure the material properties inputted for the simulation were appropriate, a number of references were referred to for each material. This is outlined in detail in the later Sections.

Only one car, the MC car, was simulated. Therefore only fire scenarios at the rear car were simulated. This was to reduce the number of grid cells thus the computation time. Both methods of defining the rate of pyrolysis for fuel surface were used i.e. HRRPUA and heat of vaporisation ΔH_v . For simulation where HRRPUA was prescribed, the FDS data file has been written such that the rate of heat release from the fuel surface followed the Cone Calorimeter HRRPUA curve (of the fuel) once its surface reached the ignition temperature. If heat of vaporisation was prescribed, the burning rate of the fuel would depend on the net heat feedback to the surface from the fire.

7.1 FDS inputs

7.1.1 Geometry

The geometry of the tunnel and the train car were taken directly from the drawings. Due to complexity in modelling some details e.g. curved geometry, a number of assumptions have been made so that to simplify the model. They were:

a) The tunnel geometry and size was based on cut and cover tunnel. There are little difference in the critical velocity and ventilation rate requirement for cut and cover and bored tunnel as the area for the two tunnel types are approximately the same (also see Section 7.1.2) therefore cut and cover tunnel geometry was used.
b) It would be difficult to model the geometry of the train head (of MC car), which is curved in shape. Therefore the train head was modelled as a rectangular shape based on equal volume method.
c) The services in the tunnel were not modelled. It was assumed that the services had little contribution to the fire growth and had negligible effect on the ventilation airflow.
d) The glass screen beside the seat was considered too small a detail to be included in the simulation. It was assumed that it had little effect on the fire growth and spread and therefore was not included in the simulation.
e) Due to limited information on the gangway construction, it was assumed that the gangway's wall and ceiling had the same thickness, density and thermal properties as the wall and ceiling constructions respectively.
f) The undercarriage (below floor) housed different equipment of different size and geometry. As it was not the intent to model fire growth and flame spread in the undercarriage it was not important to have these details captured in the model therefore they were being modelled as concrete block to simplify the model. Note that the floor was also included as part of this concrete block in the model since observations from actual metro train fires have shown that the floor was usually not involved in the fire (except for exterior fire scenario which was dealt with separately (see Section 7.1.3).

The size of the computational domain was 26.6 m long by 5.5 m wide by 4.4 m high. Three grid sizes, 300 mm, 200 mm and 150 mm, were used to investigate the sensitivity of results. There was attempt to reduce the grid size further but it proved too much for the computer to cope with. Therefore it was decided that only these three grid sizes be used for the simulations. In order to capture the important features such as details around the window which are much smaller than the defined grid size, the TRNY and TRNZ namelist groups in FDS were used to stretch the grids in y and z-directions so that the details would be included in the model. The simulation time specified for each simulation was 1800 s.

A sample FDS data file for the simulations can be found in Appendix F of this report.

7.1.2 Vents

Forced (tunnel) ventilation

Forced (tunnel) ventilation was simulated. In order to obtain the ventilation rate, the critical velocity V_{cr} needed to be calculated. From Associated Engineers (1980), critical velocity for a rail tunnel is given by:

$V_{cr} = K_{grade}\left(\frac{gH_t\dot{Q}x1000}{Fr_{cr}\rho_\infty c_p A_A T_g}\right)^{\frac{1}{3}}$	Equation 7.1

$T_g = \frac{\dot{Q}}{\rho_\infty c_p A_A V_{cr}} + T_\infty$	Equation 7.2

Where H_t is the tunnel height in m, $\dot{Q}$ is heat release rate in MW, A_A is the annular area (i.e. tunnel cross-sectional area minus train cross-sectional area) in m^2, Fr_{cr} is the critical value of the Froude Number (for a flow ventilating a fire = 4.5), T_g is the gas temperature in K and K_{grade} is grade correction factor (dimensionless) given by:

$K_{grade} = 1 + 0.0374(Grade)^{0.8}$	Equation 7.3

Where Grade is the gradient in °.

The iteration solution of Equations 7.1 and 7.2 determines the critical velocity. This criterion determines the minimum steady-state velocity of the ventilating air moving toward the fire that would require to prevent back-layering. Note that the criterion determines the required air velocity during the fire and not the air velocity in the absence of the fire which can be substantially different. The ventilation rate can then be calculated since the tunnel and train cross-sectional areas are known.

The tunnel ambient temperature T_∞, density ρ_∞ and specific heat c_p were assumed to be 305 K (32°C), 1.2 kg/m^3 and 1.0 kJ/kgK respectively. The tunnel section was assumed to be on flat ground, therefore no grade correction factor was required i.e. K_{grade} = 1. The tunnel and train cross-sectional dimensions were taken directly from the drawings. Table 7.1 below shows the calculated critical velocity and ventilation rate based on cut and cover tunnel and bored tunnel at different HRRs.

HRR	**Cut and cover tunnel**		**Bored tunnel**	
	Critical velocity	**Ventilation rate**	**Critical velocity**	**Ventilation rate**
MW	**m/s**	**m^3/s**	**m/s**	**m^3/s**
5	1.9	27	2.0	29
10	2.2	31	2.3	33
15	2.4	34	2.5	36
20	2.5	36	2.6	37
25	2.6	37	2.7	39
30	2.6	38	2.7	39
35	2.7	39	2.8	40

Table 7.1: Critical velocity and ventilation rate for cut and cover tunnel and bored tunnel

Critical velocity and ventilation rate for cut and cover tunnel and bored tunnel do not vary significantly because the areas for the two tunnel types are approximately the same. Therefore it was decided to model only the cut and cover tunnel as mentioned earlier. Deciding the ventilation rate for the simulation was a more difficult task. From Table 7.1, it can be seen that the ventilation rate varies with HRR, the parameter that is to be predicted from the simulation. In order to proceed with the simulation, an assumption needed to be made. In the end, it was decided to use the ventilation rate based on 10 MW fire as that was the fire HRR used for the design of emergency tunnel ventilation system in CCL (see Section 2.2.1).

The ventilation rate was prescribed in FDS by defining one end of the tunnel (the train head end as shown in Figure 7.1 below) to supply 31 m/s^3 of airflow into the computational domain while the other end (the gangway end as shown in Figure 7.2 below) being defined as open end. To simplify the simulation, 31 m/s^3 was being supplied into the domain at the beginning of the simulation.

Train doors

The detrainment doors and/or passenger doors were opened and/or closed depending on scenarios simulated. For scenarios whereby both the detrainment doors were opened and all the passenger doors were closed, both ends of the MC-car were 'left opened' as shown in Figure 7.1 and Figure 7.2. The velocity across the detrainment door opening was found to be about 1.71 m/s.

For scenarios whereby both the detrainment doors were closed and the passenger doors were opened, the 1st and 4th passenger doors of the MC-car facing the walkway were 'left opened' as shown in Figure 7.3. Note that because only one end (train head end) of the MC-car has detrainment door, a dummy door constructed of concrete was modelled at the other end (gangway) for this scenario. Concrete dummy door was chosen because concrete is non-combustible. The velocity across the passenger door opening was found to be about 0.34 m/s.

Finally for closed doors scenarios, all the doors in the MC-car were in 'closed position'. Concrete dummy door was also modelled at the gangway end of the train car for reason mentioned above. Note that a 100 mm thick floor gap has been provided at the concrete dummy door to simulate leakage within the MC-car compartment for closed doors scenario.

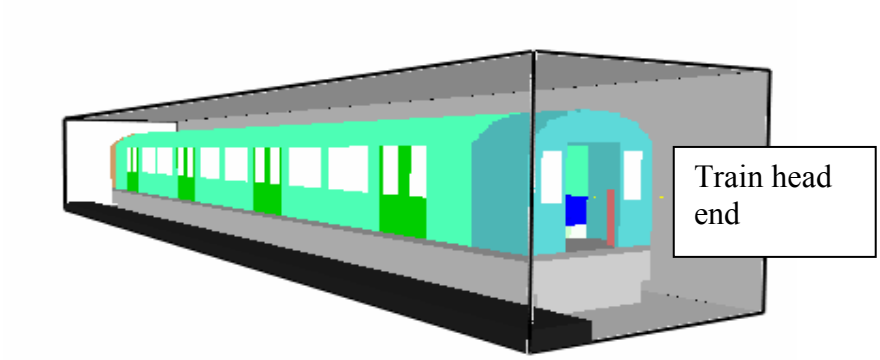

Figure 7.1 Snapshot from Smokeview showing the train head end

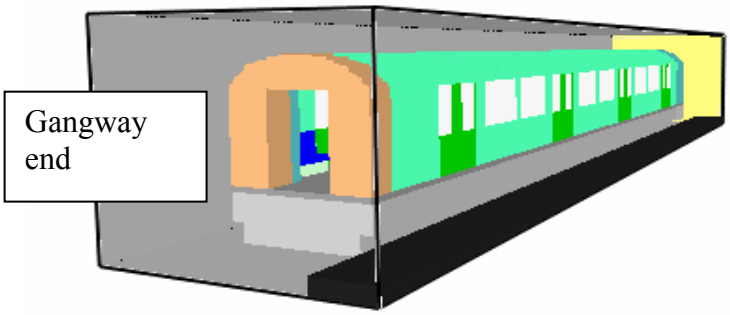

Figure 7.2: Snapshot from Smokeview showing the gangway end

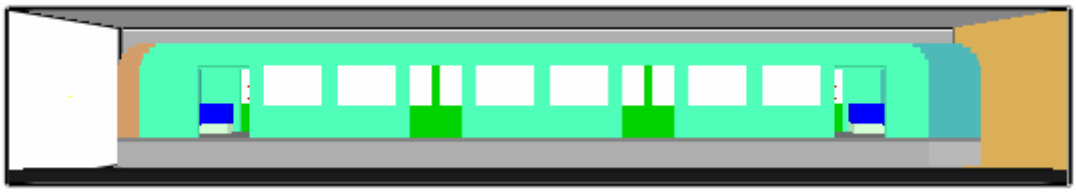

Figure 7.3: Snapshot from Smokeview showing 1st and 4th passenger doors opened

Window failure

Window failure was simulated. The failure may be due to the safety glass itself or the seal which holds the glass. Window failure was simulated by assuming that window will fail when the 'detectors' located at the window (in the model) reach a specified temperature. The temperature was based on research by Shields et al. (1998) who investigated the behaviour of large double glazed units exposed to full-scale office fire. At a compartment gas temperature of 675°C, they reported that the double-glazing window began to fracture and fall off. This temperature was taken as the criterion for window failure in this project. The author recognised that temperature is only one of the many factors that cause window failure when they are heated. But to account for all factors that cause window failure is beyond the scope of this project. This would require a window failure sub-model to be incorporated in FDS. Therefore the above assumption was made for practical reasons.

In the model each window was divided into two equal sections: upper and lower. One 'detector' was located at the centre of the window to open up the upper section and one 'detector' was located at the bottom of the window to open up the lower section. The locations of the 'detector' are illustrated in Figure 7.4 below.

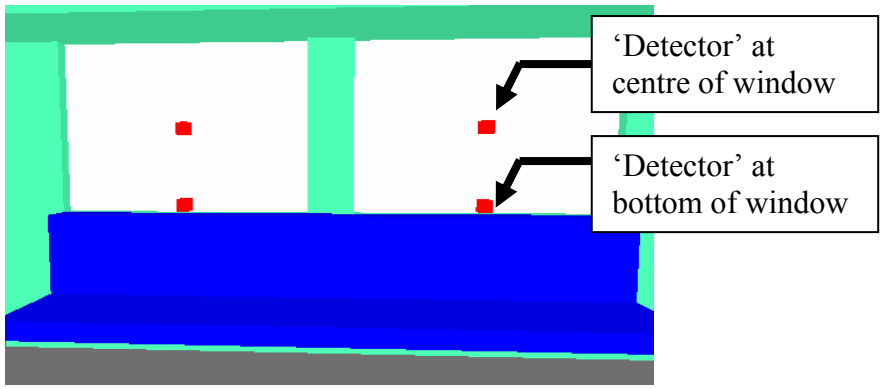

Figure 7.4: Snapshot from Smokeview showing locations of the 'detector'

7.1.3 Ignition sources

Interior fire scenario

From the literature reviewed, for interior car fire scenario, an ignition source fire size that is required to result in significant fire growth and spread is between 150 kW to 200 kW. An ignition source fire size of 200 kW was used for the simulation. This fire size was equivalent to the peak HRR of a burning trash bag or a burning luggage (Peacock et al. 2002). It is also the average HRR of two carry-bags touching and burning simultaneously (see Section 6.2). It is recognized that the credible ignition source such as burning newspaper or flammable liquid may not necessary produce a fire of such intensity. However, a 200 kW ignition source fire size was selected to eliminate the need to conduct exploratory tests for the simulation. The size of the ignition source was assumed to be 0.2 m by 0.2 m and remain constant throughout the simulation to account for the contribution of items being brought onto the train as discussed in Chapter 6, Section 6.2.

Two ignition source locations were considered in the simulation: one on top of the seat in the centre of the car and the other on the floor at one corner of the car. The first ignition source location was to simulate common fire scenario '1' - Fire due to burning newspaper or flammable liquid placed on the seat in the centre of train car (Arson), while the second ignition source location was to simulate common fire scenario '2' - Fire in the corner next to the face panel and driver console assembly (Arson or electrical fault). Figure 7.5 and Figure 7.6 show snapshots from Smokeview for the locations of the ignition sources.

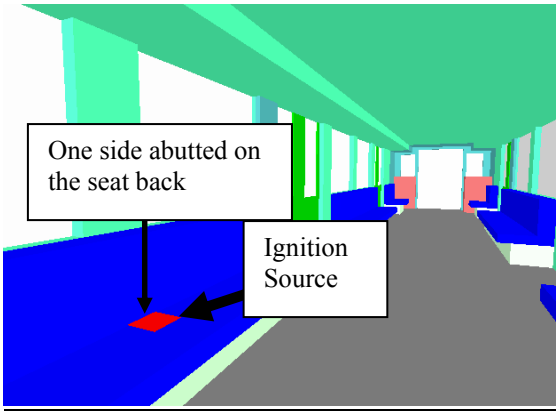

Figure 7.5: Snapshot from Smokeview showing train car interior – Ignition source on top of the seat

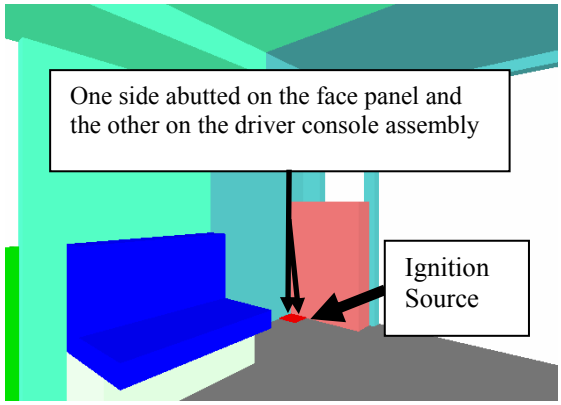

Figure 7.6: Snapshot from Smokeview showing train car interior – Ignition source on the floor

Exterior fire scenario

For exterior fire scenario, it was assumed that the exterior fire (undercarriage fire) has propagated above the fire resistance floor and burned in the car interior. The ignition source fire size, being more difficult to define, was estimated using the traditional method. Traditional method was used since it is the only known method that can be used to estimate the sub-floor components contribution to the fire. In calculating the ignition source fire size using traditional method, it was assumed that the below floor and half the floor were involved when the fire propagated above floor; and the initial fire $\dot{Q}_{\text{int}}$ was 0.7 MW (In line with design scenario – 1989 (see Section 2.2.1)). A combustion efficiency factor χ of 0.7 was included in the calculation (In line with design scenario – CCL, Singapore (see Section 2.2.1)). The formula used to calculate the ignition source fire size is as follow:

$$\dot{Q}_{is} = Ignition\ \ source\ fire\ size = \frac{(Below\ floor\ fire\ load\ (MJ) + \frac{1}{2}\ Floor\ fire\ load\ (MJ))0.7 - Q_{\text{int}}\ (MW)\,x\,1800\,(s)}{3600\,(s)}$$ Equation 7.4

The below floor and floor fire load for MC-car are 7892MJ and 3632MJ respectively. Substituting these values into Equation 7.4, the ignition source fire size equal to:

$$\dot{Q}_{is} = Ignition\ \ source\ fire\ size = \frac{(7892 + \frac{1}{2}(3632))0.7 - 0.7x1800}{3600} = 1.54\ MW = 1540\ kW$$

Some may argue that the ignition source fire size is unreasonably large and such a ignition source fire size will result in materials which are normally hard to ignite and burn to be involved in the fire. Some may even criticise whether the ignition source size is credible. But note that the assumption made for the estimation was that the exterior fire (undercarriage fire) has propagated above the fire resistance floor and burned in the car interior. If it does occur, such a fire size may not be unreasonable. Having such a large ignition source fire size would also allow the fire performance of the metro train under consideration to be tested; and is inline with the objective of establishing the peak HRR for the metro train.

The ignition source location was assumed to be on the floor directly above the battery boxes; battery charger; and the LV and IV box, with a fire area of approximately 3 m by 2 m or 6 m^2, the area occupied by the equipment. The ignition source was assumed to be constant throughout the simulation since this was the duration the exterior fire would last based on the traditional method (the other reason for assuming it to be constant was to account for the contribution of items being brought onto the train as discussed in Chapter 6, Section 6.2). Figure 7.7 shows the snapshot from Smokeview on the location of the ignition source.

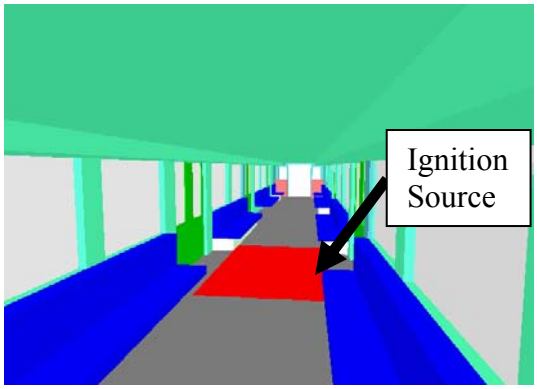

Figure 7.7: Snapshot from Smokeview showing train car interior – Ignition source on the floor directly above the battery boxes; battery charger; and the LV and IV box.

7.1.4 Materials' thickness, density and thermal properties

Table 7.2 summarises the thickness, density and thermal properties of materials used in the FDS simulation. It is important to highlight that most of these properties were based on values found in various references (at room temperature) and not from the actual materials. This was due to difficulty in obtaining information from the train supplier and their material suppliers. The main assumption made for the density and thermal properties was that they are temperature independent, which is not true in practice.

Among the materials listed, only FRP polyester and styrene butadiene were simulated as combustible surface materials. These two surface materials were assumed to be thermally thick therefore their thermal inertia $k\rho c$ was specified. This was done by specifying the thermal conductivity k, the density ρ and the specific heat c individually in FDS. Even though FDS allows change in thermal conductivity and specific heat with temperature to be prescribed, there was however no information on these properties at other temperatures except at room temperature. The author acknowledged that because of constant properties assumption, the time to ignition for the combustible surface materials might be affected.

For the wall, ceiling and door panels, they were assumed not to be involved in the fire since they are made of aluminium. There was reservation when making this assumption because the exposed side of the panel was painted with powder paint. But considering that it is only a thin coat of powder paint with low fire load content (see Chapter 5, Section 5.4), it might not contribute much to a fire even if ignited. Furthermore there was no information on the ignition properties e.g. ignition temperature and heat release properties e.g. heat of vaporisation for powder paint. Therefore wall, ceiling and door panels were assumed to be non-combustible in the trial simulations. Nevertheless the issue on whether the powder paint will contribute to the growth and spread of a fire will be addressed in the Chapter 8 whereby Cone Calorimeter test results are presented and discussed.

In order to ensure the values used were appropriate, a number of references were referred to for each material and its properties where possible. Whenever, there was a range of values for a property, the average value was used. Actual thickness and density were measured and used if sample of the materials were available. As for properties of composite components (such as laminated safety glass; wall, ceiling and door construction), they were either calculated or assumed based on information gathered for the individual materials that made up the composite component. These were the basis for the values used in the simulation. The summary of the values gathered and the calculations can be found in Appendix D of this report.

Component	**Material**	δ **(m)**	k **(W/mK)**	ρ **(kg/m^3)**	c **(kJ/kgK)**
Seats, under seat boxes, equipped cubicle assemblies, PEC module fittings, detrainment door, driving console assembly, face (wall) and ceiling panels at car end mask	FRP polyester	0.004	0.3	1795	1.51
Floor covering	Styrene butadiene	0.003	0.15	1478	1.9875
Wall construction, gangway wall construction[a]	Glass wool sandwich between aluminium panel and welded aluminium body	0.1	0.038	119	0.68
Ceiling construction, gangway ceiling construction[a]	Glass wool sandwich between aluminium panels	0.06	0.038	176	0.68
Passenger door construction	Glass wool sandwich between aluminium panels	0.35	0.038	119	0.68
Window, Passenger door's window	Laminated safety glass	0.023	0.049	1380	0.84
Tunnel wall, undercarriage[a], dummy concrete door[b]	Concrete	0.7	1.0	2100	0.88

a See Section 7.1.1
b See Section 7.1.2

Table 7.2: Thickness, density and thermal properties of materials used in the trial simulations

7.1.5 Combustion reaction parameters

The simulation was based on LES approach and therefore mixture fraction combustion model was used. In mixture fraction combustion model only one fuel can be specified for the combustion reaction. This is another limitation of the fire model because in reality there may be more than one fuel burning in the fire. In the simulation, two fuels (i.e. the FRP polyester and styrene butadiene) were specified for the simulation of fire growth and spread. But since only reaction parameters of one fuel could be inputted, it was decided to base on FRP polyester since it was the main burning material in the train car. The reaction parameters used for the simulation are shown in Table 7.3.

S/no	Parameter	Value	Remark
1	Chemical formula	$C_{5.77}H_{6.25}O_{1.63}$	
2	Energy per unit mass O_2 (kJ/kgO_2)	11900	
3	Fraction of CO from fuel (kg/kg)	0.0705	
4	Fraction of soot from fuel (kg/kg)	0.062	
5	Radiative fraction	0.35	
6	Molecular Weight of fuel	101.6	Calculated
7	Stoichiometry coefficient for CO_2	5.77	Calculated
8	Stoichiometry coefficient for H_2O	3.125	Calculated
9	Stoichiometry coefficient for O_2	6.5175	Calculated

Table 7.3: Reaction parameters for FRP polyester

The first five parameters above were selected based on criteria outlined in previous Section. The last four parameters (i.e. molecular weight of fuel, stoichiometry coefficient for CO_2, H_2O and O_2) were calculated based on the chemical formula for polyester given above. The summary of the values gathered for the first five parameters is given in Appendix D. The calculations for the last four parameters are shown in Appendix E.

7.1.6 Parameters for the modelling approach based on HRRPUA

For the modelling approach based on HRRPUA, the ignition temperatures and the Cone Calorimeter HRRPUA curves of the fuels (burning materials) were specified. The two burning materials were FRP polyester and styrene butadiene. The ignition temperatures used in the simulation were 346°C and 360°C respectively. For FRP polyester, a range of values for ignition temperature have been found (refer Appendix D), the lowest was used in the simulation.

Cone Calorimeter HRRPUA curves for the two materials were obtained from NIST's fire safety study of passenger trains (Peacock and Braun 1999). For FRP polyester, it was assumed that it had the same HRRPUA curve as the FRP wall panel tested in Peacock and Braun (1999). One of the floor coverings tested in Peacock and Braun (1999) had the same material as the floor covering used in the current study i.e. styrene butadiene, therefore it was used. The HRRPUA for the two materials are reproduced in Figure 7.8 and Figure 7.9 below for easy reference. Note that the HRRPUA curves were based on Cone Calorimeter tests at 50kW/m^2. All materials in the NIST study were only tested at this exposure heat flux level. Therefore it was not possible to prescribe the HRRPUA curves at the proposed exposure heat flux levels (depending on location of materials) as discussed in Chapter 4.

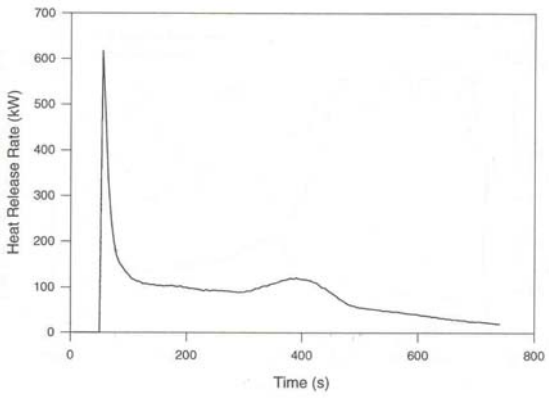

Figure 7.8: FRP wall panel (reproduced from Peacock and Braun (1999))

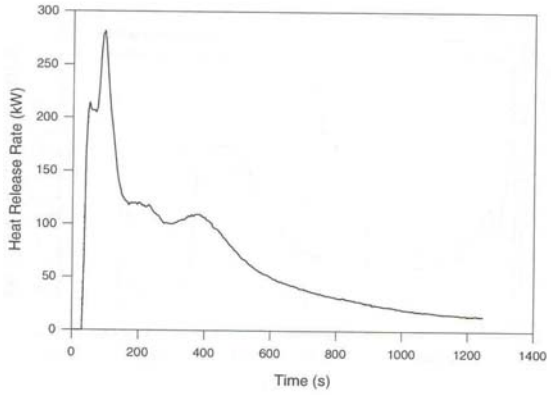

Figure 7.9: Floor covering, styrene butadiene (reproduced from Peacock and Braun (1999))

Note that only the curve from time to ignition to the end of the test was used. The incipient phase was not included in the simulation.

7.1.7 Parameters for the modelling approach based on heat of vaporisation

Important parameters such as ignition temperature, heat of vaporisation, effective heat of combustion, maximum burning rate were required in the simulation. The ignition temperatures were the same as the modelling approach based on HRRPUA and other parameters are given in Table 7.4. For FRP polyester, a range of values for heat of vaporisation has been found (refer Appendix D), the lowest was prescribed to be conservative. The effective heat of combustion values for both materials were based on information in Renie and Prevot (2003) submitted by the train supplier. The maximum burning rate was approximated from the mass loss rate curve of FRP wall panel and styrene butadiene floor covering given in Peacock and Braun (1999). Note that in the trial simulations, the critical mass flux was not prescribed as this information could not be found for the two fuels.

S/no	Parameter	FRP polyester	Styrene butadiene
1	Heat of vaporisation ΔH_v (kJ/kg)	1400	2700
2	Effective heat of combustion $\Delta H_{c,eff}$ (kJ/kg)	12870	17950
3	Maximum burning rate $\dot{m}''_{max}$ (kg/m^{2}s)	0.042	0.02

Table 7.4: Heat of vaporisation, effective heat of combustion and maximum burning rate for FRP polyester and styrene butadiene

7.2 Results and discussions for the trial simulations

Table 7.5 shows the summary of the trial simulations conducted. Note that for fire scenarios 1C, 2C and 3C i.e. scenarios with all doors closed, simulations were only conducted using 300 mm grid size.

S/no	Fire scenario	Description of fire scenario	Grid size (mm)
1	1A	Rear car fire, fire on the seat (Arson), both detrainment doors opened, all passenger doors closed	300
2			200
3			150
4	2A	Rear car fire, fire in the corner (Arson or electrical fault), both detrainment doors opened, all passenger doors closed	300
5			200
6			150
7	3A	Rear car fire, undercarriage fire (Electrical fault), both detrainment doors opened, all passenger doors closed	300
8			200
9			150
10	1B	Rear car fire, fire on the seat (Arson), both detrainment doors closed, 1st and 4th passenger doors facing the walkway opened	300
11			200
12			150
13	2B	Rear car fire, fire in the corner (Arson or electrical fault), both detrainment doors closed, 1st and 4th passenger doors facing the walkway opened	300
14			200
15			150
16	3B	Rear car fire, undercarriage fire (Electrical fault), both detrainment doors closed, 1st and 4th passenger doors facing the walkway opened	300
17			200
18			150
19	1C	Rear car fire, fire on the seat (Arson), all doors closed	300
20	2C	Rear car fire, fire in the corner (Arson or electrical fault), all doors closed	300
21	3C	Rear car fire, undercarriage fire (Electrical fault), all doors closed	300

Note: 1) Forced ventilation and window failure were simulated for all scenarios.
2) The modelling approaches based on HRRPUA and heat of vaporisation were simulated for all scenarios

Table 7.5: Summary of the trial simulations conducted.

7.2.1 Modelling approach based on HRRPUA

Figure 7.10 to Figure 7.18 show the HRR curves for the modelling approach based on HRRPUA.

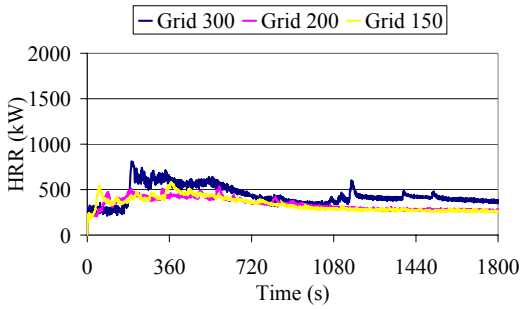

Figure 7.10: Modelling approach based on HRRPUA – Fire scenario 1A

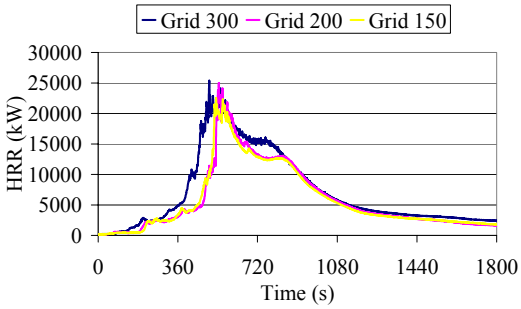

Figure 7.11: Modelling approach based on HRRPUA – Fire scenario 2A

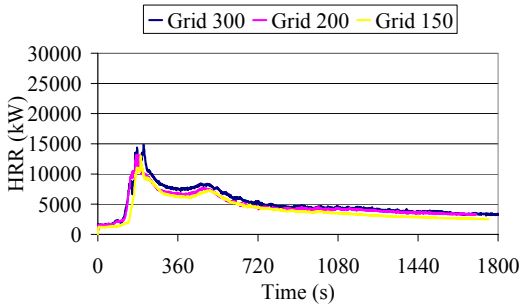

Figure 7.12: Modelling approach based on HRRPUA – Fire scenario 3A

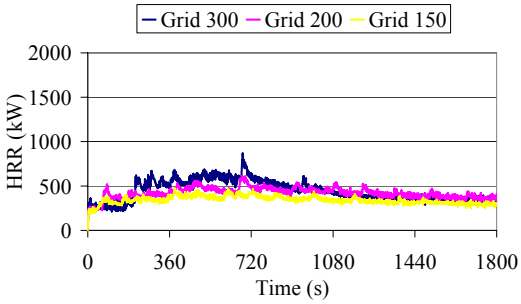

Figure 7.13: Modelling approach based on HRRPUA – Fire scenario 1B

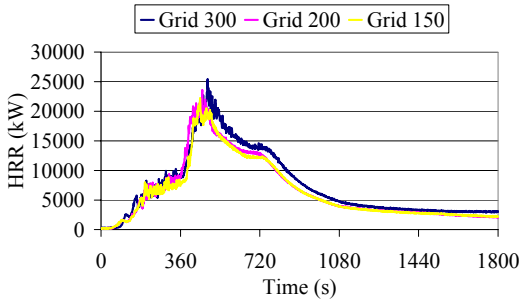

Figure 7.14: Modelling approach based on HRRPUA – Fire scenario 2B

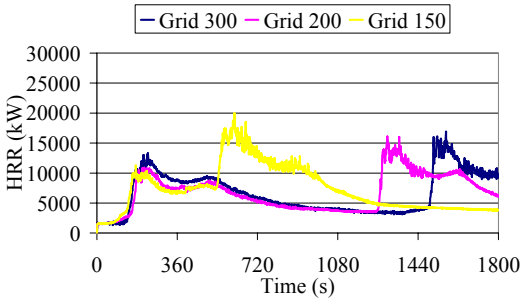

Figure 7.15: Modelling approach based on HRRPUA – Fire scenario 3B

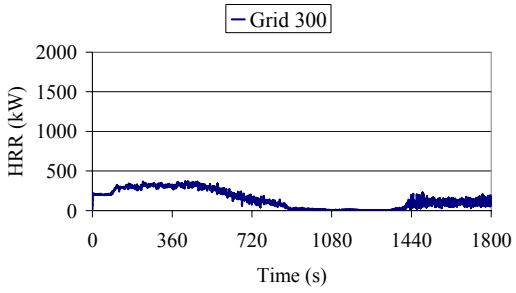

Figure 7.16: Modelling approach based on HRRPUA – Fire scenario 1C

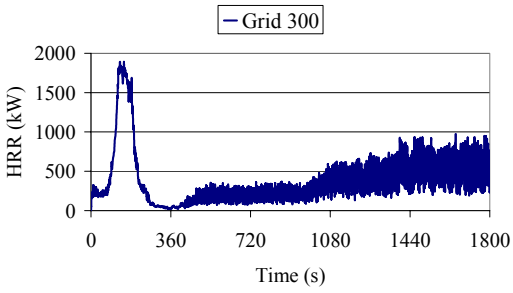

Figure 7.17: Modelling approach based on HRRPUA – Fire scenario 2C

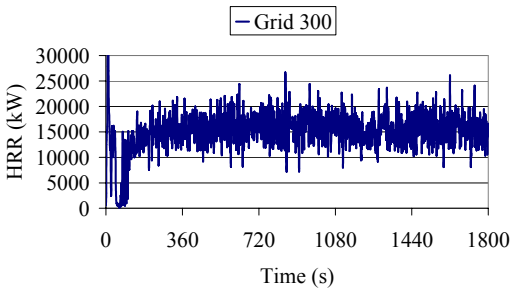

Figure 7.18: Modelling approach based on HRRPUA – Fire scenario 3C

Figure 7.19 provides the summary of predicted peak HRR values for the modelling approach based on HRRPUA.

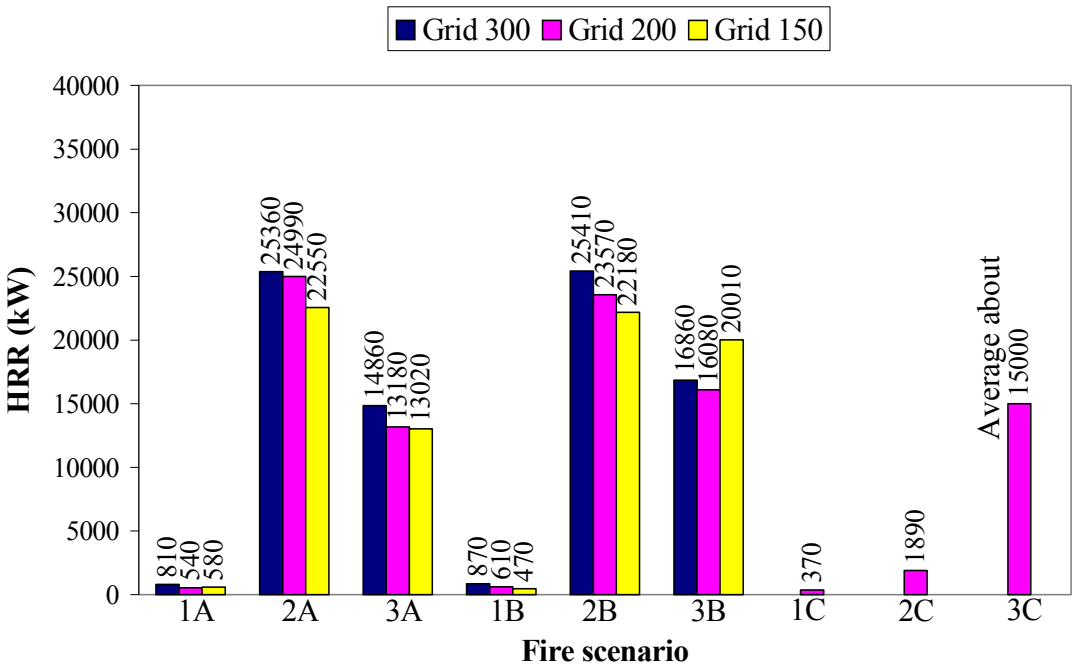

Figure 7.19: Summary of predicted peak HRR values for the modelling approach based on HRRPUA.

For fire scenarios 1A, 1B and 1C i.e. fire on the seat, the fire only managed to spread around the ignition source to the nearby seat area (see Figure 7.20). It did not spread to the wall liner and ceiling as these exposed surfaces were simulated as non-combustible. The maximum temperature in the car compartment was around 280°C implying that flashover did not take place. Because the compartment temperature was much lower than the window failure criterion, windows did not fail. With the exception of fire scenario 1C, the predicted HRRs were found to be quite sensitive to the prescribed grid sizes with grid size of 300 mm giving a more conservative prediction (see Figure 7.10, Figure 7.13 and Figure 7.19). Even so, the peak HRR values for all the seat fire scenarios at different grid sizes were all less than 1000 kW (see Figure 7.19). Ventilation conditions i.e. forced ventilation and closing of doors, did not appear to have much influence on the fire growth and flame spread for the seat fire scenarios. However for fire scenario 1C i.e. all doors closed scenario, abnormal oscillation of HRR was noted near the end of simulation (see Figure 7.16). This probably indicates the effect of numerical instability. No simulation was conducted using other grid resolution partly because of this reason.

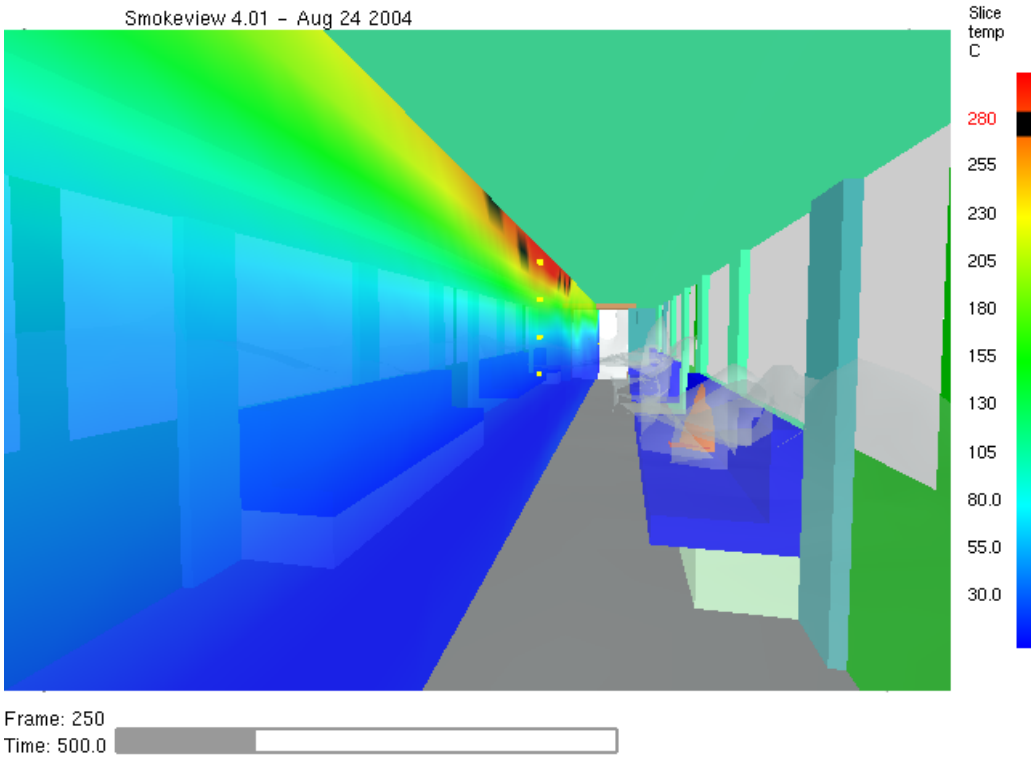

Figure 7.20: Snapshot from Smokeview for fire scenario 1A, grid 300 mm, 500 s into the simulation.

The fire in fire scenarios 2A and 2B i.e. fire in the corner, growth and spread throughout the train car compartment and resulted in almost all the windows failing (see Figure 7.21). The fire was able to grow in intensity and spreads downstream of the train car as majority of the exposed surfaces at the end mask (in the vicinity of the ignition source) were combustible. The maximum temperature in the car compartment was about 980°C. Because of high ventilation airflow velocity through the detrainment door, the fire in fire scenario 2A propagated throughout the train car faster compared with fire scenario 2B. For fire scenario 2B, because of low ventilation airflow velocity through the 1st side door, the fire burned more intensely at the end mask (in vicinity of ignition source) before spreading downstream. The difference in the growth stage can be seen from Figure 7.11 and Figure 7.14. Even though these two scenarios had different ventilation conditions, there were not significant differences in the predicted time to peak and peak HRR. One possible reason may be because FDS is not able to adjust the HRRPUA curve according to the heat feedback from the fire for the modelling approach based on HRRPUA.

For fire scenarios 2A and 2B, the simulations with different grid sizes gave a similar trend in fire growth and decay (see Figure 7.11 and Figure 7.14). For both scenarios, grid size of 300 mm provided a more conservative prediction of the peak HRR (see Figure 7.19).

For fire scenario 2C, the fire did not grow to flashover and cause window failure. Maximum temperature in the car compartment was around 430°C. HRR decreased when the oxygen level depleted within the compartment. Oscillation of HRR was noted from 450 s until the end of the simulation (see Figure 7.17). This again indicates the effect of numerical instability.

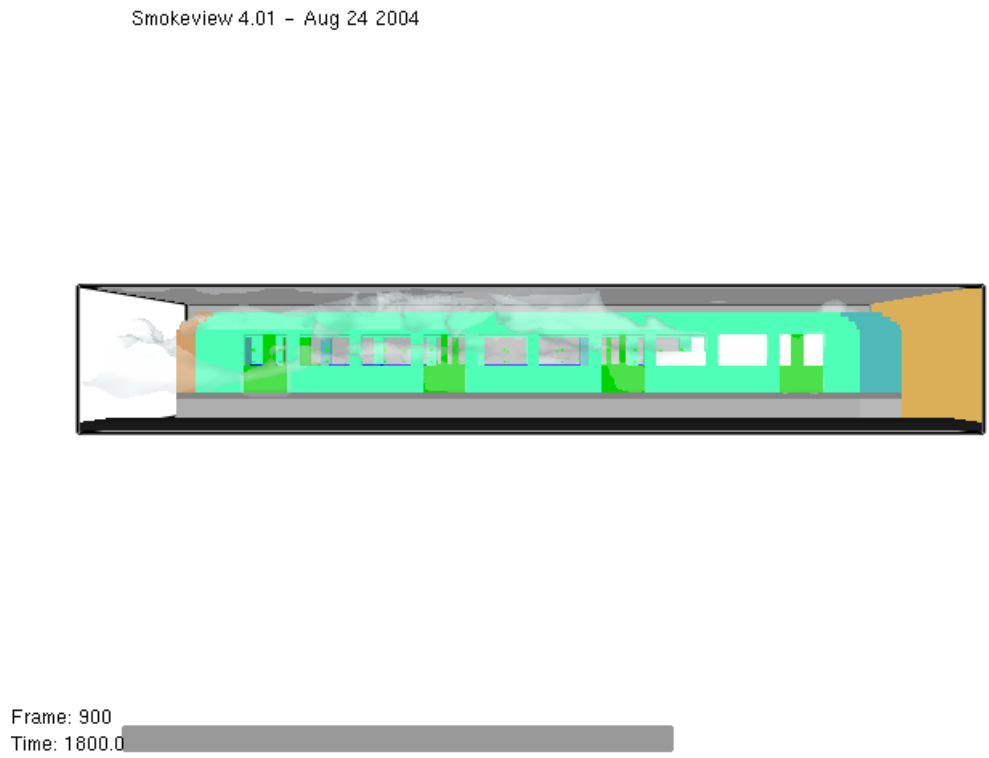

Figure 7.21: Snapshot from Smokeview for fire scenario 2A, grid 300 mm, 1800 s into the simulation.

Because the detrainment doors were opened for fire scenario 3A, the forced ventilation airflow flowed directly through the train car. High forced ventilation airflow velocity through the detrainment doors limits the fire to spread only to the downstream of the ignition source. This scenario had much lower HRR (see Figure 7.12) compared to fire scenarios 2A and 2B even though it has higher ignition source. This highlights the importance of ignition source (fire) location on the fire severity. For fire scenario 3B, the detrainment doors were closed and 1st and 4th side doors were opened. Because this scenario had lower forced ventilation airflow velocity through the doors, after the fire had spread downstream the train car, it progressed towards the end mask of the train car and resulted in second peak HRR. The second peak HRR was found to be sensitive to the grid resolutions with finer grid sizes predicting earlier occurrence of the second peak (see Figure 7.15)

For fire scenario 3C, oscillation of HRR started right from the beginning until the end of the simulation. The average HRR was about 15000 kW (see Figure 7.18) and the maximum compartment temperature was as high as 1000°C for the first 50 s (which exceeded the criterion for window failure i.e. ≥ 675°C). But unexpectedly the window did not fail and flame was observed to burn outside the train car (through the 100 mm floor gap) as shown in Figure 7.22 throughout the simulation. The odd result and strange phenomenon somewhat suggested that FDS might not be suitable for under-ventilated scenario simulation especially those with large ignition source size. The oscillation of HRR again indicates the effect of numerical instability.

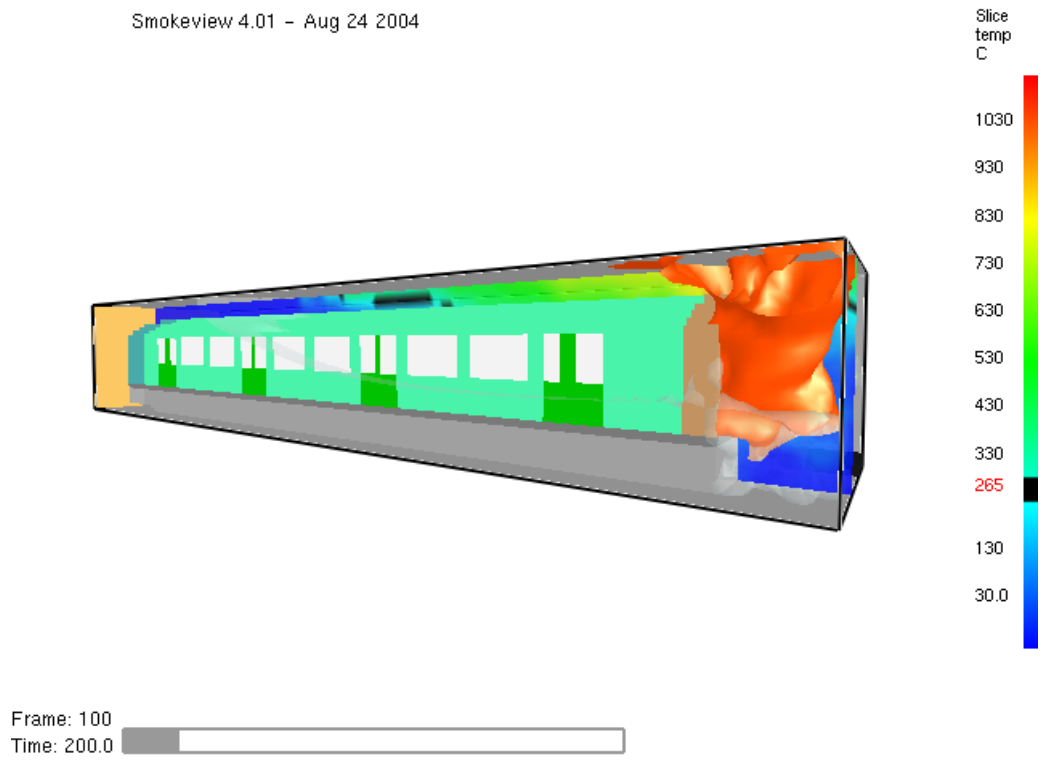

Figure 7.22: Snapshot from Smokeview for fire scenario 3C, grid 300 mm, 200 s into the simulation.

7.2.2 Modelling approach based on heat of vaporisation

Figure 7.23 to Figure 7.31 show the HRR curves for the modelling approach based on heat of vaporisation.

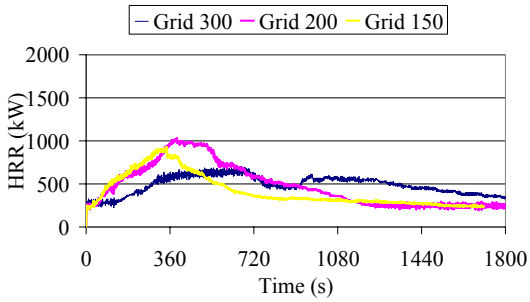

Figure 7.23: Modelling approach based on vaporisation – Fire scenario 1A

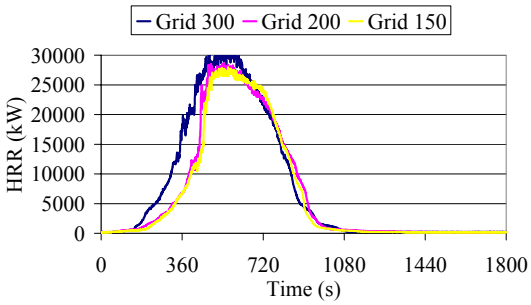

Figure 7.24: Modelling approach based on vaporisation – Fire scenario 2A

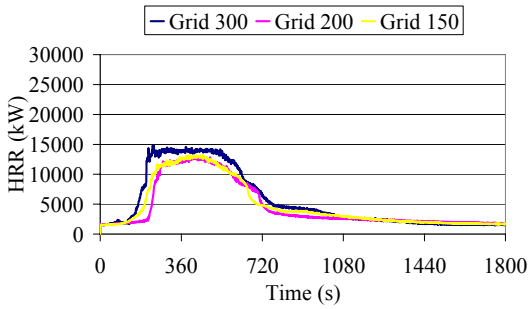

Figure 7.25: Modelling approach based on vaporisation – Fire scenario 3A

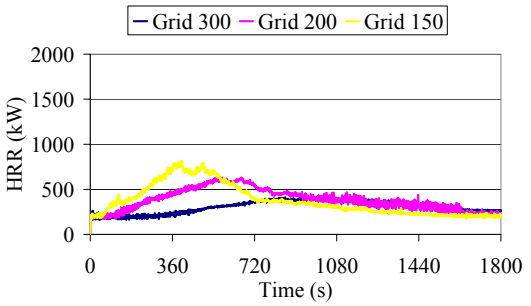

Figure 7.26: Modelling approach based on vaporisation – Fire scenario 1B

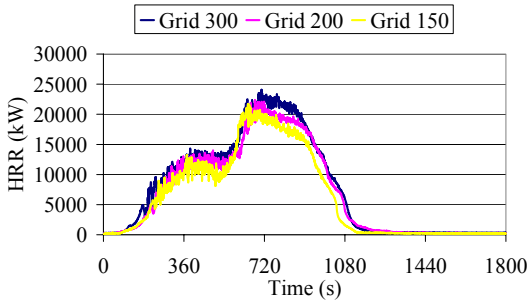

Figure 7.27: Modelling approach based on vaporisation – Fire scenario 2B

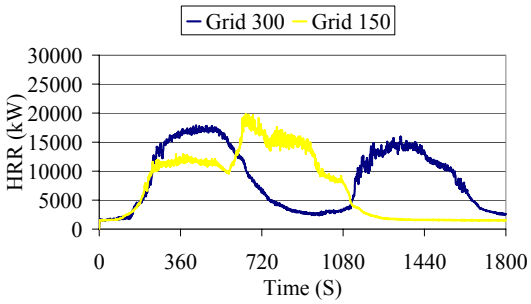

Figure 7.28: Modelling approach based on vaporisation – Fire scenario 3B

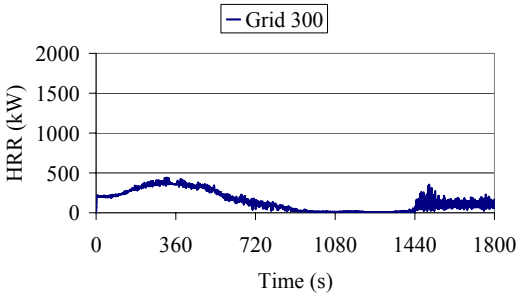

Figure 7.29: Modelling approach based on vaporisation – Fire scenario 1C

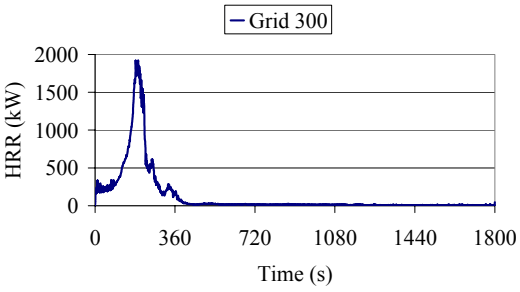

Figure 7.30: Modelling approach based on vaporisation – Fire scenario 2C

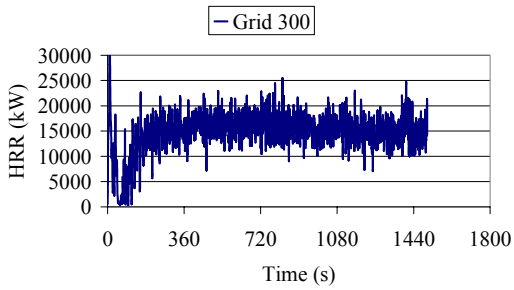

Figure 7.31: Modelling approach based on vaporisation – Fire scenario 3C

Figure 7.32 provides the summary of predicted peak HRR values for the modelling approach based on vaporisation.

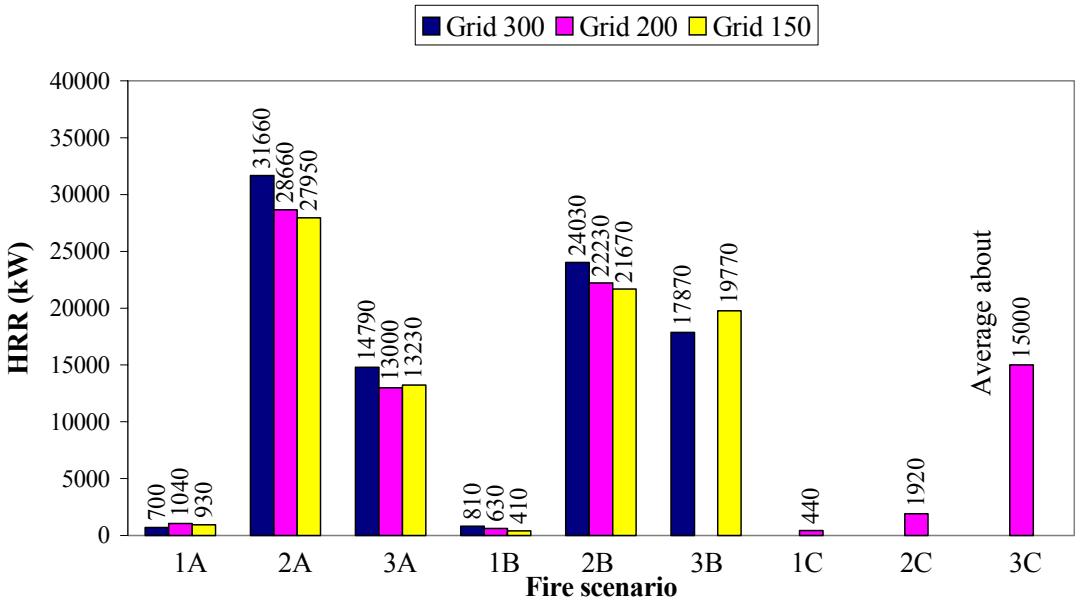

Note: For fire scenario 3B, simulation for grid size 200 mm stopped automatically at about 200 s. Therefore the peak HRR for this fire scenario is not included in the Figure.

Figure 7.32: Summary of predicted peak HRR values for the modelling approach based on vaporisation.

Coincidently, the results for both modelling approaches were quite similar even though the input data were different i.e. one prescribed HRRPUA and the other prescribed heat of vaporisation, and were from different references.

For the modelling approach based on heat of vaporisation, the fire in fire scenarios 1A, 1B and 1C i.e. fire on the seat also did not grow to flashover and cause window failure. The predicted HRRs were also sensitive to grid resolutions but unlike the modelling approach based on HRRPUA, finer grid resolutions tend to predict earlier time to peak and higher peak HRR (see Figure 7.23, Figure 7.26 and Figure 7.32). However this is not really a concern because simulations based on different grid resolutions produced consistent results in term of fire growth and spread; and for these fire scenarios the fires did not grow to flashover. The worry will be for simulations using different grid sizes to produce different predictions of fire severity as it will make selection of grid resolution for the final simulations a more difficult task. For fire scenario 1C, abnormal oscillation of HRR was also observed near the end of simulation (see Figure 7.29).

For fire scenario 2A and 2B, because of difference in ventilation conditions, dissimilarity in the growth stage was also observed (See Figure 7.24 and Figure 7.27). For fire scenario 2A, because of high ventilation airflow velocity through the detrainment doors, the fire propagated downstream the train car earlier; and the time to peak was faster and the fire grew more intense compared with fire scenario 2B. These results made more sense compared with those from the modelling approach based of HRRPUA for the same fire scenarios. For these two fire scenarios, simulations using different grid resolutions gave similar trend of fire growth and decay. A grid size of 300 mm was noted to provide a more conservative prediction of the peak HRR (see Figure 7.32). The fire in fire scenario 2B for the modelling approach based on heat of vaporisation also did not grow to flashover and cause window failure (see Figure 7.30) but unlike the modelling approach based on HRRPUA, there was no oscillation of HRR in the simulation.

For fire scenario 3A, fire spread was also limited to downstream of the ignition source because of high forced ventilation airflow velocity through the train detrainment doors. The predicted peak HRRs were also much lower compared with fire scenario 2A and 2B. Grid size of 300 mm again gave a more conservative prediction of the peak HRR (see Figure 7.32). For fire scenario 3B, two peak HRRs were also predicted. The second peak HRR occurred when the fire progressed toward the end mask of the train car. The finer grid again gave earlier prediction of the second peak. For this scenario, it was not possible to complete the simulation based on 200 mm grid size as simulation consistently stopped automatically at about 200 s. McGrattan (2005a) advised that the sketching of grids is often the cause of instabilities. This probably explains what has happened.

For fire scenario 3C (see Figure 7.31), similar result and phenomenon were observed as in the modelling approach based on HRRPUA.

7.2.3 Grid resolution for the final simulations

A grid size of 300 mm is selected for the final simulations because of the following reasons:

a) Simulations based on different grid resolutions were able to give consistent prediction of fire severity.
b) For majority of the simulations, a grid size 300 mm gave a more conservative prediction of the peak HRR.
c) For fire scenario 3C, simulation was not able to complete using 200 mm grid size.
d) Simulations based on 150 mm grid size could take up to 12 days to complete depending on fire scenario and computer speed. Not to mention that currently, only one car was simulated.

7.3 Conclusions from the trial simulations

The following conclusions can be drawn from the trial simulations:

a) For fire scenarios 1A and 1B i.e. fire on the seat, the fire did not grow to flashover. The fire only managed to spread to the nearby seat area. It did not spread to the wall liner and ceiling as these exposed surfaces were simulated as non-combustible.

b) For fire scenarios 2A and 2B i.e. the fire in the corner, the fire was able to grow in intensity and spreads downstream of the train car because majority of the exposed surfaces in the vicinity of ignition source was combustible.

c) For fire scenario 3A i.e. undercarriage fire with detrainment doors opened, the fire only spread to the surfaces downstream of the ignition source because of high forced ventilation airflow velocity through the detrainment door. For fire scenario 3B i.e. undercarriage fire with 1st and 4th passenger doors opened, two peak HRRs were predicted. The second peak HRR occurred when fire progressed to the end mask of the train car. The predicted peak HRRs for these two scenarios were lower than fire scenarios 2A and 2B even though the ignition source size was substantially larger. This highlights the importance of ignition source location on the fire severity.

d) All the simulations were able to complete except one: fire scenario 3B, grid 200 mm, the modelling approach based on heat of vaporisation. Stretching of grid might be the cause of instability for this particular simulation.

e) Simulations for fire scenarios with all doors closed i.e. fire scenarios 1C, 2C and 3C were unsteady, especially the one with large ignition source size i.e. fire scenario 3C. The results suggested that FDS might not be suitable for simulation of under-ventilated scenario.

f) A grid size 300 mm is selected for the final simulations because of reasons stated in the previous Section.

8 Cone Calorimeter tests and material properties

This Chapter describes the Cone Calorimeter tests. It also describes the procedures to derive the Cone Calorimeter heat release rates and the material properties of samples. The observations during the tests and the results will also be presented.

8.1 Cone Calorimeter

Cone Calorimeter was designed in 1982 at National Bureau of Standards (NBS), now National Institute of Standards and Technology (NIST), primarily by Babrauskas, Parker and Swanson. At present, it is the most commonly used tool for bench-scale heat release rate measurement (Janssens 2002). Besides the heat release rate, it is also possible to measure a number of other parameters, including:

a) Effective heat of combustion
b) Mass loss rate
c) Ignitability
d) Smoke and soot production
e) Production of toxic gases

During a Cone Calorimeter test, a specimen is exposed to a constant level of exposure heat flux from a conical heater. The exposure heat flux levels used can be up to 100 kW/m^2. Volatile gases, which are released from the specimen during the test, are ignited by an electric spark ignitor. Combustion gases are collected by an exhaust hood and duct system for further analysis via the gas analyser. This gas analysis may include measurements of the CO_2, CO, O_2 and other toxic gas concentrations.

The heat release rate is calculated according to the oxygen consumption method described later in Section 8.2. During the Cone Calorimeter test, the specimen is placed on a load cell, which records the mass loss of the specimen during combustion. It is possible to determine the optical smoke obscuration by measuring the attenuation of a laser beam by smoke in the exhaust duct. It is also possible to record the gravimetric soot yield i.e. grams of soot evolved, per grams of specimen burned if the Calorimeter is equipped with a soot mass sampler.

The test specimen must be flat in order to achieve a constant exposure heat flux over the entire surface. For test specimen that bends, an optional retainer frame and wire grid can be used to hold the test specimen flat and firmly in place. The retainer frame and wire grid are also used for specimens that might intumesce. The frame is designed to reduce unrepresentative edge-burning of composite specimens and to retain specimens prone to delaminating.

Standard mounting of the heater and specimen is in horizontal orientation however it is also possible to mount them in vertical orientation for special–purpose testing. In the horizontal orientation, the distance between the bottom surface of the conical heater and the top of the specimen is adjusted to be 0.025 ± 0.002 m by means of the sliding cone height adjustment to ensure that the test specimen is exposed to the designated exposure conditions.

The specimen is wrapped in a single sheet of aluminium foil, covering the sides and bottom to limit flow of molten material in case the specimen melted during the test. In order to present a standardized heat flow boundary condition to the rear face of the specimen, all specimens are backed with low loss insulating ceramic fibrous material. The specimen should be 0.1 m by 0.1 m and the thickness of 0.006 to 0.05 m.

The major components of the Cone Calorimeter are shown in Figure 8.1.

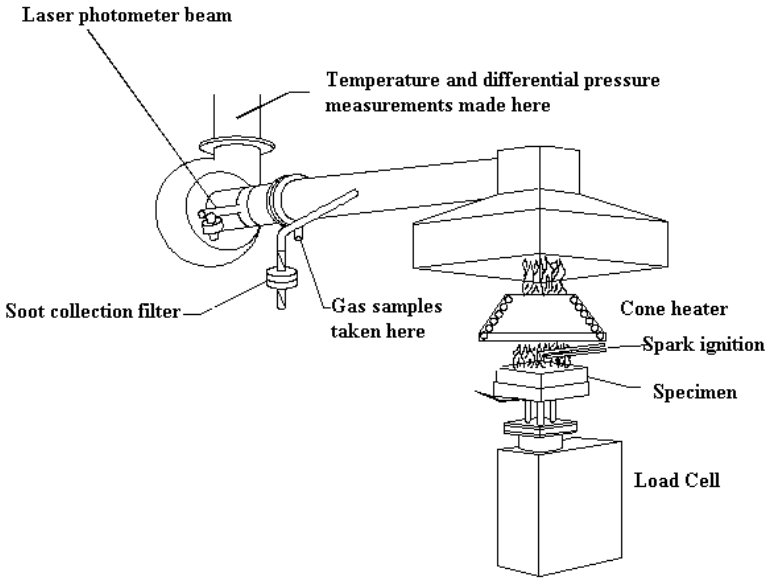

Figure 8.1: Cone Calorimeter

The test procedure is described in either NFPA 271 (NFPA 271 2004 edition), ISO 5660 (ISO 5660-1:2002; ISO 5660-2:2002; ISO 5660-3:2003), or ASTM E 1354 (ASTM E 1354 2004). Detailed descriptions of the apparatus are covered in Babrauskas (2002) whereby reader is recommended to refer to for additional information. It gives reader a clear idea of what the components are, what they do, and why they were designed to be the way they are.

8.2 Oxygen consumption method

A useful similarity between common organic materials is that the heat release per unit mass of oxygen consumed is nearly constant. Huggett (1980) investigated a wide variety of organic solids and obtained an average value for this constant of 13.1 MJ/kg of oxygen consumed. This value can be used for most practical applications and is accurate with very few exceptions to within ±5%. The heat release rate from an experiment can therefore be calculated by measuring the mass rate of oxygen consumed (Janssens 2002; Janssens and Parker 1992).

The basic requirement for using the oxygen consumption method is that all combustion gases are collected and removed through exhaust hood and duct system. At a distance downstream, where the mixing is adequate, the mass flow rate of gases, the gas temperature and the gases concentration, i.e. the mole fraction, are measured. The treatment and equations to be used varied mainly due to the extent to which gas analysis is made. As a minimum, the oxygen O_2 concentration must be measured. The accuracy of the results can be improved if the concentrations of carbon dioxide CO_2 and carbon monoxide CO (and water vapour H_2O) are also measured. In this project, the concentrations of O_2, CO_2 and CO were measured. The equations used to calculate the heat release rate with these three gases measured are described in Janssens (1991). It consists of four main steps as discuss below:

a) To calculate the mass flow rate of the gases $\dot{m}_e$

b) To obtain the mole fraction of water vapour in the incoming air $X^a_{H_2O}$

c) To calculate the oxygen depletion fraction ϕ

d) To calculate the heat release rate $\dot{q}$ in kW

8.2.1 Mass flow rate

The technique used to calculate the mass flow rate in the experiment was to measure the pressure drop across and temperature at the orifice plate. From Janssens (1991), the equation to calculate the mass flow rate is given by:

$$\dot{m}_{ex} = C_{calib}\sqrt{\frac{\Delta P}{T_e}} \qquad \text{Equation 8.1}$$

Where $\dot{m}_{ex}$ is the mass flow rate in the exhaust duct in kg/s, C_{calib} is the calibration constant, ΔP is the pressure drop across the orifice plate in Pa and T_{ex} is the gas temperature at the orifice plate in K.

The calibration constant C_{calib} was determined by carrying out a calibration (using methane). This was done prior to the day's testing to check for the proper operation of the instrument and to compensate for minor changes in mass flow determination. The pressure drop across the orifice plate and the temperature were measured during the experiment. As the pressure drop was measured in volt (1 volt equals to 1 torr), it was converted into Pa by multiplying the measured voltage by a factor of 133.

8.2.2 Mole fraction of water vapour

The mole fraction of water vapour in the incoming air X_{H2O}^{a} is given by:

$$X_{H2O}^{a} = \frac{RH}{100} \frac{\exp\left(23.2 - \frac{3816}{T_{\infty} - 46}\right)}{P_a} \qquad \text{Equation 8.2}$$

Where RH is the relative humidity in %, T_{∞} is the ambient temperature in K and P_a is the air pressure ($\approx$ 101325 Pa). The relative humidity RH and ambient temperature T_{∞} are recorded prior to the day's testing.

8.2.3 Oxygen depletion factor

With O_2, CO_2 and CO measured, the oxygen depletion factor ϕ is given by:

$$\phi = \frac{X_{O2}^{Aa}(1 - X_{CO2}^{Ae} - X_{CO}^{Ae}) - X_{O2}^{Ae}(1 - X_{CO2}^{Aa})}{(1 - X_{O2}^{Ae} - X_{CO2}^{Ae} - X_{CO}^{Ae})X_{O2}^{Aa}} \qquad \text{Equation 8.3}$$

Where X_{O2}^{Aa} and X_{CO2}^{Aa} are the measured mole fraction of O_2, CO_2 in the incoming air respectively; and X_{O2}^{Ae}, X_{CO2}^{Ae} and X_{CO}^{Ae} are the measured mole fraction of O_2, CO_2 and CO in the exhaust gases respectively.

8.2.4 Heat release rate

In Janssens (1991), the heat release rate $\dot{q}$ is given by:

$$\dot{q} = \left[E\phi - (E_{CO} - E)\frac{1-\phi}{2}\frac{X_{CO}^{Ae}}{X_{O2}^{Ae}} \right] . \frac{\dot{m}_{ex}}{1+\phi(\alpha-1)} \frac{M_{O2}}{M_a}(1 - X_{H2O}^{a})X_{O2}^{Aa} \qquad \text{Equation 8.4}$$

Where E is the amount of energy released by complete combustion per unit mass of oxygen consumed, E_{CO} is the heat release per mass unit of oxygen consumed for the combustion of CO, M_{O2} is the molecular weight of oxygen, M_a is the molecular weight of the incoming air and α is the volumetric expansion factor.

8.2.5 Constant values for calculation

Janssens (1991) recommends the following numerical values to be used in the equations:

a) E_{CO} = 17600 kJ/kg of O_2

b) M_{O2} = 32 kg/kmol

c) M_a = 29 kg/kmol

Exact values for E and α should be used, if available, to improve the accuracy (Janssens 2002). However, if actual values are not known, generic values of E = 13100 kJ/kg and α = 1.105 are recommended (Janssens 1991). In this project, these recommended values were adopted to calculate the heat release rate.

8.3 Material properties

Besides the HRR curves of Cone Calorimeter tested at various exposure heat fluxes, the following material properties are required for FDS simulation:

a) The ignition temperature T_{ig}

b) The thermal inertia $k\rho c$ if the surface material is thermally-thick. The product of $\rho c\delta$ if the surface material is thermally-thin.

c) The heat of vaporisation ΔH_v

d) The critical mass flux $\dot{m}''_{cr}$ and the maximum burning rate $\dot{m}''_{\max}$

In order to derive the material properties from the Cone Calorimeter test data, ignition data measured at a minimum of three exposure heat fluxes are required. Ideally there should be replicates tested at each exposure heat flux. The procedures to derive these properties are discussed below.

8.3.1 Ignition temperature

The procedure for determining the surface temperature for ignition T_{ig} from the Cone Calorimeter measurements is taken from Grenier (1996); Janssens (1993); Janssens and Grenier (1997). It was chosen among a few available methods as it provided a means to correlate material's ignition data based on the best fit of the data to either a semi-infinite solid (thermally thick) or thermally thin surface. The procedure is outlined below:

a) The average time to ignition t_{ig} for each exposure heat flux is calculated.

b) Correlate the average time to ignition by plotting $\left(1/t_{ig}\right)^n$ against the exposure heat fluxes. Determine the value of n between 0.547 and 1 that results in the highest correlation coefficient R^2. If the optimum n is closer to 0.547, the material behaves as a thermally-thick surface. If n is closer to 1, the material behaves as thermally-thin surface.

c) Determine the x-intercept from the best-fit line through the data. The x-intercept is taken as the critical heat flux for ignition $\dot{q}''_{cr}$. The critical heat flux for ignition is an estimate of minimum heat flux for ignition $\dot{q}''_{\min}$, the heat flux below which ignition under practical conditions cannot occur.

d) The ignition temperature T_{ig} can then be calculated by solving (by iteration) the following equation:

$$\varepsilon \dot{q}''_{cr} = h_c(T_{ig} - T_\infty) + \varepsilon\sigma(T_{ig}^4 - T_\infty^4) \qquad \text{Equation 8.5}$$

Where h_c is the convection heat transfer coefficient in kW/m^{2}K, ε is the surface emissivity at ignition, σ is the Stefan-Boltzmann's constant (5.67x10^{-11} kW/m^{2}K^4) and T_∞ is the ambient temperature.

8.3.2 Mechanical and thermal properties

If the material is identified as thermally-thick i.e. n is closer to 0.547. The thermal inertia $k\rho c$ is to be determined for the simulation. The procedure for determining the thermal inertia $k\rho c$ is also taken from Grenier (1996); Janssens (1993); Janssens and Grenier (1997) and is outlined below.

a) The total heat transfer coefficient h_{tot} is first being solved.

$$h_{tot} = \frac{\varepsilon \dot{q}''_{cr}}{(T_{ig} - T_\infty)} \qquad \text{Equation 8.6}$$

b) Correlate the ignition times again but this time use n = 0.547 and include data point $\dot{q}''_{cr}$ on the x-axis.

c) Determine the slope of a straight line drawn through the data point $\dot{q}''_{cr}$ on the x-axis and data point for the highest heat flux. This is a simplification to make the calculation easier (Wade 2003a).

d) The apparent thermal inertia $k\rho c$ in kW^{2}s/m4K^2 can then be computed using:

$$k\rho c = h_{tot}^2 \left[\frac{1}{0.73 slope \dot{q}''_{cr}} \right]^{1.828} \qquad \text{Equation 8.7}$$

If the material is identified as thermally-thin i.e. n is closer to 1. The product of $\rho c \delta$ will be determined for input into the simulation. The procedure for determining the product of $\rho c \delta$ is taken from Mikkola and Wichman (1989) and is outlined below.

a) Correlate the ignition times again but this time use n = 1.
b) Determine the slope of a linear line fit through the data.
c) The product of $\rho c \delta$ in kJ/m^{2}K can then be computed using:

$$\rho c \delta = \frac{1}{slope(T_{ig} - T_{\infty})} \qquad \text{Equation 8.8}$$

8.3.3 Heat of vaporisation

The heat of vaporisation ΔH_v for the material is determined following the procedure of Quintiere (1993) and is outlined below.

a) Peak heat release rate $\dot{q}''_{peak}$ from Cone Calorimeter tests are plotted against the exposure heat flux levels.
b) Determine the slope of a linear fit through the data. This slope is equal to effective heat of combustion $\Delta H_{c,eff}$ divided by heat of vaporisation ΔH_v.
c) The effective heat of combustion $\Delta H_{c,eff}$ is also obtained from the Cone Calorimeter test. An average value of effective heat of combustion $\Delta H_{c,eff}$ is used.
d) The heat of vaporisation can be computed using:

$$\Delta H_v = \frac{\Delta H_{c,eff}}{Slope} \qquad \text{Equation 8.9}$$

8.3.4 Critical mass flux

Critical mass flux $\dot{m}''_{cr}$ is a property that quantifies a critical condition for ignition (Janssens et al. 2003). FDS requires both this parameter and the ignition temperature T_{ig} to be specified (for the modelling approach based on heat of vaporisation) in order for the code to choose pre-exponential factor A and activation energy E_A so that the fuel burns at the critical mass flux rate when its surface temperature reaches the ignition temperature (McGrattan and Forney 2004). A method of measuring the critical mass flux was proposed by Rasbash et al. (1986) but the apparatus they used was specifically built. The author is not aware of any simple procedure or method that can be used to derive the critical mass loss rate from the Cone Calorimeter test data. This is because the critical mass flux is not commonly used to describe the piloted ignition behaviour of a material for practical reasons (Janssens et al. 2003). In order to obtain a reasonable value that can be conservatively prescribed in the simulation, the following procedure is proposed:

a) Calculate the mass loss rate of material (tested in the Cone Calorimeter test) at the lowest exposure heat flux where sustained burning occurred.
b) The mass loss rate at the time to ignition (sustained flaming) is taken as the 'critical mass flux'. This is a conservative approximation as it is expected that the 'true' critical mass flux to be lower than the value used. The average value from replicate specimens will be used in the simulation.

8.3.5 Maximum burning rate

Maximum burning rate is prescribed in FDS so that to prevent excess pyrolysis of the fuel. It limits the burning rate of the fuel to its measured maximum. To prescribe this value will require information on the burning rate of material in a real fire, which is not available. Peacock and Braun (1999) discussed the fire exposure conditions for FRA-cited test methods and in typical fires when they were deciding the exposure conditions to be used for Cone Calorimeter testing of rail car materials. The various exposure heat flux levels quoted in Peacock and Braun (1999) are summarised in Table 8.1 below.

Test method/ Fire type	**Maximum radiant energy to sample (kW/m^2)**
FRA-cited test methods	< 5 to 40
Developing fire	< 50
Post-flashover fire	≥ 50 to 75
Real-scale train fire experiments	0.5 to 62

Table 8.1: Fire exposure conditions for FRA-Cited test methods and in typical fires (adopted from Peacock and Braun (1999))

The highest exposure heat flux used in this project for material testing is 65 kW/m^2. This exposure heat flux level is higher than the exposure conditions used in FRA-cited test methods. It is also higher than the exposure conditions during a typical developing fire; and measured during the real-scale train fire experiments. Therefore it is reasonable to prescribe the maximum burning rate for simulation based on the maximum mass loss rate measured at the exposure heat flux of 65 kW/m^2. An average value from replicate specimens will be used in the simulations.

8.4 Experiments

This Section describes the Cone Calorimeter tests and reports on the observations made during the tests. It also highlights derivations from NFPA 271 (NFPA 271 2004 edition) which was the Standard referred to for the tests.

8.4.1 Train materials

The train car materials provided by LTA for the Cone Calorimeter tests are shown in Table 8.2.

S/no	Component	Material
1	Seat	FRP polyester
2	Floor covering	Styrene butadiene
3	Wall panel	Aluminium panel with a thin coat of powder paint on its exposed surface
4	Bellows (Inner)	WPE Vamac compound ref 22-003
5	Bellows (Outer)	WPE Vamac compound ref 22-004
6	Air-con duct	Glass wool with the outer surface covered with aluminium paper sheet

Table 8.2: Train car materials for Cone Calorimeter tests

Note that the seat, floor covering, bellows (Inner) and bellows (Outer) are treated with flame retardant additive as discussed in Chapter 5. Bellows (Inner) and bellows (Outer) are distinguished by their colour, which is grey and black respectively.

8.4.2 Derivations from NFPA 271

Specimen size

The Standard requires the test specimen size for the Cone Calorimeter test to be 0.1 m by 0.1 m. However, due to the available sample sizes, two of the material test specimen sizes (seat and bellows (Inner)) were smaller than the specified size. The size of the test specimens are summarised in Table 8.3 below.

Specimen thickness

The test specimen thickness should be between 0.006 m to 0.05 m. If the specimen thickness is less than 0.006 m, it should be mounted on the substrate material over which it will actually be used so that to avoid thickness effect (Babrauskas 1992). All the samples' thickness was less than 0.006 m except for the air-con duct. But since the substrate material was not available, the test specimens were all backed with calcium silicate block(s) instead.

Number of replicate specimens tested at each exposure heat flux level.

Ideally, there should be three replicate specimens tested at each exposure conditions. However, due to the available sample size, this requirement could not be met for four samples: wall panel, bellows (Inner), bellows (Outer) and air-con duct. The number of tests conducted for each material at each exposure conditions are summarised in Table 8.3 below.

S/no	Component	Sample size	δ [a] (m)	ρ [a] (kg/m^3)	$\dot{q}_e''$ (kW/m^2)	Number of tests
1	Seat	0.1 m x 0.05 m	0.004	1795	25, 35, 50 and 65	3 at each $\dot{q}_e''$
2	Floor covering	0.1 m x 0.1 m	0.003	1478	25, 35, 50 and 65	3 for each $\dot{q}_e''$
3	Wall panel	0.1 m x 0.1 m	0.0014	3011	35, 50 and 65	2 for each $\dot{q}_e''$
4	Bellows (Inner)	0.1 m x 0.068 m	0.003	1827	35, 50 and 65	2 for each $\dot{q}_e''$
5	Bellows (Outer)	0.1 m x 0.1 m	0.003	1721	35, 50 and 65	2 for each $\dot{q}_e''$
6	Air-con duct	0.1 m x 0.1 m	0.025	85.2	35, 50 and 65	2 for each $\dot{q}_e''$

a Measured from the sample

Table 8.3: Test specimen size and thickness; and number of tests conducted

8.4.3 Test specimen mounting

The Cone Calorimeter tests for all the samples were conducted in horizontal orientation. Before the test, the test specimens were wrapped in aluminium foil on all sides except for the exposed surface. The test specimens were then backed with ceramic fibrous block(s) and placed on the specimen holder. The retainer frame was used for all test specimens and wire grid was used for the specimens that might expand. The mounting details for each of material test specimen are shown from Figure 8.2 to Figure 8.7.

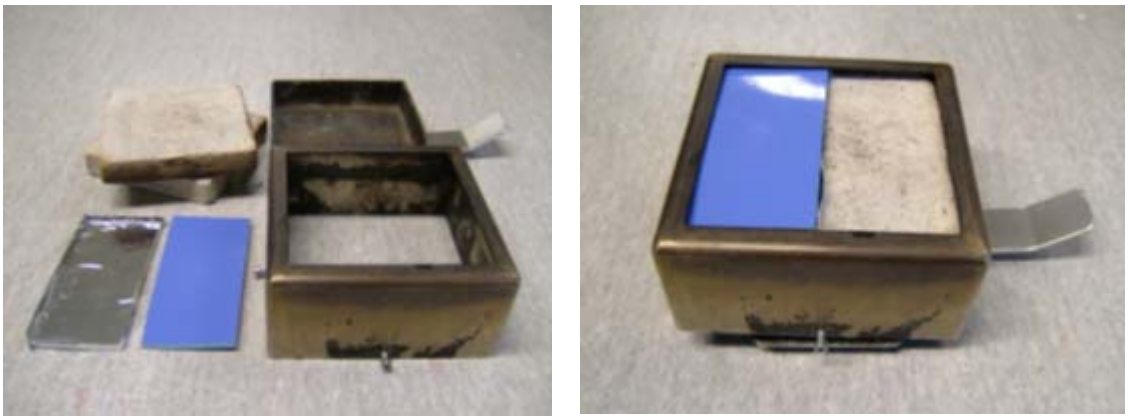

Figure 8.2: Seat test specimen mounting – Specimen holder with retainer frame

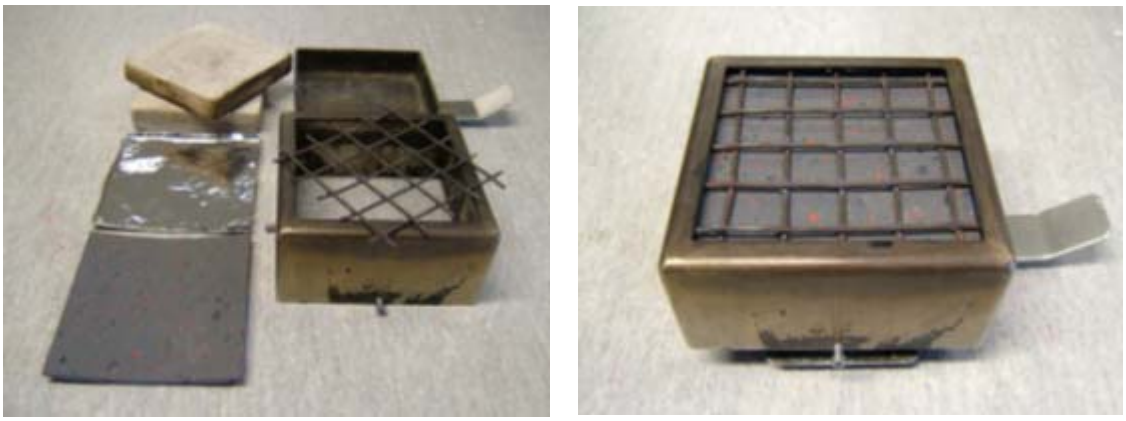

Figure 8.3: Floor covering test specimen mounting – Specimen holder with retainer frame and wire grid

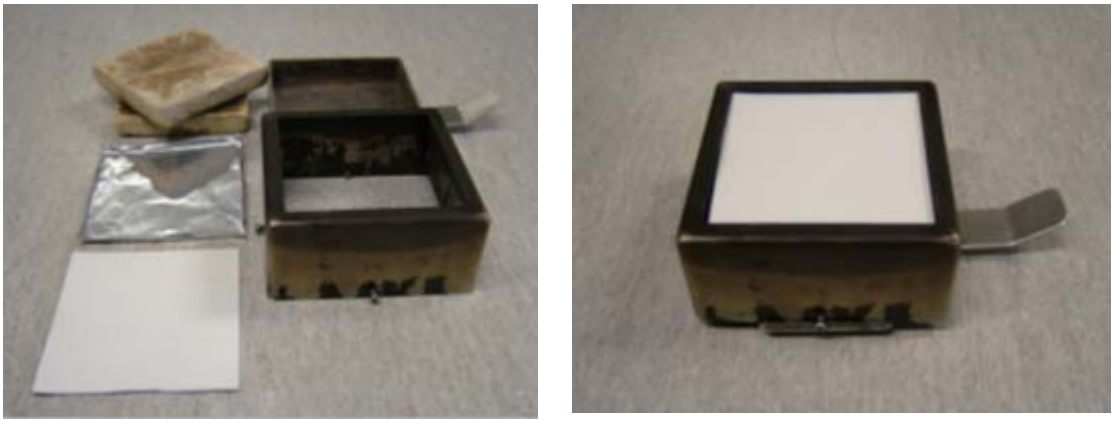

Figure 8.4: Wall panel test specimen mounting – Specimen holder with retainer frame

Figure 8.5: Bellows (Inner) test specimen mounting – Specimen holder with retainer frame and wire grid

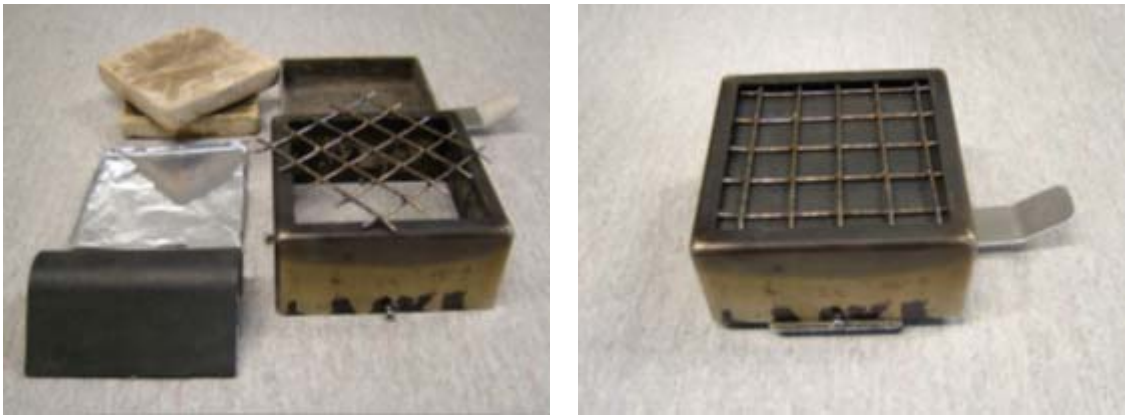

Figure 8.6: Bellows (Outer) test specimen mounting – Specimen holder with retainer frame and wire grid

Figure 8.7: Air-con duct test specimen mounting – Specimen holder with retainer frame and wire grid

8.4.4 Cone Calorimeter calibration and test procedure

The Cone Calorimeter tests were carried out at the small-scale fire laboratory at the University of Canterbury.

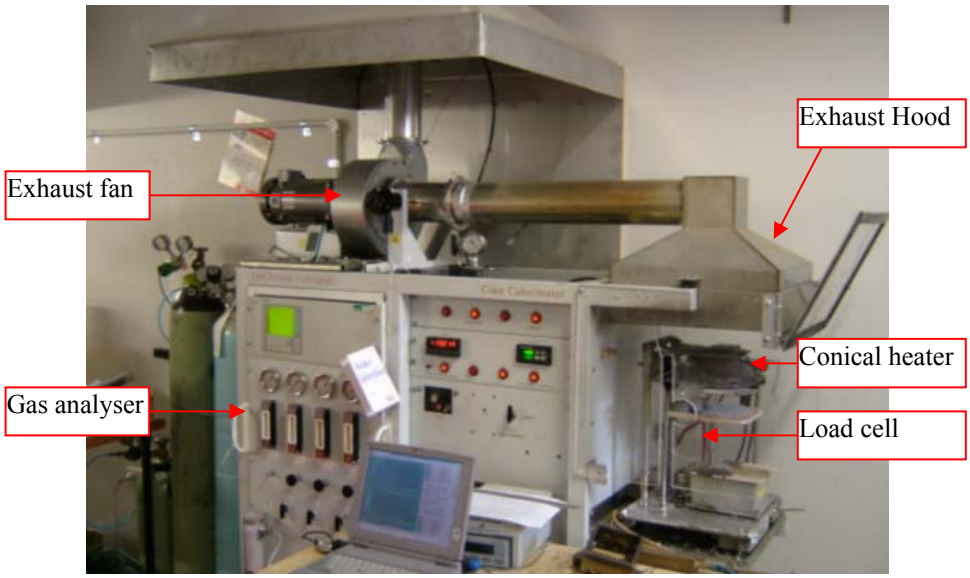

Figure 8.8: Cone Calorimeter in the small-scale fire laboratory at University of Canterbury

Prior to the day's testing, the methane calibration was performed and the calibration constant C_{calib} determined. The ambient temperature and humidity were also recorded. These values were required for the heat release rate calculation.

The distance between the bottom surface of the conical heater and the top of the specimen was adjusted to approximately 0.025 m to ensure that the test specimens were exposed to the designated exposure conditions.

A datalogger was used to acquire the data in one-second intervals and save it into a spreadsheet file. The data collected include:

a) Mole fractions of O_2, CO_2 and CO
b) Pressure drop across the orifice plate
c) Temperature at the orifice plate
d) Mass loss of test specimen

Smoke and soot production and toxic gases were not measured because the essential kit was not available.

The procedure for the Cone Calorimeter test is briefly described below:

1) Prepare the test specimen according to the pre-defined mounting details. The test specimen, the holder, the frame, the wire grid, etc, were initially at room temperature.
2) The conical heat temperature was adjusted to generate the required exposure heat flux.
3) The data acquisition program was started. The shield in front of the conical heat was closed, the spark ignitor moved into place and the test specimen held in the holder was put onto the load cell directly under the conical heater.
4) After the test specimen was properly mounted, the shield was opened. At the same time the stop-watch was started.
5) The time when sustained flaming occurs was recorded. The specimen was allowed to burn freely after the ignition until flameout. The flameout time was recorded
6) Data was collected for another two minutes after any flaming cease.
7) Steps 1 to 6 were repeated for the next specimen.
8) Note that the test was terminated when the specimen did not ignite within 15 minutes after the test was started.

8.4.5 Observations during the Cone Calorimeter tests

Seat

The material of the seat is made of FRP polyester. The test specimen size was 0.1 m by 0.05 m and 0.004 m thick. Three replicate specimens were tested at each exposure conditions. The exposure heat flux levels from the conical heater to the specimen were 25, 35, 50 and 65 kW/m^2.

Observations

When the specimen thermally decomposed, tearing or ripping sound was heard and black volatile gases were released. The sound was likely to be caused by the bursting of small tiny bubbles formed on the surface when pyrolysis occurred. After the specimen ignited, flaming tended to concentrate near the edges. The flame was observed to flicker and give an impression that it was trying to 'dig' below the surface layer from the edges. Flame extinguishment was observed to resemble those of pool fires.

At low exposure heat fluxes ($\leq$ 35 kW/m^2), 'flashing' occurred before sustained flaming. While this phenomenon only occurred once or twice for tests at 35 kW/m^2, it occurred more than 10 over times before sustained flaming happened for tests at 25 kW/m^2. For tests at 25 kW/m^2 exposure heat flux level, flashing first occurred at approximately 5 minutes and was more frequent between 6 to 8 minutes. All the three specimens at 25 kW/m^2 ignited after over 8 minutes into the tests.

During post-test observation, it was discovered that the three edges covered under the retainer frame had hardened. However delamination occurred and layers of fibre could be seen at the exposed edge. The latter observation suggested that unrepresentative burning has taken place at the 'unprotected' edge. For those tests at low heat flux (25 kW/m^2), black patches were formed on the surface which can be seen from Figure 8.9. This was likely due to incomplete combustion.

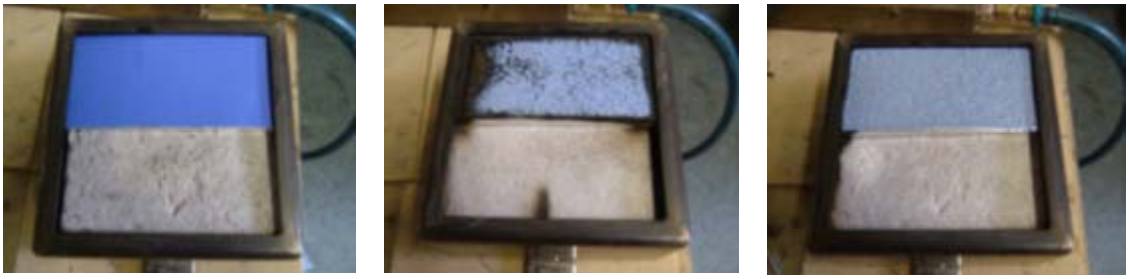

Seat specimen before test | Burned specimen at low heat flux (25 kW/m^2) | Burned specimen at high heat flux (65 kW/m^2)

Figure 8.9: Seat specimen before and after test

Floor covering

The material of the flooring covering is made of styrene butadiene, a type of synthetic rubber. The test specimen size was 0.1 m by 0.1 m and 0.003 m thick. The number of replicate specimens and the tested exposure conditions were the same as the seat specimen.

Observations

When the specimen thermally decomposed, tearing or ripping sound was heard and grey volatile gases were released. The flaming was noted to be more intense during the period immediately after ignition and during the late stage of the test. Localised burning at the edge was observed before flameout.

Transitory flaming occurred for specimens tested at low exposure heat fluxes ($\leq$35 kW/m^2). For test specimens at 35 kW/m^2, transitory flaming only occurred once but for test specimens at 25 kW/m^2, transitory flaming occurred twice or more times for the test specimens before sustained flaming happened. The floor covering was found to be more difficult to ignite compared with the seat based on the time to ignition.

At low heat flux (25 kW/m^2), the surface charred with large obvious crack lines which can be seen from Figure 8.10. At high heat flux (65 kW/m^2), the leftover was grey powder form ash on its surface and a layer of char below.

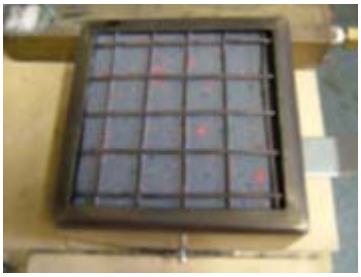
Floor covering specimen before test


Burned specimen at low heat flux (25 kW/m^2)


Burned specimen at high heat flux (65 kW/m^2)

Figure 8.10: Floor covering specimen before and after test

Wall panel

The wall panel is made of aluminium panel with a thin coat of powder paint on its exposed surface. The test specimen size was 0.1 m by 0.1 m and 0.0014 m thick. Two replicate specimens were tested at each exposure conditions. The exposure heat flux levels from the conical heater to the specimen were 35, 50 and 65 kW/m^2.

Observations

Black volatile gases were released from the test specimens at early stage of the tests. However, only specimens at 65 kW/m^2 exposure heat flux were ignited. This suggested that at lower exposure heat fluxes there were insufficient volatile gases released from the specimens to result in ignition. Even though the specimens at 65 kW/m^2 were ignited, the burning times were short: one lasted for about 18 s while the other lasted for about 30 s. This can be explained by the fact the only the powder paint on the wall panel was combustible.


Wall panel specimen before test


Non- ignited specimen (35 and 50kW/m^2)

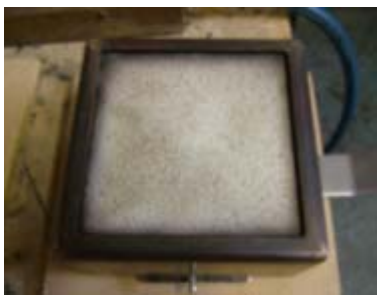
Ignited specimen (at 65kW/m^2)

Figure 8.11: Wall panel specimen before and after test

The powder paint evolved into dust after the tests. For the ignited specimens, dirty greyish spots formed on its surface which can be seen from Figure 8.11.

Bellows (Inner)

The bellows (Inner) was made of WPE Vamac compound, a type of elastomer material. The test specimen size is 0.1 m by 0.68 m and 0.003 m thick. . The number of replicate specimens and the tested exposure conditions were the same as the wall panel specimen.

Observations

Like the previous two materials i.e. seat and floor covering, tearing or ripping sound was heard when the specimen decomposed. For this material, it swelled shortly after ignition but the wire grid managed to hold the specimen firmly in place. Even though no transitory flaming was observed during the tests, it did not warrant that transitory flaming would not happened when the specimen was tested at lower exposure fluxes (since the lowest exposure heat flux level tested for this material was 35 kW/m^2). Nevertheless, this material appeared to ignite faster compared to the floor covering.

The end products were to some extent similar to the floor covering specimens at low and high heat fluxes. At low heat flux (25 kW/m^2), the surface also charred with large obvious crack lines formed on its surface which can be seen in Figure 8.12. At high heat flux (65 kW/m^2), white and powdery residue formed on its surface with a layer of char below it.

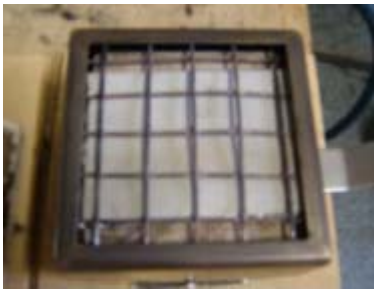

Bellows (Inner) specimen before test

Burned specimen at low heat flux (35 kW/m^2)

Burned specimen at high heat flux (65 kW/m^2)

Figure 8.12: Bellows (Inner) specimen before and after test

Bellows (Outer)

The bellows (Outer) is also made of WPE Vamac compound. The test specimen size was 0.1 m by 0.1 m and 0.003 m thick. The number of replicate specimens and the tested exposure conditions were the same as the wall panel and bellows (Inner) specimens.

Observations

The specimens gave out tearing or ripping sound when it decomposed. Shortly after ignition, the specimens swelled and expanded. The force from the expansion was so great that the wire grid bent into parabolic shape as shown in Figure 8.13. In three of the tests, the retainer frame popped up and hit the spark ignitor. This introduced errors in the recorded mass loss. Besides errors in the recorded mass loss, the heat release from the tests were likely to be inaccurate because the specimens surface were not exposed to uniform and intended heat fluxes when the above incidents took place. Charred and flaky surface was noted on the specimens during the post-test observation.

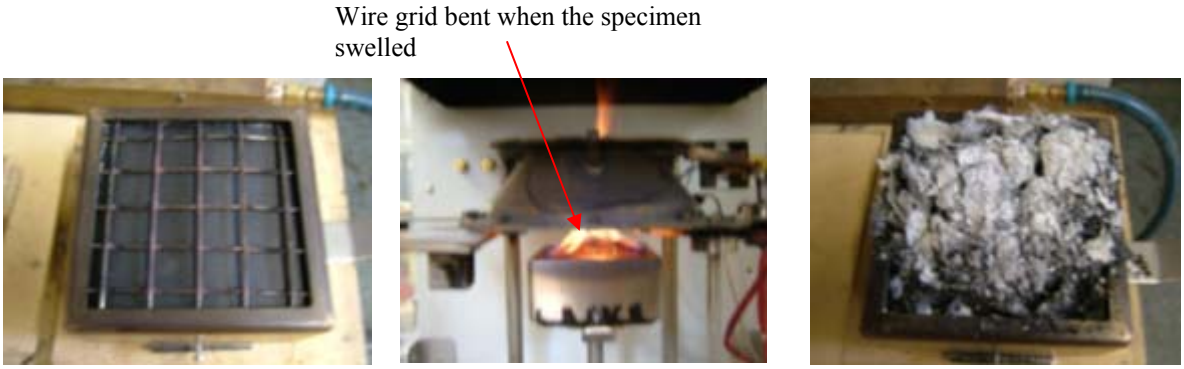

Bellows (Outer) specimen before test | The wire grid bent into parabolic shape. | Charred and flaky surface

Figure 8.13: Bellows (Outer) specimen before and after test

Air-con duct

The air-con duct is made of glass wool with the outer surface covered with aluminium paper sheet by means of adhesive. The exposed surface during the tests was the aluminium paper sheet since this would be the exposed surface during its end installation. The test specimen size was 0.1 m by 0.1 m and 0.025 m thick. The number of replicate specimens and the tested exposure conditions were the same as the wall panel and bellows (Inner and Outer) specimens.

Observations

Grey gases were released from the specimens during the tests. However, no ignition occurred at 50 and 65 kW/m^2 exposure heat flux levels. No further test was conducted at other exposure heat flux levels. The aluminium paper sheet peeled off from the surface after the tests at both exposure heat flux levels. A thin layer of char resemble that of burned paper appeared on the glass wool surface. The glass wool originally yellow in colour has turned into whitish grey. These observations can be seen from Figure 8.14.

Air- con duct specimen before test | Aluminium paper sheet peeled off from the surface. | Thin layer of char formed on the glass wool surface

Figure 8.14: Air-con duct specimen before and after test

8.5 Results and discussions for the Cone Calorimeter tests and the derived material properties

8.5.1 Heat release rate data

The calculated data from the Cone Calorimeter tests include:

a) Heat release rate $\dot{q}$ (kW)
b) HRRPUA curve (kW/m^2)
c) Mass loss rate curve (kg/sm^2)
d) Peak heat release rate $\dot{q}''_{peak}$ (kW/m^2)
e) Average $\dot{q}''$ values for the first 60, 120 and 180 s after ignition i.e. $\dot{q}''_{60}$, $\dot{q}''_{120}$ and $\dot{q}''_{180}$ (kW/m^2)
f) Total heat released by the specimen q'' (MJ/m^2)
g) Average effective heat of combustion $\Delta H_{c,eff}$ for the entire test duration (MJ/kg)

The heat release rate $\dot{q}$ was calculated using the oxygen consumption method outlined in Section 8.2. When calculating the heat release rate, the data for the gases was adjusted to account for the delay time they took to reach the gas analyser. The heat release rate per unit area at each time interval was determined by dividing the heat release rate by the specimen area in m^2.

The mass loss rate at each time interval was computed using five-point numerical differentiation method described in NFPA 271. However due the high noise disturbance, the computed mass loss rate curves were smoothed using 20 points moving average.

The peak $\dot{q}''$ and average $\dot{q}''$ values for the first 60, 120 and 180 s after ignition i.e. $\dot{q}''_{60}$, $\dot{q}''_{120}$ and $\dot{q}''_{180}$, were computed from the HRRPUA data.

As for the total heat released by the specimen, it was computed beginning with the first reading after the last negative rate of heat release reading that occurred at the beginning of the test, and continuing until the final reading recorded for the test. The average effective heat of combustion was calculated by dividing the computed total heat released by the total mass loss.

The above data for all the specimens tested in the Cone Calorimeter for current study was compiled in Appendix G of this report. This Section only reports on selective data and only the average values (of all the replicates tested at each exposure heat flux level) are reported, unless otherwise stated. The results for the air-con duct specimen are not presented since no ignition occurred at the tested exposure heat flux levels.

Seat

The time to ignition t_{ig}, peak HRR $\dot{q}''_{peak}$, average $\dot{q}''$ value for first 180 s after ignition $\dot{q}''_{180}$ and effective heat of combustion $\Delta H_{c,eff}$ at the tested exposure heat flux levels are summarised in Table 8.4. The HRRPUA and mass loss rate curves at tested exposure heat flux levels are shown in Figure 8.15 and Figure 8.16 respectively.

No of replicate	$\dot{q}''_e$ (kW/m^2)	t_{ig} (s)		$\dot{q}''_{peak}$ (kW/m^2)		$\dot{q}''_{180}$ (kW/m^2)		$\Delta H_{c,eff}$ (kJ/kg)	
		Ave	STD -EV	Ave	STD -EV	Ave	STD -EV	Ave	STD -EV
3	25	502	11	130	12	97	5	13.0	0.7
3	35	106	5	151	10	103	4	14.1	0.3
3	50	50	0	170	17	121	2	13.3	0.6
3	65	34	1	184	10	140	3	14.3	0.7

Ave = Average value of all the replicates tested at the listed exposure heat flux level
STDEV = Standard deviation of average value

Table 8.4: Summary of Cone Calorimeter ignition and heat release data for the seat sample

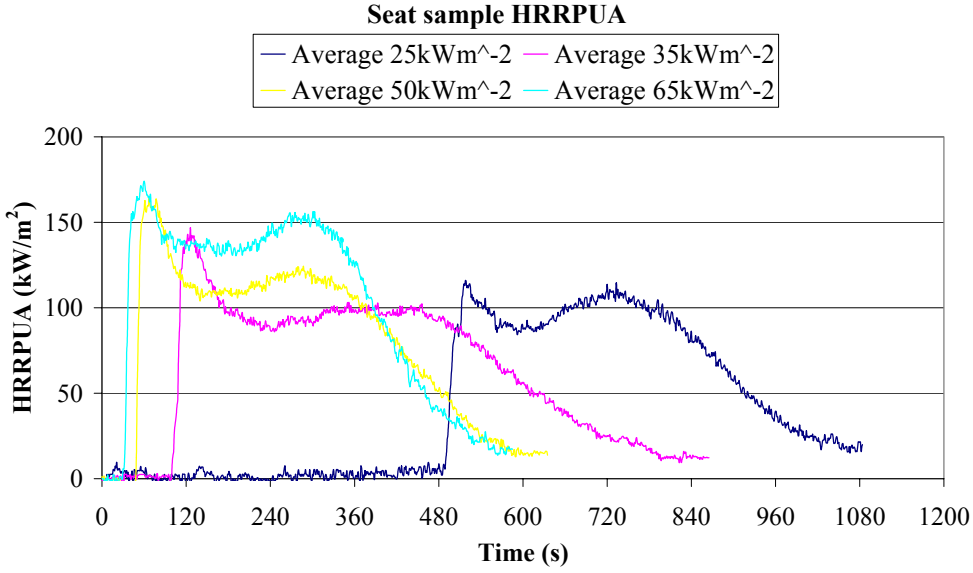

Figure 8.15: Seat sample – HRRPUA curves at tested exposure heat fluxes

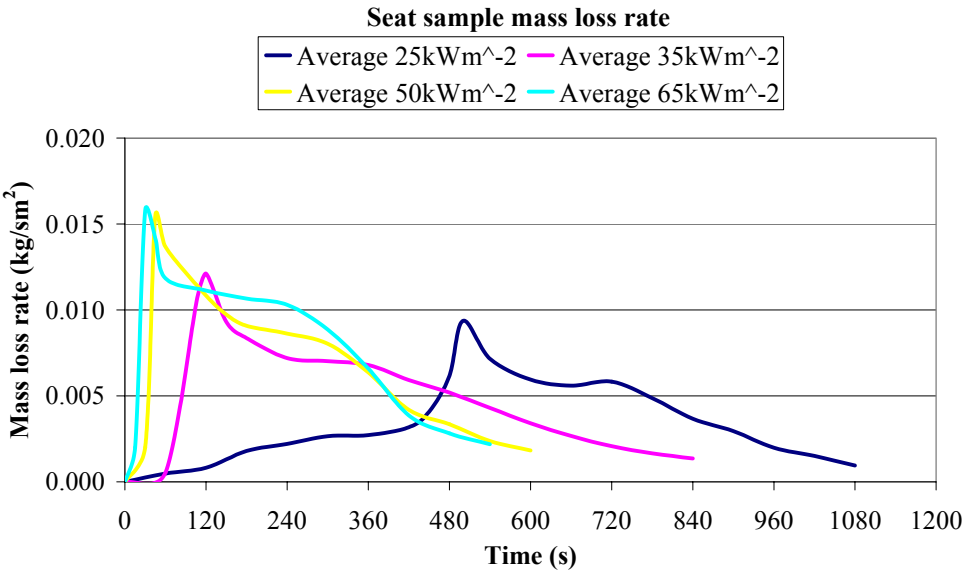

Figure 8.16: Seat sample - Mass loss rate curves at tested exposure heat fluxes

From Table 8.4, it can be seen that while there was significant increase in average time to ignition for tests at low exposure heat flux levels especially at 25 kW/m^2, the decrease in the average peak HRR was not substantial. In some cases, the peak HRR for specimen tested at e.g. 25 kW/m^2 was even higher than peak HRR for specimen tested at the next higher exposure heat flux level. This is notable by looking at the standard deviation of the average peak HRR in Table 8.4. These observations not only suggested that the material was difficult to ignite (especially at low heat flux levels); it also suggested that the material was difficult to burn. For this material, the average effective heat of combustion was found to be relatively constant with increasing exposure heat flux levels.

There were two peaks in heat release rate as shown in Figure 8.15. The first peak was likely due to burning of the surface layer. However, due to the presence of the fibreglass reinforced layer which acted as an insulation layer and physical barrier that prevented volatile gases from below the surface layer to travel out to the burning face, this resulted in decrease in the first peak HRR. The second peak might be due the delamination of the fibreglass reinforced layer which resulted in increase of the HRR again. The other possibility for the second peak HRR might be due to degradation of the unexposed back surface after the thermal wave reached the back surface.

From Figure 8.15 and Figure 8.16, it can be seen that even though the second peak HRR was not much lower than the first peak HRR, there was considerable difference in the mass loss rate when the two peak HRRs occurred. The difference in mass loss rate was most obvious for specimen tested at 25 kW/m^2 exposure heat flux level whereby both first and second peak HRR values were approximately the same. From Figure 8.16 and Table 8.4, it can be seen that for specimen tested at 25 kW/m^2 exposure heat flux level, sustained ignition did not occur until approximately 500 s into the tests, despite high mass loss rate. The likely explanation to all these results were that the material was treated with flame retardant additive. At low heat fluxes (25 and 35 kW/m^2), the additive worked effectively well to retard flaming. This might explain why flashings occurred before sustained ignition. When the specimens ignited, the additive might have decreased the effective heat of combustion during the initial stage of the test thus resulting in low HRR even though there was high mass loss rate. At the later part of the test, the effect of the additive vanished and the effective heat of combustion increased. Therefore lower mass loss rate was needed to result in same peak HRR. The other explanation for the high mass loss rate/ low HRR and low mass loss rate/ high HRR phenomena could be that the distribution of flame retardant additive was not homogenous with higher concentration near the surface. This explanation perhaps is more likely the case.

The average peak HRR for the FRP polyester seat was in the range of 130 to 184 kW/m^2 for exposure heat flux from 25 kW/m^2 to 65 kW/m^2. This was approximately 3.35 to 4.75 times lower compared with the peak HRR (618 kW/m^2) of the FRP material used in the trial simulations. Note that the HRRPUA curve for the FRP material was obtained from NIST's fire safety study of passenger trains (Peacock and Braun 1999); and was the material for wall panel tested at exposure heat flux of 50 kW/m^2. When comparing the other test data between the two FRP materials from the current study and the NIST study, at exposure heat flux level of 50 kW/m^2, it was noted that the thickness δ of the specimen in both studies was the same. The mass loss per unit area m'', time to ignition t_{ig}, second peak HRR and effective heat of combustion $\Delta H_{c,eff}$ were relatively comparable as shown in Table 8.5, despite the large difference in the peak HRR.

Data Source	δ **(m)**	t_{ig} **(s)**	m'' **(kg/m^2)**	**Second** $\dot{q}''_{peak}$ **(kW/m^2)**	$\Delta H_{c,eff}$ **(kJ/kg)**
Current study	0.004	50	3.860	132	13.3
NIST study	0.004	54[a]	4.137[a]	125[b]	13.5[a]

a Value was average of three tests listed in the report
b Approximated from the HRRPUA curve
NIST study - (Peacock and Braun 1999)

Table 8.5: Comparison of Cone Calorimeter test data between the current study and the NIST study (at exposure heat flux 50kW/m^2)

In order to make relative comparison, the test data of the seat in the current study was compared with the test data from other rail car studies as shown in Table 8.6.

Data source	$\dot{q}''_e$ **(kW/m^2)**	t_{ig} **(s)**	$\dot{q}''_{peak}$ **(kW/m^2)**	q'' **(MJ/m^2)**
Current study	25 – 65	34 - 502	130 – 184	40.1 - 60.3
NIST study[a]	50	7 - 12	260 – 420	4.5 – 61.7
Amtrak study[a]	25	0 – 16[b]	27 – 600	3.2 – 12
MARC study[a]	35 - 55	NA	164 – 192	NA
FIRESTARR[a]	25 - 35	1 – 88	98 – 525	4.3 - 92.1

a Seat cushion assembly
b Reported as ignition delay time
NA = Not available
NIST study - (Peacock and Braun 1999) Amtrak study - (Peacock and Braun 1984)
MARC study - (Gandhi et al. 1996) FIRESTARR - (Briggs et al. 2001a)

Table 8.6: Comparison of Cone Calorimeter test data of the seat between the current study and other rail car studies

The seat in the current study was moulded seat made of FRP polyester while the seat in other rail car studies was cushion seat made of combinations of foam, inter-liner and fabric. This was the main difference in the seat type. Data from Table 8.6 somewhat suggested that the seat in the current study was not easy to ignite and had relatively low peak HRR. However, in term of total heat released, it was on the high side. The might be because the amount heat released was moderately constant throughout the tests as can be seen from Figure 8.15.

Floor covering

The time to ignition t_{ig}, peak HRR $\dot{q}''_{peak}$, average $\dot{q}''$ value for first 180 s after ignition $\dot{q}''_{180}$ and effective heat of combustion $\Delta H_{c,eff}$ at the tested exposure heat flux levels are summarised in Table 8.7. The HRRPUA and mass loss rate curves at tested exposure heat flux levels are shown in Figure 8.17 and Figure 8.18 respectively.

No of replicate	$\dot{q}''_e$ (kW/m^2)	t_{ig} (s)		$\dot{q}''_{peak}$ (kW/m^2)		$\dot{q}''_{180}$ (kW/m^2)		$\Delta H_{c,eff}$ (kJ/kg)	
		Ave	STD -EV	Ave	STD -EV	Ave	STD -EV	Ave	STD -EV
3	25	603	42	45	4	31	2	11.9	2.1
3	35	232	8	82	8	44	2	16.5	0.3
3	50	118	3	80	9	61	4	14.5	1.6
3	65	76	2	101	3	77	2	15.4	1.1

Ave = Average value of all the replicates tested at the listed exposure heat flux level
STDEV = Standard deviation of average value

Table 8.7: Summary of Cone Calorimeter ignition and heat release data for the floor covering samples

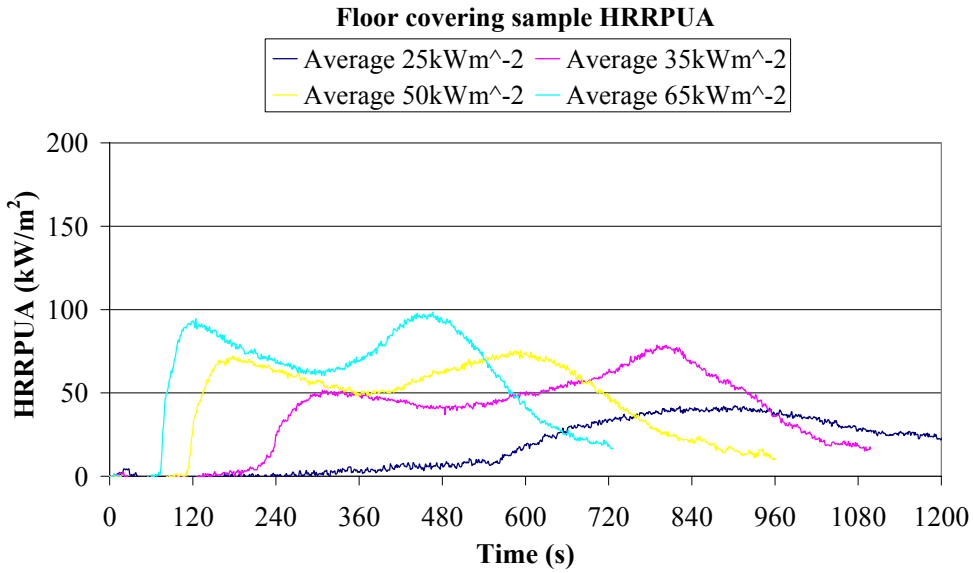

Figure 8.17: Floor covering sample – HRRPUA curves at tested exposure heat fluxes

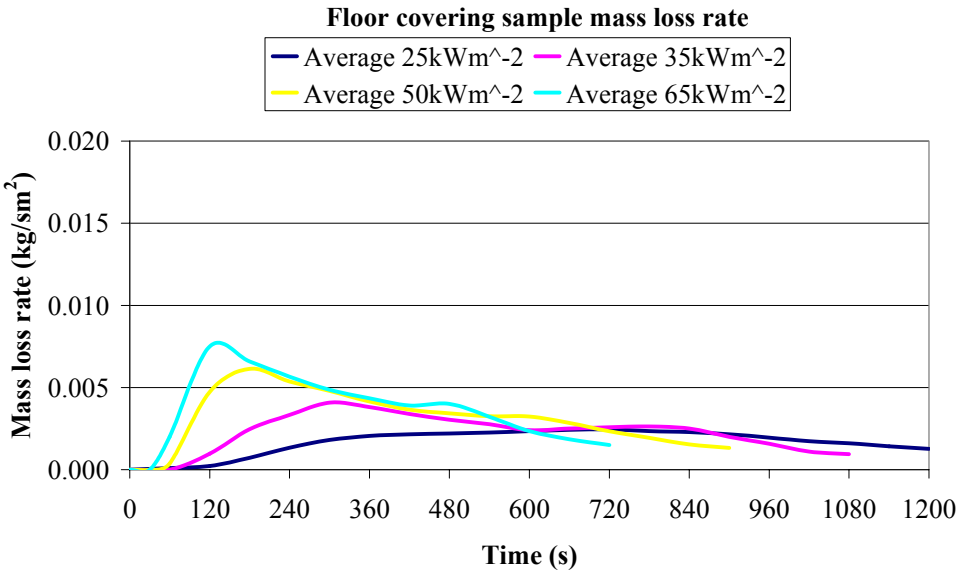

Figure 8.18: Flooring covering sample - Mass loss rate curves at tested exposure heat fluxes

Results from the Table 8.7 revealed that the floor covering was even more difficult to ignite and burn compared to the seat. There were two peak HRRs for tests at 35, 50 and 65 kW/m^2 exposure heat flux levels as shown in Figure 8.17. The first peak appeared shortly after ignition followed by gradual decrease in HRR with time. The decrease in HRR was likely due to the formation of insulating char layer near the specimen surface. The occurrence of the second peak was possibly due to heat up of the unexposed surface causing it to decompose and contribute to the HRR. At 25 kW/m^2 exposure heat flux level, there was only one peak HRR. The likely explanation was that there was insufficient energy for the thermal layer to reach the unexposed surface. The conversion of lower layer into char might also be the reason why there was only one peak HRR. Because there was only one peak HRR for tests at 25 kW/m^2, the effective heat of combustion was also relatively low compared to tests at higher exposure heat flux levels as indicated in Table 8.7.

The floor covering was also treated with flame retardant additive. This might explain why there were transitory flaming at 25 and 35 kW/m^2 exposure heat flux level; and why there were high mass loss rate / low HRR and low mass loss rate / high HRR phenomena as in tests for the seat. The second peak HRR for tests at 35 kW/m^2 exposure heat flux level was substantially higher than the first peak as shown in Figure 8.17. The first peak demonstrated good flame retardant property of the additive and the second peak suggested that there was uneven distribution of the flame retardant additive with higher concentration near the surface.

The styrene butadiene floor covering HRRPUA curve for the trial simulations was also obtained from the NIST study (Peacock and Braun 1999). Even though the material in the current study and the NIST study was the same, the peak HRR of the floor covering (281 kW/m^2) in the NIST study, at 50 kW/m^2 exposure heat flux level, was almost 3.4 times higher compared with the peak HRR (80 kW/m^2) in the current study.

Table 8.8 shows the test data of the floor covering in the current study and from other rail car studies.

Data source	$\dot{q}_e''$ **(kW/m^2)**	t_{ig} **(s)**	$\dot{q}_{peak}''$ **(kW/m^2)**	q'' **(MJ/m^2)**
Current study	25 – 65	76 – 603	45 – 101	19 – 44.3
NIST study	50	10 – 35	245 – 340	17.6 - 89.0
Amtrak study	25	95 – 117[a]	350 – 380	13 - 21

a Reported as ignition delay time
NIST study - (Peacock and Braun 1999) Amtrak study - (Peacock and Braun 1984)

Table 8.8: Comparison of Cone Calorimeter test data of the floor covering between the current study and other rail car studies

A comparison with other rail car studies shows that the floor covering in the current study was highly resistant to ignition. The peak HRR was also substantially low compared with other rail car studies. The amount of heat released was however in the middle ranges.

Wall panel

The time to ignition t_{ig}, peak HRR $\dot{q}''_{peak}$, average $\dot{q}''$ value for first 180 s after ignition $\dot{q}''_{180}$ and effective heat of combustion $\Delta H_{c,eff}$ at 65 kW/m^2 exposure heat flux levels are summarised in Table 8.9. The HRRPUA and mass loss rate curves at 65 kW/m^2 exposure heat flux levels are shown in Figure 8.19 and Figure 8.20 respectively.

No of replicate	$\dot{q}''_e$ (kW/m^2)	t_{ig} (s)		$\dot{q}''_{peak}$ (kW/m^2)		$\dot{q}''_{180}$ (kW/m^2)		$\Delta H_{c,eff}$ (kJ/kg)	
		Ave	STD -EV	Ave	STD -EV	Ave	STD -EV	Ave	STD -EV
2[a]	35	No ignition							
2[b]	50								
2	65	54	1	86	4	19	9	11.7	1.8

a No data was collected for both tests because of software problem
b No data was collected for one of the tests because of software problem
Ave = Average value of all the replicates tested at the listed exposure heat flux level
STDEV = Standard deviation of average value

Table 8.9: Summary of Cone Calorimeter ignition and heat release data for the wall panel samples

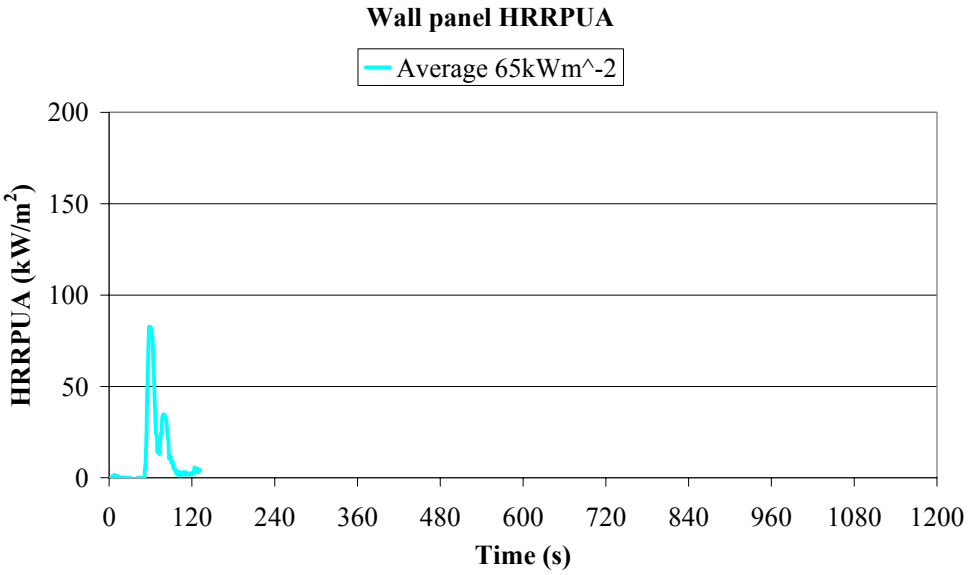

Figure 8.19: Wall panel sample - HRRPUA curve at 65kW/m^2 exposure heat flux

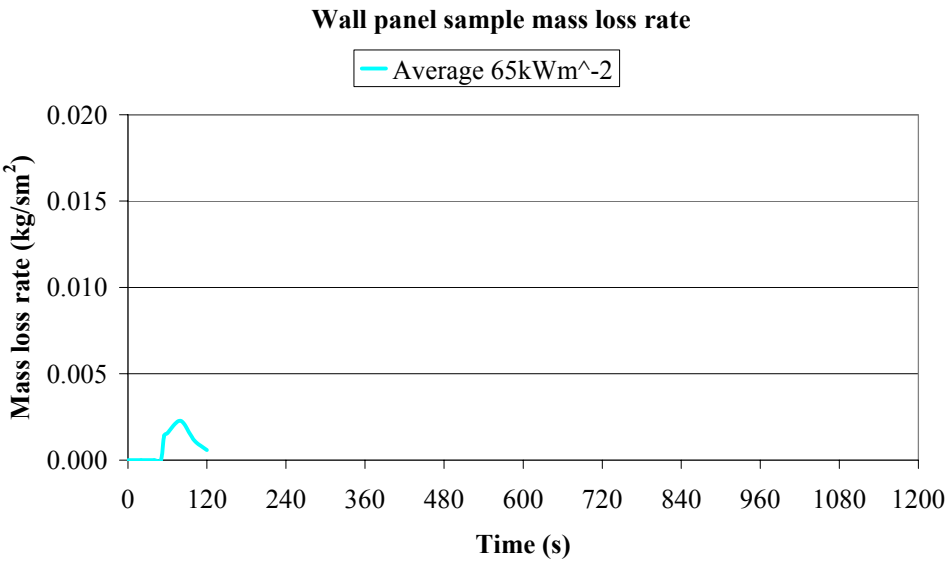

Figure 8.20: Wall panel sample - Mass loss rate curve at 65 kW/m^2 exposure heat flux

For the wall panel, there was no ignition for tests at 35 and 50 kW/m^2. This suggested that the wall panel was unlikely to contribute to the growth and spread during the developing stage of the fire. This claim could be supported based on results reported in Duggan (1997). Duggan reported the Cone Calorimeter test HRRPUA curve of a painted steel ceiling panel at 50 kW/m^2 exposure heat flux level. The HRRPUA curve is reproduced as shown in Figure 8.21.

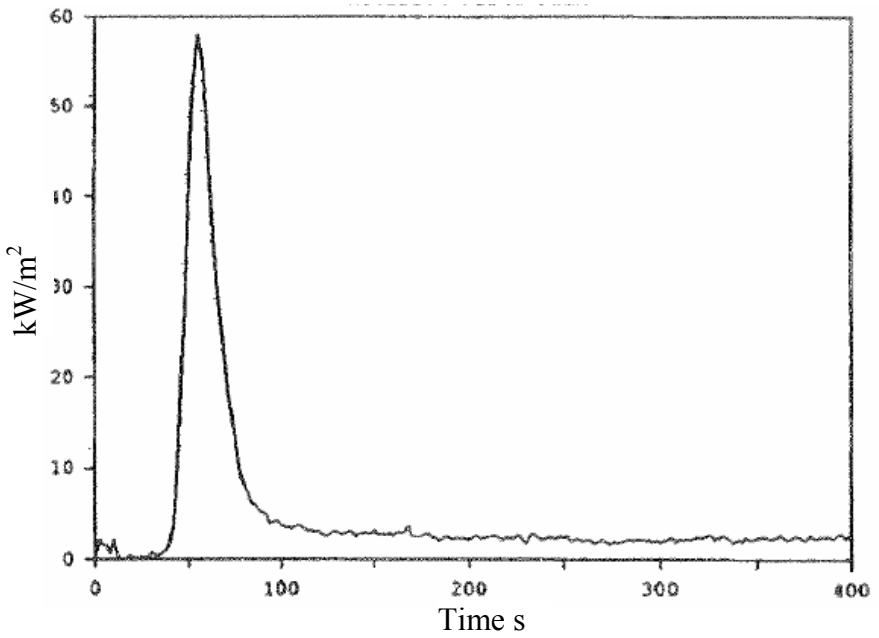

Figure 8.21: HRRPUA curve of a painted steel ceiling panel (reproduced from Duggan (1997))

The ceiling panel when tested to BS 476-Part 7 (BS 476-Part 7 1997) achieved 'Nil spread of flame'. Judging from the tested exposure heat flux level, the time to ignition and the burning period of the painted steel ceiling panel as shown in Figure 8.21, one would expect the wall panel in the current study to have better fire performance compared with the painted steel ceiling panel as ignition only occurred at 65 kW/m^2 exposure heat flux level for the wall panel. The time to ignition was also slower and the burning period was shorter for the wall panel compared with the painted steel ceiling panel even though it was tested at a higher exposure heat flux level.

The average $\dot{q}''$ for the first 180 s i.e. $\dot{q}''_{180}$ as shown in Table 8.9 was exceptionally low. This was because of short burning period of the specimen due to the fact that only the powder paint on the wall panel was combustible.

There were two peak HRRs as shown in Figure 8.19. The first peak might be due to the ignition of the top coat and the second peak due to the ignition of the primer. However note that there were insufficient tests conducted to fully support this explanation because for the two tests at 65 kW/m^2 exposure heat flux level, only one test had two peak HRRs. The HRR curve shown in Figure 8.19 was the average of the two tests.

Table 8.10 shows the test data of the wall panel in the current study and from other rail car studies.

Data source	$\dot{q}''_e$ **(kW/m^2)**	t_{ig} **(s)**	$\dot{q}''_{peak}$ **(kW/m^2)**	q'' **(MJ/m^2)**
Current study	25 – 65[a]	54	86	1.1 – 2
NIST study	50	18 - 23	120 – 270	21.5 - 66.8
Amtrak study	25	48[b]	410	3.1
MARC study	35 - 55	NA	134 - 222	NA

a Ignition occurred only at 65kW/m^2 exposure heat flux level
b Reported as ignition delay time
NA = Not available
NIST study - (Peacock and Braun 1999) Amtrak study - (Peacock and Braun 1984)
MARC study - (Gandhi et al. 1996)

Table 8.10: Comparison of Cone Calorimeter test data of the wall panel between the current study and other rail car studies

Data in Table 8.10 demonstrated good fire performance of the wall panel in the current study compared with the wall panel tested in other rail car studies. This mainly attributed to the difference in materials used to construct the panels. In other rail car studies, the wall panels were made of polymers whereby in the current study, the wall panel was made of aluminium, a non-combustible material, with a thin coat of powder paint.

Bellows (Inner)

The time to ignition t_{ig}, peak HRR $\dot{q}''_{peak}$, average $\dot{q}''$ value for first 180 s after ignition $\dot{q}''_{180}$ and effective heat of combustion $\Delta H_{c,eff}$ at the tested exposure heat flux levels are summarised in Table 8.11. The HRRPUA and mass loss rate curves at tested exposure heat flux level are shown in Figure 8.22 and Figure 8.23 respectively.

No of replicate	$\dot{q}''_e$ (kW/m^2)	t_{ig} (s)		$\dot{q}''_{peak}$ (kW/m^2)		$\dot{q}''_{180}$ (kW/m^2)		$\Delta H_{c,eff}$ (kJ/kg)	
		Ave	STD-EV	Ave	STD-EV	Ave	STD-EV	Ave	STD-EV
2[a]	35	179	n/a	111	n/a	82	n/a	Nil	n/a
2	50	81	4	147	1	104	2	15.1	0.6
2	65	58	9	170	8	109	5	13.2	1.1

a No data was collected for one of the tests. For the other tests, data acquisition stopped mid-way through the test. The effective heat of combustion could not be calculated and therefore was shown as Nil above.
Ave = Average value of all the replicates tested at the listed exposure heat flux level
STDEV = Standard deviation of average value
n/a = Not applicable since only value for one test was reported

Table 8.11: Summary of Cone Calorimeter ignition and heat release data for the bellows (Inner) samples

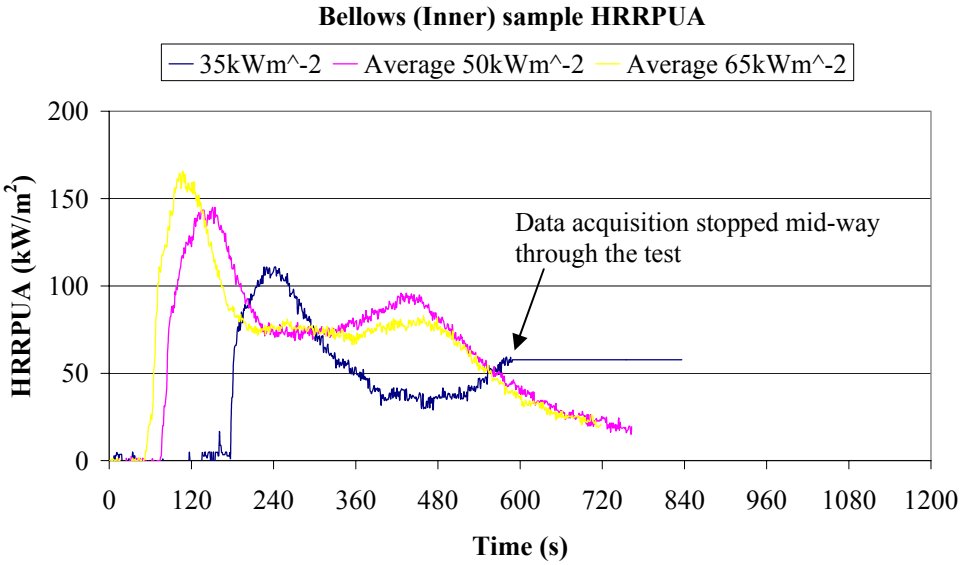

Figure 8.22: Bellows (Inner) sample - HRRPUA curves at tested exposure heat fluxes

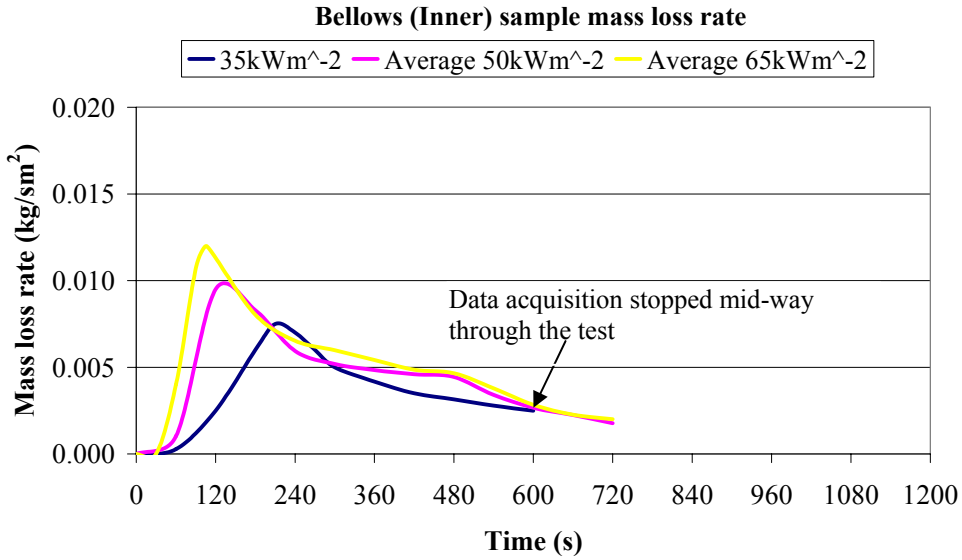

Figure 8.23: Bellows (Inner) sample - Mass loss rate curves at tested exposure heat fluxes

The bellows (Inner) exhibited the same burning behaviour as the floor covering. The material was also treated with flame retardant additive but compared with the flooring covering, it ignited slightly faster and had higher peak HRR. Unlike the floor covering, the second peak HRR was substantially lower compared with the first peak HRR at all tested exposure heat flux levels as can be seen from Figure 8.22. There was no test data to make relative comparison with, however it was noted that the fire performance of this material was better compared with the seat material in the current study.

Bellows (Outer)

The time to ignition t_{ig}, peak HRR $\dot{q}''_{peak}$, average $\dot{q}''$ value for first 180 s after ignition $\dot{q}''_{180}$ and effective heat of combustion $\Delta H_{c,eff}$ at the tested exposure heat flux levels are summarised in Table 8.12. The HRRPUA and mass loss rate curves at tested exposure heat flux levels are shown in Figure 8.24 and Figure 8.25 respectively. Note that for one of the tests at each exposure heat flux levels, the retainer frame popped up and hit the ignitor. The results for those tests were not reported here because of potential errors. However, the time to ignition was reported since it was not affected.

No of replicate	$\dot{q}''_e$ (kW/m^2)	t_{ig} (s)		$\dot{q}''_{peak}$ (kW/m^2)		$\dot{q}''_{180}$ (kW/m^2)		$\Delta H_{c,eff}$ (kJ/kg)	
		Ave	STD -EV	Ave	STD -EV	Ave	STD -EV	Ave	STD -EV
2	35	118	4	84	n/a	60	n/a	12.8	n/a
2	50	76	3	116	n/a	77	n/a	13.8	n/a
2	65	47	2	194	n/a	114	n/a	16.5	n/a

Ave = Average value of all the replicates tested at the listed exposure heat flux level
STDEV = Standard deviation of average value
n/a = Not applicable since only value for one test was reported

Table 8.12: Summary of Cone Calorimeter ignition and heat release data for the bellows (Outer) samples

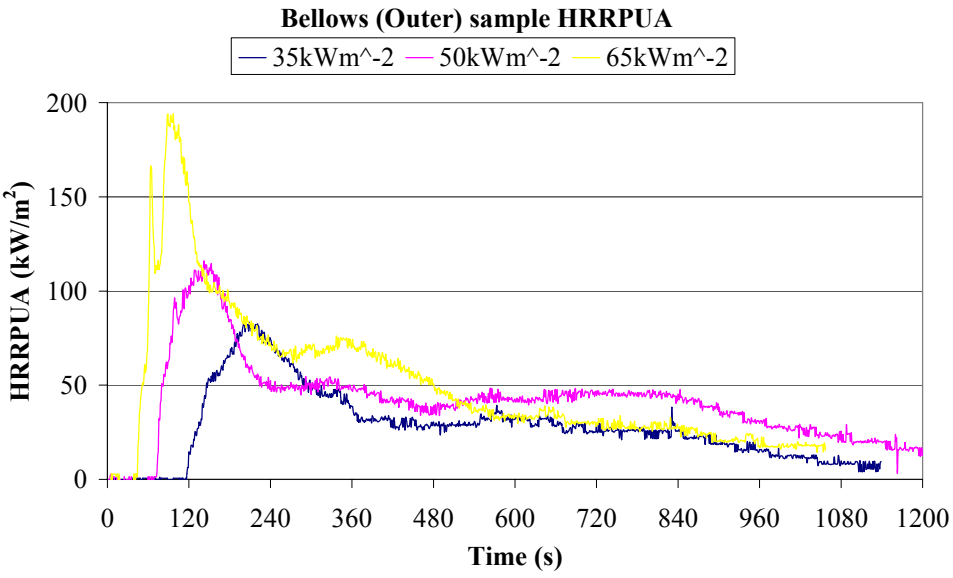

Figure 8.24: Bellows (Outer) sample - HRRPUA curves at tested exposure heat fluxes

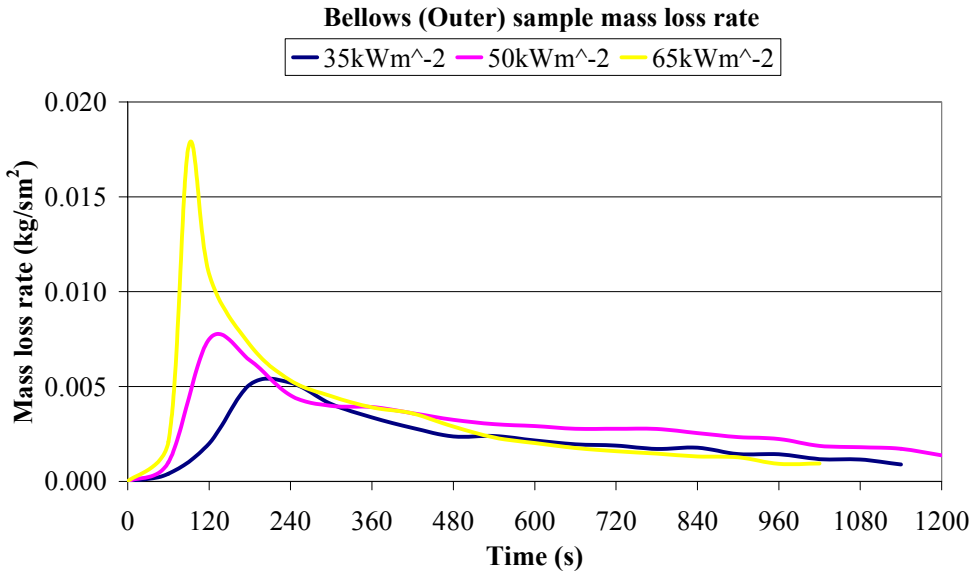

Figure 8.25: Bellows (Outer) sample - Mass loss rate curves at tested exposure heat fluxes

Both the bellows (Outer) and bellows (Inner) have the same trade name but with different identification code. It was assumed that both were made of the same material. However, from Table 8.12, it seemed that the bellows (Outer) was easier to ignite compared with the bellows (Inner). The difference in time to ignition was found to be larger at 35 kW/m^2 exposure heat flux level. The peak HRR for the bellows (Outer), however, was lower (with exception to tests at 65 kW/m^2) compared with the bellows (Inner) even though the specimens were exposed to higher exposure heat flux levels when they expanded after ignition.

There was no concrete explanation for the above. It could be due to specimen area effect since the bellows (Inner) specimen size was smaller compared with the bellows (Outer) specimen. It could be due to experimental errors or it could also be due to difference in composite ingredients that made up the two components.

Disregarding the above differences, the burning behaviour of the bellows (Outer) and bellows (Outer) were similar. The fire performance for the bellows (Outer) was also found to be better compared with the seat material in the current study. The peak HRR was below 200 kW/m^2 even with the potential errors introduced when the specimen swelled during the tests.

8.5.2 Material properties

This Section presents the results of material properties (for the exposed surface materials in the train car) derived from the Cone Calorimeter test data. Note that only the material properties for the seat and floor covering samples were derived. It was not possible to derive the material properties for wall panel due to insufficient data from the Cone Calorimeter tests. A simple assumption, however, was made to approximate the ignition temperature T_{ig} for the wall panel but the result was solely for discussion purpose only.

Ignition temperature

The ignition time correlation for the seat and floor covering are shown in Figure 8.26 and Figure 8.27 below.

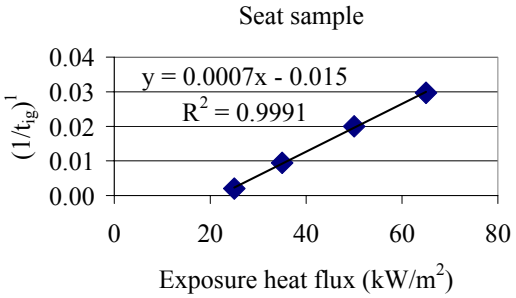

Figure 8.26: Ignition time correlation for the seat sample

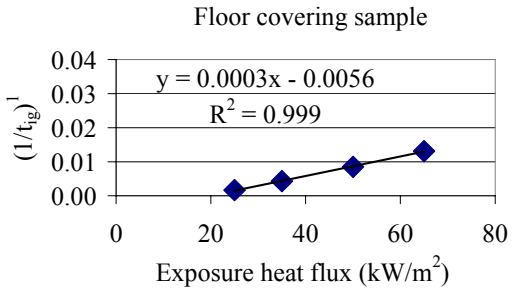

Figure 8.27: Ignition time correlation for floor covering sample

Both graphs illustrate almost perfect linear relation. The value of n that resulted in the highest correlation coefficient R^2 was 1. This indicates thermally thin behaviour.

The x-intercept is taken as the critical heat flux $\dot{q}''_{cr}$. It was determined to be 21.4 kW/m^2 for the seat and 18.7 kW/m^2 for the floor covering.

In order to determine the ignition temperature, it was necessary to solve (by iteration) Equation 8.5. Equation 8.5 is reproduced here as Equation 8.10

$$\varepsilon \dot{q}''_{cr} = h_c(T_{ig} - T_\infty) + \varepsilon\sigma(T_{ig}^4 - T_\infty^4) \qquad \text{Equation 8.10}$$

The value of ambient temperature T_∞ was assumed to be 273 K (20°C). The convective heat transfer coefficient h_c was taken as 0.0135 kW/m^{2}K, the value adopted by Grexa et al. (1996) in their study. Surface emissivity ε was taken as 0.88, the average value for a wide range of plastics and value suggested by Babrauskas (2003) for treating of the Cone Calorimeter data. Surface emissivity ε of 0.88 was also the value used by Grexa et al. (1996) in their study.

By solving Equation 8.10, the ignition temperature T_{ig} for the seat and floor covering were determined to be 448 and 419°C respectively.

These values were reasonably higher than the values used in the trial simulations which were 346 and 360°C for the seat (FRP polyester) and floor covering (styrene butadiene) respectively.

It was noted from the results above that the floor covering was determined to have lower critical heat flux $\dot{q}''_{cr}$ and ignition temperature T_{ig} compared with the seat. The results seemed to contradict with the experimental observations and HRR test data which indicated that the floor covering was more difficult to ignite. But to investigate this further was beyond the scope of this project, therefore it was decided to take the results as they were. It was also noted during the calculation process that the computed ignition temperature was sensitive to the inputted critical heat flux $\dot{q}''_{cr}$ and heat transfer coefficient h_c . Different values of heat transfer coefficient h_c were proposed by different researchers depending of the tested heat flux levels (Babrauskas 2003). However to carry out sensitivity analysis will only complicate this project therefore it was decided to abandon this attempt.

In order to approximate the ignition temperature T_{ig} for the wall panel, a crude assumption was made. The critical heat flux $\dot{q}''_{cr}$ for the wall panel was conservatively assumed to be 50 kW/m^2. Taking the ambient temperature T_∞ to be 273 K (20°C), convective heat transfer coefficient h_c to be 0.0135 kW/m^{2}K and surface emissivity ε to be 0.88. Solving by iteration of Equation 8.10, the ignition temperature T_{ig} for the wall panel was determined to be 648°C. This result again suggested that the wall panel would not be involved during the developing stage of the fire. The compartment temperature needs to be higher than 648°C to result in ignition and this will only occur during the post-flashover fire stage.

Mechanical and thermal properties

Both the seat and floor covering were found to behave as thermally thin surface, therefore the product of $\rho c \delta$ were determined for the simulation. This contrary to the assumption made in the trial simulations that the materials were thermally thick. From Figures 8.26 and 8.27, the slopes of a linear line fit through the data for the seat and floor covering were found to be 0.0007 and 0.0003 respectively. Substituting these values and the computed ignition temperatures into Equation 8.8, the products of $\rho c \delta$ for the seat and floor covering were determined to be 3.341 and 8.363 kJ/Km^2 respectively.

Heat of vaporisation

The heat release rate correlations for the seat and floor covering are shown in Figure 8.28 and Figure 8.29 below.

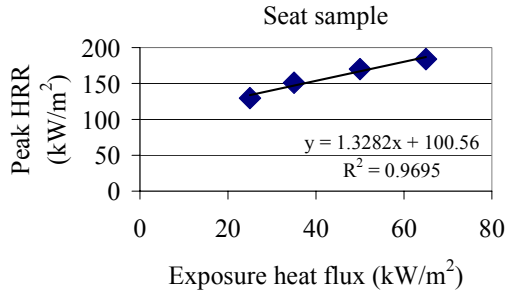

Figure 8.28: Heat release rate correlation for the seat sample

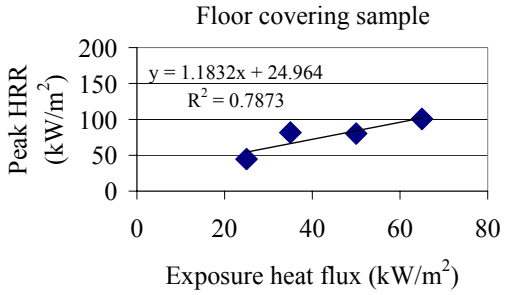

Figure 8.29: Heat release rate correlation for the floor covering sample

The average values of effective heat of combustion $\Delta H_{c,eff}$ for the seat and floor covering were determined to be 13670 and 14570 kJ/kg respectively. From Figure 8.28 and Figure 8.29, the slopes of a linear line fit through the data for the seat and floor covering were found to be 1.3282 and 1.1832 respectively. Substituting the average value of effective heat of combustion $\Delta H_{c,eff}$ and the slope into Equation 8.9, the heat of vaporisation values for the seat and floor were determined to be 10300 and 12320 kJ/kg respectively.

It was noted that the effective heat of combustion of the seat (FRP polyester) in the above calculation was higher than the value of 12870 kJ/kg used in the trial simulations. However for the floor covering (styrene butadiene), the effective heat of combustion in the calculation was lower than that prescribed in the trial simulations which was 17950 kJ/kg. The values used in the trial simulations were based on the values given in (Renie and Prevot 2003) submitted by the train supplier.

The slope or 'combustibility ratio' was found to be extremely low compared with the combustible solids quoted in Drysdale (1998). The 'combustibility ratio' for combustible solids as quoted in Drysdale (1998) was in the range of 3 (for red oak) to 30 (for rigid polystyrene foam). Drysdale (1998) reported that flame retardant could influence the 'combustibility ratio' by altering the heat for combustion and/ or heat of vaporisation. This probably explained why the 'combustibility ratio' for both the seat and floor covering were low as they were both treated with flame retardant. Having low 'combustibility ratio' somewhat suggests that the materials are 'less combustible'.

Because of low 'combustibility ratio', the computed heat of vaporisation values for both the seat and floor covering were found to be unusually high. The computed heat of vaporisation values were even higher than the heat of vaporisation values of flame retardant materials quoted in Babrauskas (2003); Drysdale (1998) and Grexa et al. (1996). The values were also substantially higher than those used in the trial simulations which were 1390 and 2700 kJ/kg for the seat (FRP polyester) and floor covering (styrene butadiene) respectively.

Critical mass flux and maximum burning rate

The critical mass flux and the maximum burning rate were determined directly from the mass loss rate data. The critical mass flux values for the seat and floor were determined to be 0.0044 and 0.0024 kg/sm^2 respectively while the maximum burning rate values were determined to be 0.0161 and 0.0079 kg/sm^2 respectively.

The critical mass flux was not prescribed in the trial simulations therefore it was not possible to make comparison. The maximum burning rate values were found to be relatively low compared with the values used in the trial simulations. The maximum burning rate values used in the trial simulations for the seat (FRP polyester) and floor covering (styrene butadiene) were 0.021 and 0.01 kg/sm^2 respectively. These values were approximated from the HRRPUA curves of similar materials tested in Peacock and Braun (1999).

Charring of samples

Because the samples charred as observed during the experiments, it posed the question whether it would be more appropriate to model the samples as thermoplastic or char former fuels. To model the samples as char former fuels will require the char density, char conductivity and char specific heat to be specified for the modelling approach based on heat of vaporisation (McGrattan 2004). These properties are on top of those that have been derived previously.

The char density could be approximated since the mass of the specimens at the end of the Cone Calorimeter tests was measured. Chen et al. (1995) described a methodology that could be used to obtain the char conductivity although in their study they found that the thermal capacity i.e. ρc of char has negligible effects on the pyrolysis process and therefore need not be quantified. However the methodology requires a thermal pyrolysis model to be created (and an assumption that the materials are thermally-thick) and a trial and error process to obtain value that best fits the predicted with the experimental mass loss rate histories for Cone Calorimeter tests at two different exposure flux levels (Delichatsios et al. 2003). How well the predicted and the experimental mass loss rate histories correlate is subjective and this will affect the char conductivity value obtained and therefore might not be suitable for engineering design.

There is no other simpler procedure to derive the char conductivity and char specific heat from the Cone Calorimeter test data. There is also no such information available for the samples modelled. In view of these constraints, it was decided to model the samples as thermoplastic fuels. It would be more conservative because the decline in first peak HRR would not be predicted. However, the author acknowledged that this is a practical problem that may affect the simulation results.

Summary of material properties derived

The material properties derived from the Cone Calorimeter test data and material properties used in the trial simulations are summarised in Table 8.13 for easy reference.

Component		T_{ig} (°C)	$\rho c \delta$ (kJ/m^{2}K)	**Ave** $\Delta H_{c,eff}$ (kJ/kg)	ΔH_v (kJ/kg)	$\dot{m}''_{cr}$ (kg/sm^2)	$\dot{m}''_{\max}$ (kg/sm^2)
Seat - FRP polyester	Derived from test data	448	3.341	13670	10300	0.0044	0.0161
	Trial simulation	346	n/a	12870	1390	Not prescribed	0.021
Floor covering - Styrene butadiene	Derived from test data	419	8.363	14570	12320	0.0024	0.0079
	Trial simulation	360	n/a	17950	2700	Not prescribed	0.01
Wall panel	Approximated	648	-	-	-	-	-

n/a = Not applicable as the material was assumed to be thermally thick. The thermal conductivity, density and specific heat i.e. $k\rho c$ were prescribed individually and were based on properties at room temperature.

Table 8.13: Summary of material properties derived from Cone Calorimeter test data

The material properties values used in the trial simulations were found to be over conservative. The train car materials are expected to be more difficult to ignite based on their derived ignition temperature. The materials are also likely to be less combustible because of low 'combustibility ratio'. The fire consequence is also expected to be less severe because of lower burning rate.

8.6 Conclusions from the Cone Calorimeter tests and the derived material properties

The following conclusions can be drawn from the Cone Calorimeter tests and the derived material properties.

a) Cone calorimeter tests were carried out for six train car materials. Among the six materials, the seat had the highest ignitability and flammability. Even so, it was more difficult to ignite and to burn compared with materials tested in other rail car studies. The flame retardant additive in the polymer materials proved to be effective in retarding ignition (especially at low heat flux levels) and reducing the heat release rate.

b) There was insufficient Cone Calorimeter test data to derive the material properties for the wall panel as the test specimens did not ignite at 35 and 50 kW/m^2. Through analysis, the wall panel is not expected to contribute to the fire growth and flame spread during the developing stage of the fire.

c) The samples charred as observed during the experiments. However as there was no information on the char properties, it was decided to model the samples as thermoplastic fuels.

d) The material properties values used in the trial simulations were found to be over conservative. The train car materials are expected to be more difficult to ignite and less combustible. The fire consequence is expected to be less severe than in the trial simulations.

9 FDS predictions of Cone Calorimeter test results

This Chapter describes the simulations carried out to compare the FDS predictions with the Cone Calorimeter test results i.e. the time to ignition and heat release rate. The purpose of the simulations is to check whether the material properties derived (and used as input into the fire model) are able to provide reasonable prediction of the experimental test results before they are used for simulation of train fires. It is particularly important to carry out this step because no full-scale test will be conducted to validate the train fire modelling results.

Since only the material properties for seat (FRP polyester) and floor covering (styrene butadiene) were derived, only these two materials were modelled.

9.1 FDS inputs

9.1.1 Geometry, vent, mechanical and thermal properties

The FDS model for the Cone Calorimeter was provided by McGrattan (2005b). The perspective views of the Cone Calorimeter model for the seat (FRP polyester) specimen and floor covering (styrene butadiene) specimen are shown in Figure 9.1 and Figure 9.2 respectively. The size of the computational domain was 0.2 m long by 0.2 m wide by 0.25 m high. All the sides were specified to be open vent i.e. open to ambient.

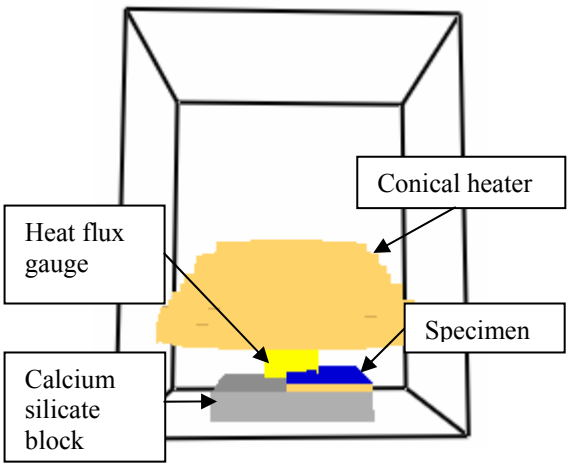

Figure 9.1: Snapshot from Smokeview – Cone Calorimeter model for seat (FRP polyester) specimen

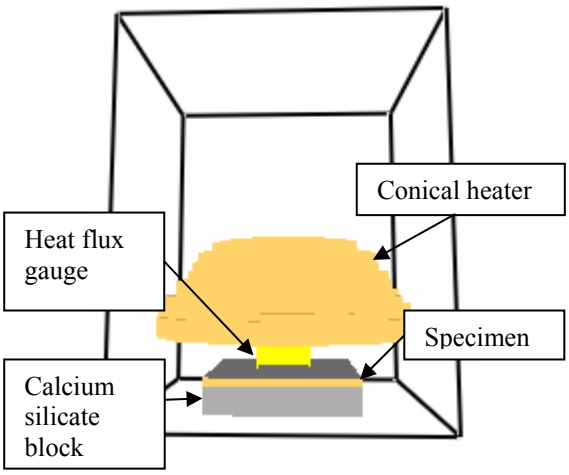

Figure 9.2: Snapshot from Smokeview – Cone Calorimeter model for floor covering (styrene butadiene) specimen

The dimensions of the specimens were specified according to their actual dimensions in the Cone Calorimeter tests. These two specimens have been found to behave as thermally-thin surface. The derived $\rho c \delta$ values for FRP polyester and styrene butadiene specimens were 3.341 and 8.363 kJ/m^{2}K respectively. These values were prescribed directly into FDS.

Both specimens were backed with 0.1 m by 0.1 m by 0.02 m thick calcium silicate block in the model. The prescribed thermal conductivity k, density ρ and specific heat c of the calcium silicate block were 0.12 W/mK, 720 kg/m^3 and 1.25 kJ/kgK respectively. These values were obtained from Wade (2003b).

The size and shape of the conical heater in the model were replicate of the conical heater in the Cone Calorimeter. The temperature of the outer surface of the conical heater was specified to be at 20°C while the temperature of the inner surface was specified according to the required incident heat flux level on the specimen. By prescribing a 'heat flux gauge' at a distance of 0.025 m below the bottom surface of conical heater and by trial and error, the calibrated temperature values as shown in Table 9.1 were obtained.

$\dot{q}_e^{"}$ **(kW/m^2)**	**Calibrated temperature (°C)**
25	633
35	712
50	808
65	883

Table 9.1: Calibrated temperatures for Cone Calorimeter model

A numerical grid size of 25 by 25 by 32 cells was chosen after conducting grid sensitivity analysis. One of the main reasons for choosing this grid size was because the proportion of grid size and characteristic fire diameter D^* given by:

$$D^* = \left(\frac{\dot{Q}}{1100} \right)^{2/5}$$ Equation 10.1

was similar for the selected grid size and characteristic fire diameter D^* for the train model as shown in Table 9.2. In the calculation, the HRR value of 1 kW for the Cone Calorimeter model was the maximum HRR in the Cone Calorimeter tests for the two specimens while the HRR value of 10000 kW for the train model (see Table 9.2) was the speculative HRR of the metro train under consideration.

Model	$\dot{Q}$ **(kW)**	D^* **(m)**	δx **(mm)**	$D^* / \delta x$
Cone Calorimeter	1	0.061	8	0.008
Train	10000	2.4	300	0.008

Table 9.2: HRR, characteristic fire diameter and grid size

This criterion was used by Hietaniemi et al. (2004) in their work to select the grid sizes for FDS models having different scales. It allows the selected grid size to relate to the HRR.

Note that in the Cone Calorimeter model, the grid has been stretched in the z-direction so that finer grid cells were allocated at lower portion of the domain where combustion took place. The simulation time specified for each simulation was 1200 s. The computers used for the simulations were Intel(R) Pentium 4(R), 3.2 GHz, 1 GB RAM computers. The times taken to complete the simulations were between 9 to 12 hours.

A sample FDS data file for the simulations can be found in Appendix H of this report.

9.1.2 Parameters for the modelling approach based on HRRPUA

For the modelling approach based on HRRPUA, the ignition temperature and the Cone Calorimeter HRRPUA curve of a specimen were specified in each simulation. The prescribed ignition temperatures for FRP polyester and styrene butadiene specimens were 448°C and 419°C respectively.

The HRRPUA curve to be prescribed should be from the time to ignition (the point where sustained flaming occurred) until the end of the test. The average HRRPUA curve of the three replicate specimens at each exposure condition was utilised.

Because the average HRRPUA curve was used, there was some uncertainty in the time to ignition especially for the specimens tested at low exposure heat flux level. This was because the visually determined ignition times showed significant scatter.

Grexa et al. (1996) proposed the use of a criterion based on the HRR to determine the time to ignition. In their study, the specimen was considered ignited when the Cone Calorimeter HRR reached 30 kW/m^2. They highlighted that the use of such criterion can greatly eliminate subjectivity because of ambiguity in the recording of ignition times. Their proposed method was therefore adopted.

After evaluation of the ignition data for the two materials in the current study, 30 kW/m^2 was also chosen as the suitable limit because the time to reach this HRR has been found to agree reasonably well with the visually determined ignition times.

9.1.3 Parameters for the modelling approach based on heat of vaporisation

The ignition temperatures prescribed were the same as the modelling approach based on HRRPUA and the other parameters for the simulations are given in Table 7.4.

S/no	Parameter	FRP polyester	Styrene butadiene
1	Heat of vaporisation ΔH_v (kJ/kg)	10300	12320
2	Effective heat of combustion $\Delta H_{c,eff}$ (kJ/kg)	13670	14570
3	Maximum burning rate $\dot{m}''_{\max}$ (kg/m^{2}s)	0.0161	0.0079
4	Critical mass flux $\dot{m}''_{cr}$ (kg/m^{2}s)	0.0044	0.0024

Table 9.3: Heat of vaporisation, effective heat of combustion, maximum burning rate and critical heat flux for FRP polyester and styrene butadiene specimens

9.2 Results and discussions for FDS prediction of Cone Calorimeter test results

9.2.1 Modelling approach based on HRRPUA

FRP polyester

Figure 9.3 to Figure 9.6 show the FDS predictions and the experimental HRR curves at different exposure conditions.

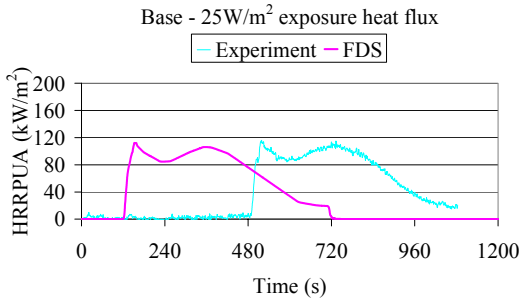

Figure 9.3: Modelling approach based on HRRPUA - FRP polyester - FDS prediction at 25 kW/m^2 exposure heat flux

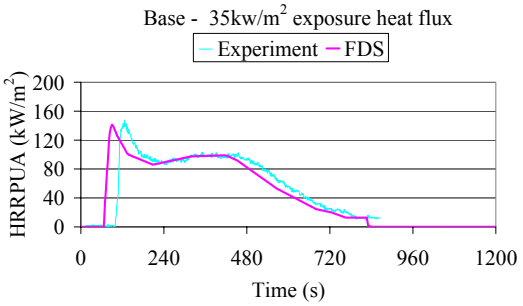

Figure 9.4: Modelling approach based on HRRPUA - FRP polyester - FDS prediction at 35 kW/m^2 exposure heat flux

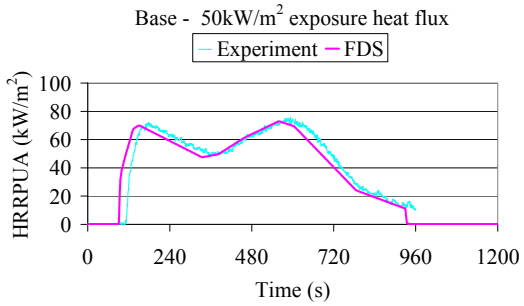

Figure 9.5: Modelling approach based on HRRPUA - FRP polyester - FDS prediction at 50 kW/m^2 exposure heat flux

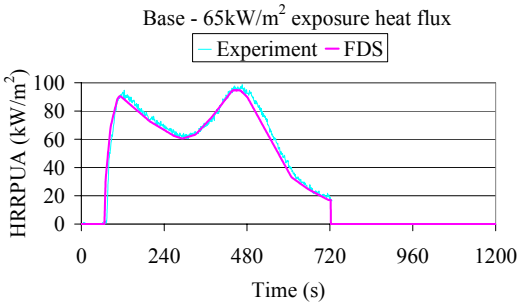

Figure 9.6: Modelling approach based on HRRPUA - FRP polyester - FDS prediction at 65 kW/m^2 exposure heat flux

For the modelling approach based on HRRPUA, the 'shape' of the heat release curves was programmed into FDS, therefore FDS was able to gave identical 'shape' as the experimental HRR curve as shown in the Figures. The predicted time to ignition was relatively accurate at high exposure heat flux levels. However, the accuracy decreases with decreasing exposure heat flux levels. At 25 kW/m^2 exposure heat flux level, the predicted time to ignition was unreasonably low. The parameters that governed the time to ignition were exposure heat flux level, $\rho c \delta$ and ignition temperature. This suggested the derived values were not suitable for prediction of time to ignition at low heat flux levels.

To improve the prediction, the $\rho c\delta$ and /or ignition temperature values may need to be calibrated since they are the parameters that influence the time to ignition. Of the two parameters, only the $\rho c\delta$ value is temperature dependent. The ignition temperature of a thermoplastic is found to be reasonably constant and independent of heat flux (Janssens et al. 2003; Thomson and Drysdale 1987; Thomson et al. 1988). Assuming the derived ignition temperature was accurate, therefore only the $\rho c\delta$ value needed to be adjusted.

By trial and error, the 'optimum' $\rho c\delta$ values as shown in Table 9.4 were obtained. From Table 9.4, it can be seen that at low exposure heat flux levels, much higher $\rho c\delta$ values were to be prescribed in order to accurately predict the time to ignition. FDS predictions using the calibrated $\rho c\delta$ values are shown from Figure 9.7 to Figure 9.10. These Figures show perfect agreement with the experimental HRR curves.

$\dot{q}_e^{"}$ **(kW/m^2)**	**Calibrated $\rho c\delta$ value (kJ/m^{2}K)**
25	13.3
35	5.4
50	3.95
65	3.6

Table 9.4: Modelling approach based on HRRPUA - Calibrated $\rho c\delta$ values for FRP polyester

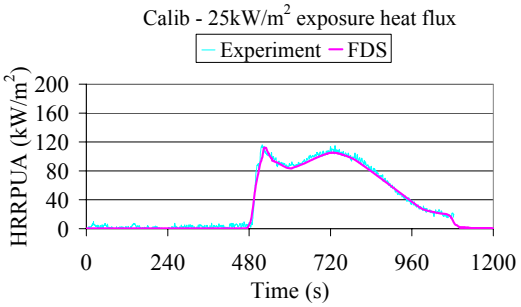

Figure 9.7: Modelling approach based on HRRPUA - FRP polyester - FDS prediction at 25 kW/m^2 exposure heat flux (Calibrated)

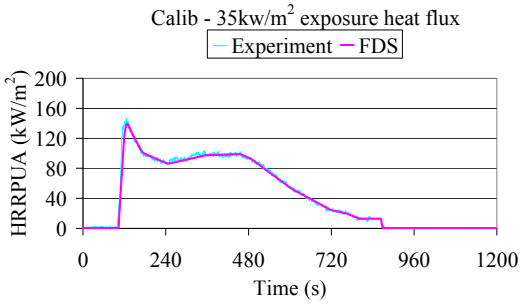

Figure 9.8: Modelling approach based on HRRPUA - FRP polyester - FDS prediction at 35 kW/m^2 exposure heat flux (Calibrated)

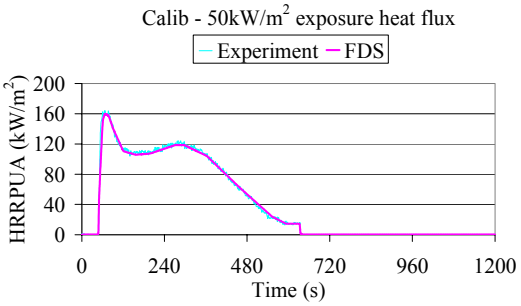

Figure 9.9: Modelling approach based on HRRPUA - FRP polyester - FDS prediction at 50 kW/m^2 exposure heat flux (Calibrated)

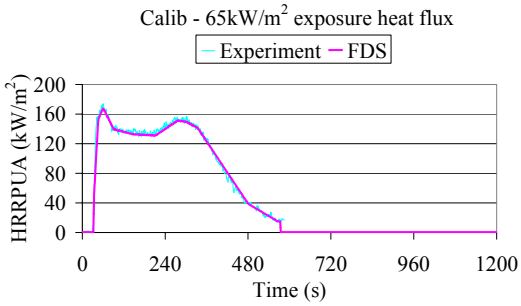

Figure 9.10: Modelling approach based on HRRPUA - FRP polyester - FDS prediction at 65 kW/m^2 exposure heat flux (Calibrated)

The author had attempted to derive a set of temperature variant properties for $\rho c\delta$ in hope that the time to ignition could be accurately predicted at various exposure heat flux levels. This was carried out by assuming T_∞ in Equation 8.8 to be the surface temperature of the materials T_{sur}. Equation 8.8 is rewritten in the following form:

$$\rho c\delta = \frac{1}{slope(T_{ig} - T_{sur})} \qquad \text{Equation 10.2}$$

The slope and the ignition temperature T_{ig} in Equation 10.2 were kept constant while T_{sur} was increased incrementally. This way, a set of temperature variant properties was derived for input into FDS for simulations. However, using the temperature variant properties for simulations did not give better results. The ignition times at low exposure heat flux levels were underestimated while the ignition times at high exposure heat flux levels were overestimated.

The calibrated $\rho c\delta$ values were plotted against the exposure heat flux levels as shown in Figure 9.11. The Figure shows that there was a steep decrease in $\rho c\delta$ values when the exposure heat flux levels increased from 25 to 35 kW/m^2. This might be the region where the fire retardant started to lose its effectiveness to retard ignition. The flame retardant was able to effectively retard ignition at low exposure heat flux level, therefore substantially greater amount of energy was required before ignition could take place, but at high heat flux intensities, lesser amount of energy was required. This might be the reason why a suitable set of temperature variant properties for the fire retardant material could not be derived.

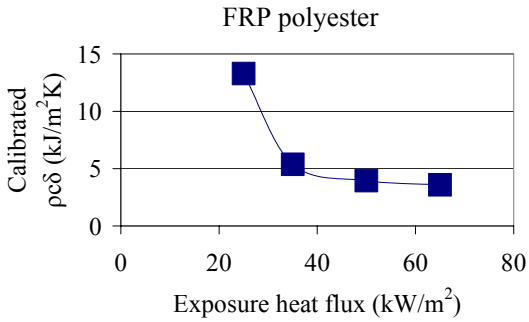

Figure 9.11: Calibrated $\rho c\delta$ values for FRP polyester at exposure different heat flux levels

A suitable set of temperature variant properties for $\rho c\delta$ could not be derived and no single constant $\rho c\delta$ value could be prescribed for the modelling approach based on HRRPUA to reasonably predict the time to ignition at different exposure heat flux levels. If the value derived from Cone Calorimeter is inputted into the train model, FDS will over-predict the HRR because the time to ignition will be underestimated especially at low heat flux levels.

To improve the prediction, a sub-model may be required. The sub-model must be able to select different prescribed property values for numerical simulation depending on the heat feedback from the fire.

The current version of FDS does not have such a sub-model. To proceed with the final simulations, it was decided to prescribe the $\rho c\delta$ values according to the locations of the components in the metro train. For wall-like surfaces, seat and driver console assembly which will be represented by HRRPUA curve tested at 35 kW/m^2, the calibrated $\rho c\delta$ value at 35 kW/m^2 exposure heat flux level i.e. 5.39 kJ/m^{2}K, will be prescribed. For ceiling which will be represented by HRRPUA curve tested at 50 kW/m^2, the calibrated $\rho c\delta$ value at 50 kW/m^2 exposure heat flux level i.e. 3.95 kJ/m^{2}K, will be prescribed. It is fully appreciated that the chosen $\rho c\delta$ values will not be able to adequately represent the conditions within the metro train but it may improve on the prediction and therefore are used for now until better modelling techniques becomes available.

Styrene butadiene (Sty but)

Figure 9.12 to Figure 9.15 show the FDS predictions and the experimental HRR curves at different exposure conditions for the styrene butadiene specimen before the $\rho c \delta$ values were being calibrated. The trend in predicted time to ignition at different exposure heat flux levels was observed to be identical with the predictions for FRP polyester specimen.

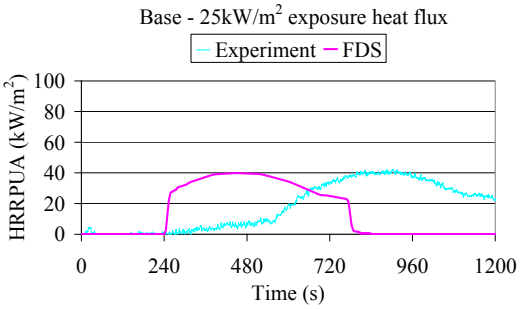

Figure 9.12: Modelling approach based on HRRPUA - Sty but - FDS prediction at 25 kW/m^2 exposure heat flux

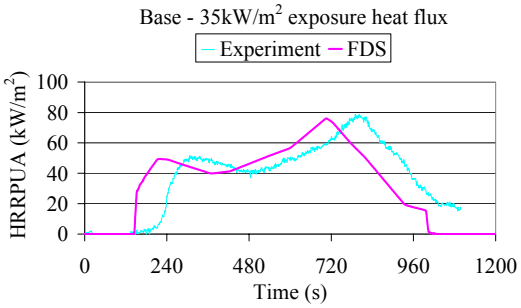

Figure 9.13: Modelling approach based on HRRPUA - Sty but - FDS prediction at 35 kW/m^2 exposure heat flux

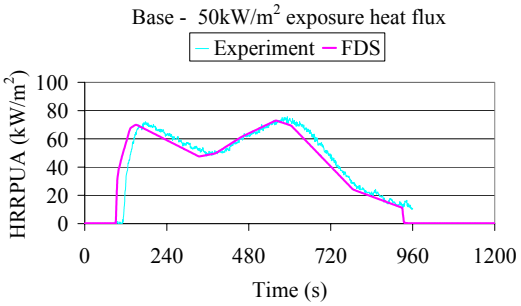

Figure 9.14: Modelling approach based on HRRPUA - Sty but - FDS prediction at 50 kW/m^2 exposure heat flux

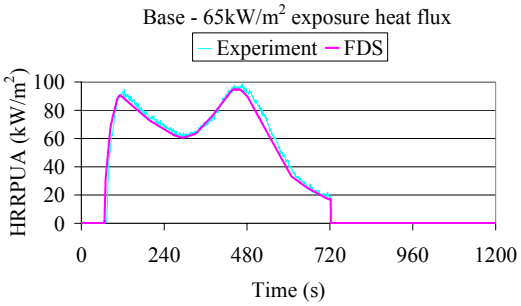

Figure 9.15: Modelling approach based on HRRPUA - Sty but - FDS prediction at 65 kW/m^2 exposure heat flux

Table 9.5 shows the calibrated $\rho c \delta$ values. Figure 9.16 to Figure 9.19 show perfect agreement of FDS predictions with the experimental HRR curves when these calibrated $\rho c \delta$ values were used.

$\dot{q}_e^{"}$ **(kW/m^2)**	**Calibrated $\rho c \delta$ (kJ/m^{2}K)**
25	22.2
35	13.3
50	10.0
65	8.65

Table 9.5: Modelling approach based on HRRPUA - Calibrated $\rho c \delta$ values for styrene butadiene

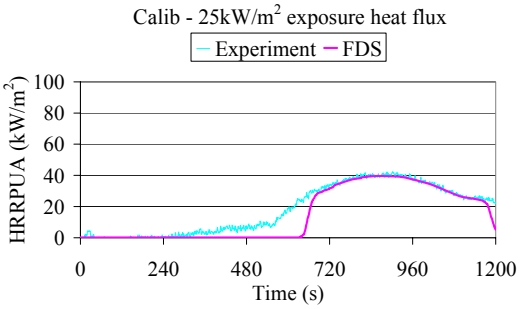

Figure 9.16: Modelling approach based on HRRPUA - Sty but - FDS prediction at 25 kW/m^2 exposure heat flux (Calibrated)

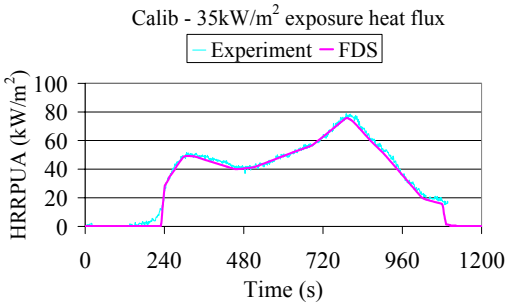

Figure 9.17: Modelling approach based on HRRPUA - Sty but - FDS prediction at 35 kW/m^2 exposure heat flux (Calibrated)

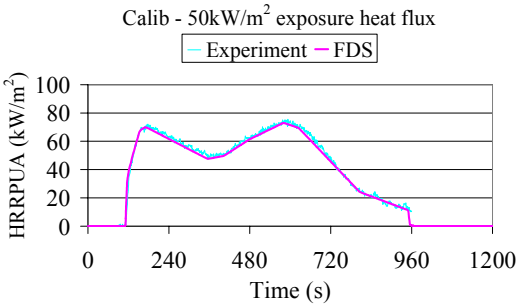

Figure 9.18: Modelling approach based on HRRPUA - Sty but - FDS prediction at 50 kW/m^2 exposure heat flux (Calibrated)

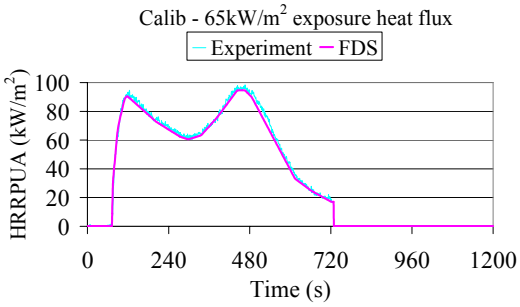

Figure 9.19: Modelling approach based on HRRPUA - Sty but - FDS prediction at 65 kW/m^2 exposure heat flux (Calibrated)

As in the case for the FRP polyester specimen, a suitable set of temperature variant properties for $\rho c \delta$ could not be derived and no single constant $\rho c \delta$ value could be prescribed for the styrene butadiene specimen for the modelling approach based on HRRPUA to reasonably predict the time to ignition at different exposure heat flux levels. Therefore for the final simulations, the $\rho c \delta$ value will also be prescribed according to the location of the component made of styrene butadiene i.e. the floor covering.

As the floor covering will be represented by HRRPUA curve tested at 25 kW/m^2 in the modelling approach based on HRRPUA, therefore the calibrated $\rho c \delta$ value at 25 kW/m^2 exposure heat flux level i.e. 22.17 kJ/m^{2}K, will be prescribed.

9.2.2 Modelling approach based on heat of vaporisation

FRP polyester

Figure 9.20 to Figure 9.23 show the FDS predictions and the experimental HRR curves at different exposure conditions.

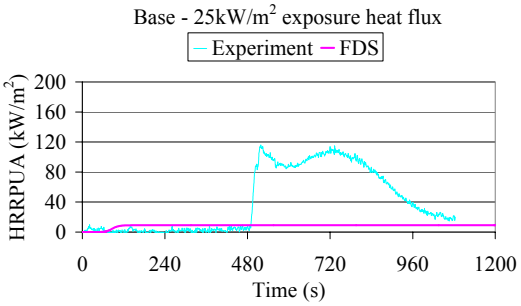

Figure 9.20: Modelling approach based on heat of vaporisation - FRP polyester - FDS prediction at 25 kW/m^2 exposure heat flux

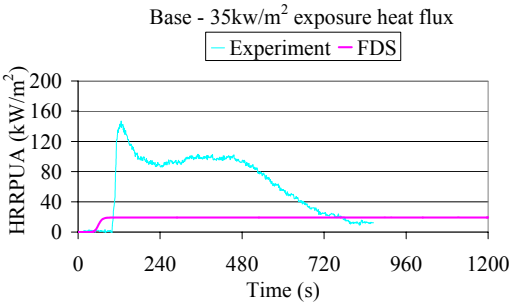

Figure 9.21: Modelling approach based on heat of vaporisation - FRP polyester - FDS prediction at 35 kW/m^2 exposure heat flux

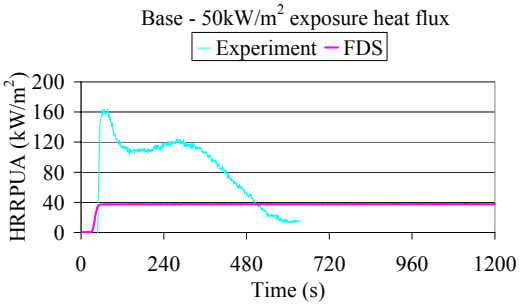

Figure 9.22: Modelling approach based on heat of vaporisation - FRP polyester - FDS prediction at 50 kW/m^2 exposure heat flux

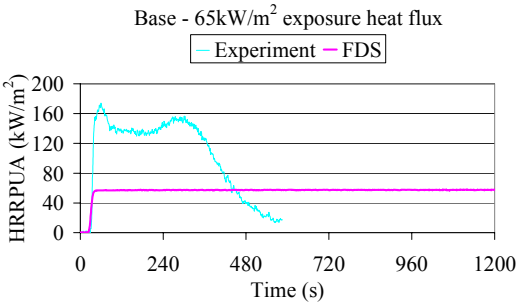

Figure 9.23: Modelling approach based on heat of vaporisation - FRP polyester - FDS prediction at 65 kW/m^2 exposure heat flux

As in the modelling approach based on HRRPUA, there were relatively good predictions in the time to ignition of specimens at high exposure heat flux levels. But at low exposure heat flux levels, the predictions were poor. Figure 9.20 to Figure 9.23 also show that the HRRs were grossly under predicted at all exposure conditions. Because the specimen was modelled as a thermoplastic and not a char former fuel, no charring properties were specified. Therefore FDS was not able to predict the decline of 1st peak HRR and increase of the 2nd peak HRR. A constant peak HRR was predicted as shown in above Figures.

The results were discouraging. It suggested that the derived properties were not suitable for use in the fire model to allow accurate prediction of ignition and fire growth. To improve the prediction, calibrations were again carried out.

In order to limit the number of simulations, it was decided to adjust only two main parameters:

a) the $\rho c \delta$ value since it affect the time to ignition
b) the heat of vaporisation ΔH_v since it affect the HRR

Since constant peak HRR would be predicted, the prediction was considered acceptable if FDS predicted the average HRR of the two peaks and the lowest point between the two peaks.

Besides problems with the time to ignition and HRR, it was also discovered that the heat released for the specimens would be over predicted if the simulation was allowed to run sufficiently long e.g. 2400 s, as the HRR would remain constant (after reaching its peak) throughout the simulation.

For FDS to estimate correct amount of heat released from the specimen, it has been found that density ρ and thickness δ of the specimen must also be prescribed in the model. Either one of these value must be adjusted so that the correct amount of heat is released. This is because in FDS the amount of heat released from a specimen is calculated by multiplying the density, thickness, surface area and effective heat of combustion i.e. $\rho \delta A_{sur} \Delta H_{e,eff}$.

From the Cone Calorimeter test data, the average amount of mass loss was found to be 54%. The prescribed thickness of the specimen was therefore adjusted so that the mass in the model was only 54% of its actual mass. As for the density, the measured value i.e. 1795 kg/m^3, was prescribed.

Table 9.6 shows the calibrated values. Figure 9.24 to Figure 9.27 show FDS predictions using the calibrated values.

$\dot{q}_e^{"}$ **(kW/m²)**	**Calibrated** δ **(m)**	**Calibrated** $\rho c \delta$ **(kJ/m²K)**	**Calibrated** ΔH_v **(kJ/kg)**
25	0.00216	13.3	2850
35	0.00216	5.4	3700
50	0.00216	3.95	4700
65	0.00216	3.6	5250

Table 9.6: Modelling approach based on heat of vaporisation - Calibrated values for FRP polyester

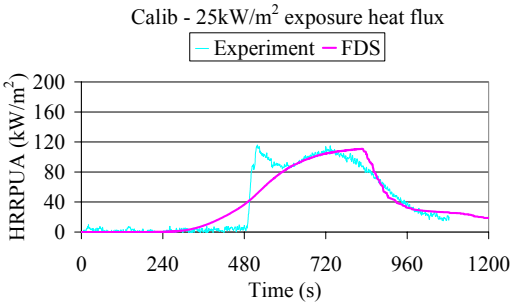

Figure 9.24: Modelling approach based on heat of vaporisation - FRP polyester - FDS prediction at 25 kW/m² exposure heat flux (Calibrated)

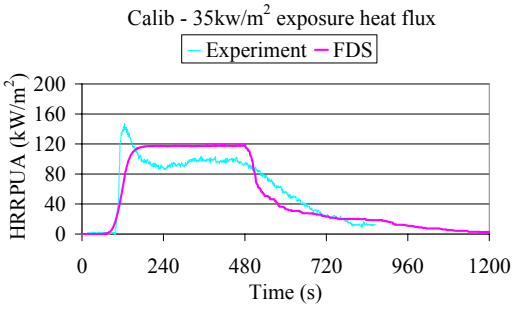

Figure 9.25: Modelling approach based on heat of vaporisation - FRP polyester - FDS prediction at 25 kW/m² exposure heat flux (Calibrated)

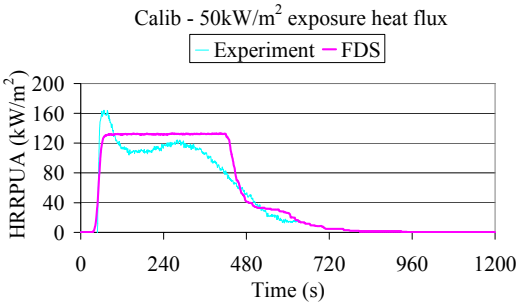

Figure 9.26: Modelling approach based on heat of vaporisation - FRP polyester - FDS prediction at 25 kW/m² exposure heat flux (Calibrated)

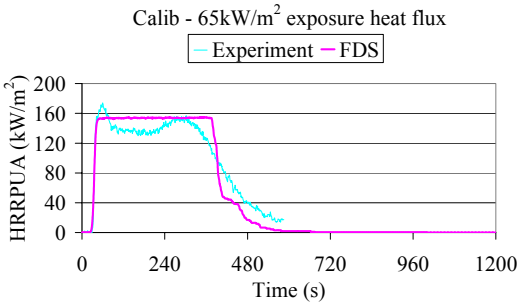

Figure 9.27: Modelling approach based on heat of vaporisation - FRP polyester - FDS prediction at 25 kW/m² exposure heat flux (Calibrated)

From Table 9.6, it can be seen that when the specimen was exposed to different exposure heat flux levels, different sets of $\rho c \delta$ and heat of vaporisation values would need to be prescribed in order to reasonably predict the time to ignition and HRR. Such a modelling technique is beyond the capabilities of FDS model at its current stage.

The derived heat of vaporisation value from Cone Calorimeter test data was 10300 kJ/kg. The calibrated values at different exposure heat flux levels were much lower than this value. This suggested that the procedure proposed by Quintiere (1993) could not derive appropriate heat of vaporisation values for fire retardant materials which could be used for fire modelling. Even though the calibrated heat of vaporisation values were lower than the derived value, it was noted that they were still higher than that used in the trial simulations.

After analysing the results, the calibrated values at 35 kW/m^2 exposure heat flux level was chosen to be the most suitable single set of values which could be used the represent the burning behaviour of the specimen over the spectrum of exposure conditions. Even though at lower heat flux level, the HRR may be slightly under-predicted, it will predict earlier ignition. At higher heat flux level, the HRR may be over-predicted but the time to ignition will be delayed. It allowed a compromise between the HRR and ignition time which both have influence on the fire severity. As maximum burning rate has been prescribed in the simulation, the maximum HRR will be limited to the experimental maximum. This will prevent the HRR to be grossly over-estimated. Therefore it was decided to use calibrated values at 35 kW/m^2 exposure heat flux level i.e. $\rho c \delta$ value of 5.39 kJ/m^{2}K and ΔH_v of 3700 kJ/kg, for the final simulations. In addition, the density and the adjusted thickness δ will be prescribed to predict a correct amount of heat released from the material.

Styrene butadiene

Figure 9.28 to Figure 9.31 show the FDS predictions and the experimental HRR curves at different exposure conditions.

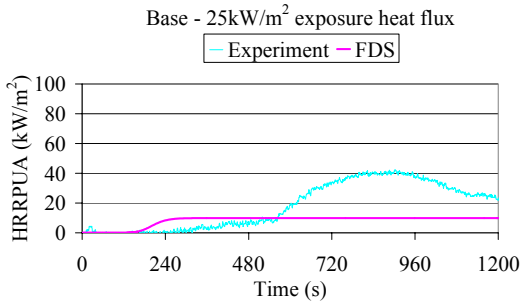

Figure 9.28: Modelling approach based on heat of vaporisation - Sty but - FDS prediction at 25 kW/m^2 exposure heat flux

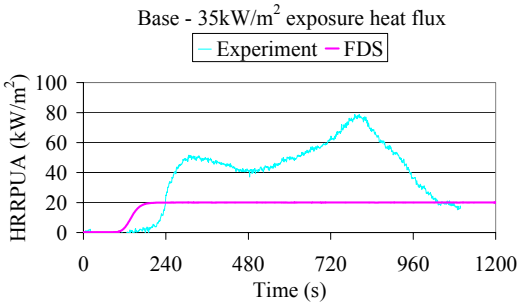

Figure 9.29: Modelling approach based on heat of vaporisation - Sty but - FDS prediction at 35 kW/m^2 exposure heat flux

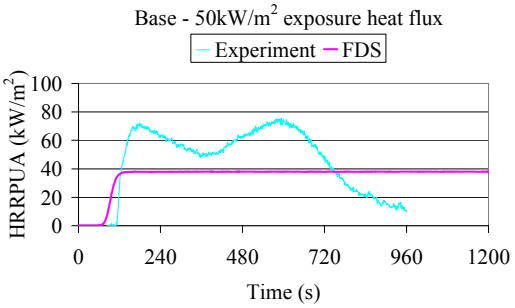

Figure 9.30: Modelling approach based on heat of vaporisation - Sty but - FDS prediction at 50 kW/m^2 exposure heat flux

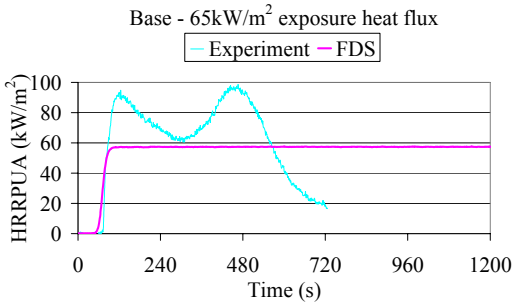

Figure 9.31: Modelling approach based on heat of vaporisation - Sty but - FDS prediction at 65 kW/m^2 exposure heat flux

These Figures show similar results as the FRP polyester specimen. Therefore calibrations were also carried out.

For the styrene butadiene specimen, the mass loss rate at 25 kW/m^2 exposure heat flux level was comparatively lower than the other three exposure heat flux levels. The average mass loss rate (of the three replicate specimens) at 25 kW/m^2 was 42%. At the other three exposure heat flux levels, the average mass loss rate was 54%. This information was used to adjust the thickness of the specimen so that correct amount of heat was released at different heat flux levels. As for the density, the measured value i.e. 1478 kg/m^3, was prescribed.

Table 9.7 shows the calibrated values. Figure 9.32 to Figure 9.35 show FDS predictions using the calibrated values.

$\dot{q}_e^{"}$ **(kW/m^2)**	**Calibrated** δ **(m)**	**Calibrated** $\rho c \delta$ **(kJ/m^{2}K)**	**Calibrated** ΔH_v **(kJ/kg)**
25	0.00126	18.6	4750
35	0.00162	13.9	6250
50	0.00162	11.0	8600
65	0.00162	9.6	9400

Table 9.7: Modelling approach based on heat of vaporisation - Calibrated values for FRP polyester

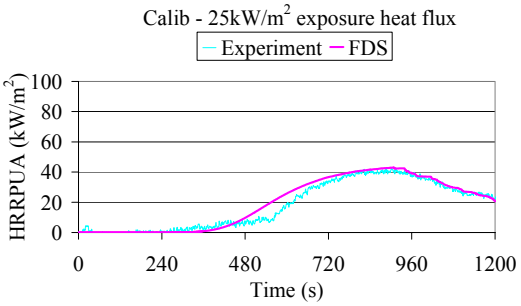

Figure 9.32: Modelling approach based on heat of vaporisation - Sty but - FDS prediction at 25 kW/m^2 exposure heat flux (Calibrated)

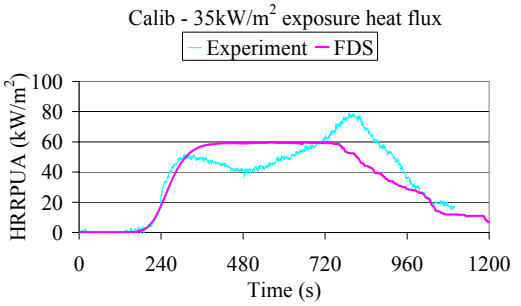

Figure 9.33: Modelling approach based on heat of vaporisation - Sty but - FDS prediction at 35 kW/m^2 exposure heat flux (Calibrated)

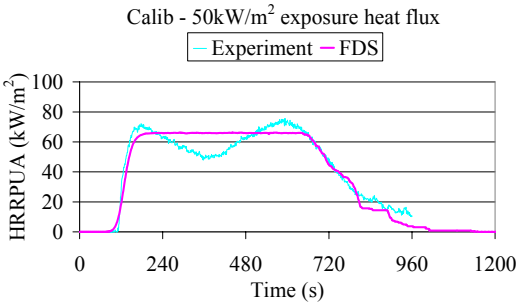

Figure 9.34: Modelling approach based on heat of vaporisation - Sty but - FDS prediction at 50 kW/m^2 exposure heat flux (Calibrated)

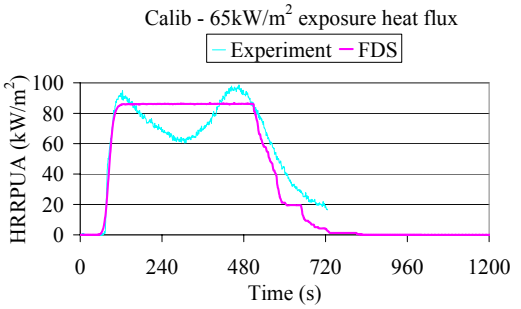

Figure 9.35: Modelling approach based on heat of vaporisation - Sty but - FDS prediction at 65 kW/m^2 exposure heat flux (Calibrated)

As in the case for FRP polyester specimen, different sets of $\rho c \delta$ and heat of vaporisation values must be prescribed at different heat flux levels in order to reasonably predict the time to ignition and HRR. The calibrated heat of vaporisation values were also lower than the derived value, but they were still higher than that used in the trial simulations.

For the final simulations, the calibrated values at 35 kW/m^2 exposure heat flux level i.e. $\rho c \delta$ value of 13.9 kJ/m^{2}K and ΔH_v of 6250 kJ/kg, will be used since only one set of values can be prescribed. The density and the adjusted thickness δ will also be prescribed to predict correct amount of heat released from the material.

9.3 Conclusions from FDS predictions of Cone Calorimeter test results

The following conclusions can be drawn after compared FDS predictions with the Cone Calorimeter test results:

a) For the modelling approach based of HRRPUA, FDS was not able predict the time to ignition at low heat flux levels using the derived properties. It was not possible to derive a suitable set of temperature variant properties for $\rho c \delta$ because the fire retardant was able to effectively retard ignition at low exposure heat flux levels.

b) For the modelling approach based of heat of vaporisation, FDS not only could not predict the time to ignition at low heat flux levels, it also under-predicted the HRR at all exposure heat flux levels.

c) It can be concluded that the procedures used cannot derive appropriate material properties for fire retardant materials which can be used in fire model to accurately predict ignition and fire growth.

d) For the modelling approach based on heat of vaporisation, it is necessary to prescribe the density and thickness of the specimen so that FDS is able to compute the heat released. In the current study, the thickness of the specimen was adjusted so that the heat released by the specimen in the model tallied with the experimental data.

e) For the modelling approach based on HRRPUA, there was no single constant $\rho c \delta$ value which could be prescribed to accurately predict the time to ignition at different exposure heat flux levels. For practical reasons, it was decided to prescribe the calibrated $\rho c \delta$ values according to the locations of the components in the metro train for the final simulations.

f) For the modelling approach based on heat of vaporisation, there was no single set of $\rho c \delta$ and heat of vaporisation values which could be prescribed to accurately predict the time to ignition and HRR at different exposure heat flux levels. For practical reasons, it was decided to prescribe the calibrated values at 35 kW/m^2 exposure heat flux level for the final simulations. In addition, the density and the adjusted δ would also be prescribed to predict correct amount of heat released from the material.

10 HRR calculations based on the current methods

This Chapter presents the HRR calculations based on the current methods. The estimations are used to make comparison with the simulation results. Estimations from three methods will be presented, namely the traditional method, Duggan (1997) method (or summation method) and the post-flashover model method. In addition, the hazard load based on method described in NFPA 130 (2003 edition) Annex D will also be estimated to examine whether self-propagating fire is possible for the CCL metro train.

10.1 Traditional method

As discussed in Chapter 2, there were two revisions to the traditional method after it was first used to estimate HRR of metro train in 1975. The latest revision i.e. design scenario – 1989, was made to incorporate the impact of the recommendations contained in NFPA 130. The HRR estimation based on this revision will be presented since the CCL metro train is designed to comply with the test methods and performance criteria specified in NFPA 130 or its equivalent.

In addition to design scenario - 1989, the modified traditional method proposed and used by the design consultant to calculate the HRR of the CCL metro train will also be presented. The modified traditional method has the same methodology as design scenario – 1989 but there are a few modifications to the assumptions. The differences will be highlighted in the later Section.

The fire loads for the MC-car and T-car are summarised in Table 10.1 below. They were computed from the fire load schedule submitted by the train supplier (Renie and Prevot 2003).

Location	Fire load (MJ)
MC-car	
Above floor	20743
Floor	3632
Below floor	7892
T-car	
Above floor	17884
Floor	3789
Below floor	8683

Table 10.1: Fire loads of MC-car and T-car

In the traditional method, the fire is assumed to start with flame ignition at the under carriage (below floor) of the metro train car. Once established in the below floor area of the car, the fire propagates through the floor (despite the use of fire resistant floor) and into the above floor area of the car. The combustibles in the car interior are assumed to ignite and result in flashover. The magnitude of the fire during flashover will result in fire spread to the adjoining car in the direction of tunnel airflow. When the fire spreads to the adjoining car, the fire is contained to the above floor due to the presence of the fire resistant floor. Fire in the adjoining car is assumed to continue to develop until flashover. The fire spread regime is assumed to continue and repeat until the entire train is being consumed. All the combustibles above and below the car floor and less than one-half of the floor materials are assumed to be burnt in the incident car while only the above floor combustibles are assumed to be involved in the second and succeeding cars.

Since the CCL metro train is made up of three cars in MC-T-MC configuration, the worst case will be for the fire to start at the MC-car (and spread downstream in the direction of airflow to the other two cars) since this will result in all three cars to be involved in the fire.

10.1.1 HRR based on design scenario – 1989

In design scenario -1989, an initial fire size $\dot{Q}_{\text{int}}$ of 0.7 MW is assumed and lasted for 30 minutes. The burning period for each car is assumed to be 60 minutes (excluding the ignition phase) while the flashover and fire-transmission rates are assumed to be 30 minutes. Up to two cars would be fully-involved at any given instant. The HRR for

the first involved car $\dot{Q}_1$ was calculated using Equation 2.4 and determined to be 8.1 MW. The HRRs of the T-car and the MC-car (at the other end of the train) were calculated using Equation 2.5 and determined to be 4.6 MW and 5.4 MW respectively. Table 10.2 below shows the tabulation of HRRs at different phases of the fire development.

Time period (min)	Car no.	HRR of car (MW)	Peak HRR (MW)	Remark
0 – 30	1	0.7	0.7	1st car under initial burning phase.
30 – 60	1 2	8.1 0.7	8.8	1st car flashover. 2nd car (T-car) under initial burning phase.
60 – 90	1 2 3	8.1 4.6 0.7	13.4	1st car continues to burn. 2nd car flashover. 3rd car (MC-car) under initial burning phase.
90 – 120	1 2 3	0 4.6 5.4	10.0	1st car completely burnt out. 2nd car continues to burn. 3rd car flashover.
120 -150	2 3	0 5.4	5.4	2nd car completely burnt out. 3rd car continues to burn.
150+	3	0	0	All cars burnt out and fire extinguished

Table 10.2: Fire development - Design scenario - 1983

From Table 10.2, the peak HRR was estimated to be 13.4 MW and the burning period was 150 minutes.

10.1.2 HRR based on modified traditional method for CCL

Initial fire size $\dot{Q}_{\text{int}}$ of 0.7 MW for 30 minutes is also assumed when calculating the HRR for CCL metro train. Only up to two cars would be fully-involved at any given instant as in design scenario -1989. However there are a few modifications in the design assumptions. They are:

a) To account for the fire resistance rating of the floor, the period from the initial ignition to fire propagation through floor is taken to be 60 minutes.
b) The burning period for the below floor, floor and above floor combustibles are assumed to be 60 minutes.
c) Combustion efficiency factor of 0.7 is included in the calculation.
d) Fire is transmitted to the adjacent car in 10 minutes after flashover.

Design Equations 2.6 to 2.9 were used to calculate the HRR for first involved car and succeeding cars. The HRR of the below floor combustibles for the first involved car; the HRR for the first involved car; the HRR of the floor and above floor combustibles for the first involved car; and the HRRs for T-car and MC-car (at the other end of the train) were determined to be 1.2, 5.6, 4.0, 3.1 and 3.7MW respectively. Table 10.3 below shows the tabulation of HRRs at different phases of the fire development.

Time period (min)	Car no.	HRR of car (MW)	Peak HRR (MW)	Remark
0 – 30	1	0.7	0.7	1st car under initial burning phase
30 – 60	1	1.2	1.2	Burning of 1st car below floor combustibles
60 – 70	1	5.6	5.6	Fire propagates above floor and cause flash-over. Entire 1st car burning
70 – 90	1 2	5.6 0.7	6.3	Entire 1st car continues to burn. 2nd car (T-car) under initial burning phase.
90 – 100	1 2	4.0 0.7	4.7	1st car below floor combustibles burnt out, 1st car above floor continues to burn, 2nd car still under initial ignition
100 – 110	1 2	4.0 3.1	7.1	1st car above floor continues to burn, 2nd car above floor flashover
110 – 120	1 2 3	4.0 3.1 0.7	**7.8**	1st and 2nd cars above floor continue to burn. 3rd car under initial burning phase
120 – 140	1 2 3	0 3.1 0.7	3.8	1st car completely burnt out. 2nd car above floor continues to burn. 3rd car still under initial ignition
140 – 150	2 3	3.1 3.7	6.8	2nd car above floor continues to burn. 3rd car above floor flash over
150 – 160	2 3	3.1 3.7	6.8	2nd and 3rd car above floor continues to burn
160 – 200	2 3	0 3.7	3.7	2nd car completely burnt. 3rd car above floor continues to burn
200+	3	0	0	All cars burnt out and fire extinguished

Table 10.3: Fire development – Modified traditional method for CCL

From Table 10.3, the peak HRR was estimated to be 7.8 MW based on the calculation method used in Circle Line. Note that the value calculated in this Section was lower than that calculated by the design consultant (10 MW) because the fire loads which the consultant based on was from the contract specification while the fire loads used here was based on the train supplier submission which was much lower.

The HRRs at different fire development stages for Design scenario - 1989 and modified traditional method for CCL are illustrated graphically in Figure 10.1 below.

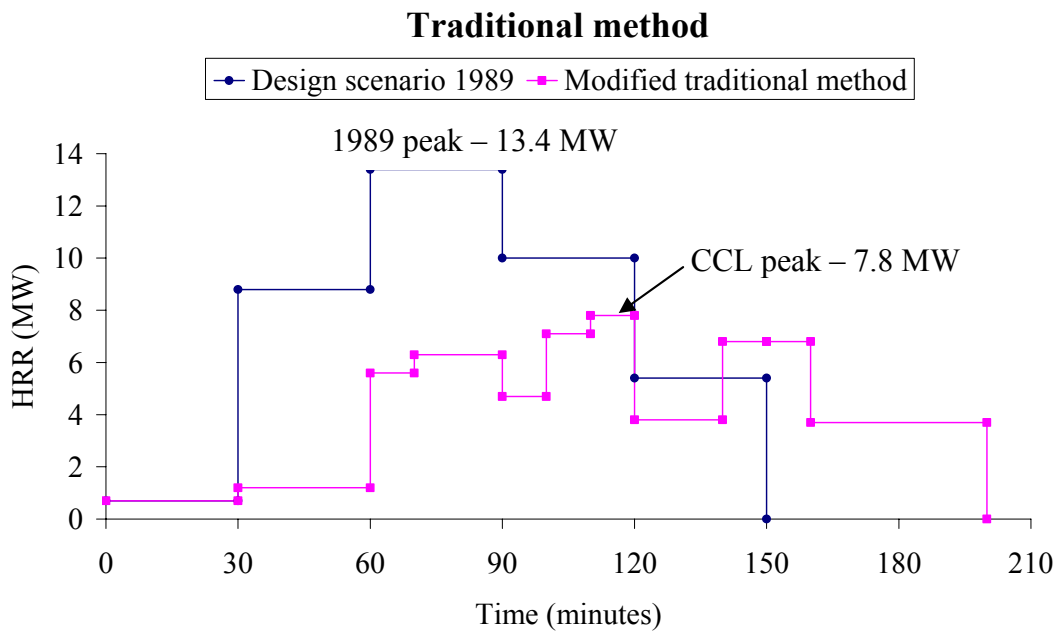

Figure 10.1: HRR vs. time for design scenario 1989 and modified traditional method for CCL

The calculation method for CCL resulted in lower peak HRR and longer burning period compared with design scenario – 1989 because of the modifications in design assumptions for the calculation. By including lapse time to account for the fire resistance rating of the floor and combustion efficiency factor reduced the peak HRR for the CCL metro train.

10.2 Duggan (1997) method

In Duggan (1997) method, the heat release rate per unit area HRRPUA curves of exposed surface materials (determined from Cone Calorimeter tests) are multiplied by their exposed area in the metro train car. The 'HRR curves' of all the exposed surface materials are then summed up. A notional 1.5 MW continuous ignition source is added to represent a severe luggage stack fire. A smoothing procedure is used to merge peaks which are resolved but close together. In addition, a notional 3 MW is added to account for other miscellaneous surfaces and items within the car when the data is used for emergency tunnel ventilation system design. The exposure heat flux levels (at which the exposed surface materials are tested) depend on their orientation in the metro train car. For a material which has a 'ceiling-like' (horizontal prone) orientation, it is tested at 50 kW/m^2. For a material which has a 'wall like' (vertical) orientation, it is 35 kW/m^2 and for a material which has a 'floor-like' (horizontal supine) orientation, it is either tested at 20 or 25 kW/m^2.

The HRRPUA curves at exposure heat flux levels of 25, 35 and 50 kW/m^2 were used for the calculation presented herein. In Duggan (1997) method, the calculation is done for only one car therefore the exposed area of surface materials in the MC-car was used as shown in Table 10.4. Note that wall, ceiling and door panels (made of aluminium panel and painted with powder paint) were not included in the calculation as the wall panel tested in the current study did not ignite at 35 and 50 kW/m^2 exposure heat flux levels.

Surface	Component	Material	$\dot{q}_e$ (kW/m^2)	Exposed area (m^2)
Horizontal supine	Floor covering	Styrene butadiene	25	53.6
	Seat base and surface of driver console assembly	FRP polyester	25	14.8
Vertical	Seat back, under seat boxes, equipped cubicle assemblies, PEC module fittings, detrainment doors, wall (face) panels at car end mask, sides of driving console assembly	FRP polyester	35	39.6
Horizontal prone	Ceiling panels at car end mask	FRP polyester	50	2.3

Table 10.4: Exposed area of surface materials

Figure 10.2 shows the 'luggage' ignition source. Figure 10.3 to Figure 10.6 show the HRR curves at listed exposure heat flux levels adjusted for area and Figure 10.7 shows the summation of HRRs. The smoothing procedure was not performed as there were no peaks close together.

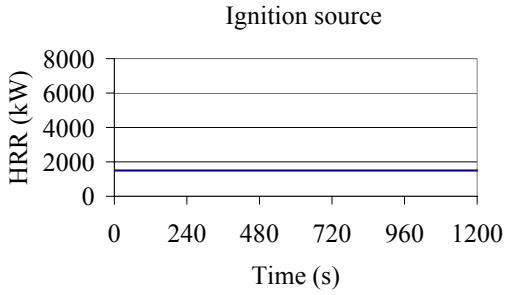

Figure 10.2: HRR curve of ignition source

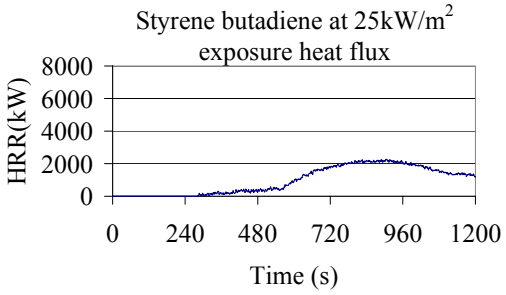

Figure 10.3: HRR curve of surface made of styrene butadiene at 25kW/m^2

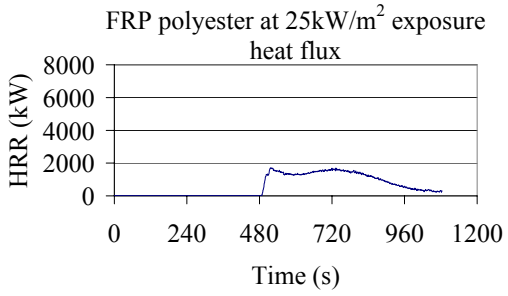

Figure 10.4: HRR curve of surfaces made of FRP polyester at 25kW/m^2

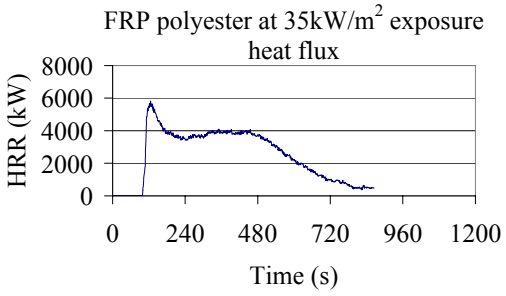

Figure 10.5: HRR curve of surfaces made of FRP polyester at 35kW/m^2

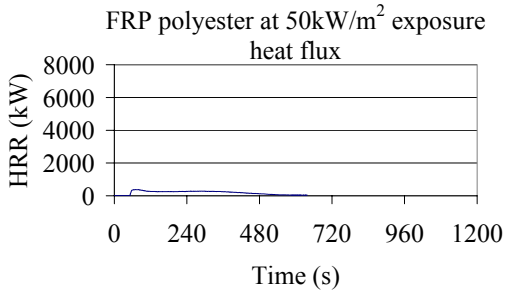

Figure 10.6: HRR curve of surfaces made of FRP polyester at 50kW/m^2

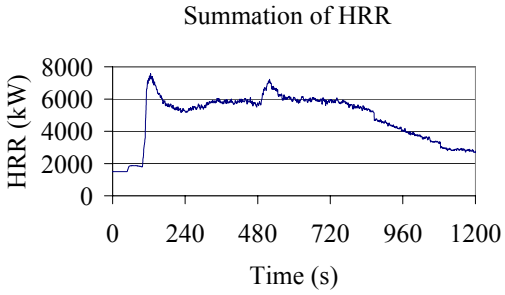

Figure 10.7: Summation of HRRs for one car

From Figure 10.3 to Figure 10.6, it can be seen that the vertical surfaces were the main contributor to the HRR. The peak HRR was found to be 7600 kW or 7.6MW as can be seen from Figure 10.7. Adding a notional 3 MW to account for other miscellaneous surfaces and items within the car gave a peak HRR of 10.6 MW.

One of the main criticisms of the Duggan (1997) method is that the calculation is done for only one car (Dowling and White 2004). Therefore another calculation was carried out by scaling the HRR curves for area of the surfaces found in two cars i.e. the MC-car and T car. Two cars were chosen because based on traditional method design scenario – 1989 and modified traditional method for CCL, only up to two cars would be fully-involved at any given instant. Three cars or a complete train were not considered for the calculation because different propensities for ignition, flame spread and heat release would make the estimation highly conservative. The summation of HRRs for two cars is show in Figure 10.8.

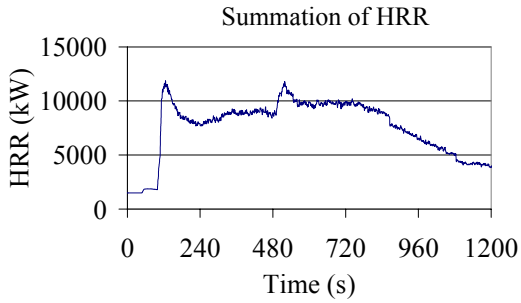

Figure 10.8: Summation of HRRs for two cars

The peak HRR was found to be 11900 kW or 11.9 MW. Adding a notional 3 MW gave a peak HRR of 14.9 MW. This value was found to be reasonably close to the estimated peak HRR of 13.4 MW using the traditional method design scenario -1989.

10.3 Post-flashover model method

Hettinger and Barnett (1991) used post-flashover computer model, COMPF2 to predict the HRR of metro train car interior (above floor). The assumption for the model is that fire is ventilation controlled during the post-flashover regime and therefore burning rate is simply function of the oxygen available for combustion.

In their study, they assumed that the material would exhibit the material properties of polycarbonate after flashover. A combustion efficiency factor χ was included and 'net' heat of combustion was based on weighted average for the combustible materials in the metro train car.

In their study, a HRR of 12.9 MW was derived based on a 'net' heat of combustion of 13650 kJ/kg, a combustion efficiency factor χ of 0.8 and the design scenario that assumed passenger doors and windows were opened. When the COMPF2 result was modified to incorporate the effect of the floor and below floor combustibles, peak HRR of 18 MW was obtained for the metro train car.

Besides having safety glass windows, the train in their study also had stainless steel shell which prevented the fire from being transmitted directly from car to car. Therefore the possibility of multiple car involvement for a fire was discounted in their study.

Then Kennedy et al. (1998) reported the COMPF2 study for the same train (and with same amount of distribution of combustibles in the train) but assumed the car had polycarbonate windows. Multi-car fire with succeeding cars being involved every 30 minutes was assumed. The peak HRR for the duration of the fire was estimated to be 23.1 MW, with two cars being fully involved at any one time.

No simulation was conducted using the COMPF2 in the current study to predict the HRR. As the opening area was approximately the same and the 'net' heat of combustion was slightly higher in the current study compared with the COMPF2 study (see Table 10.5), it was decided to approximate the HRR using the proportional method according to the above floor (car interior) heat load of the metro train cars. The average above floor fire load of MC-car and T-car was used.

Data source	Opening area per metro train car (m^2)	'Net' heat of combustion per metro train car (kJ/kg)	Above floor fire load of metro train car (MJ)
Current study	31.08	14800 (MC-car) 14100 (T-car)	19310 (average of MC and T cars)
COMPF2 study	32.67	13650	24400

Table 10.5: Opening area and 'net' heat of combustion in the current study and the COMPF2 study

Using the above proposed method, the HRR for the CCL metro train was approximated to be 18.3 MW for the multi-car fire scenario.

10.4 NFPA 130 Annex D – Hazard Load

As mentioned in Chapter 2, NFPA 130 (2003 edition) Annex D contains method to determine the hazard load in MJ/m^3 of train car volume. A suggested performance criterion of 3 MJ/m^3 is included as the maximum allowable loading to ensure self-propagating fire would not occur with an initiating fire consisting of the equivalent of 0.45 kg of newsprint or 0.23 kg of lighter fluid. To estimate the hazard load, the 180-second average heat release q''_{180} values are multiplied by the exposed area for each material and totalled. In the example calculation, the components are either exposed to 10 kW/m^2 (seat and floor) or 15 kW/m^2 (wall) or 35 kW/m^2 (ceiling) exposure heat flux level selected according to their orientation and location.

Even though there was reasonable amount of test data from the experiments, there were still two limitations for the estimation as discussed below:

a) The OSU apparatus (ASTM E 906 2004) is specified for use in the example calculation given in NFPA 130 and not the Cone Calorimeter. The OSU apparatus results, however, when compared against other measurements, have

been found to substantially underestimate the HRR (Babrauskas 1986). This was one of the reasons which led to the development of Cone Calorimeter (Peacock and Braun 1999). Therefore use of Cone Calorimeter results will be more conservative for the estimation of hazard load.

b) No test was conducted at 10 and 15 kW/m^2 exposure heat flux levels therefore no data at these heat flux levels was available. But based on the experimental results it is appropriate to assume that none of the exposed surface materials will ignite at these flux levels. The derived critical heat flux levels for FRP polyester and styrene butadiene were reasonably higher than the above exposure heat flux levels i.e. 10 and 15 kW/m^2. The critical heat flux level for the aluminium panel (with exposed surface painted with powder paint) was expected to be even much higher as no ignition occurred at 35 and 50 kW/m^2 exposure heat flux level. Therefore it is reasonable to assume the average 180-second heat release q''_{180} values for these materials to be insignificant when tested at 10 and 15 kW/m^2 exposure heat flux levels.

Considering the above, only the ceiling material tested at 35 kW/m^2 exposure heat flux in the Cone Calorimeter was required for the estimation of hazard load. This implied that only data on the ceiling panel at the end mask (made of FRP polyester) was needed for the estimation.

The exposed area of the ceiling panel was 2.3 m^2 as shown in Table 10.4. The 180-second average heat release value at 35 kW/m^2 exposure heat flux level was 18.5 MJ/m^2. The dimensions of the MC-car were 23.45 m by 2.9 m by 2.1 m high which gave a train volume of 143 m^3. Based on the information, the hazard load for the train car was determined to be 0.3 MJ/m^3 $\leq$ 3 MJ/m^3. This was 10 times lower than the specified criterion. This result suggested that self-propagating fire was unlikely to occur with an ignition source consisting of the equivalent of 0.45 kg of newsprint or 0.23 kg of lighter fluid. For fire to self-propagate, the 180-second average heat release q''_{180} value of other surfaces must exceed 1.8 MJ/m^2 (or $\dot{q}''_{180}$ >10 kW/m^2) which was a relatively high value considering that the derived critical heat flux levels of the materials were much higher than the specified exposure flux levels.

10.5 Summary

Table 10.6 summarises the peak HRRs estimated based on the various current methods.

Method	Revision	Peak HRR (MW)	Remark
Traditional method	Design scenario – 1989	13.4	
	Modified method	7.8	
Duggan method	One car	10.6	
	Two cars	14.9	
Post-flashover model method	Multi-car fire	18.3	By approximation

Table 10.6: Summary of peak HRR values estimated based the various current methods

The peak HRRs were in the range of 7.8 MW to 18.3 MW, depending on the method used to estimate it. The modified traditional method resulted in lowest HRR value whereas the post-flashover model method gave the highest HRR value. In all the current methods used to estimate the HRR, the main assumption was that the fire would grow, spread and attain flashover during a metro train fire. Because of this assumption, the HRR of the metro train might be overestimated in view that the materials tested in the current study not only complied with the stringent small-scale tests performance criteria but were also difficult to ignite and burn in the Cone Calorimeter compared with the test results from other rail car studies.

The hazard load for the metro train car was much lower than the allowable loading suggesting that self-propagating fire was unlikely to occur with an ignition source consisting of the equivalent of 0.45 kg of newsprint or 0.23 kg of lighter fluid.

11 Final Simulations

This Chapter describes the final simulations. It also presents and discusses the final simulation results. It is important to highlight that the original plan for the project is to derive thermo-physical properties for the train car exposed surface materials from the Cone Calorimeter test data and to use them as input into the FDS model for the final simulations. However, there were two unforeseen problems arose that did not allow the project to proceed as planned:

a) There was insufficient Cone Calorimeter test data to derive the material properties for the wall panel. Therefore it was not possible to simulate this component /material as combustibles in the simulation. However, through analysis, the wall panel is not expected to contribute to the fire growth and flame spread during the developing stage of the fire. Even if the fire grows to flashover, the modelling results are unlikely to be significantly affected because of low fire load content of the materials.

b) The small-scale predictions based on the derived thermo-physical properties for the other two exposed surface materials i.e. FRP polyester and styrene butadiene, have been poor. Therefore to improve the prediction, a combination of derived and calibrated properties will be used for the final simulations as discussed in Chapter 9.

11.1 Final simulations conducted

The trial simulations showed that the fire scenarios with the fire on the seat and the fire scenarios with all doors closed were not able to grow in intensity and cause window failure. This was the case even though the material properties used in the trial simulations were more conservative than the derived properties (or the calibrated properties). This led to the conclusion that these fire scenarios would be less severe compared with the other fire scenarios and therefore were not considered further in the final simulations. The other reason for not considering the fire scenarios with all doors closed was because the trial simulations have indicated that the simulations were unstable which implied that FDS was not suitable for simulating under-ventilated fire scenarios. The final simulations focused on five fire scenarios which would have higher fire severity as shown in Table 11.1.

s/no	Fire scenario	Description of fire scenario
1	2A	Rear car fire, fire in the corner (Arson or electrical fault), both detrainment doors opened, all passenger doors closed
2	3A	Rear car fire, undercarriage fire (Electrical fault), both detrainment doors opened, all passenger doors closed
3	2B	Rear car fire, fire in the corner (Arson or electrical fault), both detrainment doors closed, 1st and 4th passenger doors facing the walkway opened
4	3B	Rear car fire, undercarriage fire (Electrical fault), both detrainment doors closed, 1st and 4th passenger doors facing the walkway opened
5	3D	Middle car, undercarriage fire (Electrical fault), both detrainment doors closed, 1st and 4th passenger doors facing the walkway opened

Note: 1) Forced ventilation and window failure were simulated for all scenarios.
2) The modelling approaches based on HRRPUA and heat of vaporisation were simulated for all scenarios

Table 11.1: Summary of the final simulations conducted

11.2 FDS inputs

Since most of the details of FDS inputs for the train model were described in Chapter 7, this Section will only focus on inputs that were different from the trial simulations.

11.2.1 Geometry

In the final simulations, the complete train was modelled. Figure 11.1 and Figure 11.2 show the snapshot from Smokeview for the 3-car train. The size of the computational domain was 70 m long by 5.5 m wide by 4.4 m high. A grid size of 300 mm was selected for the simulations after conducting the grid sensitivity analysis. For the final simulations, the simulation time was increased to 3600 s. The computers used for the simulations were Intel(R) Pentium 4(R), 3.2 GHz, 1 GB RAM computers. The times taken to complete the simulations were between 20 to 80 hours each.

Figure 11.1: Snapshot from Smokeview showing exterior view of the 3-car train within a tunnel

Figure 11.2: Snapshot from Smokeview showing interior view of the 3-car train

11.2.2 Vents, ignition sources, mechanical and thermal properties and combustion reaction parameters

The vents i.e. forced ventilation, train doors and criterion for window failure, and ignition sources were as described in the trial simulations. However, at 1800 s into the simulation, the ignition sources were 'removed' to simulate burn out of the ignition source.

Besides the two burning materials i.e. FRP polyester and styrene butadiene, the thickness, the density and the thermal properties of the tunnel and other components in the train were similar to the trial simulations. The mechanical and thermal properties of FRP polyester and styrene butadiene are outlined in later Sections.

For the final simulations, the combustion reaction parameters were also based on FRP polyester since it was the main burning material in the train.

11.2.3 Parameters for the modelling approach based on HRRPUA

For the modelling approach based on HRRPUA, the ignition temperatures and the Cone Calorimeter HRRPUA curves of the burning materials i.e. FRP polyester and styrene butadiene, were specified. The ignition temperatures for FRP polyester and styrene butadiene were based on the derived values and were 448°C and 419°C respectively.

The HRRPUA curves to be prescribed in FDS depend on the locations of the materials/ components in the train and are according to the exposure heat flux levels listed in Table 4.2. The Table also shows the calibrated $\rho c \delta$ values which are prescribed according to the locations of the components in the train as discussed in Chapter 9. The FDS data file has been written such that the rate of heat release from a component followed one of the HRRPUA curves shown in Figure 11.3 to Figure 11.5 once its surface reached the ignition temperature. The curve to follow will depends on the materials and locations of the components as discussed.

Component	**Material**	$\dot{q}_e^{"}$ **(kW/m²)**	**Calibrated** $\rho c \delta$ **(kJ/m²K)**
Floor covering	Styrene butadiene	25	22.2
Seats, under seat boxes, equipped cubicle assemblies, PEC module fittings, detrainment door, driving console assembly and face panels	FRP polyester	35	5.4
Ceiling panels at car end mask	FRP polyester	50	3.95

Table 11.2: Modelling approach based on HRRPUA – Calibrated $\rho c \delta$ values

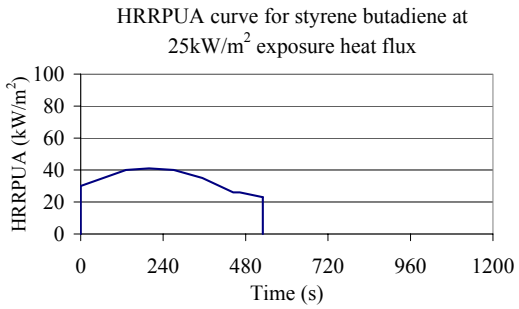

Figure 11.3: HRRPUA curve for styrene butadiene at 25 kW/m^2 exposure heat flux

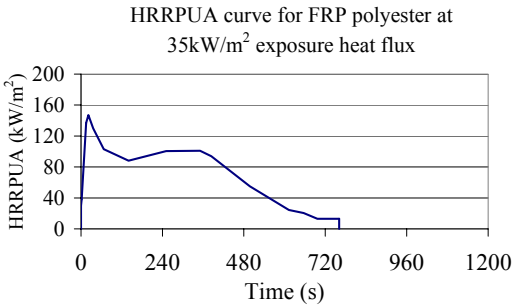

Figure 11.4: HRRPUA curve for FRP polyester at 35 kW/m^2 exposure heat flux

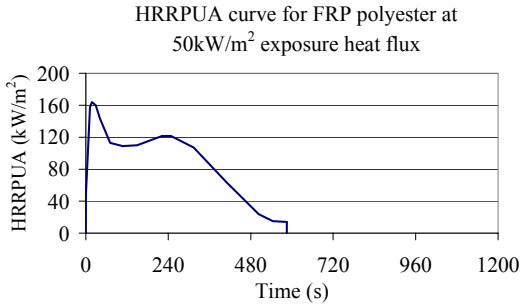

Figure 11.5: HRRPUA curve for FRP polyester at 50 kW/m^2 exposure heat flux

11.2.4 Parameters for the modelling approach based on heat of vaporisation

For completeness, the parameters prescribed for the two burning materials for the modelling approach based on heat of vaporisation are given in Table 7.4. The properties were either derived, calibrated or measured values as shown in the remark column.

s/no	Parameter	FRP polyester	Styrene butadiene	Remark
1	Ignition temperature T_{ig} (°C)	448	419	Derived
2	Heat of vaporisation ΔH_v (kJ/kg)	3700	6250	Calibrated
3	Effective heat of combustion $\Delta H_{c,eff}$ (kJ/kg)	13670	14570	Derived
4	Maximum burning rate $\dot{m}''_{\max}$ (kg/m^{2}s)	0.0161	0.0079	Derived
5	Critical mass flux $\dot{m}''_{cr}$ (kg/m^{2}s)	0.0044	0.0024	Derived
6	$\rho c \delta$ (kJ/m^{2}K)	5.4	13.9	Calibrated
7	Density ρ (kg/m^3)	1795	1478	Measured
8	Thickness δ (m)	0.00216	0.00162	Calibrated

Table 11.3: Modelling approach based on heat of vaporisation - Parameters for FRP polyester and styrene butadiene

11.3 Results and discussions for the final simulations

11.3.1 Modelling approach based on HRRPUA

Figure 7.10 to Figure 11.10 show the HRR curves while Table 11.4 shows the summary of predicted peak HRR values for the modelling approach based on HRRPUA.

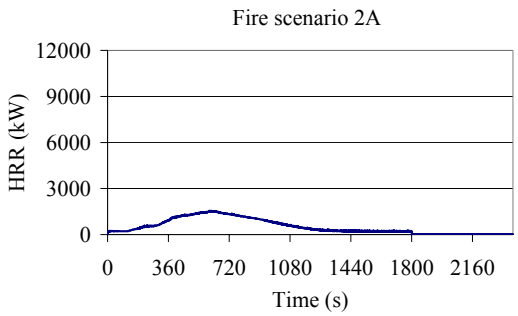

Figure 11.6: Modelling approach based on HRRPUA – Fire scenario 2A

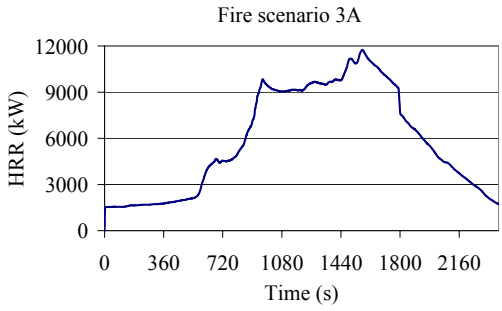

Figure 11.7: Modelling approach based on HRRPUA – Fire scenario 3A

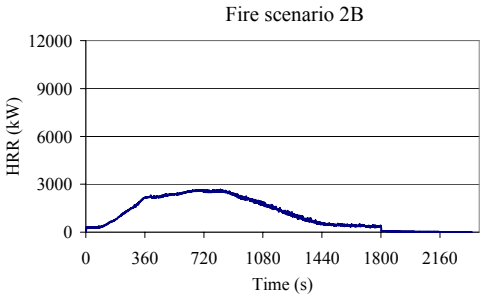

Figure 11.8: Modelling approach based on HRRPUA – Fire scenario 2B

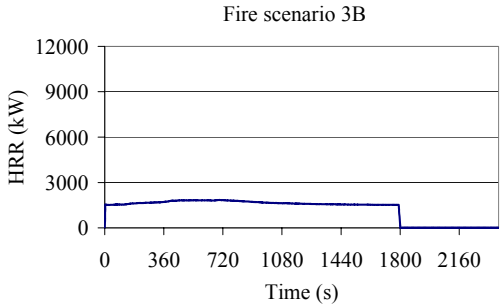

Figure 11.9: Modelling approach based on HRRPUA – Fire scenario 3B

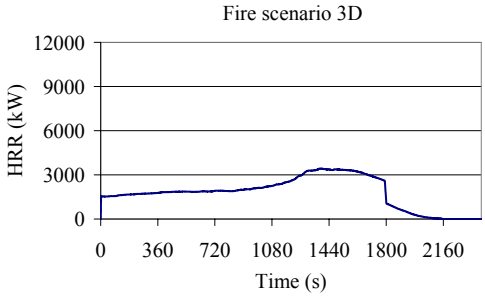

Figure 11.10: Modelling approach based on HRRPUA – Fire scenario 3D

s/no	Fire scenario	Peak HRR value for the modelling approach based on HRRPUA (kW)
1	2A	1550
2	3A	11800
3	2B	2670
4	3B	1890
5	3D	3500

Table 11.4: Final simulations - Summary of predicted peak HRR values for the modelling approach based on HRRPUA.

The fire in fire scenarios 2A and 2B i.e. fire in the corner, did not spread to the adjacent car. For fire scenario 2A, the fire was at its peak when the fire spread to the 2-seater seat area (near the ignition source) at about 620 s (see Figure 7.20). For fire scenario 2B, the fire was at its peak when the fire spread to the 7-seater seat area (near the ignition source) at about 820 s (see Figure 11.12). In both fire scenarios, the HRR started to decrease after reached the peak (see Figure 7.10 and Figure 11.8). The maximum compartment temperatures for fire scenarios 2A and 2B were 471°C and 590°C respectively. Both temperatures were below the flashover criteria implying that flashover did not take place. No window failure occurred since the compartment temperature was lower than the window failure criterion. These temperatures also would not be high enough to cause ignition of wall or ceiling since they were lower than the 'approximated' ignition temperature for wall panel (see Chapter 8, Section 8.5.2). Because the fire in fire scenario 2B was able to spread further downstream, it had slightly higher peak HRR compared with fire scenario 2A.

The results suggested that low forced ventilation airflow velocity through the passenger door has facilitated the fire growth in the vicinity of the ignition source. Although high forced ventilation airflow velocity was able to 'fan' the fire, it was not able to grow in intensity because the materials in the train car were difficult to ignite. High airflow seemed to reduce the flame temperature instead.

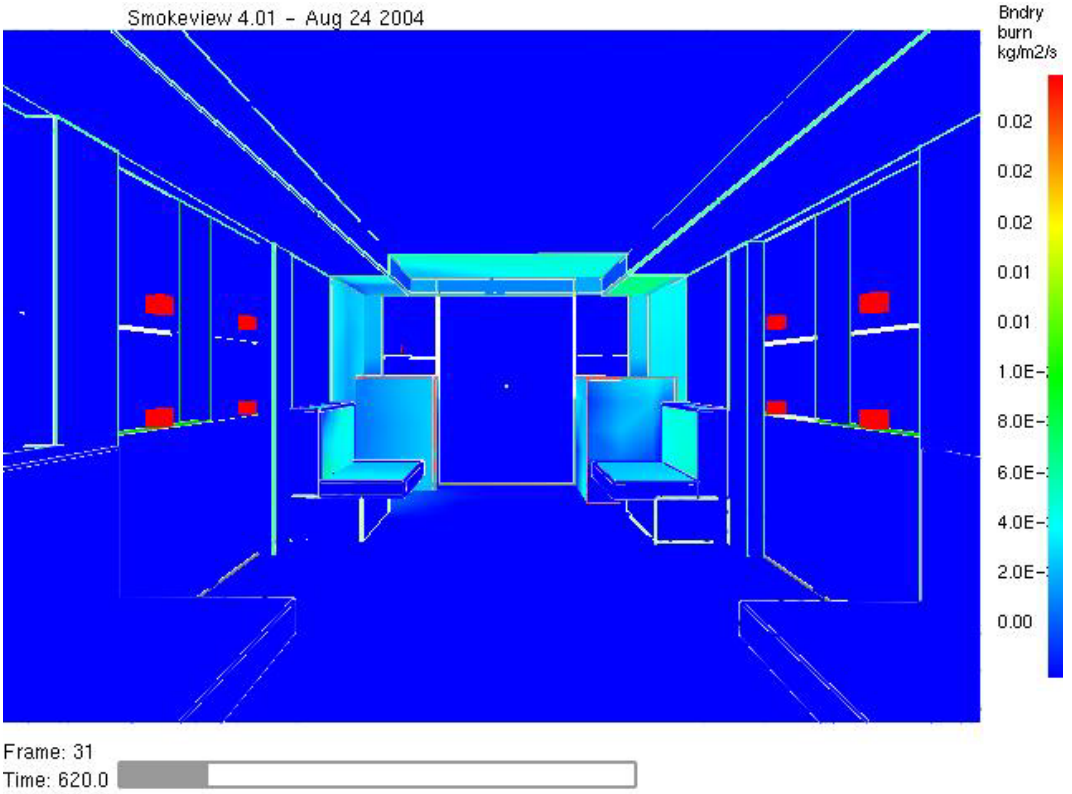

Figure 11.11: Snapshot from Smokeview for fire scenario 2A, 620 s into the simulation

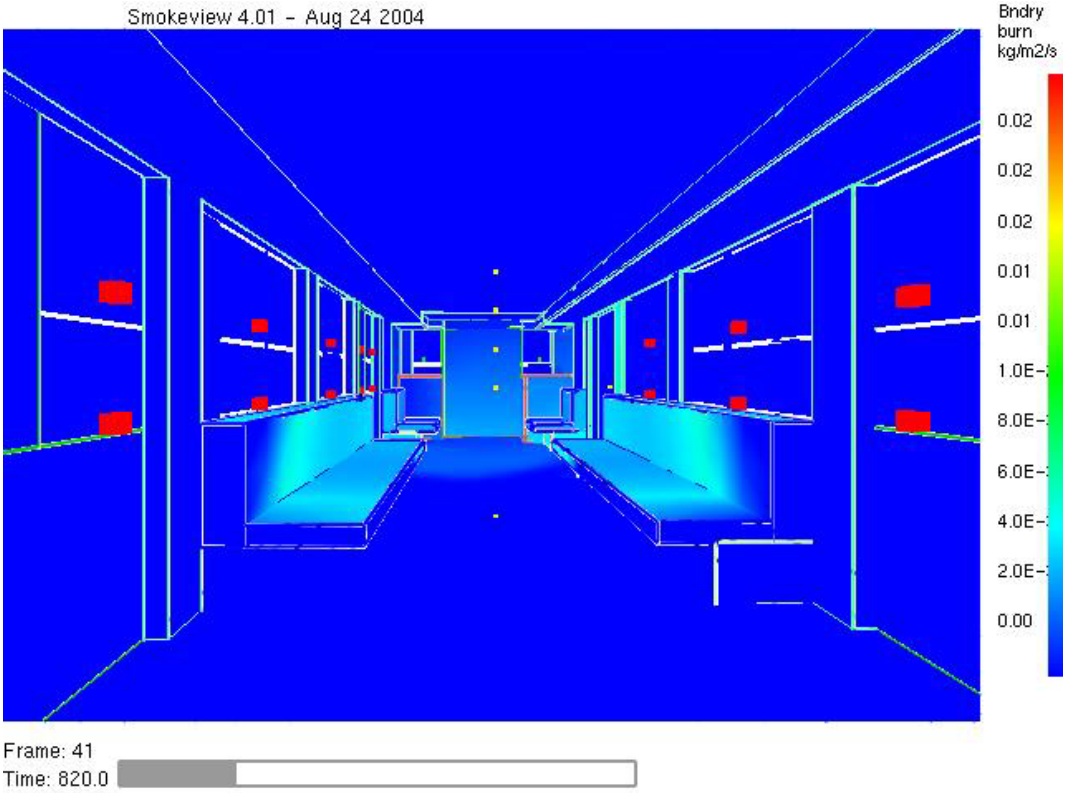

Figure 11.12: Snapshot from Smokeview for fire scenario 2B, 820 s into the simulation

However with significantly large ignition source size, high forced ventilation airflow velocity through the detrainment door would cause the fire to propagate downstream the ignition source and spread to the adjacent cars. This was the case for fire scenario 3A i.e. undercarriage fire.

For this scenario, it took about 600 s before the gas temperature in the vicinity of the ignition source was sufficiently high to cause the fire to spread to the adjacent cars. This strengthened the point made earlier that high forced ventilation airflow velocity would reduce the flame temperature and therefore it took longer time to reach a critical stage where fire spread was possible because the materials in the current study were difficult to ignite. The fire spread to adjacent cars coincided with the rapid increase in HRR as shown in Figure 11.7.

The fire spread to the second and third cars was very rapid. The assumption that the fire would spread to the next car only after the first car flashover was not valid for this particular scenario because of the high forced ventilation airflow velocity. The other reason was because there was no door installed between the train cars to prevent flame from propagating to the adjacent car due to the high airflow. Peak HRR was attained when the surfaces downstream the ignition source and the second and third cars were involved in the fire. Surfaces upstream of the ignition source were not involved in the fire because of the direction of the airflow. Maximum compartment temperature in the train was about 970°C causing almost all the windows in the second and third cars to fail (see Figure 11.13).

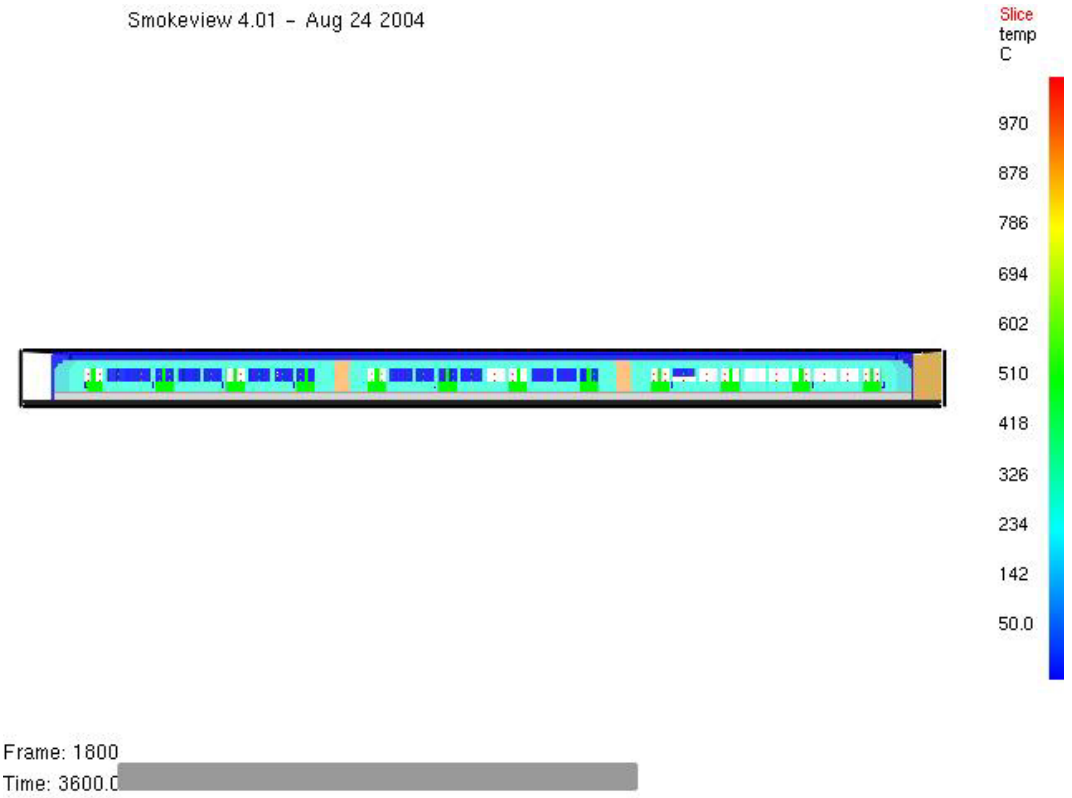

Figure 11.13: Snapshot from Smokeview for fire scenario 3A, 3600 s into the simulation

Considering the effect of direct high forced ventilation airflow velocity on the fire development, to assume the ignition source size to be constant at its peak for 1800 s was conservative. The undercarriage fire (the ignition source) might not be able to grow in the first place. Even if the emergency tunnel ventilation system was assumed to activate after the undercarriage fire has grown and propagated through the floor, the ignition source size would not remain at its peak due to the high direct airflow effect. Therefore the result from the simulation might be conservative.

Another simulation was conducted. However, as there was no better information on the likely ignition source size and burning duration, it was assumed that the ignition source size would be the same as the original simulation but this ignition source would only last for 600 s. This timing was used since this was the time taken for the compartment temperature to build up and where fire spread to adjacent cars started to occur. This again was a conservative assumption as the ignition source was unlikely to remain at its peak due to the high airflow effect as discussed earlier. The HRR curves for the original simulation and the simulation with ignition source 'removed' at 600 s are shown in Figure 11.14. From Figure 11.14, it can be seen that when the

ignition source was removed at 600 s, the fire growth was much slower. The peak HRR of 7430 kW was also substantially lower compared with the original simulation. The results from the two simulations highlighted the importance of prescribing a realistic ignition source size and its burning duration for simulations as it would have a major impact on the simulation results.

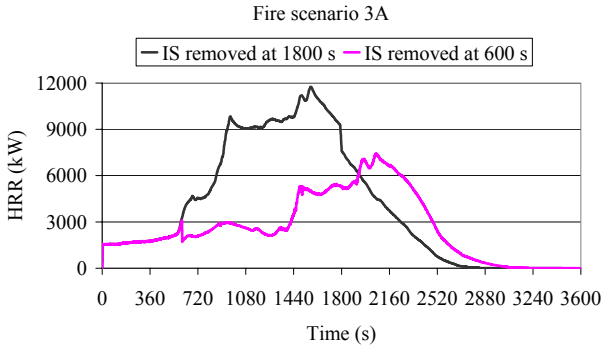

Figure 11.14: Modelling approach based on HRRPUA – Fire scenario 3A (Ignition source 'removed' at 600 s)

For fire scenarios 3B and 3D, only downstream of the ignition source was involved in the fire. The fire did not grow in intensity and spread further downstream to the adjacent car despite having a large ignition source size. The reason why the fire was not able to grow might be because of the burning area of the ignition source. Because a large burning surface (6 m^2) was defined, the flame heat flux was not as intense compared with the fire in the corner. In addition, the location of the ignition source and the location of the combustibles were also not as favourable as the fire in the corner to promote fire growth. Their HRR values were relatively constant (see Figure 11.9 and Figure 11.10) and showed signs of decay before the ignition source was 'removed' at 1800 s. The maximum compartment temperatures for fire scenarios 3B and 3D were 489 and 578°C respectively implying that flashover did not take place. There was no window failure since the compartment temperature was lower than the window failure criterion. These temperatures would also not be high enough to cause ignition of wall or ceiling since they were lower than the 'approximated' ignition temperature for wall panel (see Chapter 8, Section 8.5.2).

The simulation results for fire scenarios 3B and 3D indicated the importance of closing the detrainment door during train fire incident to prevent direct airflow

through the train that might support fire spread. Even though fire scenarios 2A and 3A have showed that high airflow would to some extent slow down the fire growth, closing the detrainment doors however could eliminate a potentially more severe fire from happening.

11.3.2 Modelling approach based on heat of vaporisation

Figure 11.15 to Figure 11.19 show the HRR curves while Table 11.5 shows the summary of predicted peak HRR values for the modelling approach based on heat of vaporisation.

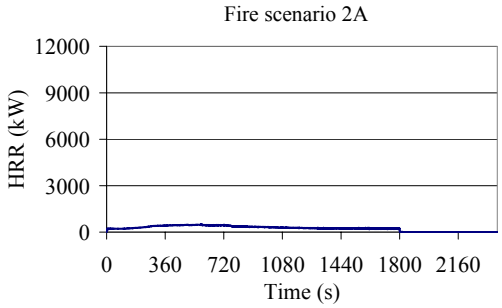

Figure 11.15: Modelling approach based on heat of vaporisation – Fire scenario 2A

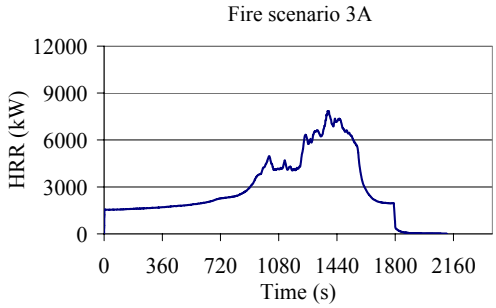

Figure 11.16: Modelling approach based on heat of vaporisation – Fire scenario 3A

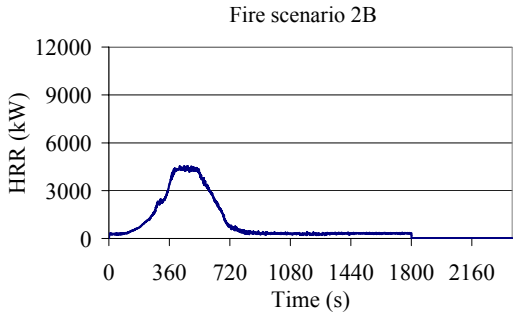

Figure 11.17: Modelling approach based on heat of vaporisation – Fire scenario 2B

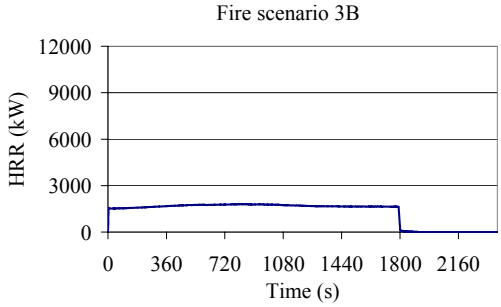

Figure 11.18: Modelling approach based on heat of vaporisation – Fire scenario 3B

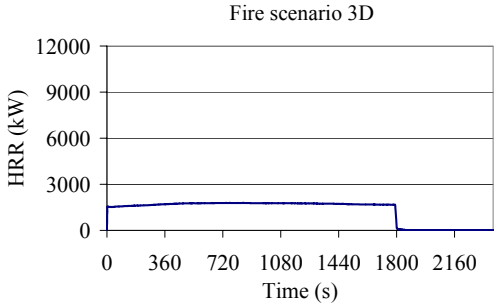

Figure 11.19: Modelling approach based on heat of vaporisation – Fire scenario 3D

s/no	Fire scenario	Peak HRR value for the modelling approach based on heat of vaporisation (kW)
1	2A	530
2	3A	8200
3	2B	4540
4	3B	1840
5	3D	1840

Table 11.5: Final simulations - Summary of predicted peak HRR values for the modelling approach based on heat of vaporisation.

The predicted fire severities for different fire scenarios were the same as the modelling approach based of HRRPUA. Low forced ventilation airflow velocity in fire scenario 2B aided the fire growth and therefore this fire scenario was more developed than fire scenario 2A. The predicted HRR for fire scenario 2B was higher than the modelling approach based on HRRPUA. Despite the difference in predicted HRR for the two modelling approaches, the furthest point the fire spread was the same i.e. to the 7-seater seat area (near the ignition source).

The fire in fire scenario 3A also spread downstream to the adjacent cars due to the influence of high forced ventilation airflow velocity. However, this only occurred at about 900 s into the simulation. The predicted HRR was also much lower than the modelling approach based on HRRPUA. As discussed in previous Section, the result for this scenario might be conservative because the ignition source size would not remain constant at its peak for 1800 s under the influence of high airflow. Another simulation was conducted by assuming the ignition source was removed at 900 s since this was the time where compartment temperature built up and fire spread to adjacent cars started to occur. The HRR curves for the original simulation and the simulation with ignition source ‘removed’ at 900 s are shown in Figure 11.20. The Figure shows that when the ignition source removed, the fire basically could not sustain itself. The results from the two simulations highlighted again the importance of prescribing a realistic ignition source size and its burning duration for simulations as it would have a major impact on the simulation results. As for the large difference in results between the two modelling approaches, it was likely because of the prescribed constant which governed the ignition and rate of pyrolysis.

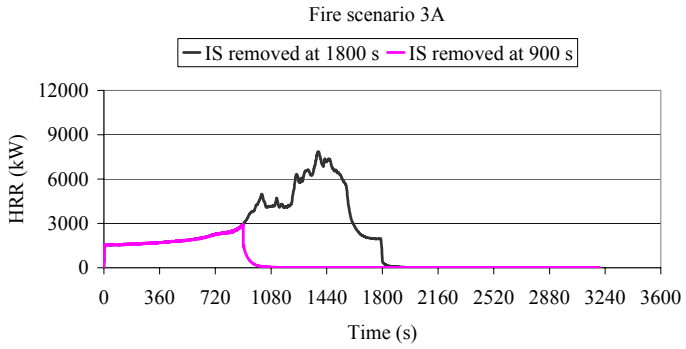

Figure 11.20: Modelling approach based on heat of vaporisation – Fire scenario 3A (Ignition source 'removed' at 900 s)

For fire scenarios 3B and 3D, the fire did not spread to adjacent car. Only downstream of the ignition source was involved in the fire. Their HRRs were almost constant until the ignition source was 'removed' at 1800 s.

11.3.3 HRR of the CCL metro train

The simulations results have allowed a full appreciation of the factors that affect the fire development. From the simulations, the influences from the following factors on the modelling results were particularly obvious:

a) Ventilation conditions (Fire scenario 2A vs. fire scenario 2B; fire scenario 3A vs. fire scenarios 3B and 3D)
b) Location of the combustibles (Fire scenarios 2A and 2B vs. fire scenarios 3A, 3B and 3D)
c) Location and size of the ignition sources (Fire scenarios 2A and 2B vs. fire scenarios 3A, 3B and 3D)
d) Burning duration of the ignition sources

Even though the two modelling approaches gave different HRR values, which were expected, they predicted the same fire consequences for different fire scenarios. Fire scenario 3A has the highest fire severity because the fire spread to adjacent cars. For this scenario, the modelling approach based on HRRPUA gave a more conservative prediction of HRR than the modelling approach based on heat of vaporisation because of the add-on effect as discussed in Chapter 4.

However, modelling results from fire scenario 3A might be conservative because the ignition source size was unlikely to remain constant at its peak for 1800 s under the direct influence of high airflow. This conclusion can be made as simulations for fire scenarios 2A and 3A have indicated that high forced ventilation airflow velocity would slow down the fire growth because materials in the current study were difficult to ignite. For the modelling approach based on HRRPUA, re-simulation result showed that the fire growth would be slower and the fire would be less severe when the ignition source was 'removed' earlier. For the modelling approach based on HRRPUA, the re-simulation result showed that the fire could not sustain itself.

The predicted peak HRR values in the final simulations were lower than the predicted peak HRR values in the trial simulations even though in the final simulations the complete train was modelled. This is because the values used in the trial simulations were over conservative as discussed in Chapter 8.

Based on the modelling results for the two modelling approaches, two peak HRR values are proposed for the metro train under consideration depending on the location of the train in the event of a fire. For a metro train fire at the station trackway i.e. the section of track next to the platform, a peak HRR value of 5 MW is proposed. Fire scenarios 2B, 3B and 3D were under the influence of low forced ventilation airflow velocity. They can also be used to represent a metro train fire at the station trackway as discussed in Chapter 6. The modelling results for both the modelling approaches for these three scenarios have showed that the HRR would not exceed 5 MW. Therefore a peak HRR value of 5 MW can conservatively be used for the design of emergency tunnel ventilation system for a train fire at the station trackway. Less than half the metro train car would be involved in the fire based on the simulations.

For a metro train fire in the tunnel, a peak HRR value of 10 MW is proposed. This HRR value coincides with the value proposed by the design consultant (see Chapter 2, Section 2.2.1). The proposed value of 10 MW allows the design to cater for the worst scenario that could probably occur in a tunnel taking into account uncertainty in size and burning duration of ignition source under the influence of high forced ventilation airflow velocity. The value was the average of predicted peak HRR for fire scenario 3A based on the two modelling approaches.

The peak HRR values estimated using the current methods were in the range of 7.8 MW to 18.3 MW, depending on the method used to estimate it. For the proposed peak HRR value of 5 MW for a metro train fire at the station trackway, the peak HRR values estimated using the current methods were higher since the main assumption used for the calculation in the current methods was that the fire would grow, spread and attain flashover during a metro train fire. The peak HRR value of 5 MW however was close to the peak HRR value computed using Frankfurt metro fire model (5.6 MW) for underground metro train car (U-Bahn) used in city of Frankfurt (see Chapter 2, Section 2.2.5). It tallied with the 5 MW value used for LAL, Hong Kong (see Chapter 2, Table 2.4) and therefore is not at odds considering the materials in the current study not only complied with the stringent small-scale tests performance criteria but were also difficult to ignite and burn in the Cone Calorimeter compared with the test results from other rail car studies.

As for the proposed peak value of 10 MW for metro train fire in the tunnel, it is at the lower limit of the estimated peak HRR values based on the current methods. It is also at the lower limit of peak HRR values adopted by various metro lines (see Chapter 2, Table 2.4). This value has been selected to cater for the worst scenario that could probably occur in a tunnel taking into account uncertainty in size and burning duration of ignition source under the influence of high forced ventilation airflow velocity. Because the size and burning duration of the ignition source used for simulations was conservative, the proposed HRR could be further reduced if better information is available.

11.3.4 Comments on the final simulations

It is important to stress that several major assumptions e.g. criterion for window failure; ignition source size and burning duration; material properties, have been made along the course of this research project so that the final simulations could be conducted. However, the assumptions made were in most case conservative so that the predicted results would be 'safe'. Efforts have also been made so that the simulations for various scenarios were realistic based on available information at hand. Comparing with the current methods of estimating HRR for a metro train, the proposed methods are still more superior as they are able to take into account factors that affect the fire development.

Nevertheless, the author has to acknowledge the proposed methods are time consuming. Besides gathering better information for simulation, there is a need to develop procedures that can derive suitable thermo-physical properties from small-scale tests for the fire retardant materials for use in fire modelling. There is also a need to improve the modelling techniques for fire growth and flame spread. The proposed methods can only become commercially viable when improvements in these areas are made. The current project can only be treated as a case study to evaluate the HRR of the metro train under consideration.

11.4 Conclusions from the final simulations

The following conclusions can be drawn from the final simulations:

a) For fire scenarios 2A and 2B i.e. fire in the corner, the fire did not grow to flashover. Low forced ventilation airflow velocity in fire scenario 2B aided the fire growth and therefore this fire scenario was more developed than fire scenario 2A. High forced ventilation airflow velocity in fire scenario 2A slowed down the fire growth due to high airflow effects.

b) With significantly large ignition source size, a high forced ventilation airflow velocity would cause the fire to spread to adjacent cars as in the case for fire scenario 3A i.e. undercarriage fire with detrainment doors opened. However, this was provided that the ignition source remained constant at its peak for 1800 s.

c) The fire in fire scenario 3B and 3D i.e. undercarriage fire with 1st and 4th passenger doors opened, was not able to grow to flashover despite having a large ignition source size. This was because the fire was less intense and the location of the ignition source and the location of the combustibles were not as favourable as fire in the corner to promote fire growth.

d) The modelling results indicated the importance of closing the detrainment door during train fire incident to prevent direct airflow through the train compartment that may support fire spread if there is a large ignition source. Closing the detrainment doors could eliminate a potentially more severe fire from happening.

e) For a scenario that will progress to flashover under the influence of high forced ventilation airflow velocity, the assumption that the fire will spread to the next car only after the first car attained flashover is not valid if there is no door installed between the train cars. The fire spread to the second and succeeding cars will be very rapid.

f) Two peak HRR values are proposed for the metro train under consideration based on the simulations. For a metro train fire at the station trackway, a peak HRR value of 5 MW is proposed and for a train fire in the tunnel, a peak HRR value of 10 MW is proposed.

12 Conclusions

The FDS CFD model was used to simulate fire growth and flame spread within a metro train in an underground trainway to predict the HRR and specifically the peak HRR for emergency tunnel ventilation system design. The main conclusions and findings from various aspects of this research are:

a) Fire on top of the seat (arson), fire in the corner (arson and electrical fault) and undercarriage fire (electrical fault) were the common fire scenarios identified for FDS simulation. The common fire scenarios were expanded to consider ventilation conditions. A total of 13 credible fire scenarios were investigated in current study.

b) From the Cone Calorimeter test data, the train materials evaluated in the current study were found to be difficult to ignite and burn compared with materials tested in other rail car studies. The fire retardant additive in the polymer materials proved to be effective in retarding ignition (especially at low heat flux levels) and reducing the heat release rate.

c) FDS predictions of Cone Calorimeter test results indicated that the procedures used in the current study were not able to derive thermo-physical properties for fire retardant materials which could be used in fire model to accurately predict the ignition and fire growth. It was not possible to derive a suitable set of temperature variant properties for $\rho c \delta$ because the fire retardant was able to effectively retard ignition at low exposure heat flux level. Different property values need to be prescribed at different exposure heat flux levels to improve the fire model prediction. Such a modelling technique is beyond the capabilities of FDS model at its current stage. For the final simulations, a combination of derived and calibrated values was prescribed to improve on the modelling results.

d) In the final simulations, the two modelling approaches predicted the same fire severity for different fire scenarios. For corner fire scenarios, a low forced ventilation airflow velocity aided the fire growth but a high forced ventilation airflow velocity slowed down the fire growth due to high airflow effects which reduced the flame temperature. However, for undercarriage fire scenarios whereas the ignition source size was significantly larger than the corner fire, a high forced ventilation velocity could cause the fire to spread to adjacent cars but the fire severity will depend on the burning duration of the ignition source.

e) It is important to close the detrainment door during a train fire incident to prevent direct airflow through the train compartment that may support fire spread if there is a large ignition source.

f) For a scenario that will progress to flashover under the influence of high ventilation airflow velocity, the assumption that the fire will spread to the next car only after the first car attained flashover is not valid if there is no door installed between the metro train cars. The fire spread to the second and succeeding cars will be very rapid.

g) Two peak HRR values are proposed for the design of emergency tunnel ventilation system for the metro train under consideration based on the final simulations. For a train fire at the station trackway, a peak HRR value of 5 MW is proposed and for a train fire in the tunnel, a peak HRR value of 10 MW is proposed.

h) The modelling results could be improved on if better information on the criterion for window failure; ignition source size and burning duration; and material properties are available. A modelling technique that allows for different prescribed property values to be selected for numerical simulations depending on the heat feedback from the fire could also improve on the modelling results.

12.1 Recommendation and future research

There is a need to develop procedures that can derive suitable thermo-physical properties for fire retardant materials for use in fire modelling from small-scale tests and also a need to improve the modelling techniques for fire growth and flame spread before the proposed methods in the current study become commercially viable. The proposed methods in the current project can only be treated as a case study to evaluate the HRR of the metro train under consideration.

As this research work has been limited in scope and duration, future work should consider the following:

a) To carry out a hazard analysis for metro train fires particularly for a scenario whereby fire occurs in the car interior and with the train stalled inside a tunnel. This scenario posed the most hazardous condition for the commuters especially if operation of emergency tunnel ventilation system is delayed.
b) To validate the modelling results if the opportunity to carry out full-scale experiments arise.

References

Alstom. (2001a). "Electrical Eqt Layout Under Seat Boxes Synop. Appareils Elecriques S/S Siege." MicroStation CAD, D830INT-ARRG0051E, ed., Alstom Transport.

Alstom. (2001b). "Final Configuration in MRT Tunnel for CSD/ SEM Tunnel Straight Alignment." MicroStation CAD, D830TUN-CSD1002A, ed., Alstom Transport.

Alstom. (2001c). "Underframe Equipment Layout MC Car Equipt. S-Chassis Voit. MC." MicroStation CAD, D830BDY-ARRG0001C, ed., Alstom Transport.

Alstom. (2001d). "Underframe Equipment Layout T Car Equipt. S-Chassis Voit. T." MicroStation CAD, D830BDY-ARRG0002C, ed., Alstom Transport.

Alstom. (2004). "Alstom Transport Project Story - Singapore Northeast Line: The Largest, Fully Automatic Metro System in the World, http://www.transport.alstom.com, accessed 10 Feb 2004." Alstom Transport.

Amtrak. (2004). "Emergency Ventilation System - Need for Fire Heat Release Rate, http://www.nfpa.org/PDF/RailSymp1.pdf, accessed 10 Aug 2004."

Anon. (2004a). "Rapid Transit, http://en.wikipedia.org/wiki/Metro, accessed 25 June 2004."

Anon. (2004b). "http://www.chandralakshmi.com/prods.htm, accessed 05 Dec 05."

Anon. (2004c). "Arson attack in the subway of Daegu, South Korea, http://www.takagi-ryo.ac/docs/id/183/lang/1, accessed 10 Dec 2004."

Arup. (2004). "Fire in a railway carriage, http://www.arup.com/fire/services/modelling/modelling.htm, accessed 24 Aug 2004."

Associated Engineers. (1980). "Subway Environment Design Handbook, Volume II, Subway Environment Simulation (SES) Computer Program, Version 3.0, Part 1: User's Manual. Prepared for the Transportation Systems Center of the U.S.D.O.T." Associated Engineers, a Joint Venture of Parsons Brinckerhoff Quade and Douglas, Inc, De Leuw Cather and Company, and Kaiser Engineers.

ASTM D 3675. (1998). "Standard Test Method for Surface Flammability of Flexible Cellular Materials Using A Radiant Heat Energy Source." American Society for Testing and Materials (ASTM), Philadelphia.

ASTM E 162. (1998). "Standard Test Method for Surface Flammability of Materials Using a Radiant Heat Energy Source." American Society for Testing and Materials (ASTM), Philadelphia.

ASTM E 906. (2004). "Standard Test Method for Heat and Visible Smoke Release Rates for Materials and Products." American Society for Testing and Materials (ASTM), Philadelphia.

ASTM E 1354. (2004). "Standard Test Method for Heat and Visible Smoke Release Rates for Materials and Products Using an Oxygen Consumption Calorimeter." American Society for Testing and Materials (ASTM), Philadelphia.

ASTM E 2061. (2000). "Guide for Fire Hazard Assessment of Rail Transportation Vehicles." American Society for Testing and Materials (ASTM), Philadelphia.

Babrauskas, V. (1979). "COMPF2: A Program for Calculating Post-Flashover Fire Temperatures. Final Report." *NBS TN 991*, National Bureau of Standards (NBS).

Babrauskas, V. (1986). "Comparative Rates of Heat Release from Five Different Types of Test Apparatuses." *Journal of Fire Sciences*, 4.

Babrauskas, V. (1992). "The Cone Calorimeter." Heat Release in Fires, V. Babrauskas and S. J. Grayson, eds., Elsevier Applied Science, pp. 61 to 91.

Babrauskas, V. (2002). "Heat Release Rates." SFPE Handbook of Fire Protection Engineering, National Fire Protection Association (NFPA), Quincy, MA, pp. 3-1 to 3-37.

Babrauskas, V. (2003). *Ignition Handbook*, Fire Science Publishers, Issaquah, WA.

Babrauskas, V., and Peacock, R. D. (1992). "Heat Release Rate: The single most important variable in fire hazard." *Fire Safety Journal*(18), pp. 255-272.

Barber, C., Gardiner, A., and Law, M. "Structural Fire Design of the Øresund Tunnel." *Proceedings of the International Conference on Fires in Tunnels*, Borås, Sweden, pp. 313 to 329.

Barnett, J. R. (1992). "Development of Analytical Techniques for Risk Management Training. University Research Final Report. Prepared for FTA, USDOT." *DOT-MA-11-0050-92-1, October 1992*, Worcester Polytechnic Institute.

Bettis, R. J., Jagger, S. F., and Moodie, K. "Reduced Scale Simulation of Fires in Partially Block Tunnels." *Proceedings of the International Conference on Fires in Tunnels*, Borås, Sweden, pp. 162 to182.

Braun, E. (1975). "A Fire Hazard Evaluation of the Interior of WMATA Metrorail Cars, Final Report. Prepared for Washington Metropolitan Area Transit Authority." *NBSIR 75-971*, National Bureau of Standards (NBS).

Braun, E. (1978). "Fire Hazard Evaluation of BART Vehicles. Prepared for Urban Mass Transportation Administration (UMTA), now Federal Transit Administration (FTA)." *NBSIR 78-1421*, National Bureau of Standards (NBS).

Brennan, E., and Lim, L. W. "Ventilating the North East Line Tunnels." *RTS Conference, Singapore 2003*, Singapore.

Briggs, P., Métral, S., Tallec, Y. L., Troïano, D., Messa, S., and Breulet, H. (2001a). "FIRESTARR - Final Report." FIRESTARR Consortium.

Briggs, P., Tallec, Y. L., Sainrat, A., Métral, S., Messa, S., and Breulet, H. "The FIRESTARR Research Project on the Reaction-To-Fire Performance of Products in European Trains." *Proceedings of the 9th International Interflam Conference 2001*, Edinburgh, Scotland, pp. 925 to 936.

BS 476-Part 7. (1997). "Fire tests on building materials and structures. Method of test to determine the classification of the surface spread of flame of products." British Standards Institution.

BSI. (1988). "Toxicity of Combustion Products, Part 2. Guide to the Relevance of Small-scale tests for Measuring the Toxicity of Combustion Products of Materials and Composites." *PD 6503: Part 2*, British Standards Institution, London.

Burdett, J. R. F., Ames, S. A., and Fardell, P. J. (1989). "Selection of Materials and Composites to Minimize Fire Hazard." King's Cross Underground Fire: Fire Dynamics and the Organisation of Safety, The Institution of Mechanical Engineers, London.

Cappuccio, J. A. (1992). "Development of Analytical Techniques for Risk Management Training," Master's thesis, Worcester Polytechnic Institute.

Carlsson, J. (2003). "Computational strategies in flame-spread modelling involving wooden surfaces - An evaluation study," Master Thesis, Lund University, Sweden.

Carvel, R. O., Beard, A. N., and Jowitt, P. W. "The Effect of Forced Longitudinal Ventilation on a HGV fire in a Tunnel." *Proceeding of the 1st International Conference on Tunnel Fires and Escape from Tunnels 1999*, Lyon, France.

Carvel, R. O., Beard, A. N., and Jowitt, P. W. "The Effect of Longitudinal Ventilation on a Pool Fire In Tunnel." *Proceeding of 8th International Interflam Conference 1999*, Edinburgh, Scotland, pp. 1267 to 1272.

Carvel, R. O., Beard, A. N., and Jowitt, P. W. "How Much Do Tunnels Enhance the Heat Release Rate of Fires?" *Proceedings of the 4th International Conference on Safety in Road and Rail Tunnels 2001*, Madrid, Spain, pp. 457 to 466.

Carvel, R. O., Beard, A. N., and Jowitt, P. W. (2001b). "The Influence of Longitudinal Ventilation Systems on Fires in Tunnels." *Tunnelling and Underground Space Technology*, 16, pp. 3 to 21.

Carvel, R. O., Beard, A. N., and Jowitt, P. W. "A Method for Making Realistic Estimates of the Heat Release Rate of a Fire in a Tunnel." *Proceedings of the 3rd International Conference on Tunnel Fires 2001*, Gaithersburg, Maryland, USA.

Carvel, R. O., Beard, A. N., Jowitt, P. W., and Drysdale, D. (2001d). "Variation of Heat Release Rate with Forced Longitudinal Ventilation for Vehicle Fires in Tunnels." *Fire Safety Journal*, 36, pp. 569 to 596.

Casale, E., and Marlair, G. "Heptane Fire Tests with Forced Ventilation." *Proceedings of International Conference of Fires in Tunnels 1994*, Borås, Sweden, pp. 37 to 50.

Castro, J. D., Rhodes, N., and Leoutsakos, G. "CFD Prediction of Smoke Movement in a Double Track Bored Tunnel, a Cut and Cover Station and a Mined Station in the Athens Metro." *Ninth International Symposium on the Aerodynamics and Ventilation of Vehicle Tunnels 1997*, Aosta Valley, Italy.

Chen, Y., Motevalli, V., and Delichatsios, M. A. (1995). "Material pyrolysis properties, Part II: methodology for derivation of pyrolysis properties for charring materials." *Combustion Science and Technology*, 104(4-6), pp. 401 to 425.

Chow, W. K. (2004). "Fire Safety of the Railway Systems." *International Journal on Architectural Science*, 5(2), pp. 35 to 42.

Chua, K. H. (2003). "Guideline for Determining Heat Release Rate for Train Fire in Underground / Enclosed Trainway (Unpublished)." Land Transport Authority, Singapore.

Cox, G. (1995). "Basic Considerations." Combustion Fundamentals of Fire, Academic Press, London.

Delichatsios, M., Bradley, P., and Bhargava, A. (2003). "Flammability properties for charring materials." *Fire Safety Journal*, 38, pp. 219 to 228.

Dowling, V. P., and Delichatsios, M. A. "Material Flammability in Train Saloons." *Proceedings: New Railways Systems, In Conjunction with Exporail (Asia) 2000*, Hong Kong.

Dowling, V. P., and Delichatsios, M. A. (2001). "Call for More Realistic Rail Fire Assessments." *Built Environment Innovation & Construction Technology*, 17.

Dowling, V. P., and White, N. "Fire Sizes in Railway Passenger Saloons." *Proceedings of the 6th Asia-Oceania Symposium on Fire Science and Technology 2004*, Daegu, Korea, pp. 601 to 611.

Drake, S., and Meeks, K. R. "Confidence Gaining by Computer Simulation of Emergency Tunnel Ventilation Design." *First International Conference, Tunnel and Underground Stations Fires 2000*.

Drysdale, D. (1998). *An Introduction to Fire Dynamics*, John Wiley & Sons Inc, London.

Drysdale, D. D., Macmillan, A. J. R., and Shilitto, D. (1992.). "King's Cross Fire: Experimental verification of the 'trench effect'." *Fire Safety Journal*, 18(1), pp. 75 to 82.

Duggan, G. J. "Usage of ISO 5660 Data in UK Railway Standards and Fire Safety Cases." *Fire Hazards, Testing, Materials and Products. A One Day Conference 1997*, Rapra Technology Ltd, Shawbury, Shrewsbury, Shropshire, UK.

ERRI. (1992a). "Coaches: Reasons for Undertaking Supplementary Studies on Improvement of the Protection of Coaches Against Fire." *ERRI B 106/RP 22*, European Rail Research Institute (ERRI), Utrecht.

ERRI. (1992b). "Feasibility Study of Computer Modelling of Fires in Railway Vehicles With a View to Improving Passenger Safety." *ERRI B 106/RP 25*, European Rail Research Institute (ERRI), Utrecht.

ERRI. (1994). "Improvement of the Protections Against Fire of Passenger Rolling Stock; Progress Report on Tests Carried Out Using a Cone Calorimeter and the Calculations with Hazard 1.1. Software Package." *ERRI C 204/RP 1*, European Rail Research Institute (ERRI), Utrecht.

ERRI. (1995). "Improvement of the Fire Protection of Passenger Rolling Stock, Results of Additional Cone Calorimeter Tests on Seat Materials and Furniture Calorimeter Tests on Mock-up Seats." *ERRI C 204.1/DT319*, European Rail Research Institute (ERRI), Utrecht.

EUREKA. (1995). "Fire protection in Traffic Tunnels - Findings from Large Scale tests within the EUREKA-project EU 499 Firetun (Final Technical Report)."

FHWA. (2004). "The Memorial Tunnel Fire Ventilation Test Program, http://www.fhwa.dot.gov/bridge/tunnel/tunres2.htm, accessed 15 Aug 2004." Federal Highway Administration (FHWA), United States Department of Transportation (USDOT).

FIT Workpackage2. (2003). "Design Fire Scenario's - 5a draft - Oct.2003 (Unpublished)." European Thematic Network on Fire in Tunnels (FIT).

Floyd, J. E., Baum, H. R., and McGrattan, K. B. "A mixture fraction combustion model for fire simulation using CFD." *Proceedings of the International Conference on Engineered Fire Protection Design 2001*, San Francisco, pp. 279 to 290.

FRA. (2002). "Code of Federal Regulations, Title 49, Transportation (49 CFR), Part 238: Passenger Equipment Safety Standards. Subpart 238.103, Fire Safety and Appendix B (As of June 25, 2002)." National Archives and Records Administration, Washington DC.

Galea, E. R., Blake, S. J., and Lawrence, P. J. "The airEXODUS Evacuation Model and its Application to Aircraft Safety." *Proceeding of International Aircraft Fire and Cabin Safety Research Conference 2001*, Trump Taj Mahal Casino Hotel, Atlantic City, NJ.

Gandhi, S., Long, R. T., and Quintiere, J. G. (1996). "Fire Tests of Passenger Rail Car Interior Materials, Final Report." *NTSB12-96-SP-034*, Prepared by Department of Fire Protection Engineering, University of Maryland for the NTSB.

Göransson, U., and Lundqvist, A. (1990). "Fires in Buses and Trains, Fire Test Methods." *SP Report 1990:45*, SP Swedish National Testing and Research Institute., Sweden.

Grenier, A. T. (1996). "Fire Characteristics of Cored Composite Materials for Marine Use," Worcester Polytechnic Institute (WPI).

Grexa, O., Janssens, M., White, R., and Dietenberger, M. "Fundamental Thermophysical Properties of Materials Derived From the Cone Calorimeter Measurements." *Proceedings of the 3rd International Scientific Conference on Wood & Fire Safety 1996*, The High Tatras, Hotel Patria, Slovak Republic.

Haack, A. "Introduction to the EUREKA-EU 499 Firetun project." *Proceedings of the International Conference on Fires in Tunnels*, Borås, Sweden, pp. 3 to 19.

Hasemi, Y., Moriyama, S., Nam, D., Tanaka, S., Okazawa, N., and Ding, W. "Fire Safety Background for Japanese Underground Railway Systems and Field Experiments on the Smoke Movement in Subway Stations." *Proceedings of the 10th International Interflam Conference 2004*, Edinburgh, Scotland, pp. 1563 to 1574.

Hettinger, J. C., and Barnett, J. R. (1991). "Evolution of the Fire Development Scenario for Subway Vehicle Fires: Historical Observations, Vehicle Design Standards, and Application of the COMPF2 Post-flashover Computer Model." *Aerodynamics and Ventilation of Vehicle Tunnels*, pp. 391 to 405.

Hietaniemi, J., Hostikka, S., and Vaari, J. (2004). "FDS Simulation of Fire Spread - Comparison of models results with experimental data." *VTT-WORK-4*, VTT Building and Transport, Kivimiehentie, Finland.

Huggett, C. (1980). "Estimation of the Rate of Heat Release by Means of Oxygen Comsumption." *Journal of Fire and Flammability*, 12.

Ingason, H., Gustavsson, S., and Dahlberg, M. (1994). "Heat Release Measurements in Tunnel Fires, BRANDFORSK Project 723-924." *SP Report 1994:08*, SP Swedish National Testing and Research Institute.

ISO 5660-1:2002. "Reaction-to-fire-tests – Heat release, smoke production and mass loss rate – Part 1: Heat release rate (cone calorimeter method)." International Organization for Standardization (ISO).

ISO 5660-2:2002. "Reaction-to-fire-tests – Heat release, smoke production and mass loss rate – Part 2: Smoke production rate (dynamic measurement)." International Organization for Standardization (ISO).

ISO 5660-3:2003. "Reaction-to-fire-tests – Heat release, smoke production and mass loss rate – Part 3: Guidance on measurement." International Organization for Standardization (ISO).

ISO 9705:1993. "Fire Tests- Full-scale room test for surface products." International Organization for Standardization (ISO).

Janssens, M. (1991). "Measuring Rate of Heat Release by Oxygen Consumption." *Fire Technology*, 27, pp. 234 -249.

Janssens, M. (2002). "Calorimetry." SFPE Handbook of Fire Protection Engineering, National Fire Protection Association (NFPA), Quincy, MA, pp. 3-38 to 3-62.

Janssens, M., Kimble, J., and D., M. "Computer Tools to Determine Material Properties for Fire growth Modelling From Cone Calorimeter Data." *Proceedings of the 8th International Conference on Fire and Materials 2003*, San Francisco, CA, pp. 377 to 387.

Janssens, M., and Parker, W. J. (1992). "Oxygen Consumption Calorimetry." Heat Release in Fires, V. Babrauskas and S. J. Grayson, eds., Elsevier Applied Science, pp. 31 to 59.

Janssens, M. L. "Improved Method of Analysis for the LIFT Apparatus, Part I: Ignition." *Proceedings of the 2nd Fire and Materials Conference 1993*, Crystal City, VA, pp. 37 to 46.

Janssens, M. L., and Grenier, A. T. "An Improved Method for Analyzing Ignition Data of Composites." *Proceedings of 23rd International Conference on Fire Safety 1997*, Millbrae, California, pp. 253-264.

Karlsson, B., and Quintiere, J. G. (2000). *Enclosure Fire Dynamics*, CRC Press, Washington, DC.

Kennedy, W. D., and Patel, S. J. "The Mount Lebanon Tunnel Ventilation System." *Sixth International Symposium on Aerodynamics and Ventilation of Vehicle Tunnels 1988*, Durham, UK.

Kennedy, W. D., Ray, R. E., and Guinan, J. W. "A Short History of Train Fire Heat Release Rate Calculations." *Annual ASHRAE Meeting 1998*, Toronto, Canada.

Könnecke, R., and Schneider, V. "A Fire Engineering Design for New and Old Existing Subway Stations." *Proceedings of the 10th International Interflam Conference 2004*, Edinburgh, Scotland, pp. 803 to 807.

Liang, M. (2002). "Evaluation Studies of the Flame Spread and Burning Rate Predictions by the Fire Dynamics Simulator," Master Thesis, University of Maryland.

Lim, L. W. (2005). Personal communication with L. W. Lim, 1 Deputy Manager, Mechanical and Electrical Services Department, Land Transport Authority, Singapore, 18 Jan 05.

Luk, K. H. (2004). "Smoke Management for Trackway Fires in Underground Train Stations," Nanyang Technological University, Singapore.

Luo, M., and Yau, R. (2002). "A Case Study: Design of a Two-way Traffic Rail Tunnel." *Tunnel Management International Journal*, 5(4).

Madrzykowski, D., Forney, G., and Walton, W. D. (2002). "Simulation of the Dynamics of a Fire in a Two-Storey Duplex - Iowa, December 22, 1999." *NISTIR 6854*, National Institute of Standards and Technology (NIST), Gaithersburg, Maryland.

Mauser, G. (2005). Personal communication - Email from Gernot Mauser, 16 Feb 2005.

McGrattan, K. (2004). "Fire Dynamics Simulator (Version 4) Technical Reference Guide." *NIST Special Publication 1018*, National Institute of Standards and Technology (NIST).

McGrattan, K. (2005a). Personal communication - Email from Kelvin McGrattan, National Institute of Standards and Technology (NIST), 15 Feb 2005.

McGrattan, K. (2005b). Personal communication - Email from Kelvin McGrattan, National Institute of Standards and Technology (NIST) to Charles Fleischmann, University of Canterbury, 7 March 2005.

McGrattan, K., and Forney, G. (2004). "Fire Dynamics Simulator (Version 4) User Guide." *NIST Special Publication 1019*, National Institute of Standards and Technology (NIST).

McGrattan, K. B., and Hamins, A. (2003). "Numerical Simulation of the Howard Street Tunnel Fire, Baltimore, Maryland, July 2001." *NUREG/CR-6793*, Joint Publication of NIST and the US Nuclear Regulatory Commission, Gaithersburg, Maryland.

Meinhardt. (2002). "Assessment of Train Fire Heat Release Rate (Unpublished)." Meinhardt (Singapore) Pte Ltd.

Mikkola, E., and Wichman, I. S. (1989). "On the ignition of Combustibles Materials." *Fire and Materials*, 14, pp. 87 to 96.

Morgan, H. P., and De Smedt, J.-C. (2002). "Prescription in Flight." *Fire Prevention and Fire Engineers Journal*, pp. 22 to 26.

Munro, J., Smith, G., Dowling, V. P., and White, N. "Combining Design Fires and Risk Assessment to Achieve Tunnel Safety." *Proceedings of the 4th International Conference on Tunnel Fires 2002*, Basel, Switzerland.

NFPA 130. (2003 edition). "Standard for Fixed Guideway Transit and Passenger Rail Systems." National Fire Protection Association, Quincy, Massachusetts.

NFPA 271. (2004 edition). "Standard Method of Test for Heat and Visible Smoke Release Rates for Materials and Products Using an Oxygen Consumption Calorimeter." National Fire Protection Association (NFPA), Quincy, Massachusetts.

Ohlemiller, T. J., and Villa, K. (1992). "Characterization of the California Technical Bulletin 133 Ignition Source and a Comparable Gas Burner." *Fire Safety Journal*, 18(4), pp. 325 to 254.

Park, H. J. "An Investigation into mysterious questions arising from the Daegu underground railway arson case through fire simulations & small-scale fire tests." *Proceedings of the 6th Asia-Oceania Symposium on Fire Science and Technology 2004*, Daegu, Korea, pp. 16 to 27.

Parker, A. "Fire Testing of Mass Transit Assemblies." *Proceedings of the 3rd International Conference on Fire and Materials 1994*, London, UK.

Peacock, R. D. (1993). "Fire Safety of Passenger Trains: A Review of U.S. and Foreign Approaches. Prepared for FRA, USDOT." *DOT/FRA/ORD-93/23*, National Institute of Standards and Technology (NIST).

Peacock, R. D., Averill, J. D., Madrzykowski, D., Stroup, D. W., Reneke, P. A., and Bukowski, R. W. (2004). "Fire Safety of Passenger Trains; Phase III: Evaluation of Fire Hazard Analysis Using Full-scale Passenger Rail Car Tests." *NISTIR 6563*, National Institute of Standards and Technology (NIST).

Peacock, R. D., and Braun, E. (1984). "Fire Tests of Amtrak Passenger Rail Vehicle Interiors. Prepared for FRA, USDOT." *Technical Note 1193*, National Bureau of Standards (NBS).

Peacock, R. D., and Braun, E. (1999). "Fire Safety of Passenger Trains; Phase I: Material Evaluation (Cone Calorimeter)." *NISTIR 6132*, National Institute of Standards and Technology (NIST).

Peacock, R. D., Bukowski, R. W., and Markos, S. H. "Evaluation of Passenger Train Car Materials in the Cone Calorimeter." *Proceedings of the 5th International Conference on Fire and Materials 1998*, San Antonio, TX.

Peacock, R. D., Jones, W. W., Bukowski, R. W., and Farney, L. C. (1991). "NIST Handbook 146, Volume II: Technical Reference Guide for HAZARD I Fire Hazard Assessment Method, Version 1.1." National Institute of Standards and Technology (NIST).

Peacock, R. D., Reneke, P. A., Averill, J. D., Bukowski, R. W., and Klote, J. H. (2002). "Fire Safety of Passenger Trains, Phase II: Application of Fire Hazard Analysis Techniques." *NISTIR 6525*, National Institute of Standards and Technology (NIST).

Peacock, R. D., Reneke, P. A., Jones, W. W., Bukowski, R. W., and Babrauskas, V. (1995). "Concepts for Fire Protection of Passenger Rail Transportation Vehicles: Past, Present, and Future." *Fire and Materials*, 19, pp. 71 to 87.

PIARC. (1999). "Fire and smoke Control in Road Tunnels." *PIARC report 05.05.B*, PIARC.

Quintiere, J. G. (1993). "A Simulation Model for Fire Growth on Materials Subject to a Room-corner Test." *Fire Safety Journal*, 20, pp. 313-339.

Rakaczky, J. A. (1980). "Fire and Flammability Characteristics of Materials Used In Rail Passenger Cars. A Literature Survey." *ARBRL-MR-03009*, U.S. Army Ballistic Research Laboratory.

Rasbash, D. J., Drysdale, D., and Deepak, D. (1986). "Critical Heat and Mass Transfer at Pilot Ignition and Extinction of a Material." *Fire Safety Journal*, 10(1), pp. 1 to 10.

Renie, G., and Prevot, R. (2003). "Passenger Vehicles - Fire Safety Design Report, Pre-Final Design Rev F (Unpublished)." *Project Reference: 83000-01-D000-VME+004 Internal Reference: CIM.W 976 001*, Alstom Transport.

Richter, I. E. "Propagation and Development of Temperatures from Tests with Railways and Road Vehicles - Comparison Between Test Data and Temperature Time Curves of Regulations." *Proceedings of the International Conference on Fires in Tunnels 1994*, Borås, Sweden, pp. 51 to 62.

Richter, I. E., and Vauquelin, O. "Description of Measuring Techniques Used in the EUREKA-Project." *Proceedings of the International Conference on Fires in Tunnels 1994*, Borås, Sweden, pp. 20 to 35.

RTI. (2002). "Introduction to the Singapore NEL Train." Rail Training International (RTI) Ltd, Traction & Rolling Stock, London, UK.

Schirmer Engineering Corporation. (1990). "Life Safety Study and Computer Modelling Analysis for New York City Railroad Tunnels and Pennsylvania Station." *Contract to the National Railway Passenger Corporation, Sec No. 15-890-29-04-00*, Schirmer Engineering Corporation.

SFPE. (2002). *SFPE Handbook of Fire Protection Engineering*, National Fire Protection Association (NFPA), Quincy, MA.

Shields, T. J., Silcock, G. W. H., and Hassani, S. K. S. (1998). "Behaviour of Glazing in a Large Simulated Office Block in a Multi-Storey Building." *Journal of Applied Fire Science*, 7(4), pp. 333-352.

Sinai, Y. (2004). "Safety in Transit." *Fire Prevention & Fire Engineers Journal*, pp. 36 to 38.

Smith, E. E. (1976). "Transit Vehicle Material Specification Using Release Rate Tests for Flammability and Smoke, Phase 1 Report. Prepared for Transit Development Corporation." Ohio State University, Department of Chemical Research, Columbus, Ohio.

Smith, E. E. "Fire Safety Evaluation of Rapid Transit System." *Proceedings of the International Conference on Fire Safety 1983*, San Francisco, CA.

Soo, W. T. (2005). Personal communication - Email from W. T. Soo, Manager, Transit Regulation Department, Land Transport Authority, Singapore, 13 Feb 2005.

SP. (2004). "Runehamar Fire Tests, http://www.sp.se/fire/Eng/Protection/Runehamar_tests.htm, accessed 1 Sept 04." SP Swedish National Testing and Research Institute.

Steinert, C. "Smoke and Heat Production in Tunnel Fires." *Proceeding of International Conference on Fires in Tunnels 1994*, Borås, Sweden, pp. 123 to137.

Tallec, Y. L., Sainrat, A., Métral, S., Briggs, P., Messa, S., and Breulet, H. "The FIRESTARR Project - Fire Protection of Railway Vehicles." *Fire and Material 2001*, Fisherman's Wharf, San Francisco, USA.

Tan, J. (2005a). Personal communication - Email from Joseph Tan, Rolling Stock Project Engineer, Land Transport Authority, Singapore, 13 Feb 2005.

Tan, J. (2005b). Personal communication - Email from Joseph Tan, Rolling Stock Project Engineer, Land Transport Authority, Singapore, 24 March 2005.

Tewarson, A. (2002). "Generation of Heat and Chemical Compounds in Fires." SFPE Handbook of Fire Protection Engineering, National Fire Protection Association (NFPA), Quincy, MA, pp. 3-82 to 3-161.

Thomson, H., and Drysdale, D. (1987). "Flammability of Plastics, I: Ignition Temperatures." *Fire and Materials*, 11, pp. 163 to 172.

Thomson, H., Drysdale, D., and Beyler, C. (1988). "An Experimental Evaluation of Critical Surface Temperature as a Criterion for Piloted Ignition of Solid Fuels." *Fire Safety Journal*, 13, pp. 185 to 196.

Tipping, G. "Composite Solutions to the Fire Performance needs of Mass Transit." *3rd International Conference on the Response of Composite Materials to Fire 2003*, Centre for Composite Materials Engineering, University of Newcastle, UK.

Vettori, R. L., Madrzykowski, D., and Walton, W. D. (2002). "Simulation of Dynamics of a Fire in a One Storey Restaurant - Texas, February 14, 2000." *NISTIR 6923*, National Institute of Standards and Technology (NIST), Gaithersburg, Maryland.

VTT. (2003). "Fire Dynamics Simulator, http://www.vtt.fi/rte/firetech/services/fire_simulation/fds.pdf , accessed 20 Feb 05."

Wade, C. A. (2003a). "BRANZFIRE Technical Reference Guide." *Student Report No. 92 (Revised 2003)*, Building Research Association of New Zealand (BRANZ), Porirua City, New Zealand.

Wade, C. A. (2003b). "BRANZFIRE Thermal Database." Microsoft Access Application, Thermal.mdb, ed., Building Research Association of New Zealand (BRANZ), Porirua City, New Zealand.

White, N., and Dowling, V. P. "Conducting a full-scale experiment on a rail passenger car." *Proceedings of the 6th Asia-Oceania Symposium on Fire Science and Engineering 2004*, Daegu, Korea, pp. 591 to 601.

Wilk, E. (2002). "Bericht zur Bestimmung eines Bemessungsbrandes für Triebfahrzeuge der U-Bahn/ Frankfurt a. M., Anlage 8." Brandschutz Consult mbH, Leipzig.

Wolinska, J. R. (2002). "Passenger Train Fire In tunnel." *Tunnel Management International Journal*, 5(4).

Wu, Y. "Smoke Control in Tunnels with Slope using Longitudinal Ventilation Effect of Tunnel Slope on Critical Velocity." *Proceedings of the 11th International Symposium on Aerodynamics and Ventilation of Vehicle Tunnels 2003*, Luzern, Switzerland, pp. 77 to 86.

Yau, R., Lai, F., Li, J., and Lau, B. (2002). "Design of Tunnel Ventilation System of Underground Rapid Transit System in Bangkok."

Young, R. "Development of Heat Release Techniques Within European Railways." *Proceedings of the Fire Safety by Design Conference 1995*, University of Sunderland, UK.

Appendix A: NFPA 130 and FRA test methods and performance criteria

Materials		Flammability and smoke emission	
Category[a]	**Function of material**[a]	**Test method**	**Performance criteria**
Cushions, mattress	All	ASTM D 3675	$I_s \leq 25$
		ASTM E 662	D_s (1.5 min) ≤ 100 D_s (4.0 min) ≤ 175
Fabrics	All	14 CFR 25, Appendix F, Part I (vertical test)	Flame time $\leq$ 10 s Burn length $\leq$ 150 mm
		ASTM E 662	D_s (4.0 min) ≤ 200
Interior vehicle components	Sear and mattress frames, wall and ceiling lining and panels, seat and toilet shrouds, trays and other tables, partitions, shelves, opaque windscreens, and combustible signage	ASTM E 162	$I_s \leq 35$
		ASTM E 662	D_s (1.5 min) ≤ 100 D_s (4.0 min) ≤ 200
	Flexible cellular foams used in armrest and seat and mattress padding	ASTM D 3675	$I_s \leq 25$
		ASTM E 662	D_s (1.5 min) ≤ 100 D_s (4.0 min) ≤ 175
	Thermal and acoustical insulation	ASTM E 162	$I_s \leq 25$
		ASTM E 662	D_s (4.0 min) ≤ 100
	HVAC ducting	ASTM E 162	$I_s \leq 25$[b]
		ASTM E 662	D_s (4.0 min) ≤ 100
	Floor covering	ASTM E 648	CRF $\geq$ 5 kW/m^2
		ASTM E 662	D_s (1.5 min) ≤ 100 D_s (4.0 min) ≤ 200
	Light diffusers, windows and transparent plastic windscreens	ASTM E 162	$I_s \leq 100$
		ASTM E 662	D_s (1.5 min) ≤ 100 D_s (4.0 min) ≤ 200
Elastomers	Window gaskets, door nosings, intercar diaphragms, and roof mats	ASTM C 1166	Average flame propagation < 100 mm
		ASTM E 662	D_s (1.5 min) ≤ 100 D_s (4.0 min) ≤ 200
Exterior vehicle components[c]	End caps, roof housing, articulation bellows, exterior shells, and component boxes and covers	ASTM E 162	$I_s \leq 35$
		ASTM E 662	D_s (1.5 min) ≤ 100 D_s (4.0 min) ≤ 175
Wire and Cable[c]	All	UL 1581, CSA C22.2, UL 1685, ANSL/ UL 1666, NFPA 262, ASTM E 662	Pass
	Control and low voltage	ICEA S-19/ NEMA WC 3, UL 44, UL 83	Pass
	Fire alarm cable	IEC 60331-11	Pass
Structural Components	Flooring, other	ASTM E 199	Pass

a Categories and functions follow NFPA 130.

b FRA requirement is $I_s \leq 35$

c NPFA 130 only

Table A1: NFPA 130 and FRA test methods and performance criteria for the flammability and smoke emission characteristic of materials used in fixed guideway vehicles and passenger rail cars.

Note:

1) I_s is flame spread index
2) D_s is an instantaneous measure of the optical density at a particular instant in time
3) CRF is critical radiant flux

References

FRA. (2002). "Code of Federal Regulations, Title 49, Transportation (49 CFR), Part 238: Passenger Equipment Safety Standards. Subpart 238.103, Fire Safety and Appendix B (As of June 25, 2002)." National Archives and Records Administration, Washington DC.

NFPA 130. (2003 edition). "Standard for Fixed Guideway Transit and Passenger Rail Systems." National Fire Protection Association, Quincy, Massachusetts.

Appendix B: Major metro train fires in tunnel from 1970 to 2003

City, Country	Date	Description	Reference
Daegu, South Korea	18 Feb 2003	An arsonist started fire when he was on a train by spreading flammable liquid into one of the carriages of a six-car train when it reached Jungangno Station. Two six-car trains were destroyed, and 198 people killed.	(Anon 2004c)
Berlin, Germany	7 July 2001	The fire was started by an arc lamp in the rear carriage of the roughly 100 m long train, in a tunnel between the stations at "Kurt-Schumacher-Platz" and "Afrikanische Strasse". Despite the small size of fire, the amount of smoke in the carriage and the tunnel area was considerable.	(Anon 2004d)
Berlin, Germany	8 July 2000	Electrical short-circuit caused arcing on the body of the last car of an eight-car train. The car superstructure ignited upon entering the Deutsche Oper station. Passengers were evacuated from both underground trains in the station. Last car of the incident train was completely burned out.	(FIT Workpackage2 2003)
Amsterdam, Netherlands	12 July 1999	The brakes on the bogie started the fire of a high-speed tram when it was in Weesperplein underground station. The driver and a member of station staff tried to extinguish the fire but failed and the entire station got filled with smoke. Evacuation was initiated. The firemen eventually put off the fire. Two persons were slightly injured (smoke poisoning).	(Colombo 2001)
Baku, Aserbadjain	28 Oct 1995	A fully loaded five-car train stopped about 200 m after Uldus station due to sparkover/ electric arc in electrical equipment in the rear bogie of the fourth car. 289 people were killed and 265 injured.	(FIT Workpackage2 2003)

New York City, US	21 Dec 1994	An arsonist exploded a homemade bomb that sent a fireball whooshing through a subway car injuring himself and 47 others. The crude bomb went off while the subway train was parked in a station.	(Anon 2004e)
New York City, US	28 Dec 1990	Electrical fire in the subway tunnel near Clark Street, Brooklyn kills two and injures 188.	(Anon 2004e)
Moscow, Russia	1987	A burning train stopped in a tunnel to evacuate passengers. Inaccessibility made fire fighting difficult, and the fire reached major proportions before firemen arrived. Tunnel draughts caused problems from smoke and gases.	(Andersen 2004a)
Hamburg, Germany	20 Sep 1984	A fire started in a seat on a three-car train late at night. The train was stopped and evacuated at Landungsbrucken station, where the fire spread to cables. Two cars were destroyed, and one passenger was affected by smoke.	(Andersen 2004a)
München, Germany	5 Sep 1983	An electrical fault caused a train fire; after discharging passengers at HW the driver continued to a stabling siding where firemen extinguished the blaze. Two vehicles were destroyed, and seven passengers affected by smoke.	(Andersen 2004a)
London, UK	11 Aug 1982	A short circuit on a Piccadilly line train in a tunnel between Wood Green and Bounds Green caused a fire which destroyed one vehicle. Over 50 passengers were evacuated along the tunnel; 15 of them were affected by smoke.	(Andersen 2004a)
New York City, US	2 Jun 1982	A PATH train stabled near Exchange Place station caught fire, and the fire service took six hours to bring it under control. Four cars were destroyed, and several people were affected by smoke.	(Andersen 2004a)
New York City, US	16 Mar 1982	A fault in under-floor control gear started a train fire in the running tunnel near Christopher Street. Rapid spread of smoke led to the evacuation of some 400 passengers; 86 of them were injured, and one vehicle was destroyed.	(Andersen 2004a)

Bonn, Germany	11 Sep 1981	A technical fault caused a fire on a light rail car in the running tunnel near Ramersdorf station. The fire was extinguished within 25 minutes, with no passengers injured; the car was destroyed.	(Andersen 2004a)
Moscow, Russia	1 Jun 1981	An electrical fault caused a fire on a train at Oktyabrskaya station, and two cars were engulfed before the fire brigade arrived. Heat and smoke made the firefighting difficult. Over 2000 passengers were evacuated from various trains by firemen in breathing apparatus. Seven people were reported to have died.	(Andersen 2004a)
New York City, US	1980 – 1981	Between June 1980 and July 1981, eight fires on the New York Subway necessitated evacuation of passengers. A total of 50 people were hospitalised. Several of the fires were started by electrical faults in under floor control equipment.	(Andersen 2004a)
London, UK	21 Jun 1980	A discarded cigarette is believed to have started a fire in a cross-passage between the Northern Line running tunnels at Goodge Street. Poisonous smoke given off by burning cables caused one fatality.	(Andersen 2004a)
Hamburg, Germany	8 Apr 1980	A fire was deliberately started in a seat near the front of a train, and spread rapidly down the train. Two cars were destroyed, and four passengers were affected by smoke.	(Andersen 2004a)
New York City, US	8 Sep 1979	A discarded cigarette ignited oil to start a fire at Grand Central Terminal on the Lennox Avenue line, creating dense smoke. Two cars of 12 stabled nearby were burnt out. Poor communication between train crews and controllers and between firemen and managers delayed evacuation of 100 people, resulting in four being injured.	(Andersen 2004a)
Philadelphia, US	6 Sep 1979	A transformer fire and explosion in a train carrying 1100 people at Septa's Erie Street station. The train's doors failed to open, causing panic. 148 passengers were injured in the crush as people left through the windows.	(Andersen 2004a)

Paris, France	25 Mar 1979	A short circuit caused by a foreign body on the line at Reuilly-Diderot station on Line 1 started a fire on a passenger train, destroying one car. Thick smoke hampered rescue operations, affecting 26 people.	(Andersen 2004a)
San Francisco, US	17 Jan 1979	A current collector fault on a BART train passing through the trans-Bay tunnel caused a short circuit and fire on the following train. Lack of communication between driver and control centre, poor co-ordination and errors of judgement hampered rescue of the passengers. One person died, and 56 were affected by smoke. Five cars were involved in varying degree.	(Andersen 2004a; Associated Engineers 1980)
Köln, Germany	24 Oct 1978	A discarded cigarette set fire to a light rail car in the pre-metro tunnel at Hansaring station, and eight passengers were evacuated. Because of the smoke only firemen with breathing equipment could enter.	(Andersen 2004a)
Toronto, Canada	15 Oct 1976	An arsonist started a fire in a train at Christie Street station, resulting in the destruction of four vehicles.	(Andersen 2004a)
Lisboan, Portugal	25 May 1976	A traction failure led to a fire on a train; passengers were evacuated at a station, but four cars were destroyed.	(Andersen 2004a)
San Francisco, US	March 1975 - Nov 1976	There have been 27 fire or smoke incidents on subway cars of the BART system. All but three of these incidents occurred below the car floor and did not penetrate into the passenger compartment. The remaining three cases involved interior car fires that produced minor damage (Two burning trash fires and one aborted arson attempt to ignite a seat cushion with a pile of matches).	(Braun 1978)
Boston, US	2 Jul 1975	Broken overhead wires in the light-rail tunnel near Kenmore Square station ignited the front of a car during the morning peak. Over 400 people were evacuated, and 34 were affected by smoke.	(Andersen 2004a)

Montreal, Canada	23 Jan 1974	Faulty rubber tyres on a train caused a short circuit south of Rosemard station, starting a fire and leading to the destruction of nine vehicles and 300 m of cabling. Over 1000 passengers had to be evacuated.	(Andersen 2004a)
Paris, France	27 Mar 1973	An empty car in a Line 7 train was set on fire near Porte d'Italie by an arsonist igniting a seat. Despite rapid action by the fire services, the car was destroyed and two passengers at the station were killed by smoke.	(Andersen 2004a)
Stockholm, Sweden	1972 - 1978	Over this period seven fires broke out on board trains, resulting in destruction of the cars in each case. All the fires were thought to be arson.	(Andersen 2004a)
East Berlin, Germany	4 Oct 1972	A train car stabled at Alexanderplatz caught fire, damaging the station buildings and destroying four vehicles.	(Andersen 2004a)
Montreal, Canada	12 Dec 1971	A train collided with the end of the tunnel at Henri Bourassa metro station, followed by a short circuit and fire which spread to train-sets stationed nearby. 36 cars were destroyed, and the driver killed.	(Andersen 2004a)

Table B1: Major metro train fires in tunnel from 1970 to 2003

References

Andersen, T. (2004a). "Significant metro fires 1970-1987, http://home.no.net/lotsberg/artiklar/brann/metro_fires.html, accessed 20 Dec 2004."

Anon. (2004c). "Arson attack in the subway of Daegu, South Korea, http://www.takagi-ryo.ac/docs/id/183/lang/1, accessed 10 Dec 2004."

Anon. (2004d). "Berlin: Fire in a subway station, http://alt.brandschutz-zeitschrift.de/english/article_subwayberlin.htm, accessed 23 Dec 2004."

Anon. (2004e). "NYC Subway Accidents, http://www.nycsubway.org/faq/accidents.html, accessed 24 Dec 2004."

Anon. (2004f). "Fire Incidents in Tunnels (1990-2003), http://sci-fire.members.beeb.net/tunnelfiresafety/tunnelfires.html, accessed 20 Dec 2004."

Associated Engineers. (1980). "Subway Environment Design Handbook, Volume II, Subway Environment Simulation (SES) Computer Program, Version 3.0, Part 1: User's Manual. Prepared for the Transportation Systems Center of the U.S.D.O.T." Associated Engineers, a Joint Venture of Parsons Brinckerhoff Quade and Douglas, Inc, De Leuw Cather and Company, and Kaiser Engineers.

Braun, E. (1978). "Fire Hazard Evaluation of BART Vehicles. Prepared for Urban Mass Transportation Administration (UMTA), now Federal Transit Administration (FTA)." *NBSIR 78-1421*, National Bureau of Standards (NBS).

Colombo, A. G. (2001). "NEDIES PROJECT - Lessons Learnt from Tunnel Accidents." *EUR Report March 2001*, Institute for Systems, Informatics and Safety (ISIS) of the EC Joint Research Centre (JRC).

FIT Workpackage2. (2003). "Design Fire Scenario's - 5a draft - Oct.2003 (Unpublished)." European Thematic Network on Fire in Tunnels (FIT).

Note: There were several other metro fire incidents reported in (Anon 2004f). They were not included here because it contained quite a number of errors in the reported date of incident.

Appendix C: Emergency tunnel ventilation system operating direction for Circle Line (CCL) under various fire scenarios

All the stations in Circle Line are built underground and are provided with air-conditioning. Full height platform screens are installed at the edges of the platform to conserve energy and also to prevent passengers from falling or getting onto the track (see Figure C1). Platform screen doors (PSD) are located along the platform screens and are inline with the metro train passenger doors when the metro train stopped at the station (see Figure C2).

Figure C1: Platform screens and platform screen doors (in closed position)

Figure C2: Platform screen doors inline with the metro train passenger doors when metro train stopped at station

If a metro train on fire is stopped at the station trackway i.e. the section of track next to the station platform, the tunnel ventilation fans at both ends of the station will operate in exhaust mode to extract smoke and hot gases generated from the fire[1]. The PSD will be opened to allow passenger evacuation and for replacement air. The operation of the system should prevent the spread of smoke from the trackway into the station platform (except for some spillage from an undercarriage fire that is unavoidable) and to induce a stream of uncontaminated air in the direction of escape. This will prevent causing unnecessary panic and ensuring tenable environment is maintained along the means of escape within the station (Chua 2003).

1 The emergency ventilation strategy used in CCL is one of the strategies normally used to handle train fires at the station trackway. Luk (2004) discussed in detail the other strategies that have been adopted by different metro lines /stations. He highlighted that the layout of the station and trackway, location of fire, the fire size, the capacities of the ventilation systems, etc are factors that affect the selection of a ventilation strategy for a train fires at the station trackway.

However, if a metro train on fire is stalled inside a tunnel, passenger evacuation inside the tunnel will be required. The emergency tunnel ventilation system needs to be operated so that it provides a clear and safe path for passenger evacuation in the tunnel. This is achieved by operating the emergency tunnel ventilation system in a push-pull mode by operation staff in the operation control centre (OCC). The direction of the emergency tunnel ventilation airflow will be in the opposite the direction of evacuation which in turn depends on the position of the fire (front car, middle car or rear car) and the location of trains.

The various fire scenarios that might occur in the tunnel and the emergency tunnel ventilation system operating directions are discussed below.

C1 Only incident metro train inside tunnel section (between stations)

Fire location unknown

In event that the location of the metro train fire cannot be identified, it is recommended that the direction of emergency tunnel ventilation airflow be set in the normal train travelling direction.

Front car fire, external metro train fire

If the front car of the metro train is on fire, the direction of the emergency tunnel ventilation airflow should be set in the normal train travelling direction.

Rear car fire, external metro train fire

If the rear car of the metro train is on fire, the direction of the emergency tunnel ventilation airflow should be set in the opposite direction of a normal train travelling direction.

Middle car fire, external metro train fire

If middle car of the metro train is on fire, the direction of the emergency tunnel ventilation airflow should be based on the evacuation arrangement determined by the operation staff in the OCC and the Customer Service Officer[2] (CSO).

Internal metro train fire

With an internal metro train fire, the metro train should be able to move towards the next station for passenger evacuation. However, if the incident metro train is disabled in the tunnel, the direction of the emergency tunnel ventilation airflow should be based on the evacuation arrangement determined by the operation staff in the OCC and the CSO.

C2 Incident metro train and non-incident metro train inside tunnel section (between stations)

External metro train fire

If any non-incident metro train is stopped behind the incident train, the emergency tunnel ventilation airflow should be set in a direction to prevent smoke from flowing towards the non-incident metro train regardless of the metro train fire location.

Internal metro train fire

With an internal metro train fire, the metro train should be able to move towards the next station for passenger evacuation. However, if the incident metro train is disabled in the tunnel and there is another metro train stopped behind it, the emergency tunnel ventilation air flow should be set in a direction that prevent the smoke from flowing towards the non-incident metro train regardless of the metro train fire location.

2 Unlike typical metro system, the Circle Line trains will be driverless. However, there would be one customer service officer (CSO) in each train. CSOs are trained to handle passengers' queries, manage emergency situations, report metro train faults and abnormalities to the OCC and they are also qualified train drivers.

References

Brennan, E., and Lim, L. W. "Ventilating the North East Line Tunnels." *RTS Conference, Singapore 2003*, Singapore.

Chua, K. H. (2003). "Guideline for Determining Heat Release Rate for Train Fire in Underground / Enclosed Trainway (Unpublished)." Land Transport Authority, Singapore.

Luk, K. H. (2004). "Smoke Management for Trackway Fires in Underground Train Stations," Nanyang Technological University, Singapore.

Appendix D: Material properties

D1 FRP polyester

The components that are made of FRP polyester are the seats, under seat boxes, equipped cubicle assemblies, PEC module fittings, detrainment doors, driver console assembly, face (wall) and the ceiling panels at car end mask. The material properties for FRP polyester obtained from various references are compiled in Table D1. Note that since only the seat sample is available, it is assumed that the thickness and density of other components made of FRP polyester are the same as the seat.

Properties	Value	Value selected	Remark	Reference
Thickness δ (m)	0.004	0.004	Measured from the seat sample	
Thermal conductivity k (W/mK)	0.3	0.295 (Ave)	Polyester, FRP	(Anon 2004g)
	0.29		Polyester, glass filler (18-36%)	(Tewarson et al. 1999)
Density ρ (kg/m^3)	1795	1795 (measured value)	Measured from the seat sample	
	1950		Polyester, FRP	(Anon 2004g)
	1480 - 1730		Polyester, glass filler (18-36%)	(Tewarson et al. 1999)
Specific heat c (kJ/kgK)	1.51	1.6735 (Ave)	Polyester, FRP	(Anon 2004g)
	1.2-2.3		Polyester, unsaturated	(SFPE 2002) Appendix C Table C3
	1.1 - 1.3		Polyester, glass filler (18-36%)	(Tewarson et al. 1999)
	1.047		Polyester, chopped glass filler	(Hilado 1990) Table 2.3
Chemical Formula	$C_{5.77}H_{6.25}O_{1.63}$	$C_{5.77}H_{6.25}O_{1.63}$	Polyester, unsaturated	(SFPE 2002) Appendix C Table C3
Energy per unit mass O_2 (kJ/kg of O_2)	11900	11900	Polyester, unsaturated	(SFPE 2002) Appendix C Table C3

Fraction of CO_2 from fuel (kg/kg)	0.71 -1.47	Not used	Polyester, FRP	(Tewarson 2002) Table 3-4.14
	1.38		Wall panel, FRP Cone Calorimeter test average	(Peacock and Braun 1999) Table D-6
Fraction of CO from fuel (kg/kg)	0.039 – 0.102	0.0705 (Ave)	Polyester, FRP	(Tewarson 2002) Table 3-4.14
	0.094		Wall panel, FRP Cone Calorimeter test average	(Peacock and Braun 1999) Table D-6
Fraction of soot from fuel (kg/kg)	0.054 – 0.07	0.062 (Ave)	Polyester, FRP	(Tewarson 2002) Table 3-4.14
Radiative fraction	0.3 – 0.4	0.35 (Ave)	Polyester, FRP	(Tewarson 2002) Table 3-4.14
Ignition Temperature T_{ig} (°C)	346 - 399	346 (lowest)	Polyester, glass fibre laminate (glass reinforced)	(Hilado 1990) Table 2.5
Heat of vaporisation ΔH_v (kJ/kg)	1400 – 6400	1390 (lowest)	Polyester, FRP	(Tewarson 2002) Table 3-4-7
	1390		Polyester (glass fibre reinforced)	(Drysdale 1998) Table 5.8
	1750		Fire Rated Polyester (glass fibre reinforced)	(Drysdale 1998) Table 5.8
	350 – 410		Polyester, unsaturated	(Babrauskas 2003)
Effective heat of combustion $\Delta H_{c,eff}$ (kJ/kg)	9300 – 19000	12870 (use supplier figure)	Polyester, FRP	(Tewarson 2002) Table 3-4.14
	13500		Wall panel, FRP Cone Calorimeter test average	(Peacock and Braun 1999) Table D-6
Maximum burning rate $\dot{m}''_{\max}$ (kg/m^{2}s)	0.021	0.042	Wall panel, FRP	(Peacock and Braun 1999) Figure D-24

Table D1: Material properties for FRP polyester

D2 Styrene butadiene

The floor covering is made of styrene butadiene. The material properties obtained from various references are compiled in Table D2.

Properties	Value	Value selected	Remark	Reference
Thickness δ (m)	0.003	0.003	Measured from the floor covering sample	
Thermal conductivity k (W/mK)	0.15	0.19 (Ave)	Styrene butadiene	(Hilado 1990) Table 2.4
	0.23		Synthetic rubber	(Bejan 1993) Appendix B
Density ρ (kg/m^3)	1478	1478 (measured value)	Measured from the floor covering sample	
	1150		Synthetic rubber	(Bejan 1993) Appendix B
Specific heat c (kJ/kgK)	1.883 – 2.092	1.9875 (Ave)	Styrene butadiene	(Hilado 1990) Table 2.3
	1.97		Synthetic rubber	(Bejan 1993) Appendix B
	1.94		Butadiene/styrene 8.58% copolymer	(SFPE 2002) Appendix C Table C3
	1.82		Butadiene/styrene 25.5% copolymer	(SFPE 2002) Appendix C Table C3
Ignition Temperature T_{ig} (°C)	360	360	Styrene butadiene	(Babrauskas 2003)
Heat of vaporisation ΔH_v (kJ/kg)	2700	2700	Styrene butadiene	(Tewarson 2002) Table 3-4-7
Effective heat of combustion $\Delta H_{c,eff}$ (kJ/kg)	42490	17950 (use supplier figure)	Butadiene/styrene 8.58% copolymer	(SFPE 2002) Appendix C Table C3
	41950		Butadiene/styrene 25.5% copolymer	(SFPE 2002) Appendix C Table C3
	29500		Floor cover - Styrene-Butadiene Cone Calorimeter test average	(Peacock and Braun 1999) Table D-6
Maximum burning rate $\dot{m}''_{max}$ (kg/m^{2}s)	0.01	0.01	Floor cover - Styrene-Butadiene	(Peacock and Braun 1999) Figure D-33

Table D2: Material properties for styrene butadiene

D3 Concrete

The tunnel wall is made of concrete. The material properties obtained from various references are compiled in Table D3.

Properties	Value	Value selected	Remark	Reference
Thickness δ (m)	0.7	0.7		(Alstom 2001b)
Thermal conductivity k (W/mK)	1.28	1.1 (Ave)		(Bejan 1993) Appendix B
	1.0			FDS database
	0.81 – 1.4			(Chapman 1974; Karlsson and Quintiere 2000)
Density ρ (kg/m^3)	2200	2100 (Ave)		(Bejan 1993) Appendix B
	2100			FDS database
	1900 – 2300			(Chapman 1974; Karlsson and Quintiere 2000)
Specific heat c (kJ/kgK)	0.88	0.88		(Bejan 1993) Appendix B and FDS database

Table D3: Material properties for concrete

D4 Window

The window consists of two sheets of laminated glass: one 5 mm thick and the other 6 mm thick, with 12 mm air-gap in between. The thermal conductivity and the specific heat for the laminated glass are assumed to be the same as the float glass. The thermal conductivity and the specific heat for the float glass from various references are complied in Table D4 while the thermal conductivity and the specific heat for air at 300 K taken from (Incropera and DeWitt 2002) are 0.0263 W/mK and 1.007 kJ/kgK respectively.

Properties	Value	Value selected	Remark	Reference
Thermal conductivity k (W/mK)	0.78	0.78 (Ave)		(SFPE 2002) Table B.7
	0.76			(Parry 2002) and FDS database
	0.81			(Bejan 1993) Appendix B and (Kreith and Bohn 1986)
Specific heat c (kJ/kgK)	0.84	0.84 (Ave)		(SFPE 2002) Table B.7 and FDS database
	0.88			(Anon 2004h)
	0.8			(Bejan 1993) Appendix B and (Kreith and Bohn 1986)

Table D4: Material properties for float glass

The laminated glass has a lower specific heat compared with the air. Therefore it is assumed that the specific heat for the window is the same as the float glass since lesser energy is required to raise the temperature of the window and thus more conservative. For the thermal conductivity, it can be calculated since for composite wall,

$$U \equiv \frac{k_{window}}{\delta_{window}} \qquad \text{Equation D1}$$

and

$$U = \frac{1}{\frac{\delta_{glass(5mm)}}{k_{glass}} + \frac{\delta_{air}}{k_{air}} + \frac{\delta_{glass(6mm)}}{k_{glass}}}$$ Equation D2

Where U is the overall heat transfer coefficient in W/m^{2}K.

This is valid since one-dimensional heat transfer will be performed in FDS if the thermal conductivity, the density and the specific heat are prescribed for the window.

Finally the density of the window, which is measured since sample is available. The material properties for the window are complied in Table D5 below.

Properties	**Value used**	**Remark**
Thickness δ (m)	0.023	Measured from the window sample
Thermal conductivity k (W/mK)	0.049	Calculated
Density ρ (kg/m^3)	1380	Measured from the window sample
Specific heat c (kJ/kgK)	0.84	Assumed to be same as float glass

Table D5: Material properties for the window

D5 Wall, ceiling and passenger door constructions

The thickness for the wall, ceiling and passenger door constructions are 0.1, 0.6 and 0.35 m respectively. The constructions consist of glass wool sandwiched between the aluminium panel and the welded aluminium body or between two aluminium panels. The material properties for the aluminium and glass wool from various references are compiled in Table D6 and Table D7 respectively.

Properties	Value	Value selected	Remark	Reference
Thermal conductivity k (W/mK)	237	223 (Ave)		(Incropera and DeWitt 2002) Appendix A Table A.1
	204			(Bejan 1993) Appendix B
	229			(Chapman 1974)
Density ρ (kg/m^3)	3011	3011 (measured value)	Measured from the wall panel sample	
	2700			(Incropera and DeWitt 2002) Appendix A Table A.1 and (Bejan 1993) Appendix B and (Chapman 1974)
Specific heat c (kJ/kgK)	0.9	0.9		(Incropera and DeWitt 2002) Appendix A Table A.1 and (Bejan 1993) Appendix B and (Chapman 1974)
Melting point (°C)	660	660		(Incropera and DeWitt 2002) Appendix A Table A.1

Table D6: Material properties for aluminium

Properties	**Value**	**Value selected**	**Remark**	**Reference**
Thermal conductivity k (W/mK)	0.038	0.038 (Ave)		(SFPE 2002) Table B.7
	0.037			(Bejan 1993) Appendix B
	0.036-0.04		Density varies from 50 to 200 kg/m^3	(Kreith and Bohn 1986)
Density ρ (kg/m^3)	16 - 54	35 (Ave)		(Alstom 2001a; Renie and Prevot 2003)
Specific heat c (kJ/kgK)	0.7	0.68 (Ave)		(SFPE 2002)Table B.7
	0.66			(Bejan 1993) Appendix B
	0.67			(Kreith and Bohn 1986)

Table D7: Material properties for glass wool

The glass wool has a lower specific heat compared with the aluminium. Therefore it is assumed that the specific heat for the wall, ceiling and passenger door constructions is the same as the glass wool since lesser energy is required to raise the temperature of the constructions and thus more conservative. The thermal conductivities for the constructions are obtained using the same calculation method as for the window. As for the densities of the constructions, they can be calculated since information on the density and thickness of the aluminium panel and the glass wool for each construction is available. The material properties for the wall, ceiling and passenger door constructions are compiled in Table D8, Table D9 and Table D10 respectively.

Properties	**Value used**	**Remark**	**Reference**
Thickness δ (m)	0.1		(Alstom 2001a)
Thermal conductivity k (W/mK)	0.038	Calculated	
Density ρ (kg/m^3)	119	Calculated	
Specific heat c (kJ/kgK)	0.68	Assumed to be the same as glass wool	

Table D8: Material properties for the wall construction

Properties	**Value used**	**Remark**	**Reference**
Thickness δ (m)	0.06		(Alstom 2001a)
Thermal conductivity k (W/mK)	0.038	Calculated	
Density ρ (kg/m^3)	176	Calculated	
Specific heat c (kJ/kgK)	0.68	Assumed to be the same as glass wool	

Table D9: Material properties for the ceiling construction

Properties	**Value used**	**Remark**	**Reference**
Thickness δ (m)	0.035		(Alstom 2001a)
Thermal conductivity k (W/mK)	0.038	Calculated	
Density ρ (kg/m^3)	276	Calculated	
Specific heat c (kJ/kgK)	0.68	Assumed to be the same as glass wool	

Table D10: Material properties for the passenger door construction

References

Alstom. (2001a). "Electrical Eqt Layout Under Seat Boxes Synop. Appareils Elecriques S/S Siege." MicroStation CAD, D830INT-ARRG0051E, ed., Alstom Transport.

Alstom. (2001b). "Final Configuration in MRT Tunnel for CSD/ SEM Tunnel Straight Alignment." MicroStation CAD, D830TUN-CSD1002A, ed., Alstom Transport.

Anon. (2004g). "Fiberglass Reinforced, Polyester, http://www.matweb.com/search/SpecificMaterial.asp?bassnum=PPREMI01, accessed 6 Nov 2004."

Anon. (2004h). "http://www.mikroglas.com/material/htm, accessed 7 Nov 2004."

Babrauskas, V. (2003). *Ignition Handbook*, Fire Science Publishers, Issaquah, WA.

Bejan, A. (1993). *Heat Transfer*, John Wiley & Sons, Inc., New York.

Chapman, A. J. (1974). *Heat Transfer*, Macmillan Publishing Co., Inc, New York.

Drysdale, D. (1998). *An Introduction to Fire Dynamics*, John Wiley & Sons Inc, London.

Hilado, C. J. (1990). *Flammability Handbook for Plastics*, Technomic Publishing Company, Inc., Lancaster, Pennsylvania.

Incropera, F. P., and DeWitt, D. P. (2002). *Fundamental of Heat and Mass Transfer*, John Wiley & Sons, Inc., London.

Karlsson, B., and Quintiere, J. G. (2000). *Enclosure Fire Dynamics*, CRC Press, Washington, DC.

Kreith, F., and Bohn, M. S. (1986). *Principles of Heat Transfer*, Harper & Row Publishers, New York.

Parry, R. (2002). "Implementation of a Glass Fracture Module for the BRANZFIRE Compartment Fire Zone Modelling Software," Master thesis, University of Canterbury, Christchurch.

Peacock, R. D., and Braun, E. (1999). "Fire Safety of Passenger Trains; Phase I: Material Evaluation (Cone Calorimeter)." *NISTIR 6132*, National Institute of Standards and Technology (NIST).

Renie, G., and Prevot, R. (2003). "Passenger Vehicles - Fire Safety Design Report, Pre-Final Design Rev F (Unpublished)." *Project Reference: 83000-01-D000-VME+004 Internal Reference: CIM.W 976 001*, Alstom Transport.

SFPE. (2002). *SFPE Handbook of Fire Protection Engineering*, National Fire Protection Association (NFPA), Quincy, MA.

Tewarson, A. (2002). "Generation of Heat and Chemical Compounds in Fires." SFPE Handbook of Fire Protection Engineering, National Fire Protection Association (NFPA), Quincy, MA, page 3-82 to 3-161.

Tewarson, A., Abu-Isa, I. A., Cummings, D. R., and LaDue, D. E. "Characterization of the ignition behaviour of polymers commonly used in the automotive industry." *Proceedings of the 6th International Symposium on Fire Safety Science 1999*, Poitiers, France, Page 991-1002.

Appendix E: FRP polyester - Calculation of molecular weight and stoichiometry coefficient for CO_2, H_2O and O_2

E1 Molecular weight

The chemical formula for polyester is given as $C_{5.77}H_{6.25}C_{1.63}$. The atomic weights of C, H and O are 12, 1 and 16 respectively. Therefore the molecular weight = (12 x 5.77) + (1 x 6.25) + (16 x 1.63) = 101.6

E2 Stoichiometry coefficient for CO_2, H_2O and O_2

Consider stoichiometric reaction in air with the general form:

$$Fuel(C,H,O) + Air \rightarrow \Pr oduct(CO_2, H_2O, N_2) \qquad \text{Equation E1}$$

$$C_aH_bO_c + d(O_2 + 3.76N_2) \rightarrow aCO_2 + \frac{b}{2}H_2O + 3.76dN_2 \qquad \text{Equation E2}$$

Where

$$d = a + \frac{b}{4} - \frac{c}{2} \qquad \text{Equation E3}$$

The chemical formula of polyester is given by $C_{5.77}H_{6.25}C_{1.63}$. Therefore a = 5.77, b = 6.25, c = 1.63 and

$$d = 5.77 + \frac{6.25}{4} - \frac{1.63}{2} = 6.5175$$

Thus Equation E2 can be written as:

$$C_{5.77}H_{6.25}O_{1.63} + 6.5175(O_2 + 3.76N_2) \rightarrow 5.77CO_2 + \frac{6.25}{2}H_2O + 3.76(6.5175)N_2$$

$$C_{5.77}H_{6.25}O_{1.63} + 6.5175(O_2 + 3.76N_2) \rightarrow 5.77CO_2 + 3.125H_2O + 24.5N_2$$

Therefore, stoichiometry coefficient for CO_2, H_2O and O_2 are 5.77, 3.125 and 6.5175 respectively

References

Karlsson, B., and Quintiere, J. G. (2000). *Enclosure Fire Dynamics*, CRC Press, Washington, DC.

Appendix F: Sample FDS data file for trial simulations

Define name for output files

…….....

&HEAD CHID ='MCSimulation1Grid300',TITLE ='Circle Line - Train Fire' / All output files will have names beginning with "MCSimulation1Grid300"

Define grid size and computational domain

…….....

Grid size (choose only 1 grid size)

**,,,

Based on 150mm grid

,,,

```
    KS        = 0.038
    DELTA     = 0.06
    BACKING   = 'EXPOSED'/ 60mm ceiling

&SURF ID        = 'SIDEDOOR_CONSTRUCTION'
    FYI       = 'Aluminium-Glass wool-Aluminium'
    C_P       = 0.68
    DENSITY   = 276.
    KS        = 0.038
    DELTA     = 0.035
    BACKING   = 'EXPOSED' / 35mm door

&SURF ID        = 'LAMINATED_SAFETY_GLASS'
    RGB       = 1.0,1.0,0.75
    KS        = 0.049
    C_P       = 0.84
    DENSITY   = 1380.
    DELTA     = 0.023
    BACKING   = 'EXPOSED' /

&SURF ID        = 'CONCRETE'
    FYI       = 'Quintiere, Fire Behavior'
    RGB       = 0.66,0.66,0.66
    C_P       = 0.88
    DENSITY   = 2100.
    KS        = 1.1
    DELTA     = 0.7 /
```

Flammability parameters (Choose either simulation based on heat of vaporisation or HRRPUA)

.....

Simulation based on heat of vaporisation

**,,,

```
    DENSITY   = 1478.
    C_P = 1.9875
    DELTA     = 0.003
    TMPIGN    = 360.
    BACKING   = 'INSULATED'
    HRRPUA    = 281.
    RAMP_Q    = 'SB' /
RAMP ID = 'SB', T =      0.0      , F =     0.00     /
RAMP ID = 'SB', T =      15.0     , F =     0.76     /
RAMP ID = 'SB', T =      35.0     , F =     0.74     /
RAMP ID = 'SB', T =      60.0     , F =     1.00     /
RAMP ID = 'SB', T =      125.0    , F =     0.43     /
RAMP ID = 'SB', T =      192.0    , F =     0.40     /
RAMP ID = 'SB', T =      255.0    , F =     0.36     /
RAMP ID = 'SB', T =      345.0    , F =     0.39     /
RAMP ID = 'SB', T =      520.0    , F =     0.20     /
RAMP ID = 'SB', T =      665.0    , F =     0.14     /
RAMP ID = 'SB', T =      878.0    , F =     0.09     /
RAMP ID = 'SB', T =      1212.0   , F =     0.06     /

SURF ID       = 'FRP_POLYESTER'
    KS   = 0.295
    DENSITY     = 1795.
    C_P = 1.6735
    DELTA     = 0.004
    TMPIGN    = 346.
    BACKING    = 'INSULATED'
    HRRPUA      = 618.
    RAMP_Q      = 'PEST'/
RAMP ID = 'PEST', T =    0.0      , F =     0.00     /
RAMP ID = 'PEST', T =    3.0      , F =     1.00     /
RAMP ID = 'PEST', T =    25.0     , F =     0.28     /
RAMP ID = 'PEST', T =    48.0     , F =     0.20     /
RAMP ID = 'PEST', T =    248.0    , F =     0.15     /
RAMP ID = 'PEST', T =    338.0    , F =     0.20     /
RAMP ID = 'PEST', T =    433.0    , F =     0.10     /
RAMP ID = 'PEST', T =    689.0    , F =     0.03     /
```

Ignition Source

…….....

Fire size (Choose only 1 fire size)

**,,,

Walkway

.....

&OBST XB=-36.,36.,-3.1,-1.85,-0.3,0.33, RGB=0.1,0.1,0.1/ Walkway in tunnel

Undercarriage

.....

&OBST XB= 11.4,34.55,-1.3,1.3,-0.3,0.4 / Right MC car Undercarriage
&OBST XB= 11.4,34.55,-1.55,1.55,0.4,1. / Right MC car Undercarriage

Door position (For closed doors simulation, select all. For passenger doors opened simulation, select only OBST under 'Detrainment Doors'. For detrainment doors opened simulation, select all items under ' 1st and 4th passenger doors')

.....

Detrainment Doors

,,

&OBST XB= 11.4, 11.5,-0.7,0.7,1.2,3.025, RGB=0.0,0.8,0.0/
Detrainment Door Left (with 100mm leakage).
&OBST XB= 34.45,34.55,-0.7,0.7,1.1,3.1, RGB=0.0,0.8,0.0, SURF_ID='FRP_POLYESTER'/
Detrainment Door Right

1st and 4th Passenger Doors

**,,,,,,,,,,,,,,,,,,,

```
'LAMINATED_SAFETY_GLASS',HEAT_REMOVE='det35a' / Passenger Door Window Front Right 4b
HEAT XYZ=13.8125,-1.477,2.5,RTI=100,ACTIVATION_TEMPERATURE=675.,LABEL='det35a'/
OBST XB=13.5625,14.0625,-1.55,-1.527,1.975,2.5,RGB=1.0,1.0,1.0, SURF_ID=
'LAMINATED_SAFETY_GLASS',HEAT_REMOVE='det35b' / Passenger Door Window Front Right 4b
HEAT XYZ=13.8125,-.477,2.025,RTI=100,ACTIVATION_TEMPERATURE=675.,LABEL='det35b'/
```

MC-car Geometry (Right)

```
.....
&OBST XB=11.4,34.55,-1.55,1.55,1.0,1.1,RGB=0.5,0.5,0.5, SURF_ID = 'STYRENE_BUTADIENE' /
      Floor Cover

&OBST XB=12.0,33.25,-1.55,-0.9,3.025,3.05,RGB=0.3,1,0.7, SURF_ID=
'CEILING_CONSTRUCTION',SAWTOOTH=.FALSE / Ceiling
&OBST XB=12.0,33.25,-1.55,-0.9,3.05,3.1,RGB=0.3,1,0.7, SURF_ID=
'CEILING_CONSTRUCTION',SAWTOOTH=.FALSE / Ceiling
&OBST XB=12.0,33.25,-1.5,-0.9,3.1,3.15,RGB=0.3,1,0.7, SURF_ID=
'CEILING_CONSTRUCTION',SAWTOOTH=.FALSE / Ceiling
&OBST XB=12.0,33.25,-1.45,-0.9,3.15,3.2,RGB=0.3,1,0.7, SURF_ID=
'CEILING_CONSTRUCTION',SAWTOOTH=.FALSE / Ceiling
&OBST XB=12.0,33.25,0.9,1.55,3.025,3.05,RGB=0.3,1,0.7, SURF_ID=
'CEILING_CONSTRUCTION',SAWTOOTH=.FALSE / Ceiling
&OBST XB=12.0,33.25,0.9,1.55,3.05,3.1,RGB=0.3,1,0.7, SURF_ID=
'CEILING_CONSTRUCTION',SAWTOOTH=.FALSE / Ceiling
&OBST XB=12.0,33.25,0.9,1.5,3.1,3.15,RGB=0.3,1,0.7, SURF_ID=
'CEILING_CONSTRUCTION',SAWTOOTH=.FALSE / Ceiling
&OBST XB=12.0,33.25,0.9,1.45,3.15,3.2,RGB=0.3,1,0.7, SURF_ID=
'CEILING_CONSTRUCTION',SAWTOOTH=.FALSE / Ceiling

&OBST XB=12.0,33.25,-1.4,1.4,3.2,3.25,RGB=0.3,1,0.7, SURF_ID=
'CEILING_CONSTRUCTION',SAWTOOTH=.FALSE / Ceiling
&OBST XB=12.0,33.25,-1.31,1.31,3.25,3.3,RGB=0.3,1,0.7, SURF_ID=
'CEILING_CONSTRUCTION',SAWTOOTH=.FALSE/ Ceiling
&OBST XB=12.0,33.25,-1.27,1.27,3.3,3.35,RGB=0.3,1,0.7, SURF_ID=
'CEILING_CONSTRUCTION',SAWTOOTH=.FALSE / Ceiling
&OBST XB=12.0,33.25,-1.2,1.2,3.35,3.4,RGB=0.3,1,0.7, SURF_ID=
'CEILING_CONSTRUCTION',SAWTOOTH=.FALSE/ Ceiling
&OBST XB=12.0,33.25,-1.15,1.15,3.4,3.45,RGB=0.3,1,0.7, SURF_ID=
'CEILING_CONSTRUCTION',SAWTOOTH=.FALSE / Ceiling
&OBST XB=12.0,33.25,-1.075,1.075,3.45,3.5,RGB=0.3,1,0.7, SURF_ID=
'CEILING_CONSTRUCTION',SAWTOOTH=.FALSE/ Ceiling
&OBST XB=12.0,33.25,-0.925,0.925,3.5,3.55,RGB=0.3,1,0.7, SURF_ID=
'CEILING_CONSTRUCTION',SAWTOOTH=.FALSE / Ceiling
&OBST XB=12.0,33.25,-0.825,0.825,3.55,3.6,RGB=0.3,1,0.7, SURF_ID=
'CEILING_CONSTRUCTION',SAWTOOTH=.FALSE / Ceiling
&OBST XB=12.0,33.25,-0.7,0.6,3.6,3.65,RGB=0.3,1,0.7, SURF_ID=
'CEILING_CONSTRUCTION',SAWTOOTH=.FALSE / Ceiling
&OBST XB=12.0,33.25,-0.375,0.375,3.65,3.7,RGB=0.3,1,0.7, SURF_ID=
'CEILING_CONSTRUCTION', SAWTOOTH=.FALSE / Ceiling

&OBST XB=33.25,34.55,-1.55,-0.9,3.025,3.05,RGB= 0.3,0.7,0.7, SURF_ID= 'FRP_POLYESTER',
SAWTOOTH=.FALSE / Ceiling at End Mask
&OBST XB=33.25,34.55,-1.55,-0.9,3.05,3.1,RGB= 0.3,0.7,0.7, SURF_ID= 'FRP_POLYESTER',
SAWTOOTH=.FALSE / Ceiling at End Mask
&OBST XB=33.25,34.55,-1.5,-0.9,3.1,3.15,RGB= 0.3,0.7,0.7, SURF_ID= 'FRP_POLYESTER',
SAWTOOTH=.FALSE / Ceiling at End Mask
&OBST XB=33.25,34.55,-1.45,-0.9,3.15,3.2,RGB= 0.3,0.7,0.7, SURF_ID= 'FRP_POLYESTER',
SAWTOOTH=.FALSE / Ceiling at End Mask
&OBST XB=33.25,34.55,0.9,1.55,3.025,3.05,RGB= 0.3,0.7,0.7, SURF_ID= 'FRP_POLYESTER',
SAWTOOTH=.FALSE / Ceiling at End Mask
&OBST XB=33.25,34.55,0.9,1.55,3.05,3.1,RGB= 0.3,0.7,0.7, SURF_ID= 'FRP_POLYESTER',
```

```
SAWTOOTH=.FALSE. / Ceiling at End Mask
&OBST XB=33.25,34.55,0.9,1.5,3.1,3.15,RGB= 0.3,0.7,0.7, SURF_ID= 'FRP_POLYESTER',
SAWTOOTH=.FALSE. / Ceiling at End Mask
&OBST XB=33.25,34.55,0.9,1.45,3.15,3.2,RGB= 0.3,0.7,0.7, SURF_ID= 'FRP_POLYESTER',
SAWTOOTH=.FALSE. / Ceiling at End Mask

&OBST XB=33.25,34.55,-1.4,1.4,3.2,3.25,RGB= 0.3,0.7,0.7, SURF_ID=
'FRP_POLYESTER',SAWTOOTH=.FALSE / Ceiling at End Mask
&OBST XB=33.25,34.55,-1.31,1.31,3.25,3.3,RGB= 0.3,0.7,0.7, SURF_ID=
'FRP_POLYESTER',SAWTOOTH=.FALSE/ Ceiling at End Mask
&OBST XB=33.25,34.55,-1.27,1.27,3.3,3.35,RGB= 0.3,0.7,0.7, SURF_ID=
'FRP_POLYESTER',SAWTOOTH=.FALSE / Ceiling at End Mask
&OBST XB=33.25,34.55,-1.2,1.2,3.35,3.4,RGB= 0.3,0.7,0.7, SURF_ID=
'FRP_POLYESTER',SAWTOOTH=.FALSE/ Ceiling at End Mask
&OBST XB=33.25,34.55,-1.15,1.15,3.4,3.45,RGB= 0.3,0.7,0.7, SURF_ID=
'FRP_POLYESTER',SAWTOOTH=.FALSE / Ceiling at End Mask
&OBST XB=33.25,34.55,-1.075,1.075,3.45,3.5,RGB= 0.3,0.7,0.7, SURF_ID=
'FRP_POLYESTER',SAWTOOTH=.FALSE/ Ceiling at End Mask
&OBST XB=33.25,34.55,-0.925,0.925,3.5,3.55,RGB= 0.3,0.7,0.7, SURF_ID=
'FRP_POLYESTER',SAWTOOTH=.FALSE / Ceiling at End Mask
&OBST XB=33.25,34.55,-0.825,0.825,3.55,3.6,RGB= 0.3,0.7,0.7, SURF_ID=
'FRP_POLYESTER',SAWTOOTH=.FALSE / Ceiling at End Mask
&OBST XB=33.25,34.55,-0.7,0.6,3.6,3.65,RGB= 0.3,0.7,0.7, SURF_ID=
'FRP_POLYESTER',SAWTOOTH=.FALSE / Ceiling at End Mask
&OBST XB=33.25,34.55,-0.375,0.375,3.65,3.7,RGB= 0.3,0.7,0.7, SURF_ID=
'FRP_POLYESTER',SAWTOOTH=.FALSE / Ceiling at End Mask

&OBST XB=11.4,12.0,-1.55,1.55,3.025,3.05,RGB=0.8,0.6,0.4, SURF_ID=
'CEILING_CONSTRUCTION',SAWTOOTH=.FALSE / Gangway Ceiling
&OBST XB=11.4,12.0,-1.55,1.55,3.05,3.1,RGB=0.8,0.6,0.4, SURF_ID=
'CEILING_CONSTRUCTION',SAWTOOTH=.FALSE / Gangway Ceiling
&OBST XB=11.4,12.0,-1.5,1.5,3.1,3.15,RGB=0.8,0.6,0.4, SURF_ID=
'CEILING_CONSTRUCTION',SAWTOOTH=.FALSE / Gangway Ceiling
&OBST XB=11.4,12.0,-1.45,1.45,3.15,3.2,RGB=0.8,0.6,0.4, SURF_ID=
'CEILING_CONSTRUCTION',SAWTOOTH=.FALSE / Gangway Ceiling
&OBST XB=11.4,12.0,-1.4,1.4,3.2,3.25,RGB=0.8,0.6,0.4, SURF_ID=
'CEILING_CONSTRUCTION',SAWTOOTH=.FALSE / Gangway Ceiling
&OBST XB=11.4,12.0,-1.31,1.31,3.25,3.3,RGB=0.8,0.6,0.4, SURF_ID=
'CEILING_CONSTRUCTION',SAWTOOTH=.FALSE/ Gangway Ceiling
&OBST XB=11.4,12.0,-1.27,1.27,3.3,3.35,RGB=0.8,0.6,0.4, SURF_ID=
'CEILING_CONSTRUCTION',SAWTOOTH=.FALSE / Gangway Ceiling
&OBST XB=11.4,12.0,-1.2,1.2,3.35,3.4,RGB=0.8,0.6,0.4, SURF_ID=
'CEILING_CONSTRUCTION',SAWTOOTH=.FALSE/ Gangway Ceiling
&OBST XB=11.4,12.0,-1.15,1.15,3.4,3.45,RGB=0.8,0.6,0.4, SURF_ID=
'CEILING_CONSTRUCTION',SAWTOOTH=.FALSE / Gangway Ceiling
&OBST XB=11.4,12.0,-1.075,1.075,3.45,3.5,RGB=0.8,0.6,0.4, SURF_ID=
'CEILING_CONSTRUCTION',SAWTOOTH=.FALSE/ Gangway Ceiling
&OBST XB=11.4,12.0,-0.925,0.925,3.5,3.55,RGB=0.8,0.6,0.4, SURF_ID=
'CEILING_CONSTRUCTION',SAWTOOTH=.FALSE / Gangway Ceiling
&OBST XB=11.4,12.0,-0.825,0.825,3.55,3.6,RGB=0.8,0.6,0.4, SURF_ID=
'CEILING_CONSTRUCTION',SAWTOOTH=.FALSE / Gangway Ceiling
&OBST XB=11.4,12.0,-0.7,0.6,3.6,3.65,RGB=0.8,0.6,0.4, SURF_ID=
'CEILING_CONSTRUCTION',SAWTOOTH=.FALSE / Gangway Ceiling
&OBST XB=11.4,12.0,-0.375,0.375,3.65,3.7,RGB=0.8,0.6,0.4, SURF_ID=
'CEILING_CONSTRUCTION',SAWTOOTH=.FALSE / Gangway Ceiling

&OBST XB=21.1,24.5,-1.275,-0.825,1.4,1.5,RGB=0.0,0.0,1.0, SURF_ID='FRP_POLYESTER' /
      Seat Front Centre
&OBST XB=21.1,24.5,-1.45,-1.275,1.4,1.975,RGB=0.0,0.0,1.0, SURF_ID='FRP_POLYESTER' /
      Seat Front Centre
```

```
&OBST XB=21.1,24.5,0.825,1.275,1.4,1.5,RGB=0.0,0.0,1.0, SURF_ID='FRP_POLYESTER' /
      Seat Back Centre
&OBST XB=21.1,24.5,1.275,1.45,1.4,1.975,RGB=0.0,0.0,1.0, SURF_ID='FRP_POLYESTER' /
      Seat Back Centre

&OBST XB=26.8,30.2,-1.275,-0.825,1.4,1.5,RGB=0.0,0.0,1.0, SURF_ID='FRP_POLYESTER' /
      Seat Front Right1
&OBST XB=26.8,30.2,-1.45,-1.275,1.4,1.975,RGB=0.0,0.0,1.0, SURF_ID='FRP_POLYESTER' /
      Seat Front Right1
&OBST XB=26.8,30.2,0.825,1.275,1.4,1.5,RGB=0.0,0.0,1.0, SURF_ID='FRP_POLYESTER' /
      Seat Back Right1
&OBST XB=26.8,30.2,1.275,1.45,1.4,1.975,RGB=0.0,0.0,1.0, SURF_ID='FRP_POLYESTER' /
      Seat Back Right1
&OBST XB=32.25,33.25,-1.275,-0.825,1.4,1.5,RGB=0.0,0.0,1.0, SURF_ID='FRP_POLYESTER' /
      Seat Front Right2
&OBST XB=32.25,33.25,-1.45,-1.275,1.4,1.975,RGB=0.0,0.0,1.0, SURF_ID='FRP_POLYESTER' /
      Seat Front Right2
&OBST XB=32.25,33.25,0.825,1.275,1.4,1.5,RGB=0.0,0.0,1.0, SURF_ID='FRP_POLYESTER' /
      Seat Back Right2
&OBST XB=32.25,33.25,1.275,1.45,1.4,1.975,RGB=0.0,0.0,1.0, SURF_ID='FRP_POLYESTER' /
      Seat Back Right2

&OBST XB=15.4,18.8,-1.275,-0.825,1.4,1.5,RGB=0.0,0.0,1.0, SURF_ID='FRP_POLYESTER' /
      Seat Front Left1
&OBST XB=15.4,18.8,-1.45,-1.275,1.4,1.975,RGB=0.0,0.0,1.0, SURF_ID='FRP_POLYESTER' /
      Seat Front Left1
&OBST XB=15.4,18.8,0.825,1.275,1.4,1.5,RGB=0.0,0.0,1.0, SURF_ID='FRP_POLYESTER' /
      Seat Back Left1
&OBST XB=15.4,18.8,1.275,1.45,1.4,1.975,RGB=0.0,0.0,1.0, SURF_ID='FRP_POLYESTER' /
      Seat Back Left1
&OBST XB=12.35,13.35,-1.275,-0.825,1.4,1.5,RGB=0.0,0.0,1.0, SURF_ID='FRP_POLYESTER' /
      Seat Front Left2
&OBST XB=12.35,13.35,-1.45,-1.275,1.4,1.975,RGB=0.0,0.0,1.0, SURF_ID='FRP_POLYESTER' /
      Seat Front Left2
&OBST XB=12.35,13.35,0.825,1.275,1.4,1.5,RGB=0.0,0.0,1.0, SURF_ID='FRP_POLYESTER' /
      Seat Back Left2
&OBST XB=12.35,13.35,1.275,1.45,1.4,1.975,RGB=0.0,0.0,1.0, SURF_ID='FRP_POLYESTER' /
      Seat Back Left2

&OBST XB=28.65,30.2,1.527,1.55,2.5,3.025,RGB=1.0,1.0,1.0, SURF_ID=
'LAMINATED_SAFETY_GLASS', HEAT_REMOVE='det2a' / Window Back Right 1
&HEAT XYZ=29.425,1.477,2.5,RTI=100,ACTIVATION_TEMPERATURE=675.,LABEL='det2a'/
&OBST XB=28.65,30.2,1.527,1.55,1.975,2.5,RGB=1.0,1.0,1.0, SURF_ID=
'LAMINATED_SAFETY_GLASS', HEAT_REMOVE='det2b' / Window Back Right 1
&HEAT XYZ=29.425,1.477,2.025,RTI=100,ACTIVATION_TEMPERATURE=675.,LABEL='det2b'/
&OBST XB=26.8,28.35,-1.55,-1.527,2.5,3.025,RGB=1.0,1.0,1.0, SURF_ID=
'LAMINATED_SAFETY_GLASS' ,HEAT_REMOVE='det3a'/ Window Front Right 2
&HEAT XYZ=27.575,-1.477,2.5,RTI=100,ACTIVATION_TEMPERATURE=675.,LABEL='det3a'/
&OBST XB=26.8,28.35,-1.55,-1.527,1.975,2.5,RGB=1.0,1.0,1.0, SURF_ID=
'LAMINATED_SAFETY_GLASS' ,HEAT_REMOVE='det3b'/ Window Front Right 2
&HEAT XYZ=27.575,-.477,2.025,RTI=100,ACTIVATION_TEMPERATURE=675.,LABEL='det3b'/
&OBST XB=26.8,28.35,1.527,1.55,2.5,3.025,RGB=1.0,1.0,1.0, SURF_ID=
'LAMINATED_SAFETY_GLASS', HEAT_REMOVE='det4a'/ Window Back Right 2
&HEAT XYZ=27.575,1.477,2.5,RTI=100,ACTIVATION_TEMPERATURE=675.,LABEL='det4a'/
&OBST XB=26.8,28.35,1.527,1.55,1.975,2.5,RGB=1.0,1.0,1.0, SURF_ID=
'LAMINATED_SAFETY_GLASS', HEAT_REMOVE='det4b'/ Window Back Right 2
&HEAT XYZ=27.575,1.477,2.025,RTI=100,ACTIVATION_TEMPERATURE=675.,LABEL='det4b'/
&OBST XB=22.95,24.5,-1.55,-1.527,2.5,3.025,RGB=1.0,1.0,1.0, SURF_ID=
'LAMINATED_SAFETY_GLASS' ,HEAT_REMOVE='det5a'/ Window Front 3*Centre
&HEAT XYZ=23.725,-1.477,2.5,RTI=100,ACTIVATION_TEMPERATURE=675.,LABEL='det5a'/
```

```
&OBST XB=22.95,24.5,-1.55,-1.527,1.975,2.5,RGB=1.0,1.0,1.0, SURF_ID=
'LAMINATED_SAFETY_GLASS', HEAT_REMOVE='det5b'/ Window Front 3*Centre
&HEAT XYZ=23.725,-.477,2.025,RTI=100,ACTIVATION_TEMPERATURE=675.,LABEL='det5b'/
&OBST XB=22.95,24.5,1.527,1.55,2.5,3.025,RGB=1.0,1.0,1.0, SURF_ID=
'LAMINATED_SAFETY_GLASS', HEAT_REMOVE='det6a'/ Window Back 3**Centre
&HEAT XYZ=23.725,1.477,2.5,RTI=100,ACTIVATION_TEMPERATURE=675.,LABEL='det6a'/
&OBST XB=22.95,24.5,1.527,1.55,1.975,2.5,RGB=1.0,1.0,1.0, SURF_ID=
'LAMINATED_SAFETY_GLASS', HEAT_REMOVE='det6b'/ Window Back 3**Centre
&HEAT XYZ=23.725,1.477,2.025,RTI=100,ACTIVATION_TEMPERATURE=675.,LABEL='det6b'/
&OBST XB=21.1,22.65,-1.55,-1.527,2.5,3.025,RGB=1.0,1.0,1.0, SURF_ID=
'LAMINATED_SAFETY_GLASS', HEAT_REMOVE='det7a'/ Window Front 4**Centre
&HEAT XYZ=21.875,-1.477,2.5,RTI=100,ACTIVATION_TEMPERATURE=675.,LABEL='det7a'/
&OBST XB=21.1,22.65,-1.55,-1.527,1.975,2.5,RGB=1.0,1.0,1.0, SURF_ID=
'LAMINATED_SAFETY_GLASS', HEAT_REMOVE='det7b'/ Window Front 4**Centre
&HEAT XYZ=21.875,-.477,2.025,RTI=100,ACTIVATION_TEMPERATURE=675.,LABEL='det7b'/
&OBST XB=21.1,22.65,1.527,1.55,2.5,3.025,RGB=1.0,1.0,1.0, SURF_ID=
'LAMINATED_SAFETY_GLASS', HEAT_REMOVE='det8a' / Window Back 4**Centre
&HEAT XYZ=21.875,1.477,2.5,RTI=100,ACTIVATION_TEMPERATURE=675.,LABEL='det8a'/
&OBST XB=21.1,22.65,1.527,1.55,1.975,2.5,RGB=1.0,1.0,1.0, SURF_ID=
'LAMINATED_SAFETY_GLASS', HEAT_REMOVE='det8b' / Window Back 4**Centre
&HEAT XYZ=21.875,1.477,2.025,RTI=100,ACTIVATION_TEMPERATURE=675.,LABEL='det8b'/
&OBST XB=17.25,18.8,-1.55,-1.527,2.5,3.025,RGB=1.0,1.0,1.0, SURF_ID=
'LAMINATED_SAFETY_GLASS', HEAT_REMOVE='det9a'/ Window Front Left 5
&HEAT XYZ=18.025,-1.477,2.5,RTI=100,ACTIVATION_TEMPERATURE=675.,LABEL='det9a'/
&OBST XB=17.25,18.8,-1.55,-1.527,1.975,2.5,RGB=1.0,1.0,1.0, SURF_ID=
'LAMINATED_SAFETY_GLASS', HEAT_REMOVE='det9b'/ Window Front Left 5
&HEAT XYZ=18.025,-.477,2.025,RTI=100,ACTIVATION_TEMPERATURE=675.,LABEL='det9b'/
&OBST XB=17.25,18.8,1.527,1.55,2.5,3.025,RGB=1.0,1.0,1.0, SURF_ID=
'LAMINATED_SAFETY_GLASS', HEAT_REMOVE='det10a'/ Window Back Left 5
&HEAT XYZ=18.025,1.477,2.5,RTI=100,ACTIVATION_TEMPERATURE=675.,LABEL='det10a'/
&OBST XB=17.25,18.8,1.527,1.55,1.975,2.5,RGB=1.0,1.0,1.0, SURF_ID=
 'LAMINATED_SAFETY_GLASS', HEAT_REMOVE='det10b'/ Window Back Left 5
&HEAT XYZ=18.025,1.477,2.025,RTI=100,ACTIVATION_TEMPERATURE=675.,LABEL='det10b'/
&OBST XB=15.4,16.95,-1.55,-1.527,2.5,3.025,RGB=1.0,1.0,1.0, SURF_ID=
'LAMINATED_SAFETY_GLASS' ,HEAT_REMOVE='det11a'/ Window Front Left 6
&HEAT XYZ=16.175,-1.477,2.5,RTI=100,ACTIVATION_TEMPERATURE=675.,LABEL='det11a'/
&OBST XB=15.4,16.95,-1.55,-1.527,1.975,2.5,RGB=1.0,1.0,1.0, SURF_ID=
'LAMINATED_SAFETY_GLASS' ,HEAT_REMOVE='det11b'/ Window Front Left 6
&HEAT XYZ=16.175,-1.477,2.025,RTI=100,ACTIVATION_TEMPERATURE=675.,LABEL='det11b'/
&OBST XB=15.4,16.95,1.527,1.55,2.5,3.025,RGB=1.0,1.0,1.0, SURF_ID=
 'LAMINATED_SAFETY_GLASS', HEAT_REMOVE='det12a'/ Window Back Left 6
&HEAT XYZ=16.175,1.477,2.5,RTI=100,ACTIVATION_TEMPERATURE=675.,LABEL='det12a'/
&OBST XB=15.4,16.95,1.527,1.55,1.975,2.5,RGB=1.0,1.0,1.0, SURF_ID=
'LAMINATED_SAFETY_GLASS', HEAT_REMOVE='det12b'/ Window Back Left 6
&HEAT XYZ=16.175,1.477,2.025,RTI=100,ACTIVATION_TEMPERATURE=675.,LABEL='det12b'/

&OBST XB=21.1,24.5,-1.45,-0.975,1.1,1.4,RGB=0.8,1,0.8, SURF_ID='FRP_POLYESTER' /
        Underseat Boxes Front Centre
&OBST XB=21.1,24.5,0.975,1.45,1.1,1.4,RGB=0.8,1,0.8, SURF_ID='FRP_POLYESTER' /
        Underseat Boxes Back Centre
&OBST XB=26.8,30.2,-1.45,-0.975,1.1,1.4,RGB=0.8,1,0.8, SURF_ID='FRP_POLYESTER' /
        Underseat Boxes Front Centre1
&OBST XB=32.25,33.25,-1.45,-0.975,1.1,1.4,RGB=0.8,1,0.8, SURF_ID='FRP_POLYESTER' /
        Underseat Boxes Front Left
&OBST XB=32.25,33.25,0.975,1.45,1.1,1.4,RGB=0.8,1,0.8, SURF_ID='FRP_POLYESTER' /
        Underseat Boxes Back Left
&OBST XB=12.35,13.35,-1.45,-0.975,1.1,1.4,RGB=0.8,1,0.8, SURF_ID='FRP_POLYESTER' /
        Underseat Boxes Front Right
&OBST XB=12.35,13.35,0.975,1.45,1.1,1.4,RGB=0.8,1,0.8, SURF_ID='FRP_POLYESTER' /
        Underseat Boxes Back Right
```

```
&OBST XB=22.65,22.95,-1.55,-1.45,1.975,3.025,RGB=0.3,1,0.7, SURF_ID= 'WALL_CONSTRUCTION'/
      Wall Front Centre
&OBST XB=21.1,24.5,-1.55,-1.45,1.1,1.975,RGB=0.3,1,0.7, SURF_ID='WALL_CONSTRUCTION' /
      Wall Front Centre
&OBST XB=24.5,24.9,-1.55,-1.45,1.1,3.025,RGB=0.3,1,0.7, SURF_ID='WALL_CONSTRUCTION' /
      Wall Front Centre
&OBST XB=20.7,21.1,-1.55,-1.45,1.1,3.025,RGB=0.3,1,0.7, SURF_ID='WALL_CONSTRUCTION' /
      Wall Front Centre
&OBST XB=22.65,22.95,1.45,1.55,1.975,3.025,RGB=0.3,1,0.7, SURF_ID= 'WALL_CONSTRUCTION' /
      Wall Back Centre
&OBST XB=21.1,24.5,1.45,1.55,1.1,1.975,RGB=0.3,1,0.7, SURF_ID='WALL_CONSTRUCTION' /
      Wall Back Centre
&OBST XB=24.5,24.9,1.5,1.55,1.1,3.025,RGB=0.3,1,0.7, SURF_ID='WALL_CONSTRUCTION' /
      Wall Back centre
&OBST XB=20.7,21.1,1.45,1.55,1.1,3.025,RGB=0.3,1,0.7, SURF_ID='WALL_CONSTRUCTION' /
      Wall Back Centre

&OBST XB=24.5,24.9,1.45,1.5,1.1,3.025,RGB=0.3,0.7,0.7, SURF_ID='FRP_POLYESTER' / PEC

&OBST XB=28.35,28.65,-1.55,-1.45,1.975,3.025,RGB=0.3,1,0.7, SURF_ID= 'WALL_CONSTRUCTION'/
      Wall Front Right1
&OBST XB=26.8,30.2,-1.55,-1.45,1.1,1.975,RGB=0.3,1,0.7, SURF_ID='WALL_CONSTRUCTION' /
      Wall Front Right1
&OBST XB=30.2,30.6,-1.55,-1.5,1.1,3.025,RGB=0.3,1,0.7, SURF_ID='WALL_CONSTRUCTION' /
      Wall Front Right1
&OBST XB=26.4,26.8,-1.55,-1.45,1.1,3.025,RGB=0.3,1,0.7, SURF_ID='WALL_CONSTRUCTION' /
      Wall Front Right1
&OBST XB=28.35,28.65,1.45,1.55,1.975,3.025,RGB=0.3,1,0.7, SURF_ID= 'WALL_CONSTRUCTION' /
      Wall Back Right1
&OBST XB=26.8,30.2,1.45,1.55,1.1,1.975,RGB=0.3,1,0.7, SURF_ID='WALL_CONSTRUCTION' /
      Wall Back Right1
&OBST XB=30.2,30.6,1.45,1.55,1.1,3.025,RGB=0.3,1,0.7, SURF_ID='WALL_CONSTRUCTION' /
      Wall Back Right1
&OBST XB=26.4,26.8,1.45,1.55,1.1,3.025,RGB=0.3,1,0.7, SURF_ID='WALL_CONSTRUCTION' /
      Wall Back Right1

&OBST XB=30.2,30.6,-1.5,-1.45,1.1,3.025,RGB=0.3,0.7,0.7, SURF_ID='FRP_POLYESTER' / PEC

&OBST XB=16.95,17.25,-1.55,-1.45,1.975,3.025,RGB=0.3,1,0.7, SURF_ID= 'WALL_CONSTRUCTION'/
      Wall Front Left1
&OBST XB=15.4,18.8,-1.55,-1.45,1.1,1.975,RGB=0.3,1,0.7, SURF_ID='WALL_CONSTRUCTION' /
      Wall Front Left1
&OBST XB=15.0,15.4,-1.55,-1.45,1.1,3.025,RGB=0.3,1,0.7, SURF_ID='WALL_CONSTRUCTION' /
      Wall Front Left1
&OBST XB=18.8,19.2,-1.55,-1.5,1.1,3.025,RGB=0.3,1,0.7, SURF_ID='WALL_CONSTRUCTION' /
      Wall Back Left1
&OBST XB=16.95,17.25,1.45,1.55,1.975,3.025,RGB=0.3,1,0.7, SURF_ID= 'WALL_CONSTRUCTION' /
      Wall Back Left1
&OBST XB=15.4,18.8,1.45,1.55,1.1,1.975,RGB=0.3,1,0.7, SURF_ID='WALL_CONSTRUCTION' /
      Wall Back Left1
&OBST XB=15.0,15.4,1.5,1.55,1.1,3.025,RGB=0.3,1,0.7, SURF_ID='WALL_CONSTRUCTION' /
      Wall Back Left1
&OBST XB=18.8,19.2,1.45,1.55,1.1,3.025,RGB=0.3,1,0.7, SURF_ID='WALL_CONSTRUCTION' /
      Wall Back Left1

&OBST XB=18.8,19.2,-1.5,-1.45,1.1,3.025,RGB=0.3,0.7,0.7, SURF_ID='FRP_POLYESTER' / PEC
&OBST XB=15.0,15.4,1.45,1.5,1.1,3.025,RGB=0.3,0.7,0.7, SURF_ID='FRP_POLYESTER' / PEC

&OBST XB=32.25,33.25,-1.55,-1.45,1.1,3.025,RGB=0.3,1,0.7, SURF_ID= 'WALL_CONSTRUCTION' /
      Wall Front Left2
```

```
&OBST XB=32.25,33.25,1.45,1.55,1.1,3.025,RGB=0.3,1,0.7, SURF_ID='WALL_CONSTRUCTION' /
      Wall Back Left2
&OBST XB=32.1,32.25,-1.55,-1.45,1.1,3.025,RGB=0.3,1,0.7, SURF_ID='WALL_CONSTRUCTION' /
      Wall Front Left2
&OBST XB=32.1,32.25,1.45,1.55,1.1,3.025,RGB=0.3,1,0.7, SURF_ID='WALL_CONSTRUCTION' /
      Wall Back Left2
&OBST XB=12.0,12.15,-1.55,-1.45,1.1,3.025,RGB=0.3,1,0.7, SURF_ID='WALL_CONSTRUCTION' /
      Wall Front Left2
&OBST XB=12.15,12.25,-1.55,-1.45,1.1,3.025,RGB=0.3,1,.7, SURF_ID= 'WALL_CONSTRUCTION',
SAWTOOTH=.FALSE / Wall Front Left2
&OBST XB=12.25,12.35,-1.55,-1.45,1.1,3.025,RGB=0.3,1,.7, SURF_ID= ‘WALL_CONSTRUCTION',
SAWTOOTH=.FALSE / Wall Front Left2
&OBST XB=12.0,12.15,1.45,1.55,1.1,3.025,RGB=0.3,1,0.7, SURF_ID='WALL_CONSTRUCTION' /
      Wall Back Left2
&OBST XB=12.15,12.25,1.45,1.55,1.1,3.025,RGB=0.3,1,0.7, SURF_ID= 'WALL_CONSTRUCTION',
SAWTOOTH=.FALSE / Wall Back Left2
&OBST XB=12.25,12.35,1.45,1.55,1.1,3.025,RGB=0.3,1,0.7, SURF_ID= 'WALL_CONSTRUCTION',
SAWTOOTH=.FALSE / Wall Back Left2
&OBST XB=12.35,13.35,-1.55,-1.45,1.1,3.025,RGB=0.3,1,0.7, SURF_ID= 'WALL_CONSTRUCTION' /
      Wall Front Left2
&OBST XB=12.35,13.35,1.45,1.55,1.1,3.025,RGB=0.3,1,0.7, SURF_ID='WALL_CONSTRUCTION' /
      Wall Back Left2
&OBST XB=13.35,13.5,-1.55,-1.45,1.1,3.025,RGB=0.3,1,0.7, SURF_ID='WALL_CONSTRUCTION' /
      Wall Front Left2
&OBST XB=13.35,13.5,1.45,1.55,1.1,3.025,RGB=0.3,1,0.7, SURF_ID='WALL_CONSTRUCTION' /
      Wall Back Left2

&OBST XB=12.0,12.15,-1.45,-0.7,1.1,3.025,RGB=0.3,0.7,0.7, SURF_ID='FRP_POLYESTER' /
      Equipped Cubicle Front Left
&OBST XB=12.15,12.25,-1.45,-0.75,1.1,3.025,RGB=0.3,0.7,.7, SURF_ID= 'FRP_POLYESTER',
SAWTOOTH=.FALSE /  Equipped Cubicle Front Left
&OBST XB=12.25,12.35,-1.45,-0.9,1.1,3.025,RGB=0.3,0.7,.7, SURF_ID= 'FRP_POLYESTER',
SAWTOOTH=.FALSE /  Equipped Cubicle Front Left
&OBST XB=12.0,12.15,0.7,1.45,1.1,3.025,RGB=0.3,0.7,0.7, SURF_ID='FRP_POLYESTER' /
      Equipped Cubicle Back Left
&OBST XB=12.15,12.25,0.75,1.45,1.1,3.025,RGB=0.3,0.7,0.7, SURF_ID= 'FRP_POLYESTER',
SAWTOOTH=.FALSE / Equipped Cubicle Back Left
&OBST XB=12.25,12.35,0.9,1.45,1.1,3.025,RGB=0.3,0.7,0.7, SURF_ID= 'FRP_POLYESTER',
SAWTOOTH=.FALSE /  Equipped Cubicle Back Left

&OBST XB=32.0375,32.1,1.515,1.55,1.975,3.025,RGB=0.0,0.8,0.0, SURF_ID=
'SIDEDOOR_CONSTRUCTION' / Passenger Door Back C1
&OBST XB=31.1625,31.5375,1.515,1.55,1.975,3.025,RGB=0.0,0.8,0.0, SURF_ID=
'SIDEDOOR_CONSTRUCTION' / Passenger Door Back C1
&OBST XB=30.6,30.6625,1.515,1.55,1.975,3.025,RGB=0.0,0.8,0.0, SURF_ID=
'SIDEDOOR_CONSTRUCTION' / Passenger Door Back C1
&OBST XB=30.6,32.1,1.515,1.55,1.1,1.975,RGB=0.0,0.8,0.0, SURF_ID=
'SIDEDOOR_CONSTRUCTION' / Passenger Door Back C1

&OBST XB=26.3375,26.4,-1.55,-1.515,1.975,3.025,RGB=0.0,0.8,0.0, SURF_ID=
'SIDEDOOR_CONSTRUCTION' / Passenger Door Front C2
&OBST XB=25.4625,25.8375,-1.55,-1.515,1.975,3.025,RGB=0.0,0.8,0.0, SURF_ID=
'SIDEDOOR_CONSTRUCTION' / Passenger Door Front C2
&OBST XB=24.9,24.9625,-1.55,-1.515,1.975,3.025,RGB=0.0,0.8,0.0, SURF_ID=
'SIDEDOOR_CONSTRUCTION' / Passenger Door Front C2
&OBST XB=24.9,26.4,-1.55,-1.515,1.1,1.975,RGB=0.0,0.8,0.0, SURF_ID=
'SIDEDOOR_CONSTRUCTION' / Passenger Door Front C2
&OBST XB=26.3375,26.4,1.515,1.55,1.975,3.025,RGB=0.0,0.8,0.0, SURF_ID=
'SIDEDOOR_CONSTRUCTION' / Passenger Door Back C2
&OBST XB=25.4625,25.8375,1.515,1.55,1.975,3.025,RGB=0.0,0.8,0.0, SURF_ID=
'SIDEDOOR_CONSTRUCTION' / Passenger Door Back C2
```

```
&OBST XB=24.9,24.9625,1.515,1.55,1.975,3.025,RGB=0.0,0.8,0.0, SURF_ID=
'SIDEDOOR_CONSTRUCTION' / Passenger Door Back C2
&OBST XB=24.9,26.4,1.515,1.55,1.1,1.975,RGB=0.0,0.8,0.0, SURF_ID=
'SIDEDOOR_CONSTRUCTION' / Passenger Door Back C2

&OBST XB=19.2,19.2625,-1.55,-1.515,1.975,3.025,RGB=0.0,0.8,0.0, SURF_ID=
'SIDEDOOR_CONSTRUCTION' / Passenger Door Front C3
&OBST XB=19.7625,20.1375,-1.55,-1.515,1.975,3.025,RGB=0.0,0.8,0.0, SURF_ID=
'SIDEDOOR_CONSTRUCTION' / Passenger Door Front C3
&OBST XB=20.6375,20.7,-1.55,-1.515,1.975,3.025,RGB=0.0,0.8,0.0, SURF_ID=
'SIDEDOOR_CONSTRUCTION' / Passenger Door Front C3
&OBST XB=19.2,20.7,-1.55,-1.515,1.1,1.975,RGB=0.0,0.8,0.0, SURF_ID=
'SIDEDOOR_CONSTRUCTION' / Passenger Door Front C3
&OBST XB=19.2,19.2625,1.515,1.55,1.975,3.025,RGB=0.0,0.8,0.0, SURF_ID=
'SIDEDOOR_CONSTRUCTION' / Passenger Door Back C3
&OBST XB=19.7625,20.1375,1.515,1.55,1.975,3.025,RGB=0.0,0.8,0.0, SURF_ID=
'SIDEDOOR_CONSTRUCTION' / Passenger Door Back C3
&OBST XB=20.6375,20.7,1.515,1.55,1.975,3.025,RGB=0.0,0.8,0.0, SURF_ID=
'SIDEDOOR_CONSTRUCTION' / Passenger Door Back C3
&OBST XB=19.2,20.7,1.515,1.55,1.1,1.975,RGB=0.0,0.8,0.0, SURF_ID=
'SIDEDOOR_CONSTRUCTION' / Passenger Door Back C3

&OBST XB=13.5,13.5625,1.515,1.55,1.975,3.025,RGB=0.0,0.8,0.0, SURF_ID=
'SIDEDOOR_CONSTRUCTION' / Passenger Door Back C4
&OBST XB=14.0625,14.4375,1.515,1.55,1.975,3.025,RGB=0.0,0.8,0.0, SURF_ID=
'SIDEDOOR_CONSTRUCTION' / Passenger Door Back C4
&OBST XB=14.9375,15.0,1.515,1.55,1.975,3.025,RGB=0.0,0.8,0.0, SURF_ID=
'SIDEDOOR_CONSTRUCTION' / Passenger Door Back C4
&OBST XB=13.5,15.0,1.515,1.55,1.1,1.975,RGB=0.0,0.8,0.0, SURF_ID=
'SIDEDOOR_CONSTRUCTION' / Passenger Door Back C4

&OBST XB=31.5375,32.0375,1.527,1.55,2.5,3.025,RGB=1.0,1.0,1.0, SURF_ID=
'LAMINATED_SAFETY_GLASS', HEAT_REMOVE='det22a'/ Passenger Door Window Back Left 1a
&HEAT XYZ=31.7825,1.477,2.5,RTI=100,ACTIVATION_TEMPERATURE=675.,LABEL='det22a'/
&OBST XB=31.5375,32.0375,1.527,1.55,1.975,2.5,RGB=1.0,1.0,1.0, SURF_ID=
'LAMINATED_SAFETY_GLASS', HEAT_REMOVE='det22b'/ Passenger Door Window Back Left 1a
&HEAT XYZ=31.7825,1.477,2.025,RTI=100,ACTIVATION_TEMPERATURE=675.,LABEL='det22b'/
&OBST XB=30.6675,31.1675,1.527,1.55,2.5,3.025,RGB=1.0,1.0,1.0, SURF_ID=
 'LAMINATED_SAFETY_GLASS', HEAT_REMOVE='det24a'/ Passenger Door Window Back Left 1b
&HEAT XYZ=30.9175,1.477,2.5,RTI=100,ACTIVATION_TEMPERATURE=675.,LABEL='det24a'/
&OBST XB=30.6675,31.1675,1.527,1.55,1.975,2.5,RGB=1.0,1.0,1.0, SURF_ID=
'LAMINATED_SAFETY_GLASS', HEAT_REMOVE='det24b'/ Passenger Door Window Back Left 1b
&HEAT XYZ=30.9175,1.477,2.025,RTI=100,ACTIVATION_TEMPERATURE=675.,LABEL='det24b'/
&OBST XB=25.8375,26.3375,-1.55,-1.527,2.5,3.025,RGB=1.0,1.0,1.0, SURF_ID=
 'LAMINATED_SAFETY_GLASS',HEAT_REMOVE='det25a' / Passenger Door Window Front Left 2a
&HEAT XYZ=26.0875,-1.477,2.5,RTI=100,ACTIVATION_TEMPERATURE=675.,LABEL='det25a'/
&OBST XB=25.8375,26.3375,-1.55,-1.527,1.975,2.5,RGB=1.0,1.0,1.0, SURF_ID=
 'LAMINATED_SAFETY_GLASS',HEAT_REMOVE='det25b' / Passenger Door Window Front Left 2a
&HEAT XYZ=26.0875,-1.477,2.025,RTI=100,ACTIVATION_TEMPERATURE=675.,LABEL='det25b'/
&OBST XB=25.8375,26.3375,1.527,1.55,2.5,3.025,RGB=1.0,1.0,1.0, SURF_ID=
 'LAMINATED_SAFETY_GLASS', HEAT_REMOVE='det26a' / Passenger Door Window Back Left 2a
&HEAT XYZ=26.0875,1.477,2.5,RTI=100,ACTIVATION_TEMPERATURE=675.,LABEL='det26a'/
&OBST XB=25.8375,26.3375,1.527,1.55,1.975,2.5,RGB=1.0,1.0,1.0, SURF_ID=
'LAMINATED_SAFETY_GLASS', HEAT_REMOVE='det26b' / Passenger Door Window Back Left 2a
&HEAT XYZ=26.0875,1.477,2.025,RTI=100,ACTIVATION_TEMPERATURE=675.,LABEL='det26b'/
&OBST XB=24.9625,25.4625,-1.55,-1.527,2.5,3.025,RGB=1.0,1.0,1.0, SURF_ID=
'LAMINATED_SAFETY_GLASS' ,HEAT_REMOVE='det27a'/ Passenger Door Window Front Left 2b
&HEAT XYZ=25.2125,-1.477,2.5,RTI=100,ACTIVATION_TEMPERATURE=675.,LABEL='det27a'/
&OBST XB=24.9625,25.4625,-1.55,-1.527,1.975,2.5,RGB=1.0,1.0,1.0, SURF_ID=
'LAMINATED_SAFETY_GLASS' ,HEAT_REMOVE='det27b'/ Passenger Door Window Front Left 2b
&HEAT XYZ=25.2125,-1.477,2.025,RTI=100,ACTIVATION_TEMPERATURE=675.,LABEL='det27b'/
&OBST XB=24.9625,25.4625,1.527,1.55,2.5,3.025,RGB=1.0,1.0,1.0, SURF_ID=
```

```
 'LAMINATED_SAFETY_GLASS', HEAT_REMOVE='det28a'/ Passenger Door Window Back Left 2b
&HEAT XYZ=25.2125,1.477,2.5,RTI=100,ACTIVATION_TEMPERATURE=675.,LABEL='det28a'/
&OBST XB=24.9625,25.4625,1.527,1.55,1.975,2.5,RGB=1.0,1.0,1.0, SURF_ID=
'LAMINATED_SAFETY_GLASS', HEAT_REMOVE='det28b'/ Passenger Door Window Back Left 2b
&HEAT XYZ=25.2125,1.477,2.025,RTI=100,ACTIVATION_TEMPERATURE=675.,LABEL='det28b'/
&OBST XB=20.1375,20.6375,-1.55,-1.527,2.5,3.025,RGB=1.0,1.0,1.0, SURF_ID=
 'LAMINATED_SAFETY_GLASS' ,HEAT_REMOVE='det29a'/ Passenger Door Window Front Right 3a
&HEAT XYZ=20.3875,-1.477,2.5,RTI=100,ACTIVATION_TEMPERATURE=675.,LABEL='det29a'/
&OBST XB=20.1375,20.6375,-1.55,-1.527,1.975,2.5,RGB=1.0,1.0,1.0, SURF_ID=
 'LAMINATED_SAFETY_GLASS' ,HEAT_REMOVE='det29b'/ Passenger Door Window Front Right 3a
&HEAT XYZ=20.3875,-1.477,2.025,RTI=100,ACTIVATION_TEMPERATURE=675.,LABEL='det29b'/
&OBST XB=20.1375,20.6375,1.527,1.55,2.5,3.025,RGB=1.0,1.0,1.0, SURF_ID=
'LAMINATED_SAFETY_GLASS', HEAT_REMOVE='det30a'/ Passenger Door Window Back Right 3a
&HEAT XYZ=20.3875,1.477,2.5,RTI=100,ACTIVATION_TEMPERATURE=675.,LABEL='det30a'/
&OBST XB=20.1375,20.6375,1.527,1.55,1.975,2.5,RGB=1.0,1.0,1.0, SURF_ID=
'LAMINATED_SAFETY_GLASS', HEAT_REMOVE='det30b'/ Passenger Door Window Back Right 3a
&HEAT XYZ=20.3875,1.477,2.025,RTI=100,ACTIVATION_TEMPERATURE=675.,LABEL='det30b'/
&OBST XB=19.2625,19.7625,-1.55,-1.527,2.5,3.025,RGB=1.0,1.0,1.0, SURF_ID=
'LAMINATED_SAFETY_GLASS' ,HEAT_REMOVE='det31a'/ Passenger Door Window Front Right 3b
&HEAT XYZ=19.5125,-1.477,2.5,RTI=100,ACTIVATION_TEMPERATURE=675.,LABEL='det31a'/
&OBST XB=19.2625,19.7625,-1.55,-1.527,1.975,2.5,RGB=1.0,1.0,1.0, SURF_ID=
 'LAMINATED_SAFETY_GLASS' ,HEAT_REMOVE='det31b'/ Passenger Door Window Front Right 3b
&HEAT XYZ=19.5125,-1.477,2.025,RTI=100,ACTIVATION_TEMPERATURE=675.,LABEL='det31b'/
&OBST XB=19.2625,19.7625,1.527,1.55,2.5,3.025,RGB=1.0,1.0,1.0, SURF_ID=
'LAMINATED_SAFETY_GLASS', HEAT_REMOVE='det32a'/ Passenger Door Window Back Right 3b
&HEAT XYZ=19.5125,1.477,2.5,RTI=100,ACTIVATION_TEMPERATURE=675.,LABEL='det32a'/
&OBST XB=19.2625,19.7625,1.527,1.55,1.975,2.5,RGB=1.0,1.0,1.0, SURF_ID=
 'LAMINATED_SAFETY_GLASS', HEAT_REMOVE='det32b'/ Passenger Door Window Back Right 3b
&HEAT XYZ=19.5125,1.477,2.025,RTI=100,ACTIVATION_TEMPERATURE=675.,LABEL='det32b'/
&OBST XB=14.4375,14.9375,1.527,1.55,2.5,3.025,RGB=1.0,1.0,1.0, SURF_ID=
'LAMINATED_SAFETY_GLASS', HEAT_REMOVE='det34a'/ Passenger Door Window Back Right 4a
&HEAT XYZ=14.6875,1.477,2.5,RTI=100,ACTIVATION_TEMPERATURE=675.,LABEL='det34a'/
&OBST XB=14.4375,14.9375,1.527,1.55,1.975,2.5,RGB=1.0,1.0,1.0, SURF_ID=
'LAMINATED_SAFETY_GLASS', HEAT_REMOVE='det34b'/ Passenger Door Window Back Right 4a
&HEAT XYZ=14.6875,1.477,2.025,RTI=100,ACTIVATION_TEMPERATURE=675.,LABEL='det34b'/
&OBST XB=13.5625,14.0625,1.527,1.55,2.5,3.025,RGB=1.0,1.0,1.0, SURF_ID=
'LAMINATED_SAFETY_GLASS', HEAT_REMOVE='det36a'/ Passenger Door Window Back Right 4b
&HEAT XYZ=13.8125,1.477,2.5,RTI=100,ACTIVATION_TEMPERATURE=675.,LABEL='det36a'/
&OBST XB=13.5625,14.0625,1.527,1.55,1.975,2.5,RGB=1.0,1.0,1.0, SURF_ID=
'LAMINATED_SAFETY_GLASS', HEAT_REMOVE='det36b'/ Passenger Door Window Back Right 4b
&HEAT XYZ=13.8125,1.477,2.025,RTI=100,ACTIVATION_TEMPERATURE=675.,LABEL='det36b'/

&OBST XB=11.4,12.0,-1.55,-0.7,1.1,3.025,RGB=0.8,0.6,0.4, SURF_ID='WALL_CONSTRUCTION' /
      Gangway Wall Front Left
&OBST XB=11.4,12.0,0.7,1.55,1.1,3.025,RGB=0.8,0.6,0.4, SURF_ID='WALL_CONSTRUCTION' /
      Gangway Wall Back Left
&OBST XB=33.25,34.55,-1.55,-1.45,1.1,3.025,RGB=0.3,0.7,0.7, SURF_ID='FRP_POLYESTER' /
      Face Panel at End Mask
&OBST XB=33.25,34.55,1.45,1.55,1.1,3.025,RGB=0.3,0.7,0.7, SURF_ID='FRP_POLYESTER' /
      Face Panel at End Mask
&OBST XB=34.45,34.55,-1.55,-0.7,1.1,2.0,RGB=0.3,0.7,0.7, SURF_ID='FRP_POLYESTER' /
      Face Panel at End Mask
&OBST XB=34.45,34.55,0.7,1.55,1.1,2.0,RGB=0.3,0.7,0.7, SURF_ID='FRP_POLYESTER' /
      Face Panel at End Mask
&OBST XB=34.45,34.55,-1.45,-1.25,2.,3.025,RGB=0.3,0.7,0.7, SURF_ID='FRP_POLYESTER' /
      Face Panel at End Mask
&OBST XB=34.45,34.55,1.25,1.45,2.,3.025,RGB=0.3,0.7,0.7, SURF_ID='FRP_POLYESTER' /
      Face Panel at End Mask
&OBST XB=34.45,34.55,-1.45,-0.8,2.95,3.025,RGB=0.3,0.7,0.7, SURF_ID='FRP_POLYESTER' /
      Face Panel at End Mask
&OBST XB=34.45,34.55,0.8,1.45,2.95,3.025,RGB=0.3,0.7,0.7, SURF_ID='FRP_POLYESTER' /
      Face Panel at End Mask
```

```
&OBST XB=34.45,34.55,-0.8,-0.7,1.7,3.025,RGB=0.3,0.7,0.7, SURF_ID='FRP_POLYESTER' /
      Face Panel at End Mask
&OBST XB=34.45,34.55,0.7,0.8,1.7,3.025,RGB=0.3,0.7,0.7, SURF_ID='FRP_POLYESTER' /
      Face Panel at End Mask
&OBST XB=34.45,34.55,-0.9,-0.7,3.025,3.2,RGB=0.3,0.7,0.7, SURF_ID='FRP_POLYESTER' /
      Face Panel at End Mask
&OBST XB=34.45,34.55,0.7,0.9,3.025,3.2,RGB=0.3,0.7,0.7, SURF_ID='FRP_POLYESTER' /
      Face Panel at End Mask
&OBST XB=34.45,34.55,-0.7,0.7,3.1,3.2,RGB=0.3,0.7,0.7, SURF_ID='FRP_POLYESTER' /
      Face Panel at End Mask

&OBST XB=34.527,34.55,-1.25,-0.8,2.475,2.95,RGB=1.0,1.0,1.0, SURF_ID=
'LAMINATED_SAFETY_GLASS',HEAT_REMOVE='det51a' / Window at End Mask
&HEAT XYZ=34.477,-1.025,2.475,RTI=100,ACTIVATION_TEMPERATURE=675.,LABEL='det51a'/
&OBST XB=34.527,34.55,-1.25,-0.8,2.,2.475,RGB=1.0,1.0,1.0, SURF_ID=
 'LAMINATED_SAFETY_GLASS',HEAT_REMOVE='det51b' / Window at End Mask
&HEAT XYZ=34.477,-1.025,2.05,RTI=100,ACTIVATION_TEMPERATURE=675.,LABEL='det51b'/
&OBST XB=34.527,34.55,0.8,1.25,2.475,2.95,RGB=1.0,1.0,1.0, SURF_ID=
 'LAMINATED_SAFETY_GLASS', HEAT_REMOVE='det52a' / Window at End Mask
&HEAT XYZ=34.477,1.025,2.475,RTI=100,ACTIVATION_TEMPERATURE=675.,LABEL='det52a'/
&OBST XB=34.527,34.55,0.8,1.25,2.,2.475,RGB=1.0,1.0,1.0, SURF_ID=
'LAMINATED_SAFETY_GLASS',HEAT_REMOVE='det52b' / Window at End Mask
&HEAT XYZ=34.477,1.025,2.05,RTI=100,ACTIVATION_TEMPERATURE=675.,LABEL='det52b'/

&OBST XB=33.65,34.45,-1.45,-0.75,1.1,2.2,RGB=0.8,0.4,0.4, SURF_ID='FRP_POLYESTER' /
      Driver Console Assembly
&OBST XB=34.25,34.45,0.75,1.45,1.1,2.2,RGB=0.8,0.4,0.4, SURF_ID='FRP_POLYESTER' /
      Driver Console Assembly
```

Output from FDS

```
.............................
&BNDF QUANTITY='GAUGE_HEAT_FLUX', DTSAM=1. / Data written to file every 1 s
&BNDF QUANTITY='WALL_TEMPERATURE', DTSAM=1./ Data written to file every 1 s
&BNDF QUANTITY='BURNING_RATE', DTSAM=1. / Data written to file every 1 s
&ISOF QUANTITY='MIXTURE_FRACTION', VALUE(1)=0.114,VALUE(2)=0.001, DTSAM=2./
      Data written to file every 2 s
&SLCF PBX=22.8, QUANTITY='TEMPERATURE', DTSAM=2./ Data written to file every 2 s
&SLCF PBY=0., QUANTITY='TEMPERATURE', DTSAM=2./ Data written to file every 2 s
&SLCF PBZ=2.6, QUANTITY='TEMPERATURE', DTSAM=2. / Data written to file every 2 s

&THCP XYZ=17.1,0.,2.1,QUANTITY='TEMPERATURE',LABEL='MC_car_FO_TempL1' /
&THCP XYZ=17.1,0.,2.4,QUANTITY='TEMPERATURE',LABEL='MC_car_FO_TempL2' /
&THCP XYZ=17.1,0.,2.7,QUANTITY='TEMPERATURE',LABEL='MC_car_FO_TempL3' /
&THCP XYZ=17.1,0.,3.0,QUANTITY='TEMPERATURE',LABEL='MC_car_FO_TempL4' /

&THCP XYZ=22.8,0.,2.1,QUANTITY='TEMPERATURE',LABEL='MC_car_FO_TempC1' /
&THCP XYZ=22.8,0.,2.4,QUANTITY='TEMPERATURE',LABEL='MC_car_FO_TempC2' /
&THCP XYZ=22.8,0.,2.7,QUANTITY='TEMPERATURE',LABEL='MC_car_FO_TempC3' /
&THCP XYZ=22.8,0.,3.0,QUANTITY='TEMPERATURE',LABEL='MC_car_FO_TempC4' /

&THCP XYZ=28.5,0.,2.1,QUANTITY='TEMPERATURE',LABEL='MC_car_FO_TempR1' /
&THCP XYZ=28.5,0.,2.4,QUANTITY='TEMPERATURE',LABEL='MC_car_FO_TempR2' /
&THCP XYZ=28.5,0.,2.7,QUANTITY='TEMPERATURE',LABEL='MC_car_FO_TempR3' /
&THCP XYZ=28.5,0.,3.0,QUANTITY='TEMPERATURE',LABEL='MC_car_FO_TempR4' /

&THCP XYZ=17.1,0.,1.1,QUANTITY='GAUGE_HEAT_FLUX',IOR=3,
LABEL='MC_car_FO_Heat_FluxLeft' /
&THCP XYZ=22.8,0.,1.1,QUANTITY='GAUGE_HEAT_FLUX',IOR=3,
LABEL='MC_car_FO_Heat_FluxCentre' /
&THCP XYZ=28.5,0.,1.1,QUANTITY='GAUGE_HEAT_FLUX',IOR=3,
```

```
LABEL='MC_car_FO_Heat_FluxRight' /

&THCP XB=9.4,9.4,-3.1,2.4,0.0,4.4,QUANTITY='VOLUME FLOW',LABEL='Left_VOLUME' /
&THCP XB=36.0,36.0,-3.1,2.4,0.0,4.4,QUANTITY='VOLUME FLOW',LABEL='Right_VOLUME' /
&THCP XB=9.4,9.4,-3.1,2.4,0.0,4.4,QUANTITY='HRR',LABEL='Left_HRR' /
&THCP XB=36.0,36.0,-3.1,2.4,0.0,4.4,QUANTITY='HRR',LABEL='Right_HRR' /

&THCP XB=11.4,11.4,-0.7,0.7,1.1,3.1,QUANTITY='VOLUME
FLOW',LABEL='DD_Left_VOLUME' /
&THCP XB=34.55,34.55,-0.7,0.7,1.1,3.1,QUANTITY='VOLUME
FLOW',LABEL='DD_Right_VOLUME' /
&THCP XB=11.4,11.4,-0.7,0.7,1.1,3.1,QUANTITY='HRR',LABEL='DD_Left_HRR' /
&THCP XB=34.55,34.55,-0.7,0.7,1.1,3.1,QUANTITY='HRR',LABEL='DD_Right_HRR' /

&THCP XB=30.6,32.1,-1.55,-1.55,1.1,3.025,QUANTITY='VOLUME
FLOW',LABEL='1stSide_door_VOLUME' /
&THCP XB=13.5,15.0,-1.55,-1.55,1.1,3.025,QUANTITY='VOLUME
FLOW',LABEL='4thSide_door_VOLUME' /
&THCP XB=30.6,32.1,-1.55,-1.55,1.1,3.025,QUANTITY='HRR',LABEL='1stSide_door_HRR' /
&THCP XB=13.5,15.0,-1.55,-1.55,1.1,3.025,QUANTITY='HRR',LABEL='4thSide_door_HRR' /
```

Appendix G: Cone Calorimeter test data

This Appendix contains data sheets; and HRRPUA and mass loss rate curves for the specimens tested in the Cone Calorimeter for this study. However, note that for tests whereby not ignition occurred, no graphs are presented.

Component:	Train car seat	Test orientation:	Horizontal
Material:	FRP polyester	Mounting:	Specimen holder with retainer frame Specimen wrapped with aluminium foil
Specimen size:	0.1 m x 0.05 m x 0.004 m thick	Data recording interval:	1 s
		Problem:	Nil

Exposure heat flux	Sample no	Initial mass	Final mass	Time to ignition	Flameout time	1st $\dot{q}''_{peak}$	Time to 1st $\dot{q}''_{peak}$	2nd $\dot{q}''_{peak}$	Time to 2nd $\dot{q}''_{peak}$	$\dot{q}''_{60}$	$\dot{q}''_{120}$	$\dot{q}''_{180}$	q''	$\Delta H_{c,eff}$	Mass loss rate at t_{ig}	Max mass loss rate
kW/m^2		g	g	s	s	kW/m^2	s	kW/m^2	s	kW/m^2	kW/m^2	kW/m^2	MJ/m^2	MJ/kg	kg/sm^2	kg/sm^2
25	1	36.5	17.9	500	1139	143	505	109	720	116	105	103	51.1	13.8	.0045	n/r
	2	33.5	17.7	492	1010	121	498	126	731	98	93	95	40.1	12.7	.0043	n/r
	3	35.9	18.1	513	1153	120	519	114	764	103	93	93	44.7	12.6	.0044	n/r
35	1	37.0	16.1	100	800	150	126	110	380	123	112	106	58.5	14.0	n/r	n/r
	2	36.5	17.2	110	797	137	143	104	450	119	105	99	53.4	13.9	n/r	n/r
	3	33.6	16.7	108	804	162	126	107	352	124	109	103	49.0	14.5	n/r	n/r
50	1	36.5	16.5	50	676	156	77	132	364	136	126	122	55.6	13.9	n/r	n/r
	2	33.4	12.5	51	666	189	61	131	287	150	130	122	52.9	12.7	n/r	n/r
	3	33.5	16.5	50	558	164	68	132	253	135	122	119	45.5	13.4	n/r	n/r
65	1	33.6	12.0	33	565	173	42	149	231	148	140	137	58.4	13.5	n/r	.0161
	2	36.7	16.4	34	530	192	60	159	303	153	147	144	60.3	14.9	n/r	.0169
	3	35.4	15.4	34	510	170	54	186	294	147	144	141	58.1	14.5	n/r	.0152

n/r = The mass loss rate at t_{ig} and max mass loss rate at other heat fluxes are not reported since the information is not required for the simulation.

Table G1: Cone Calorimeter test data for the seat specimens

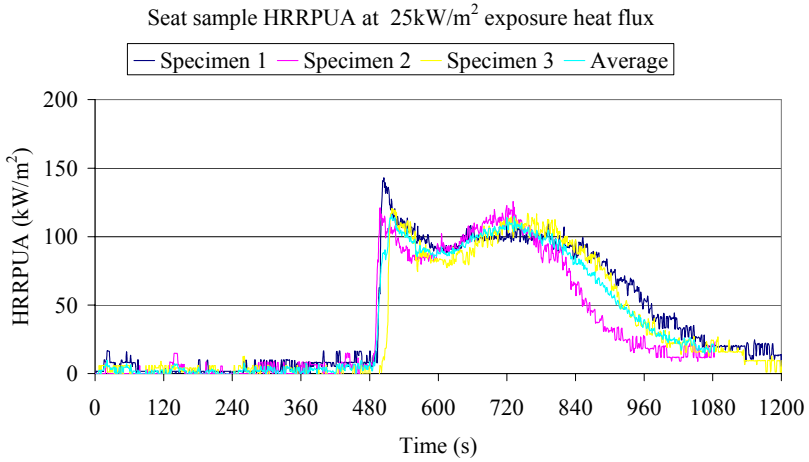

Figure G1: Seat sample HRRPUA at 25 kW/m^2

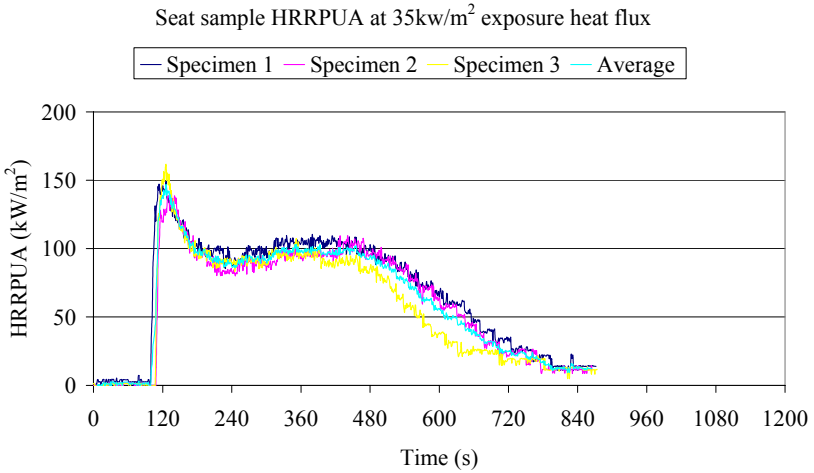

Figure G2: Seat sample HRRPUA at 35 kW/m^2

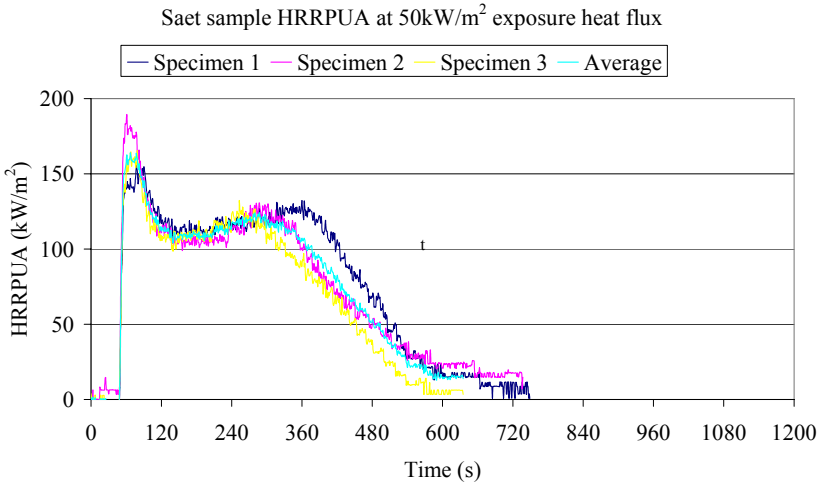

Figure G3: Seat sample HRRPUA at 50 kW/m^2

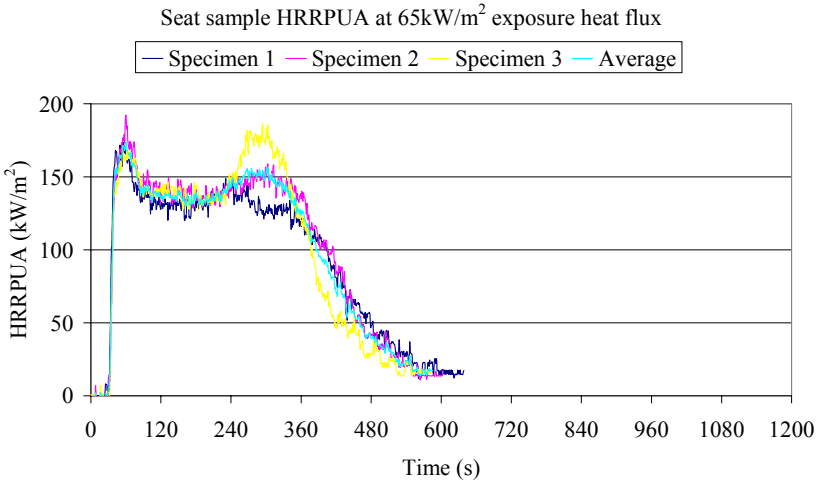

Figure G4: Seat sample HRRPUA at 65 kW/m^2

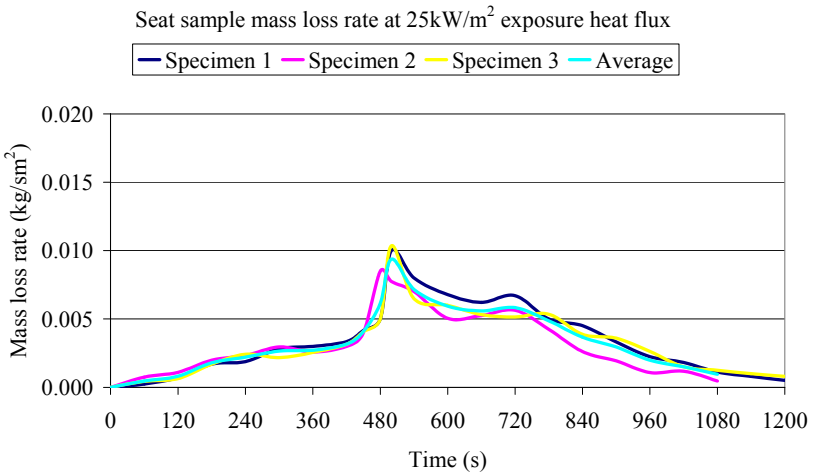

Figure G5: Seat sample mass loss rate at 25 kW/m^2

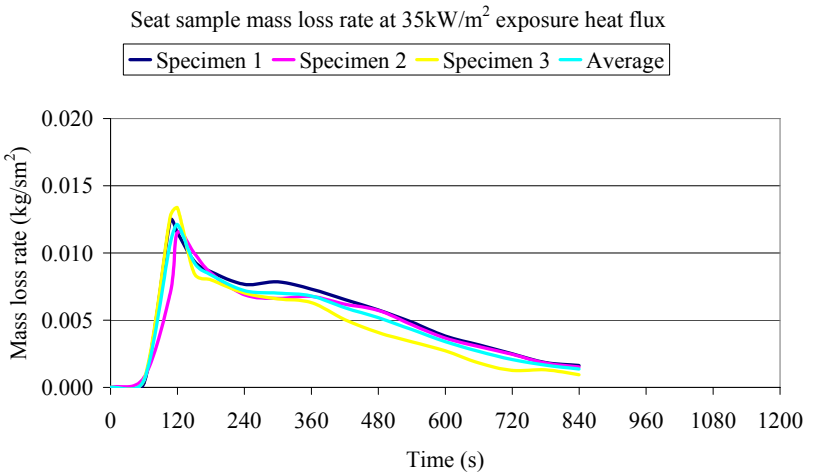

Figure G6: Seat sample mass loss rate at 35 kW/m^2

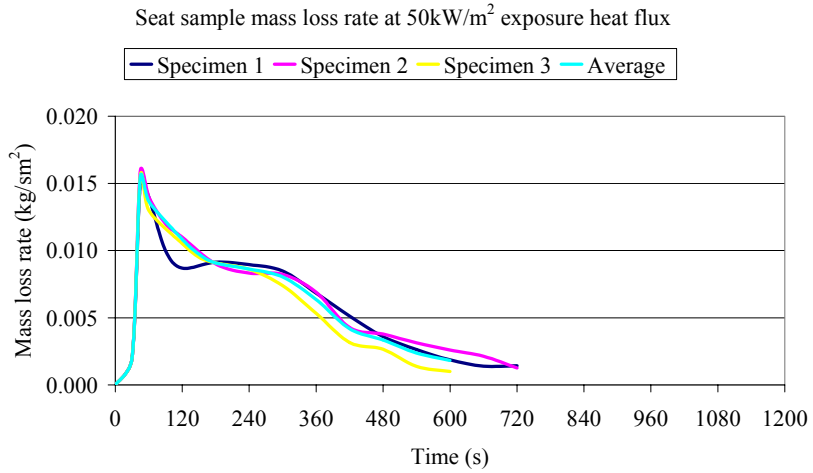

Figure G7: Seat sample mass loss rate at 50 kW/m^2

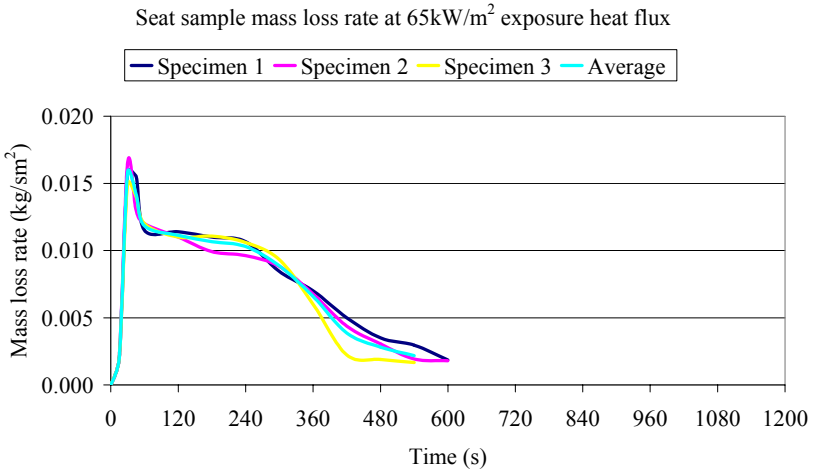

Figure G8: Seat sample mass loss rate at 65 kW/m^2

Component:	Train car floor covering	Test orientation:	Horizontal
Material:	Styrene butadiene	Mounting:	Specimen holder with retainer frame and wire grid Specimen wrapped with aluminium foil
Specimen size:	0.1 m x 0.1 m x 0.003 m thick	Data recording interval:	1 s
		Problem:	Nil

Exposure heat flux	Sample no	Initial mass	Final mass	Time to ignition	Flameout time	1st $\dot{q}''_{peak}$	Time to 1st $\dot{q}''_{peak}$	2nd $\dot{q}''_{peak}$	Time to 2nd $\dot{q}''_{peak}$	$\dot{q}''_{60}$	$\dot{q}''_{120}$	$\dot{q}''_{180}$	q''	$\Delta H_{c,eff}$	Mass loss rate at t_{ig}	Max mass loss rate
kW/m^2		g	g	s	s	kW/m^2	s	kW/m^2	s	kW/m^2	kW/m^2	kW/m^2	MJ/m^2	MJ/kg	kg/sm^2	kg/sm^2
25	1	51.2	28.8	650	1436	44	821	Nil[a]	Nil[a]	26	30	33	29.2	13.0	.0025	n/r
	2	50.5	28.3	570	1383	49	919	Nil[a]	Nil[a]	24	28	31	29.2	13.2	.0024	n/r
	3	52.5	32.4	590	1159	41	837	Nil[a]	Nil[a]	23	26	29	19.0	9.5	.0023	n/r
35	1	50.3	24.4	224	1038	54	334	79	801	36	43	44	41.8	16.2	n/r	n/r
	2	51.2	26.5	233	1165	54	338	74	776	33	41	43	41.6	16.8	n/r	n/r
	3	50.5	24.6	240	1032	55	296	91	790	42	46	46	42.5	16.4	n/r	n/r
50	1	51.1	19.8	120	985	70	169	64	514	55	59	58	40.6	12.3	n/r	n/r
	2	52.7	22.3	118	893	74	185	88	639	57	62	61	44.2	14.5	n/r	n/r
	3	51.5	24.3	115	900	79	178	82	552	59	66	65	43.8	16.1	n/r	n/r
65	1	52.0	21.2	78	749	96	120	97	468	83	81	77	43.8	14.2	n/r	.0078
	2	50.3	21.9	75	710	100	124	102	453	77	81	79	44.3	15.6	n/r	.0079
	3	51.5	25.6	76	650	93	114	102	436	76	78	75	42.5	16.4	n/r	.0078

a Nil because there is no 2nd peak HRR.

n/r = The mass loss rate at t_{ig} and max mass loss rate at other heat fluxes are not reported since the information is not required for the simulation.

Table G2: Cone Calorimeter test data for the floor covering specimens

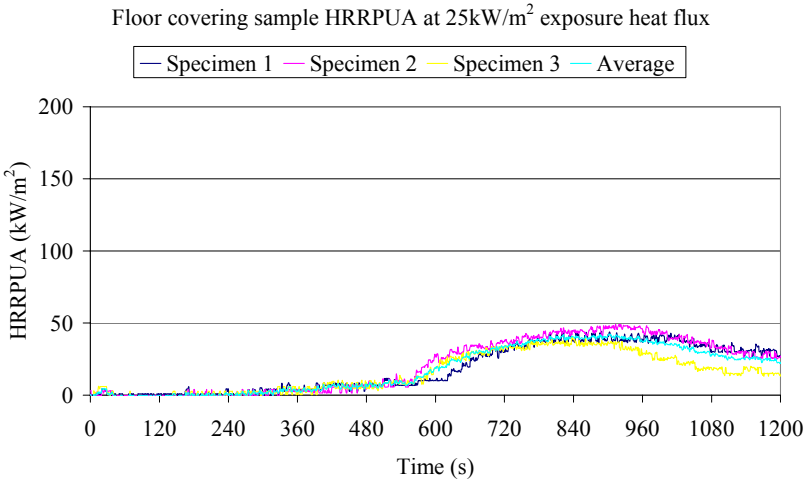

Figure G9: Floor covering sample HRRPUA at 25 kW/m^2

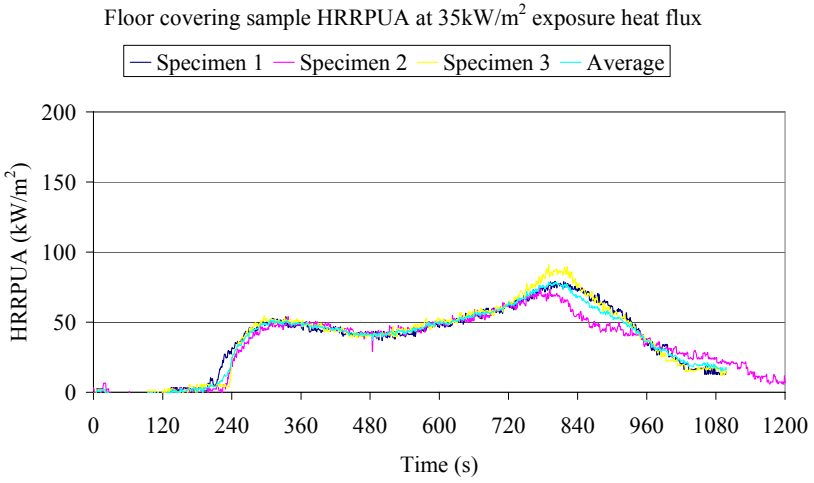

Figure G10: Floor covering sample HRRPUA at 35 kW/m^2

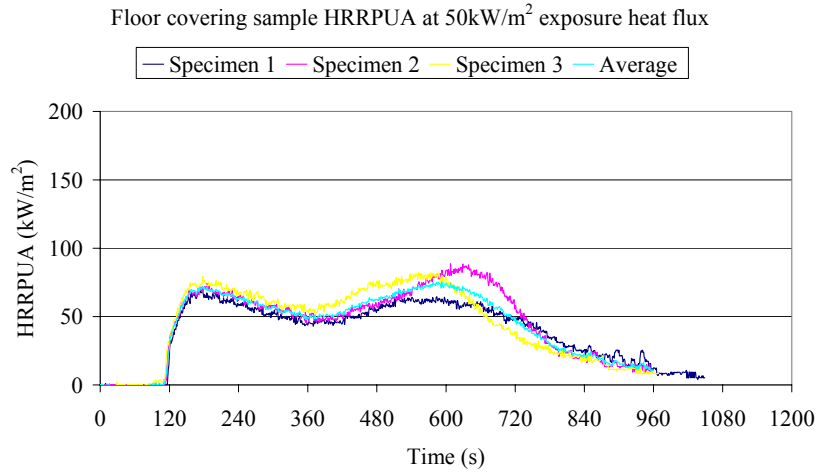

Figure G11: Floor covering sample HRRPUA at 50 kW/m^2

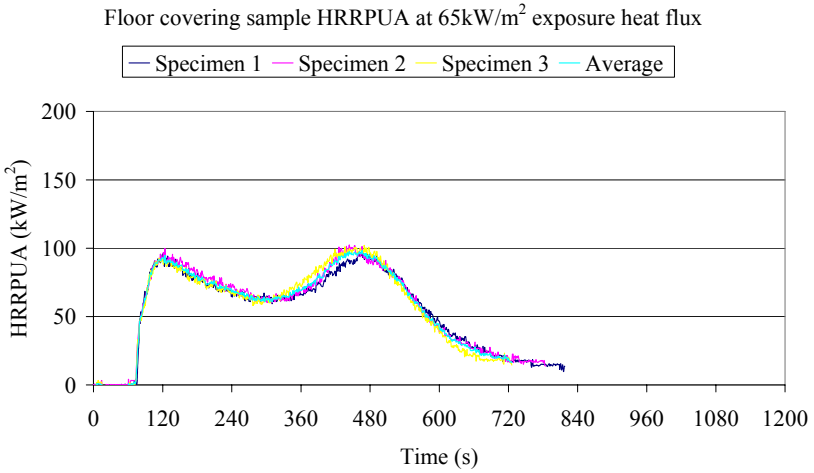

Figure G12: Floor covering sample HRRPUA at 65 kW/m^2

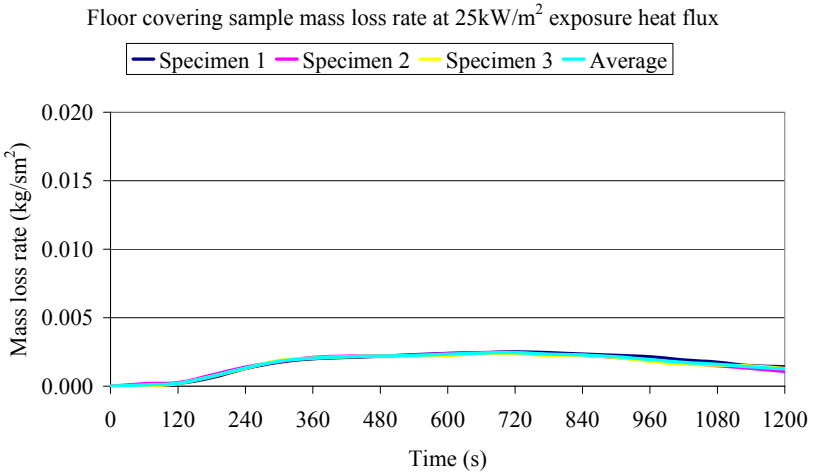

Figure G13: Floor covering sample mass loss rate at 25 kW/m^2

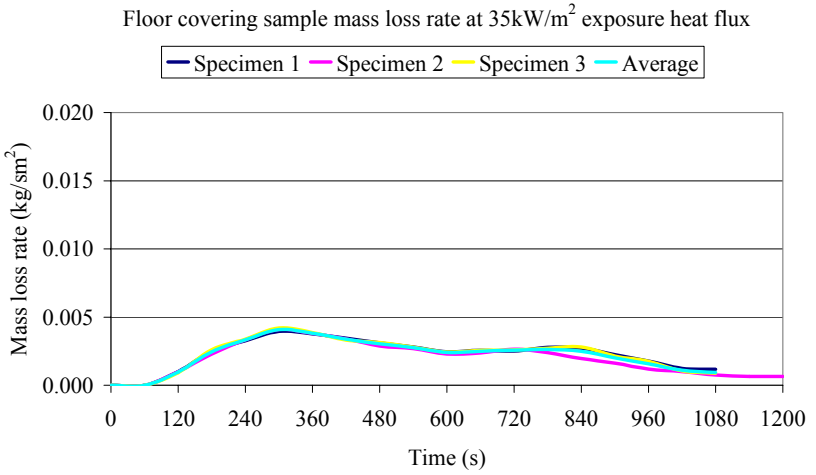

Figure G14: Floor covering sample mass loss rate at 35 kW/m^2

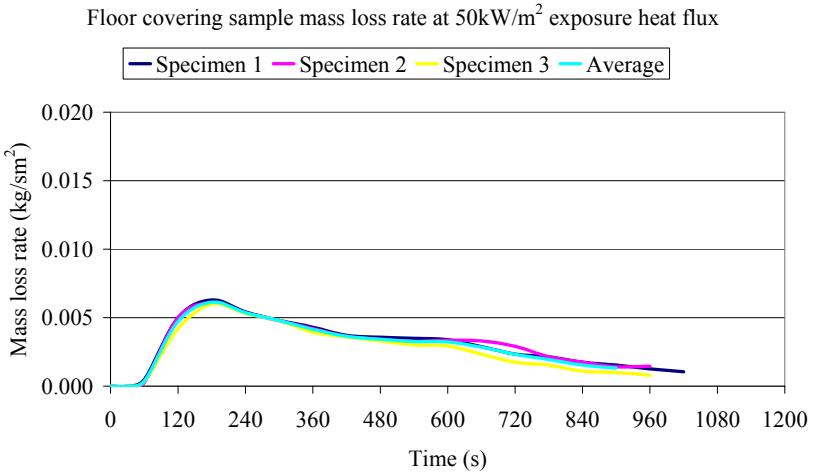

Figure G15: Floor covering sample mass loss rate at 50 kW/m^2

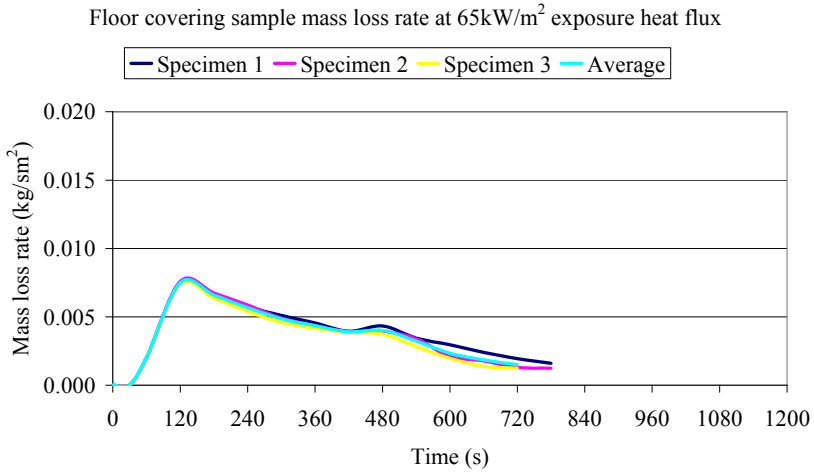

Figure G16: Floor covering sample mass loss rate at 65 kW/m^2

Component:	Train car wall panel	Test orientation:	Horizontal
Material:	Aluminium panel with exposed surface painted with powder paint	Mounting:	Specimen holder with retainer frame Specimen wrapped with aluminium foil
Specimen size:	0.1 m x 0.1 m x 0.0014 m thick	Data recording interval:	1 s
		Problem:	No data was collected for the two tests at 35 kW/m^2 and one test at 50 kW/m^2 because of software problem.

Exposure heat flux	Sample no	Initial mass	Final mass	Time to ignition	Flameout time	1st $\dot{q}''_{peak}$	Time to 1st $\dot{q}''_{peak}$	2nd $\dot{q}''_{peak}$	Time to 2nd $\dot{q}''_{peak}$	$\dot{q}''_{60}$	$\dot{q}''_{120}$	$\dot{q}''_{180}$	q''	$\Delta H_{c,eff}$	Mass loss rate at t_{ig}	Max mass loss rate
kW/m^2		g	g	s	s	kW/m^2	s	kW/m^2	s	kW/m^2	kW/m^2	kW/m^2	MJ/m^2	MJ/kg	kg/sm^2	kg/sm^2
35	1	Data not collected/ NI														
	2															
50	1															
	2	42.5	40.5	NI	NI	8	332	NI	NI	2	2	2	NI	NI	n/r	n/r
65	1	42.5	40.5	55	92	88	63	67	78	32	26	26	2.0	10.4	n/r	.0035
	2	42.7	41.9	53	66	83	58	Nil[a]	Nil[a]	16	13	13	1.1	12.9	n/r	.0028

a Nil because there is no 2nd peak HRR

NI = No ignition.

n/r = Not reported because not required for the simulation

Note: For a specimen that did not show sustained flaming, the peak heat release rate $\dot{q}''_{peak}$, and the average $\dot{q}''$ values for the first 60, 120 and 180 s were tabulated for periods beginning with the first reading after the last negative rate of heat release reading that occurs at the beginning of the test.

Table G3: Cone Calorimeter test data for the wall panel specimens

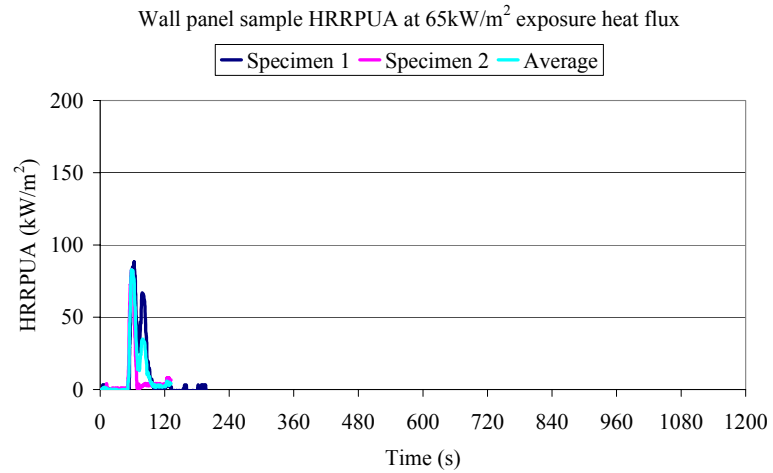

Figure G17: Wall panel sample HRRPUA at 65 kW/m^2

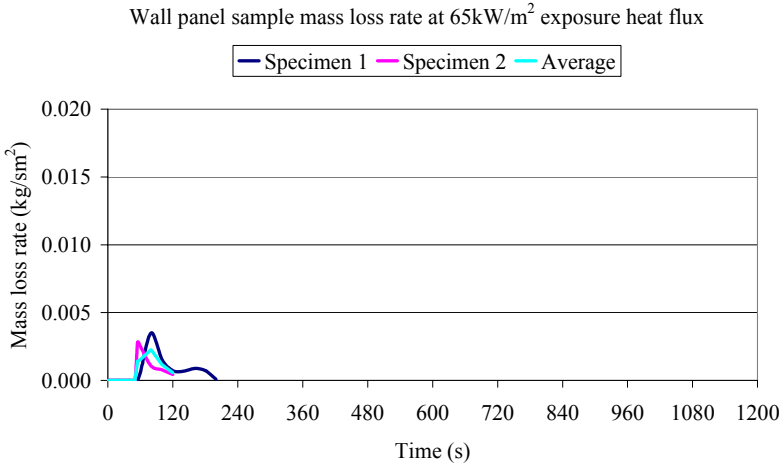

Figure G18: Wall panel sample mass loss rate at 65 kW/m^2

Component:	Train car bellows (Inner)	Test orientation:	Horizontal
Material:	WPE Vamac compound ref 22-003, grey	Mounting:	Specimen holder with retainer frame and wire grid Specimen wrapped with aluminium foil
Specimen size:	0.1 m x 0.1 m x 0.003 m thick	Data recording interval:	1 s
		Problem:	No data was collected for one of the tests at 35 kW/m^2 exposure heat flux level. For the other test at 35 kW/m^2, data acquisition stopped mid-way through the test.

Exposure heat flux	Sample no	Initial mass	Final mass	Time to ignition	Flameout time	1st $\dot{q}''_{peak}$	Time to 1st $\dot{q}''_{peak}$	2nd $\dot{q}''_{peak}$	Time to 2nd $\dot{q}''_{peak}$	$\dot{q}''_{60}$	$\dot{q}''_{120}$	$\dot{q}''_{180}$	q''	$\Delta H_{c,eff}$	Mass loss rate at t_{ig}	Max mass loss rate
kW/m^2		g	g	s	s	kW/m^2	s	kW/m^2	s	kW/m^2	kW/m^2	kW/m^2	MJ/m^2	MJ/kg	kg/sm^2	kg/sm^2
35	1	Data not collected														
	2	35.8	Nil[a]	179	900	111	242	Nil[a]	Nil[a]	91	92	82	Nil[a]	Nil[a]	n/r	n/r
50	1	38.0	14.5	84	844	147	151	89	423	116	118	105	50.9	14.7	n/r	n/r
	2	35.8	15.0	78	684	148	136	107	426	108	115	102	47.3	15.5	n/r	n/r
65	1	36.2	10.8	64	720	165	97	78	370	136	121	106	46.3	12.4	n/r	n/r
	2	37.6	12.8	51	717	176	109	100	457	140	130	113	50.6	13.9	n/r	n/r

a Nil because data acquisition stopped mid-way through the test.
n/r = Not reported because not required for the simulation

Table G4: Cone Calorimeter test data for the bellows (Inner) specimens

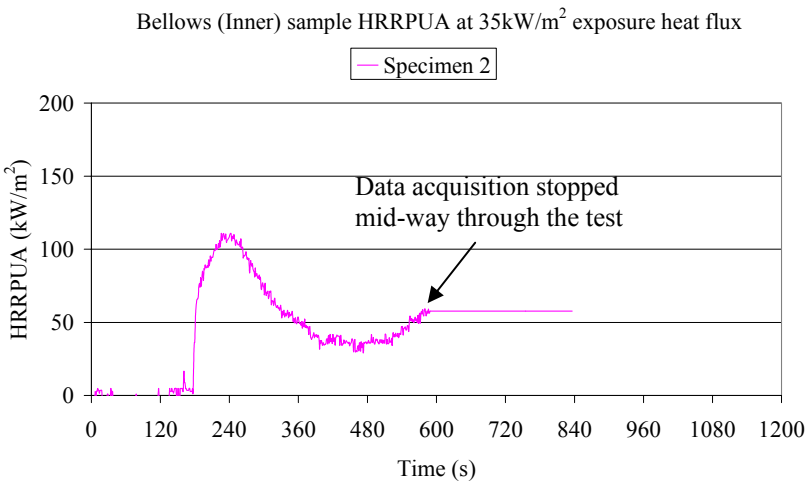

Figure G19: Bellows (Inner) sample HRRPUA at 35 kW/m^2

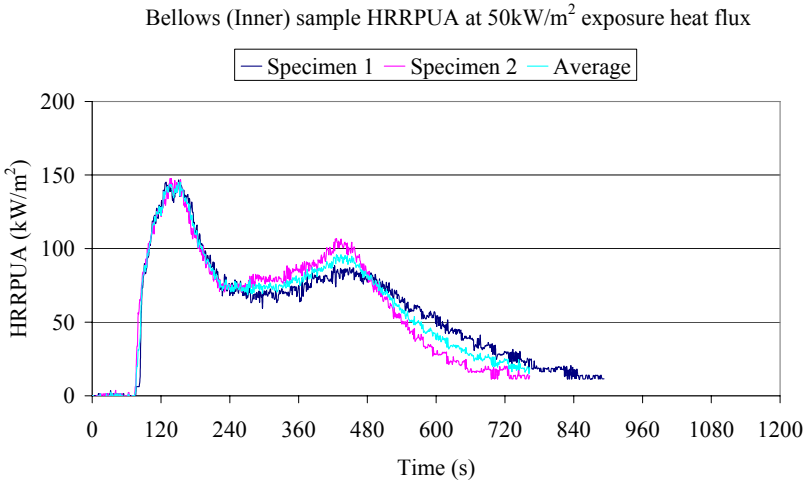

Figure G20: Bellows (Inner) sample HRRPUA at 50 kW/m^2

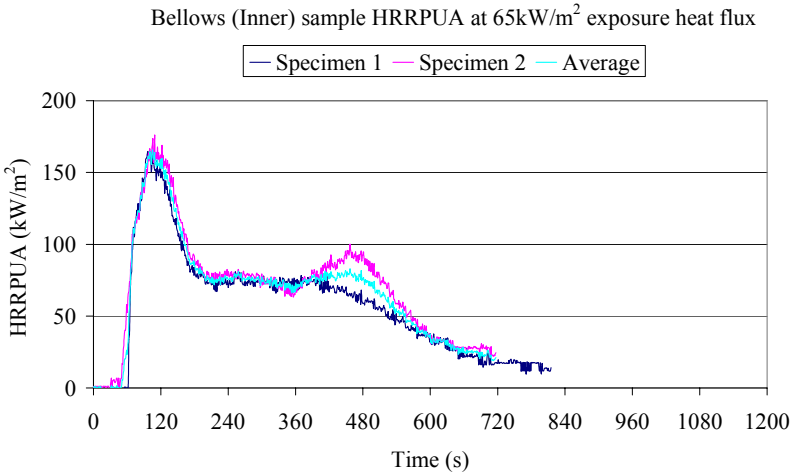

Figure G21: Bellows (Inner) sample HRRPUA at 65 kW/m^2

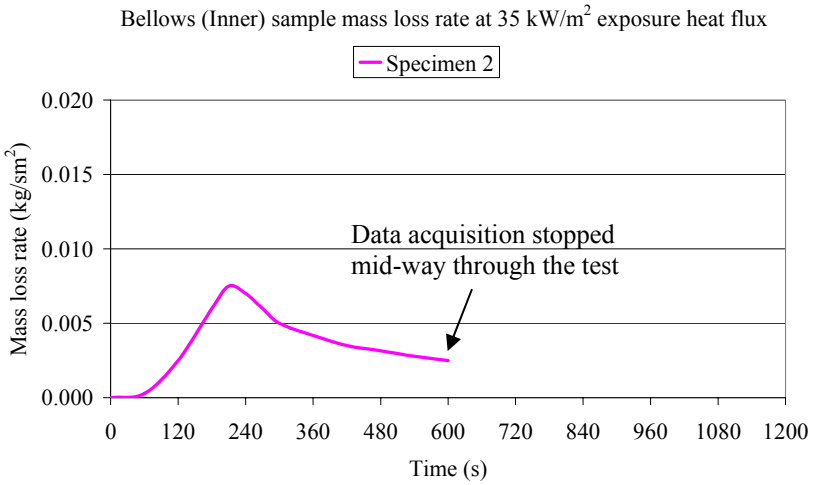

Figure G22: Bellows (Inner) sample mass loss rate at 35 kW/m^2

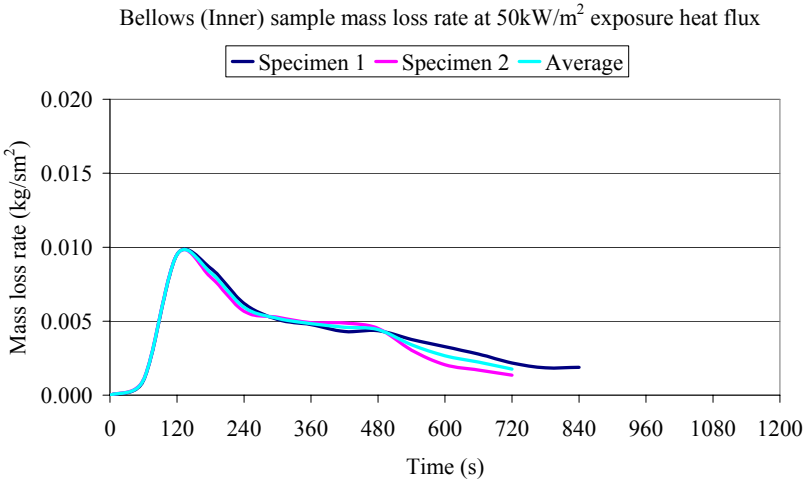

Figure G23: Bellows (Inner) sample mass loss rate at 50 kW/m^2

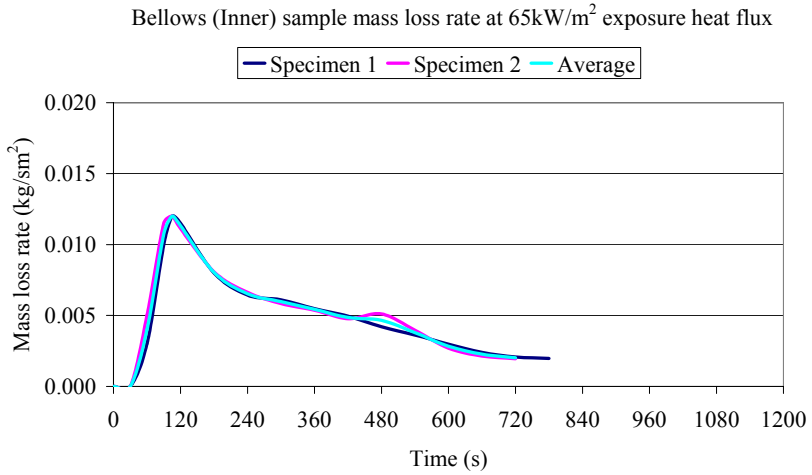

Figure G24: Bellows (Inner) sample mass loss rate at 65 kW/m^2

Component:	Train car bellows (Outer)	Test orientation:	Horizontal
Material:	WPE Vamac compound ref 22-004, black	Mounting:	Specimen holder with retainer frame and wire grid Specimen wrapped with aluminium foil
Specimen size:	0.1 m x 0.1 m x 0.003 m thick	Data recording interval:	1 s
		Problem:	The retainer frame popped up and hit the ignitor during the tests for specimen 1 at 35 and 50 kW/m^2 and specimen 2 at 65 kW/m^2 exposure heat flux levels. For all the tests, the wire grid bent into parabolic shape when the specimen expanded.

Exposure heat flux	Sample no	Initial mass	Final mass	Time to ignition	Flameout time	1st $\dot{q}''_{peak}$	Time to 1st $\dot{q}''_{peak}$	2nd $\dot{q}''_{peak}$	Time to 2nd $\dot{q}''_{peak}$	$\dot{q}''_{60}$	$\dot{q}''_{120}$	$\dot{q}''_{180}$	q''	$\Delta H_{c,eff}$	Mass loss rate at t_{ig}	Max mass loss rate
kW/m^2		g	g	s	s	kW/m^2	s	kW/m^2	s	kW/m^2	kW/m^2	kW/m^2	MJ/m^2	MJ/kg	kg/sm^2	kg/sm^2
35	1	52.2	Nil[a]	115	1090	104	209	53	611	48	67	63	41.6	Nil[a]	n/r	n/r
	2	53.2	28.3	120	1077	84	201	39	573	45	61	60	31.7	12.8	n/r	n/r
50	1	53.0	Nil[a]	78	812	134	140	87	482	82	92	83	47.5	Nil[a]	n/r	n/r
	2	52.3	15.9	74	1226	116	142	48	566	81	89	77	50.5	13.8	n/r	n/r
65	1	53.4	20.8	45	995	194	89	76	337	128	127	114	53.7	16.5	n/r	n/r
	2	53.1	Nil[a]	48	525	369	86	102	274	220	190	160	54.9	Nil[a]	n/r	n/r

a Nil because there was error in the mass loss data

n/r = Not reported because not required for the simulation

Table G5: Cone Calorimeter test data for the bellows (Outer) specimens

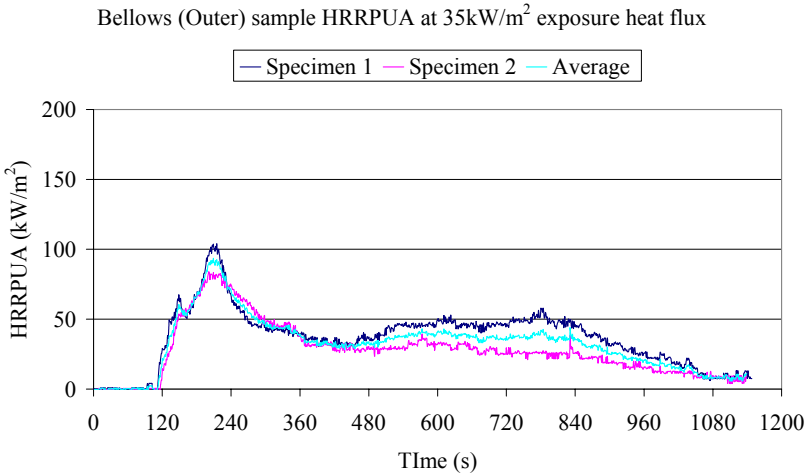

Figure G25: Bellows (Outer) sample HRRPUA at 35 kW/m^2

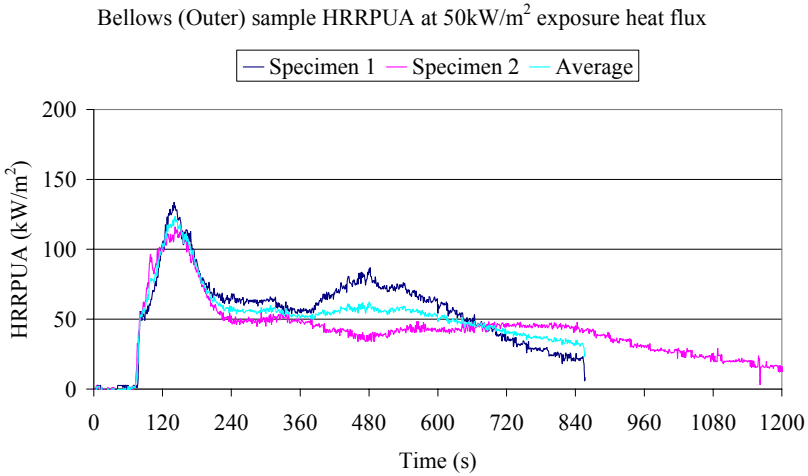

Figure G26: Bellows (Outer) sample HRRPUA at 50 kW/m^2

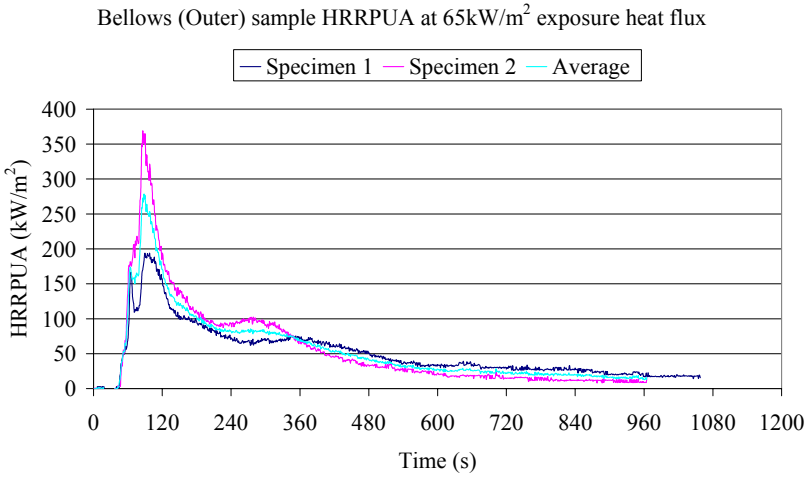

Figure G27: Bellows (Outer) sample HRRPUA at 65 kW/m^2

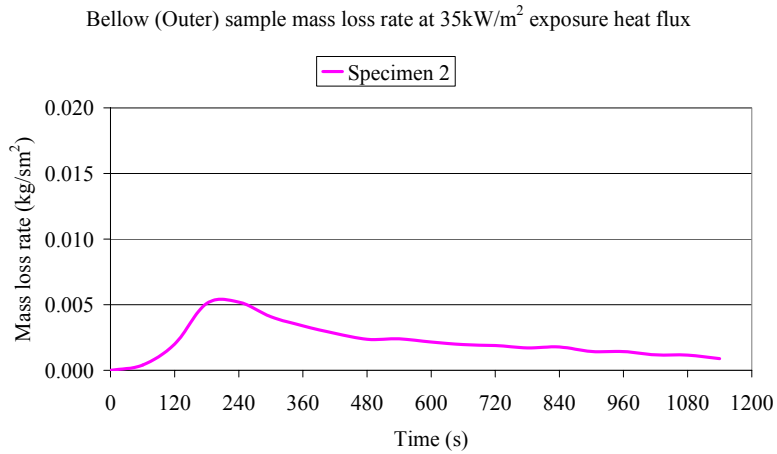

Figure G28: Bellows (Outer) sample mass loss rate at 35 kW/m^2

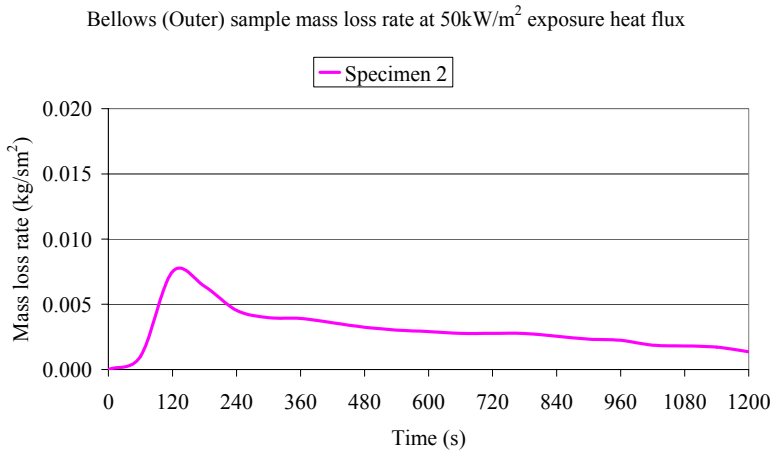

Figure G29: Bellows (Outer) sample mass loss rate at 50 kW/m^2

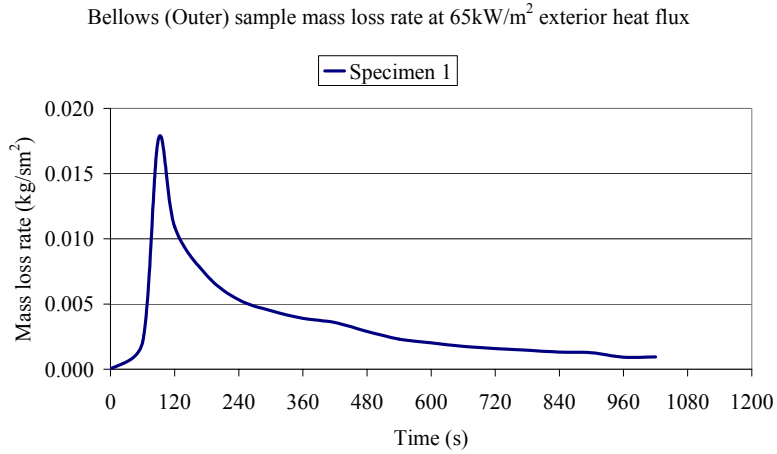

Figure G30: Bellows (Outer) sample mass loss rate at 65 kW/m^2

Note: Mass loss rate curves for specimen 1 at 35 and 50 kW/m^2 and specimen 2 at 65 kW/m^2 exposure heat flux levels are not shown because of errors in the mass loss measurement.

Component:	Train car air-con duct	Test orientation:	Horizontal
Material:	Glass wool with the outer surface covered with a layer aluminium paper sheet	Mounting:	Specimen holder with retainer frame Specimen wrapped with aluminium foil
Specimen size:	0.1 m x 0.1 m x 0.025 m thick	Data recording interval:	1 s
		Problem:	Nil

Exposure heat flux	Sample no	Initial mass	Final mass	Time to ignition	Flameout time	1st $\dot{q}''_{peak}$	Time to 1st $\dot{q}''_{peak}$	2nd $\dot{q}''_{peak}$	Time to 2nd $\dot{q}''_{peak}$	$\dot{q}''_{60}$	$\dot{q}''_{120}$	$\dot{q}''_{180}$	q''	$\Delta H_{c,eff}$	Mass loss rate at t_{ig}	Max mass loss rate
kW/m^2		g	g	s	s	kW/m^2	s	kW/m^2	s	kW/m^2	kW/m^2	kW/m^2	MJ/m^2	MJ/kg	kg/sm^2	kg/sm^2
35	1	Test not conducted														
	2															
50	1	20.7	19.0	NI	NI	12	463	NI	NI	2	2	2	NI	NI	n/r	n/r
	2	21.2	18.5	NI	NI	8	316	NI	NI	3	3	3	NI	NI	n/r	n/r
65	1	20.6	16.7	NI	NI	10	405	NI	NI	2	2	2	NI	NI	n/r	n/r
	2	21.4	15.9	NI	NI	12	547	NI	NI	2	2	2	NI	NI	n/r	n/r

NI = No ignition
n/r = Not reported because not required for the simulation
Note: The peak heat release rate $\dot{q}''_{peak}$, and the average $\dot{q}''$ values for the first 60, 120 and 180 s were tabulated for periods beginning with the first reading after the last negative rate of heat release reading that occurs at the beginning of the test.

Table G6: Cone Calorimeter test data for the air-con duct specimens

Appendix H: Sample FDS data file for Cone Calorimeter model

Define name for output files

.....……

```
&HEAD CHID='ConeSimulation1', TITLE='CONE CALORIMETER' /
```

All output files will have names beginning with "ConeSimulation1"

Define grid size and computational domain

.....……..….....

Grid size

,,,,,,,,,,,,,,,,

```
&GRID IBAR=25,JBAR=35,KBAR=32 /
```

Computational domain

,,

```
&PDIM XBAR0 = -0.1, XBAR = 0.1,
     YBAR0 = -0.1, YBAR = 0.1,
     ZBAR0 = -0.05, ZBAR = 0.20 /
```

Stretching the grid in z-direction

.....……....

```
&TRNZ IDERIV=0,CC=0.04,PC=0.01/
&TRNZ IDERIV=1,CC=0.04,PC=0.6 /
```

Simulation time (in s)

.....……...

```
&TIME TWFIN=1200. /
```

Miscellaneous input parameters

.....…….....

```
&MISC AUTOMATIC_Z = .FALSE., NFRAMES=1200 /
```

Material properties of calcium silicate block

.....……

```
&SURF ID    = 'Block'
     RGB   = 0.66,0.66,0.66
     C_P   = 1.25
     DENSITY=720.
     KS    = 0.12
     DELTA = 0.02 /
```

Flammability parameters (choose either simulation based on heat of vaporisation or HRRPUA. Note only one material can be selected)

.....……

Simulation based on heat of vaporisation

**,,,,,,,,,,,,,,,,,,,

```
     HEAT_OF_COMBUSTION   = 13670. /

SURF ID        = 'STYRENE_BUTADIENE'
     RGB       = 0.5,0.5,0.5
     C_DELTA_RHO= 8.363
     TMPIGN     = 419.
     BACKING    = 'INSULATED'
     MASS_FLUX_CRITICAL   = 0.0024
     BURNING_RATE_MAX     = 0.0079
     HEAT_OF_VAPORIZATION = 12320.
     HEAT_OF_COMBUSTION   = 14570. /
```

Simulation based on HRRPUA

,,,

```
RAMP ID = 'PEST1', T =  251       , F =      0.68      /
RAMP ID = 'PEST1', T =  351       , F =      0.69      /
RAMP ID = 'PEST1', T =  384       , F =      0.64      /
RAMP ID = 'PEST1', T =  498       , F =      0.37      /
RAMP ID = 'PEST1', T =  613       , F =      0.17      /
RAMP ID = 'PEST1', T =  656       , F =      0.14      /
RAMP ID = 'PEST1', T =  697       , F =      0.09      /
RAMP ID = 'PEST1', T =  720       , F =      0.09      /
RAMP ID = 'PEST1', T =  761       , F =      0.09      /
RAMP ID = 'PEST1', T =  761       , F =      0.00      /

HRRPUA curve for test at 50 kw/m2 exposure heat flux
----------------------------------------------------------------------
SURF ID       = '50FRP_POLYESTER'
     RGB      = 0.0,0.0,1.0
     C_DELTA_RHO = 3.341
     TMPIGN     = 448.
     BACKING    = 'INSULATED'
     HRRPUA     = 164.
     RAMP_Q     = 'PEST1'/
RAMP ID = 'PEST1', T =  0         , F =      0.00      /
RAMP ID = 'PEST1', T =  0         , F =      0.18      /
RAMP ID = 'PEST1', T =  0         , F =      0.28      /
RAMP ID = 'PEST1', T =  12        , F =      0.96      /
RAMP ID = 'PEST1', T =  18        , F =      1.00      /
RAMP ID = 'PEST1', T =  29        , F =      0.98      /
RAMP ID = 'PEST1', T =  41        , F =      0.88      /
RAMP ID = 'PEST1', T =  71        , F =      0.69      /
RAMP ID = 'PEST1', T =  107       , F =      0.66      /
RAMP ID = 'PEST1', T =  149       , F =      0.67      /
RAMP ID = 'PEST1', T =  222       , F =      0.74      /
RAMP ID = 'PEST1', T =  248       , F =      0.74      /
RAMP ID = 'PEST1', T =  314       , F =      0.65      /
RAMP ID = 'PEST1', T =  409       , F =      0.39      /
RAMP ID = 'PEST1', T =  503       , F =      0.15      /
RAMP ID = 'PEST1', T =  544       , F =      0.09      /
RAMP ID = 'PEST1', T =  585       , F =      0.09      /
RAMP ID = 'PEST1', T =  585       , F =      0.00      /

HRRPUA curve for test at 65 kw/m2 exposure heat flux
----------------------------------------------------------------------
SURF ID       = '65FRP_POLYESTER'
     RGB      = 0.0,0.0,1.0
     C_DELTA_RHO = 3.341
     TMPIGN     = 448.
     BACKING    = 'INSULATED'
     HRRPUA     = 172.
     RAMP_Q     = 'PEST1'/
RAMP ID = 'PEST1', T =  0         , F =      0.00      /
RAMP ID = 'PEST1', T =  0         , F =      0.17      /
RAMP ID = 'PEST1', T =  0         , F =      0.26      /
RAMP ID = 'PEST1', T =  13        , F =      0.91      /
RAMP ID = 'PEST1', T =  27        , F =      1.00      /
RAMP ID = 'PEST1', T =  58        , F =      0.83      /
RAMP ID = 'PEST1', T =  114       , F =      0.79      /
RAMP ID = 'PEST1', T =  179       , F =      0.78      /
RAMP ID = 'PEST1', T =  243       , F =      0.90      /
RAMP ID = 'PEST1', T =  268       , F =      0.89      /
RAMP ID = 'PEST1', T =  301       , F =      0.84      /
RAMP ID = 'PEST1', T =  448       , F =      0.23      /
```

```
RAMP ID = 'PEST1', T =  533       , F =      0.09      /
RAMP ID = 'PEST1', T =  541       , F =      0.09      /
RAMP ID = 'PEST1', T =  541       , F =      0.00      /

Styrene butadiene (Choose only one depending on tested exposure heat flux simulated)
================================================================
HRRPUA curve for test at 25 kw/m2 exposure heat flux
----------------------------------------------------------------
&SURF ID          = '25STYRENE_BUTADIENE'
     RGB      = 0.5,0.5,0.5
     C_DELTA_RHO = 8.363
     TMPIGN     = 419.
     BACKING    = 'INSULATED'
     HRRPUA     = 41.
     RAMP_Q     = 'SB' /
&RAMP ID = 'SB', T =    0         , F =      0.00      /
&RAMP ID = 'SB', T =    0         , F =      0.73      /
&RAMP ID = 'SB', T =    132       , F =      0.98      /
&RAMP ID = 'SB', T =    199       , F =      1.00      /
&RAMP ID = 'SB', T =    271       , F =      0.98      /
&RAMP ID = 'SB', T =    354       , F =      0.85      /
&RAMP ID = 'SB', T =    444       , F =      0.63      /
&RAMP ID = 'SB', T =    463       , F =      0.63      /
&RAMP ID = 'SB', T =    530       , F =      0.56      /
&RAMP ID = 'SB', T =    530       , F =      0.00      /

HRRPUA curve for test at 35 kw/m2 exposure heat flux
----------------------------------------------------------------
&SURF ID          = '35STYRENE_BUTADIENE'
     RGB      = 0.5,0.5,0.5
     C_DELTA_RHO = 8.363
     TMPIGN     = 419.
     BACKING    = 'INSULATED'
     HRRPUA     = 78.5
     RAMP_Q     = 'SB' /
&RAMP ID = 'SB', T =    0         , F =      0.00      /
&RAMP ID = 'SB', T =    0         , F =      0.38      /
&RAMP ID = 'SB', T =    9         , F =      0.42      /
&RAMP ID = 'SB', T =    64        , F =      0.65      /
&RAMP ID = 'SB', T =    96        , F =      0.64      /
&RAMP ID = 'SB', T =    124       , F =      0.61      /
&RAMP ID = 'SB', T =    220       , F =      0.52      /
&RAMP ID = 'SB', T =    275       , F =      0.54      /
&RAMP ID = 'SB', T =    395       , F =      0.68      /
&RAMP ID = 'SB', T =    451       , F =      0.74      /
&RAMP ID = 'SB', T =    557       , F =      1.00      /
&RAMP ID = 'SB', T =    575       , F =      0.96      /
&RAMP ID = 'SB', T =    628       , F =      0.78      /
&RAMP ID = 'SB', T =    669       , F =      0.66      /
&RAMP ID = 'SB', T =    786       , F =      0.25      /
&RAMP ID = 'SB', T =    852       , F =      0.20      /
&RAMP ID = 'SB', T =    852       , F =      0.00      /

HRRPUA curve for test at 50 kw/m2 exposure heat flux
----------------------------------------------------------------
&SURF ID          = '50STYRENE_BUTADIENE'
     RGB      = 0.5,0.5,0.5
     C_DELTA_RHO = 8.363
     TMPIGN     = 419.
     BACKING    = 'INSULATED'
```

```
     HRRPUA      = 75.
     RAMP_Q      = 'SB' /
&RAMP ID = 'SB', T =    0        , F =     0.00     /
&RAMP ID = 'SB', T =    0        , F =     0.40     /
&RAMP ID = 'SB', T =    5        , F =     0.53     /
&RAMP ID = 'SB', T =    40       , F =     0.93     /
&RAMP ID = 'SB', T =    57       , F =     0.96     /
&RAMP ID = 'SB', T =    241      , F =     0.65     /
&RAMP ID = 'SB', T =    289      , F =     0.68     /
&RAMP ID = 'SB', T =    365      , F =     0.84     /
&RAMP ID = 'SB', T =    466      , F =     1.00     /
&RAMP ID = 'SB', T =    511      , F =     0.95     /
&RAMP ID = 'SB', T =    692      , F =     0.33     /
&RAMP ID = 'SB', T =    839      , F =     0.15     /
&RAMP ID = 'SB', T =    839      , F =     0.00     /

HRRPUA curve for test at 65 kw/m2 exposure heat flux
----------------------------------------------------------------------
&SURF ID          = '65STYRENE_BUTADIENE'
     RGB       = 0.5,0.5,0.5
     C_DELTA_RHO = 8.363
     TMPIGN      = 419.
     BACKING     = 'INSULATED'
     HRRPUA      = 97.
     RAMP_Q      = 'SB' /
&RAMP ID = 'SB', T =    0        , F =     0.00     /
&RAMP ID = 'SB', T =    0        , F =     0.31     /
&RAMP ID = 'SB', T =    16       , F =     0.73     /
&RAMP ID = 'SB', T =    36       , F =     0.94     /
&RAMP ID = 'SB', T =    43       , F =     0.96     /
&RAMP ID = 'SB', T =    129      , F =     0.77     /
&RAMP ID = 'SB', T =    200      , F =     0.66     /
&RAMP ID = 'SB', T =    224      , F =     0.64     /
&RAMP ID = 'SB', T =    262      , F =     0.67     /
&RAMP ID = 'SB', T =    309      , F =     0.80     /
&RAMP ID = 'SB', T =    369      , F =     1.00     /
&RAMP ID = 'SB', T =    392      , F =     1.00     /
&RAMP ID = 'SB', T =    412      , F =     0.95     /
&RAMP ID = 'SB', T =    540      , F =     0.35     /
&RAMP ID = 'SB', T =    589      , F =     0.26     /
&RAMP ID = 'SB', T =    647      , F =     0.18     /
```

Specify the sides of the computational domain as open vent

.....……

```
&VENT CB='XBAR0',SURF_ID='OPEN' /
&VENT CB='XBAR' ,SURF_ID='OPEN' /
&VENT CB='YBAR0',SURF_ID='OPEN' /
&VENT CB='YBAR' ,SURF_ID='OPEN' /
&VENT CB='ZBAR0',SURF_ID='OPEN' /
&VENT CB='ZBAR' ,SURF_ID='OPEN' /
```

Specify the temperature of the outer surface of the conical heater

.....……

```
&SURF ID='SHIELD',TMPWAL = 20. /
```

Specify the temperature of the inner surface of the conical heater (Choose only one depending on the exposure heat flux simulated)

.....……

SURF ID='CONE', TMPWAL = 883./ 65kWm^-2 heat flux
SURF ID='CONE', TMPWAL = 808./ 50kWm^-2 heat flux
SURF ID='CONE', TMPWAL = 712./ 35kWm^-2 heat flux
&SURF ID='CONE', TMPWAL = 633./ 25kWm^-2 heat flux

Specimen and calcium silicate block geometry (Choose only one depending on material simulated)

.....……

For FRP polyester

,,,,,,,,,,,,,,,,,,,,,,,,

&OBST XB=-.050,0.050,-.050,0.000,-0.029,-
0.025,SURF_ID6='INERT','INERT','INERT','INERT','INERT','FRP_POLYESTER' /
&OBST XB=-.050,0.050,-.050,0.050,-0.049,-0.029,SURF_ID='BLOCK' /

For styrene butadiene

,,,,,,,,,,,,,,,,,,,,,,,,,,,,,,,,

&OBST XB=-.050,0.050,-.050,0.000,-0.028,-
0.025,SURF_ID6='INERT','INERT','INERT','INERT','INERT','STYRENE_BUTADIENE' /
&OBST XB=-.050,0.050,-.050,0.050,-0.048,-0.028,SURF_ID='BLOCK' /

Conical heater geometry

**.....……..... **

&OBST XB=-.0140,-.0120,-.0920,-.0900,0.0008,0.0125, SURF_ID='SHIELD' /
&OBST XB=-.0120,-.0100,-.0920,-.0900,0.0008,0.0125, SURF_ID='SHIELD' /
&OBST XB=-.0100,-.0080,-.0920,-.0900,0.0008,0.0125, SURF_ID='SHIELD' /
.
.
.
.
.
&OBST XB=-.0160,-.0140,-.0820,-.0800,0.0008,0.0281, SURF_ID='SHIELD' /
&OBST XB=-.0140,-.0120,-.0820,-.0800,0.0008,0.0281, SURF_ID='SHIELD' /
&OBST XB=-.0120,-.0100,-.0820,-.0800,0.0008,0.0125, SURF_ID='CONE' /
&OBST XB=-.0120,-.0100,-.0820,-.0800,0.0125,0.0225, SURF_ID='SHIELD' /
&OBST XB=-.0120,-.0100,-.0820,-.0800,0.0125,0.0281, SURF_ID='SHIELD' /
&OBST XB=-.0100,-.0080,-.0820,-.0800,0.0008,0.0125, SURF_ID='CONE' /
&OBST XB=-.0100,-.0080,-.0820,-.0800,0.0125,0.0225, SURF_ID='SHIELD' /
&OBST XB=-.0100,-.0080,-.0820,-.0800,0.0125,0.0281, SURF_ID='SHIELD' /
&OBST XB=-.0080,-.0060,-.0820,-.0800,0.0008,0.0125, SURF_ID='CONE' /
&OBST XB=-.0080,-.0060,-.0820,-.0800,0.0125,0.0225, SURF_ID='SHIELD' /
&OBST XB=-.0080,-.0060,-.0820,-.0800,0.0125,0.0281, SURF_ID='SHIELD' /
&OBST XB=-.0060,-.0040,-.0820,-.0800,0.0008,0.0125, SURF_ID='CONE' /
&OBST XB=-.0060,-.0040,-.0820,-.0800,0.0125,0.0225, SURF_ID='SHIELD' /
&OBST XB=-.0060,-.0040,-.0820,-.0800,0.0125,0.0281, SURF_ID='SHIELD' /
&OBST XB=-.0040,-.0020,-.0820,-.0800,0.0008,0.0125, SURF_ID='CONE' /
&OBST XB=-.0040,-.0020,-.0820,-.0800,0.0125,0.0225, SURF_ID='SHIELD' /
&OBST XB=-.0040,-.0020,-.0820,-.0800,0.0125,0.0281, SURF_ID='SHIELD' /
&OBST XB=-.0020,0.0000,-.0820,-.0800,0.0008,0.0125, SURF_ID='CONE' /
&OBST XB=-.0020,0.0000,-.0820,-.0800,0.0125,0.0225, SURF_ID='SHIELD' /
&OBST XB=-.0020,0.0000,-.0820,-.0800,0.0125,0.0281, SURF_ID='SHIELD' /
&OBST XB=0.0000,0.0020,-.0820,-.0800,0.0008,0.0125, SURF_ID='CONE' /
&OBST XB=0.0000,0.0020,-.0820,-.0800,0.0125,0.0225, SURF_ID='SHIELD' /
&OBST XB=0.0000,0.0020,-.0820,-.0800,0.0125,0.0281, SURF_ID='SHIELD' /
&OBST XB=0.0020,0.0040,-.0820,-.0800,0.0008,0.0125, SURF_ID='CONE' /

```
&OBST XB=0.0020,0.0040,-.0820,-.0800,0.0125,0.0225, SURF_ID='SHIELD' /
&OBST XB=0.0020,0.0040,-.0820,-.0800,0.0125,0.0281, SURF_ID='SHIELD' /
&OBST XB=0.0040,0.0060,-.0820,-.0800,0.0008,0.0125, SURF_ID='CONE' /
&OBST XB=0.0040,0.0060,-.0820,-.0800,0.0125,0.0225, SURF_ID='SHIELD' /
&OBST XB=0.0040,0.0060,-.0820,-.0800,0.0125,0.0281, SURF_ID='SHIELD' /
&OBST XB=0.0060,0.0080,-.0820,-.0800,0.0008,0.0125, SURF_ID='CONE' /
&OBST XB=0.0060,0.0080,-.0820,-.0800,0.0125,0.0225, SURF_ID='SHIELD' /
&OBST XB=0.0060,0.0080,-.0820,-.0800,0.0125,0.0281, SURF_ID='SHIELD' /
&OBST XB=0.0080,0.0100,-.0820,-.0800,0.0008,0.0125, SURF_ID='CONE' /
&OBST XB=0.0080,0.0100,-.0820,-.0800,0.0125,0.0225, SURF_ID='SHIELD' /
&OBST XB=0.0080,0.0100,-.0820,-.0800,0.0125,0.0281, SURF_ID='SHIELD' /
&OBST XB=0.0100,0.0120,-.0820,-.0800,0.0008,0.0125, SURF_ID='CONE' /
&OBST XB=0.0100,0.0120,-.0820,-.0800,0.0125,0.0225, SURF_ID='SHIELD' /
&OBST XB=0.0100,0.0120,-.0820,-.0800,0.0125,0.0281, SURF_ID='SHIELD' /
&OBST XB=0.0120,0.0140,-.0820,-.0800,0.0008,0.0281, SURF_ID='SHIELD' /
&OBST XB=0.0140,0.0160,-.0820,-.0800,0.0008,0.0281, SURF_ID='SHIELD' /
&OBST XB=0.0160,0.0180,-.0820,-.0800,0.0008,0.0242, SURF_ID='SHIELD' /
                                        .
                                        .
                                        .
                                        .
                                        .
&OBST XB=0.0080,0.0100,0.0900,0.0920,0.0008,0.0125, SURF_ID='SHIELD' /
&OBST XB=0.0100,0.0120,0.0900,0.0920,0.0008,0.0125, SURF_ID='SHIELD' /
&OBST XB=0.0120,0.0140,0.0900,0.0920,0.0008,0.0125, SURF_ID='SHIELD' /
```

Output from FDS

```
.....……....
&PL3D DTSAM=10000. /

&THCP XYZ=0.00,0.00,-.025,IOR= 3,QUANTITY='GAUGE_HEAT_FLUX',LABEL='Surface Heat
Flux' /

&SLCF PBY=0.00,QUANTITY='TEMPERATURE' /
&SLCF PBY=0.00,QUANTITY='RADIANT_INTENSITY' /
&SLCF PBY=0.00,QUANTITY='HRRPUV' /

&BNDF QUANTITY='GAUGE_HEAT_FLUX' /
&BNDF QUANTITY='WALL_TEMPERATURE' /
&BNDF QUANTITY='BURNING_RATE' /
```

Note: It will require two hundred over pages to include all the input data for the conical heater geometry. Therefore only portion of it can be shown in this Appendix for practical reason.